

CLEITON LOPES AGUIAR

**Caracterização da plasticidade sináptica e padrões oscilatórios na via
hipocampo-córtex pré-frontal medial in vivo: possíveis implicações para o
estudo de comorbidades psiquiátricas em modelos experimentais de
epilepsia**

Tese apresentada à Faculdade de
Medicina de Ribeirão Preto da
Universidade de São Paulo, como parte
das exigências para a obtenção do título
de Doutor em Ciências. Área de
concentração: Neurociência

Orientador: Prof. Dr. João Pereira Leite
Co-orientador: Prof. Dr. Rodrigo Neves
Romcy-Pereira

RIBEIRÃO PRETO – SP

2014

Autorizo a reprodução e divulgação total ou parcial deste trabalho, por qualquer meio convencional ou eletrônico, para fins de estudo e pesquisa, desde que citada a fonte

Lopes-Aguiar, Cleiton

Caracterização da plasticidade sináptica e padrões oscilatórios na via hipocampo-córtex pré-frontal medial in vivo: possíveis implicações para o estudo de comorbidades psiquiátricas em modelos experimentais de epilepsia / Cleiton Lopes Aguiar. Ribeirão Preto, 2014.

118p. : il.; 30 cm

Orientador: João Pereira Leite

Tese (doutorado) – Faculdade de Medicina de Ribeirão Preto da Universidade de São Paulo. Área de concentração: Neurociências.

1. Córtex pré-frontal. 2. Potenciação de longa-duração. 3. CA1 do hipocampo. 4. Plasticidade sináptica. 5. Cetamina. 6. Pós-descarga única hipocampal. 7. Padrões oscilatórios. 8. Anestesia por uretana.

Lopes-Aguiar C. Caracterização da plasticidade sináptica e padrões oscilatórios na via hipocampo-córtex pré-frontal medial in vivo: possíveis implicações para o estudo de comorbidades psiquiátricas em modelos experimentais de epilepsia. Tese apresentada à Faculdade de Medicina de Ribeirão Preto da Universidade de São Paulo, como parte das exigências para a obtenção do título de Doutor em Ciências. Área de concentração: Neurociências.

Aprovado em:

Banca examinadora

Prof. Dr.: _____ Instituição: _____

Julgamento: _____ Assinatura: _____

Prof. Dr.: _____ Instituição: _____

Julgamento: _____ Assinatura: _____

Prof. Dr.: _____ Instituição: _____

Julgamento: _____ Assinatura: _____

Prof. Dr.: _____ Instituição: _____

Julgamento: _____ Assinatura: _____

Prof. Dr.: _____ Instituição: _____

Julgamento: _____ Assinatura: _____

Dedico este trabalho à
Minha esposa, e parceira de
todas as horas, Gisele.
*Obrigado por estar **sempre***
ao meu lado!

E ao meu pai, mãe e irmã
(Roseli, Vitor e Leisa) pelo
imenso carinho e suporte

Agradeço:

Aos meus orientadores Dr. João Pereira Leite e Dr. Rodrigo N. Romcy-Pereira, pela amizade, visão de ciência que me proporcionaram e por todos os ótimos momentos que tivemos nesses 8 anos que participei do Laboratório de Investigação em Epilepsia.

À Fundação de Amparo à Pesquisa do Estado de São Paulo (FAPESP) pelo financiamento de bolsa regular de doutorado no país (#2009/54410-0) e de bolsa de estágio no exterior (# 2012/07107-2).

À Cooperação Interinstitucional de Apoio a Pesquisas sobre o Cérebro (CInAPCe) da FAPESP, Conselho Nacional de Desenvolvimento Científico e Tecnológico (CNPq), Coordenação de Aperfeiçoamento de Pessoal de Nível Superior (CAPES), Fundação de Apoio ao Ensino, Pesquisa e Assistência do Hospital das Clínicas da Faculdade de Medicina de Ribeirão Preto da Universidade de São Paulo (FAEPA), por apoiar, direta ou indiretamente, o presente trabalho;

À minha família, pelo amor e suporte. Gisele, Vitor, Roseli e Leisa, sou extremamente grato por estarem ao meu lado nos momentos que mais precisei;

Aos meus “irmãos” Rafael Naime Ruggiero, Milton Àvila, Caio Moreira e Matheus T. Rossignoli pelo enorme apoio nas horas difíceis e amizade sincera;

Aos amigos de laboratório que contribuíram direta ou indiretamente para a melhoria do presente trabalho: Ana Clara Broggin, Ingrid Esteves, José Peixoto, Lézio S. Bueno Jr., Ludmyla Kandravicius e Raquel do Val da Silva.

Aos demais amigos de laboratório pela excelente convivência e pelas discussões valiosas sobre neurociências: Danilo, Mariana, Patrícia e Priscila

À técnica de nosso laboratório (Sra. Renata Scandiuzzi) por tudo o que me ensinou e pela maneira gentil, qualificada e prestativa que sempre nos ajudou;

Ao técnico do departamento de Neurociências e Ciências do Comportamento (Sr. Renato Meireles) pela assistência qualificada e eficiente ao nosso laboratório e pela gentileza e amizade;

À secretária do programa de pós-graduação em Neurologia/Neurociências (Sra. Silvana Lo Turco), pela gentileza com que sempre me tratou e pela imensa ajuda que me deu nessa reta final.

“O intelecto humano evoluiu em um contexto que era necessário vencer tanto no mundo natural como no social. Assim, nossa mente é composta por módulos que nos tornam capazes de raciocinar sobre como funcionam objetos, artefatos, seres vivos e outros seres humanos. Como diz o ditado: se você der um martelo a um menino, o mundo inteiro irá se tornar um prego. Se você der a uma espécie uma compreensão elementar de mecânica, biologia e psicologia, o mundo inteiro torna-se uma máquina, uma selva e uma sociedade”.

Steven Pinker (1999) em seu livro: Como a mente funciona.

Resumo

Lopes-Aguiar, C. Caracterização da plasticidade sináptica e padrões oscilatórios na via hipocampo-córtex pré-frontal medial *in vivo*: possíveis implicações para o estudo de comorbidades psiquiátricas em modelos experimentais de epilepsia [Tese]. Ribeirão Preto: Universidade de São Paulo, Faculdade de Medicina de Ribeirão Preto, 2014. 118 p.

Transtornos psicóticos afetam cerca de 20% dos pacientes acometidos por epilepsia do lobo temporal (ELT) e resultam de disfunções, ainda pouco compreendidas, presentes em vários níveis de organização neurobiológica. Em modelos animais, o desequilíbrio entre os sistemas excitatório e inibitório em circuitos límbico-corticais gera disfunções secundárias no sistema dopaminérgico, levando a alterações comportamentais que se assemelham a psicose. Em longo prazo, a disfunção da plasticidade sináptica cortical nessas vias parece estar subjacente aos sintomas negativos e prejuízos cognitivos, observados na esquizofrenia ou na psicose associada a ELT. O objetivo do presente trabalho foi caracterizar os efeitos da indução de pós-descarga única no hipocampo (AD; possível modelo de psicose pós-ictal) e da injeção sistêmica de cetamina S+ (KET-S+; modelo farmacológico de psicose) sobre a plasticidade sináptica e padrões oscilatórios da via CA1-córtex pré-frontal medial (mPFC) *in vivo*. Além disso, testamos se a indução de potenciação de longa duração (LTP) no mPFC seria capaz de modular as alterações eletrofisiológicas promovidas por KET e AD. Ratos adultos anestesiados com uretana receberam implantes de eletrodos de estimulação e registro, em CA1 e no mPFC, respectivamente. Dois pulsos elétricos quadrados monofásicos (intervalo entre pulsos = 80 ms) foram aplicados em CA1 a 0,05 Hz para eliciar potenciais pós-sinápticos de campo (fPSP1 e fPSP2) no mPFC. Avaliamos a plasticidade de curta duração por meio da facilitação por pulso emparelhado, calculada pela razão entre as amplitudes de fPSP2 e fPSP1. Após 90min de registros de linha de base, grupos independentes de animais receberam aplicação de pós-descarga no hipocampo, injeção de KET-S+ (12,5 mg/kg i.p.) ou injeção de veículo, e foram monitorados por mais 120min. Em outro experimento registramos 30min de linha de base e aplicamos estímulos de alta frequência para indução de LTP aos 30 e 60min. Trinta minutos depois, os animais receberam KET-S+, AD ou veículo e tiveram seus potenciais corticais registrados por mais 120 min. Potenciais de campo locais em CA1 e no mPFC foram registrados simultaneamente durante todo o experimento. Nossos resultados mostram que AD reduz (-50%; $p < 0,05$ – ANOVA de duas vias de medidas repetidas) a eficiência de transmissão basal na via CA1-mPFC, enquanto KET-S+ promove aumento de 10% ($p < 0,05$ - ANOVA). Ambos os tratamentos promovem prejuízo da plasticidade pré-sináptica na mesma via. Além disso, observamos que a indução prévia de LTP atenua as alterações da eficiência basal e bloqueia os prejuízos de plasticidade pré-sináptica na via CA1-mPFC induzidos por KET-S+ e AD. A indução prévia de LTP também atenua o aumento aberrante induzido por KET-S+ na comodulação entre fase de delta e amplitude de gama no córtex, mas não no hipocampo. Nossos achados indicam que a plasticidade sináptica e a sincronia hipocampo-cortical são alterados em modelos de psicose e psicose pós-ictal. A prevenção de tais efeitos por indução de LTP prévia, está de acordo com evidências recentes de que o aumento da eficiência de receptores glutamatérgicos atenua os prejuízos cognitivos em modelos animais de psicose. Portanto, a estimulação de alta frequência em CA1 pode ser uma ferramenta útil para compreender melhor como prevenir prejuízos de plasticidade sináptica observados em modelos experimentais de psicose e psicose pós-ictal.

Palavras-chave: psicose pós-ictal, plasticidade sináptica, via CA1-córtex pré-frontal medial, potenciação de longa duração, pós-descarga hipocampal, esquizofrenia, cetamina, epilepsia

Lopes-Aguiar, C. Characterization of the synaptic plasticity and oscillatory patterns in the hippocampus-medial prefrontal cortex pathway *in vivo*: possible implications for psychiatry comorbidities studies in temporal lobe epilepsy experimental models. [Thesis]. Ribeirão Preto: University of São Paulo, Ribeirão Preto School of Medicine, 2014. 118 p.

Abstract

Psychotic disorders affect around 20% of the patients with temporal lobe epilepsy (TLE). This condition is resulted of dysfunctions in different levels of neurobiological organization. In animal models, it has been shown that the excitatory/inhibitory unbalance in cortico-limbic circuits produces secondary dysfunctions in the dopaminergic system, leading to psychotic-like behavioral abnormalities. At long-term, the synaptic plasticity dysfunction in the cortex seems to underlie the negative symptoms and cognitive deficits observed in schizophrenia or psychosis associated to TLE. The present work aimed to characterize the effects of hippocampal after-discharge (AD; putative model of post-ictal psychosis) or ketamine S+ (KET-S+; pharmacological model of psychosis) on the synaptic plasticity and oscillatory patterns in the CA1-medial prefrontal cortex (mPFC) pathway. Also, we tested whether the induction of cortical long-term potentiation (LTP) was able to prevent the presynaptic plasticity impairment induced by AD or KET-S+. Electrodes were stereotaxically positioned into CA1 and mPFC in urethane-anesthetized rats. Squared-monophasic paired-pulses of electrical stimuli were applied to CA1 in order to evoke field post-synaptic potentials (fPSP 1 and fPSP 2) in the mPFC every at 0,05 Hz. Short-term plasticity was evaluated by measuring paired-pulse facilitation (PPF), defined as the amplitude ratio fPSP2/ fPSP1. After 90min of baseline recordings, three independent groups of animals received hippocampal-AD, KET-S+ (12.5mg/kg, i.p.) or vehicle (NaCl 0.15M) followed by 120min of evoked response monitoring. In an additional experiment, two applications of high-frequency stimuli (HFS) were performed at 30 and 60min after baseline. Thirty minutes after the second HFS, the rats received KET-S+, AD or vehicle and their cortical evoked potentials were monitored for further 120min. Our results showed that AD significantly decreased (-50%; $p < 0,05$ – Two way ANOVA repeated measures) whereas KET-S+ enhanced (+10%) CA1-mPFC basal synaptic transmission. In addition, AD and KET-S+ similarly impaired short-term plasticity in the mPFC (-15%). Interestingly, induction of LTP in the mPFC prevented the PPF disruption and the aberrant enhancement of the cortical comodulation (high-gamma amplitude/delta phase) induced by KET and AD. Altogether, our findings support recent evidences that positive allosteric modulators of NMDA and AMPA receptors attenuate cognitive impairments in animal models of psychosis. Therefore, HFS in CA1 might be a useful tool to better understand how to prevent synaptic plasticity disruptions observed in experimental models of psychosis and post-ictal psychosis.

Keywords: post-ictal psychosis, synaptic plasticity, CA1-medial prefrontal cortex pathway, long-term potentiation, hippocampal afterdischarge, schizophrenia, ketamine, epilepsy

Lista de figuras

Figura S1. Método para avaliação imunohistoquímica	41
Figura 1. Medidas eletrofisiológicas, estímulos elétricos e paradigmas experimentais	76
Figura 2. Propriedades dos potenciais evocados na via CA1-mPFC <i>in vivo</i>	78
Figura 3. Efeitos de curto prazo induzidos por AD	79
Figura 4. Alteração da dinâmica dos estados oscilatórios no hipocampo e córtex sob uretana induzido por KET S+	81
Figura 5. Efeitos de KET sobre os padrões oscilatórios no hipocampo e mPFC	83
Figura 6. Efeitos de KET S+ e AD sobre a eficiência basal e plasticidade pré-sináptica da via CA1-mPFC	85
Figura 7. Correlações entre padrões oscilatórios e potenciais evocados na via CA1-mPFC ..	86
Figura 8. Efeitos da indução prévia de LTP sobre as alterações induzidas por KET e AD na via CA1-mPFC	88
Figura 9. Modulação da LTP sobre as alterações induzidas por KET S+ nos padrões oscilatórios do mPFC	90
Figura 10. KET S+ aumenta a comodulação entre amplitude de gama-alta e fase de delta induzido no hipocampo e mPFC	91
Figura 11. Indução prévia de LTP atenua o aumento do MI induzido por KET S+ especificamente no mPFC	93
Figura 12. Exemplo de relação não-linear entre MI e potência de delta no mPFC e hipocampo antes e após KET S+	95
Figura 13. Análise imunohistoquímica de BDNF no hipocampo e mPFC	97

Lista de abreviações

AMPA	Ácido alfa-amino-3-hidroxi-5-metil-4-isoxazolpropiônico
BDNF	Fator neurotrófico derivado do cérebro
CA1i	Subregião intermediária de CA1
CA1v	Subregião ventral de CA1
D2	Receptor dopaminérgico do tipo 2
DG	Giro denteado
DV	Dorso-ventral
E/S	Curva de entrada e saída
ELT	Epilepsia do lobo temporal
fMRI	Ressonância magnética funcional/Functional magnetic resonance imaging
fPSP1 e fPSP2	Potenciais pós-sinápticos de campo
GABA	Ácido gama-amino butírico
GLIT	Transportador de glicina
GSK-3	Glicogênio Sintase Cinase 3/Glycogen synthase kinase 3
HFS	Estimulação elétrica em alta frequência/High-frequency stimulation
KET	Cloridrato de cetamina
KET-R	Cloridrato cetamina racêmica
KET-S+	Cloridrato de cetamina S+
LTD	Depressão de longa duração
LTP	Potenciação de longa duração
LY451395	Modulador alostérico positivo de AMPA
M1	Receptor muscarínico do tipo 1
M4	Receptor muscarínico do tipo 4
MI	Índice de modulação/Modulation index
MK-801	Dizocilpina
ML	Médio-lateral
mPFC	Córtex pré-frontal medial
NAcc	Núcleo accumbens
NMDAR	receptor de N-metil-D-aspartato
PBS	Tampão fosfato salina
PCP	Fenciclidina
PFA	Solução fixadora de paraformaldeído
PFC	Córtex pré-frontal
PL	Região pré-límbica do mPFC
PPD	Depressão por pulso emparelhado/Paired pulse depression
PPF	Facilitação por pulso emparelhado/Paired pulse facilitation
PPI	Inibição do sobressalto acústico induzido por pré-pulso/Prepulse inhibition
PSD	Densidade espectral
REM	Rapid eye movement
SAL	Solução salina estéril 0,9%
SWS	Estágio de ondas lentas/Slow-wave sleep
VTA	Área tegmentar ventral

Sumário

FUNDAMENTOS TEÓRICOS E ACHADOS RECENTES DO NOSSO LABORATÓRIO	12
INTRODUÇÃO	23
COMORBIDADES PSIQUIÁTRICAS EM EPILEPSIA DO LOBO TEMPORAL	23
MODELOS DE PSICOSE BASEADOS NA HIPÓTESE GLUTAMATÉRGICA DA ESQUIZOFRENIA	26
DISFUNÇÕES DA COMUNICAÇÃO NA VIA CA1-MPFC EM MODELOS DE PSICOSE	29
NOVOS ALVOS TERAPÊUTICOS NA PSICOSE EXPERIMENTAL	31
OBJETIVOS	34
MATERIAIS E MÉTODOS	35
SUJEITOS	35
CIRURGIA ESTEREOTÁXICA PARA IMPLANTE DE ELETRODOS	35
APARATO EXPERIMENTAL	37
CURVAS DE ENTRADA E SAÍDA E PROTOCOLOS DE ESTIMULAÇÃO	37
DESENHO EXPERIMENTAL	38
IMUNOHISTOQUÍMICA: MÉTODO	40
IMUNOHISTOQUÍMICA: AVALIAÇÃO	41
ANÁLISES DE PADRÕES OSCILATÓRIOS	42
ANÁLISE ESTATÍSTICA DOS POTENCIAIS EVOCADOS	43
RESULTADOS	43
DISCUSSÃO	55
CONCLUSÃO	75
FIGURAS E LEGENDAS	76
REFERÊNCIAS BIBLIOGRÁFICAS	98
ANEXOS	119
ANEXO 1: ARTIGO PUBLICADO NA NEUROPHARMACHOLOGY	

ANEXO 2: PAINEL APRESENTADO NO SIMPÓSIO INTERNACIONAL SOBRE CÓRTEX PRÉ-FRONTAL

ANEXO 3: RELATÓRIO DE ESTÁGIO DE PESQUISA NO EXTERIOR – BEPE – FAPESP

ANEXO 4: ARTIGO DE REVISÃO PUBLICADO NA REVISTA BRASILEIRA DE PSIQUIATRIA

ANEXO 5: RESUMO EXPANDIDO VENCEDOR DO PRÊMIO ARISTIDES LEÃO (CONGRESSO BRASILEIRO DE EPILEPSIA)

ANEXO 6: ARTIGO PUBLICADO NA PLOS ONE

1. Fundamentos teóricos e achados recentes do nosso laboratório

1.1. Modelos de plasticidade sináptica

Atualmente a principal hipótese sobre o mecanismo fundamental de plasticidade sináptica postula que as conexões neuronais em mais alta atividade tendem a se fortalecer e a se estabilizar ao contrário das conexões menos ativas (Hebb, 1949). A primeira observação experimental de um fenômeno de potenciação sináptica, de duração compatível com a manutenção da memória, foi observada estudando-se os potenciais pós-sinápticos de campo (fPSPs) eliciados no giro denteado do hipocampo, após estimulação da via perfurante de coelhos anestesiados (Bliss e Lomo, 1973). Este fenômeno foi chamado de potenciação de longa duração (LTP, do inglês *long-term potentiation*) (Bliss e Collingridge, 1993). Estudos subsequentes descreveram suas principais propriedades como cooperatividade, associatividade e especificidade, que se tornaram fortes argumentos em favor da hipótese de que a LTP pode ser um dos substratos neuronais do aprendizado e processamento de memórias. Atualmente, um conjunto significativo de trabalhos comportamentais, eletrofisiológicos, moleculares e farmacológicos reforça essa ideia (Lynch, 2004; Nicoll e Roche, 2013). Já a depressão de longa duração (ou LTD do inglês, *long-term depression*) é induzida por protocolos de estimulação elétrica em baixas frequências; mostrando que

também é um modelo de plasticidade sináptica atividade-dependente (Malenka e Bear, 2004; Jo *et al.*, 2006; Citri e Malenka, 2008).

A LTP e a LTD compartilham algumas características importantes como: (1) dependência de ativação de receptores de L-glutamato do tipo N-metil-D-aspartato (NMDARs), (2) manutenção dependente de síntese de novas proteínas (Citri e Malenka, 2008) e (3) curso temporal equivalente a processos mnemônicos (Bliss e Collingridge, 1993; Takita *et al.*, 1999). Adicionalmente, foi demonstrado que LTP e LTD também podem ser induzidas em diversas outras regiões do encéfalo de roedores, como amígdala, cerebelo, córtex perirrinal e córtex pré-frontal medial (mPFC) (Lynch, 2004; Massey e Bashir, 2007; Takita *et al.*, 2010).

Contudo, LTP e LTD diferem substancialmente quanto às suas cascatas de sinalização intracelulares (Citri e Malenka, 2008). Resumidamente, uma maior mobilização de proteínas cinases ativa cascatas de sinalização responsáveis pela inserção de novos receptores glutamatérgicos do tipo não-NMDA [e.g. ácido alfa-amino-3-hidroxi-5-metil-4-isoxazolpropiónico (AMPA) e cainato] no terminal pós-sináptico, potencializando a eficiência da transmissão sináptica. Ao passo que a mobilização de fosfatases ativa cascatas de sinalização responsáveis pela endocitose de receptores AMPA e cainato, deprimindo a eficiência da transmissão sináptica (Wang e Kelly, 1996). A compreensão das interações entre LTP e LTD é um fator chave para entender a relação entre flexibilidade da eficiência sináptica em circuitos específicos, cognição e manifestação de transtornos psiquiátricos (Collingridge *et al.*, 2010; Goto *et al.*, 2010; Keifer e Zheng, 2010).

Já a plasticidade sináptica de curta duração pode ser estudada aplicando-se dois estímulos emparelhados em um neurônio pré-sináptico com proximidade temporal suficiente para gerar facilitação (PPF do inglês, *paired pulse facilitation*) ou depressão (PPD

do inglês, *paired pulse depression*) relativa dos fPSPs. Estes dois mecanismos influenciam a transmissão sináptica em uma escala temporal muito curta (dezenas de milissegundos), alterando a probabilidade de disparos do neurônio pós-sináptico de acordo com a frequência de disparos do terminal pré-sináptico. São considerados propriedades importantes para o processamento e filtro de informações sensoriais, além da codificação exigida durante mudanças rápidas de estratégias comportamentais (Citri e Malenka, 2008).

1.2. Comunicação hipocampo-cortical e cognição

O principal elo entre o hipocampo e o neocórtex é o córtex transicional, composto pelos córtices perirrinal, parahipocampal e entorrinal. Os dois primeiros recebem informações dos estágios mais elevados do processamento neocortical em cada uma das principais modalidades sensoriais. Após processar um estímulo, os córtices perirrinal e parahipocampal enviam a informação para a região do córtex entorrinal onde as diferentes modalidades sensoriais podem ser combinadas, formando uma representação polimodal do ambiente. O córtex entorrinal, por sua vez, envia estas informações ao hipocampo, onde se tornam ainda mais complexas. As informações processadas pelo hipocampo são enviadas de volta ao neocórtex, via CA1 hipocampal, completando assim a alça de comunicação córtex – hipocampo – córtex (Squire *et al.*, 2004). Além de projetar para o córtex entorrinal, a região CA1 projeta, ipsilateralmente, para o mPFC (Vertes, 2006). Diversos estudos clínicos e experimentais indicaram que o mPFC está envolvido no processo de aprendizagem e memória, especialmente de trabalho (Goldman-Rakic, 1995b; a). Além disso, o mPFC contribui para: (1) a ordenação temporal de eventos espaciais e não espaciais; (2) a organização de informações e planejamento de respostas; (3) o processamento de informações que requerem atenção seletiva; ou ainda (4) o processamento de informações

e planejamento de comportamentos relacionados ao medo e ansiedade (Dalley *et al.*, 2004). É bem documentada também o envolvimento de disfunções no mPFC em transtornos psiquiátricos, tais como: transtorno bipolar, depressão, psicose e transtorno de ansiedade (Drevets *et al.*, 1997; Cerqueira *et al.*, 2007). Portanto, o estudo da comunicação entre hipocampo e mPFC parece ser uma peça fundamental para a melhor compreensão dos mecanismos subjacentes as funções executivas em condições não patológicas e aos prejuízos cognitivos associados a transtornos psiquiátricos e outras neuropatologias (Damasio, 1989; Laroche *et al.*, 2000; Kandratavicius, Lopes-Aguiar, *et al.*, 2012).

1.3. A via CA1-mPFC

1.3.1. Características gerais e plasticidade sináptica

A via hipocampo–mPFC origina-se em CA1 e subículo e: (1) é direta e monossináptica; (2) estende-se, ipsilateralmente, via fórnix, ao mPFC, (3) é unidirecional, (4) é excitatória, e (5) dependente de ativação de receptores AMPA no mPFC (Laroche *et al.*, 2000; Godsil *et al.*, 2013). Além disso, a via CA1-mPFC está sujeita a indução de LTP, LTD, despotenciação (estimulação que, quando aplicada após indução de LTP, produz volta rápida da eficiência sináptica para a linha de base) e bidirecionalidade (conversão entre LTP e LTD, e vice-versa). Tanto a indução de LTP, quanto a de LTD, dependem de ativação de receptores NMDA no mPFC (Laroche *et al.*, 1990; Jay *et al.*, 1995; 1996; Takita *et al.*, 1999; Laroche *et al.*, 2000; Lopes-Aguiar *et al.*, 2013). A plasticidade sináptica no mPFC é modulada pela atividade dos sistemas serotoninérgico, colinérgico e dopaminérgico (Jay *et al.*, 2004; Lopes Aguiar *et al.*, 2008; Zhong *et al.*, 2008). Além disso, a LTP na via CA1-mPFC é prejudicada por tratamento crônico com anfetamina, um modelo farmacológico de psicose (Ishikawa *et al.*, 2005); e o antipsicótico atípico, clozapina, aumenta a LTP nessa via, por meio de ativação de receptores

dopaminérgicos do tipo D1 (Matsumoto *et al.*, 2008). É interessante notar que ocorre aumento dos níveis extracelulares de dopamina no mPFC e núcleo *accumbens* (NAcc) logo após aplicação de estimulação elétrica em alta-frequência (HFS, do inglês *high-frequency stimulation*) utilizada para indução de LTP na via CA1-mPFC (Jay *et al.*, 2004), sugerindo que a manipulação da plasticidade sináptica nessa via possa produzir efeitos secundários em redes mais amplas.

1.3.2. Evidências da natureza monossináptica da via CA1-mPFC

Experimentos utilizando marcação retrógrada e registros extracelulares em CA1 após estimulação antidrômica no mPFC sugerem que a via CA1-mPFC seja, monossináptica. Ferino *et al.* (1987) mostraram que a latência média entre o estímulo dos terminais axônicos no mPFC e os *spikes* evocados em CA1 em ratos anestesiados foi de $15,6 \pm 3,6$ ms (Ferino *et al.*, 1987). Posteriormente, (Degenetais *et al.*, 2003) realizaram registros intracelulares de neurônios piramidais do mPFC após estimulação em CA1 também de ratos anestesiados. Os autores mostraram que mais de 90% das células registradas apresentaram potenciais excitatórios pós-sinápticos (EPSP). Consistente com (Ferino *et al.*, 1987), a latência média dos EPSPs evocados foi de $14,6 \pm 4$ ms. Intensidades crescentes de corrente aplicadas em CA1 (de 100 a 500 μ A) foram capazes de aumentar os EPSPs corticais, sem alterar sua latência. Apenas 19% dos neurônios registrados apresentaram *spikes* juntamente com os EPSPs evocados. Os autores ainda confirmaram, em parte das células piramidais registradas, que é possível induzir diferentes formas de plasticidade sináptica (PPD, PPF e LTP) na via CA1-mPFC (Degenetais *et al.*, 2003). Em seguida, o mesmo grupo reportou evidências sobre a influência das projeções hipocâmpais sobre os interneurônios do mPFC de ratos anestesiados (Tierney *et al.*, 2004). Os autores utilizaram estimulação elétrica em CA1,

seguido de registros unitários extracelulares no mPFC, associados a injeções justacelulares de biotina para posterior identificação das células registradas. Os resultados mostraram que a maioria dos interneurônios registrados (70%) no mPFC apresentaram spikes após aplicação de pulsos únicos em CA1. Além disso, os autores demonstraram que os interneurônios dispararam mais (a maioria das vezes em salvas) e com latências médias mais curtas (12 a 14 ms) do que os neurônios piramidais. Esses resultados, em conjunto, sugerem que as projeções hipocámpicas excitatórias aos interneurônios do mPFC seriam responsáveis por restringir, no tempo e espaço, a influência do hipocampo sobre os neurônios piramidais do mPFC, além de gerar localmente ritmos corticais com alta precisão temporal (e.g. oscilações teta, 4 – 10 Hz; gama, 30 a 100 Hz e *ripples*, 100 a 200 Hz). Os autores ainda sugerem que a aplicação de HFS em CA1, além de aumentar a eficiência global da comunicação da via hipocampo-mPFC, também seria capaz de gerar alterações de longo prazo no sistema inibitório local do mPFC. Isso poderia explicar como os ritmos hipocámpicos endógenos de alta frequência (e.g. *sharp-wave ripples*, 100 a 250 Hz) seriam capazes de influenciar, por longo-prazo, o processamento local e saída de informação do mPFC (Goldman-Rakic, 1996; Tierney *et al.*, 2004). Contudo, os autores não testaram se a indução de LTP afeta as respostas subsequentes dos interneurônios do mPFC aos estímulos elétricos em CA1.

1.3.3. A via CA1-mPFC é composta por duas rotas distintas

1.3.3.1. Evidências anatômicas e eletrofisiológicas

Recentemente, devido a um acúmulo de evidências neuroanatômicas e eletrofisiológicas, ficou mais claro que a via CA1-mPFC parece ser constituída de duas rotas com origens distintas, porém convergentes. A primeira origina-se na região intermediária de CA1 (via iCA1 – mPFC); e a segunda origina-se na porção ventral de CA1 (via vCA1 – mPFC;

(Takita *et al.*, 2013). É importante salientar que a região CA1 do hipocampo anterior não projeta ao mPFC (Ferino *et al.*, 1987; Vertes, 2006). Contudo, ainda não está claro se tais rotas também apresentam propriedades eletrofisiológicas e/ou funções distintas. Resumidamente, foram reportadas semelhanças entre as latências dos fPSP e magnitude/duração da LTP das vias iCA1-mPFC e vCA1-mPFC de ratos anestesiados com uretana (Izaki *et al.*, 2002; Izaki *et al.*, 2003). Os mesmos autores encontraram, entretanto, diferenças em relação a indução de plasticidade sináptica de curto prazo. Enquanto a via iCA1-mPFC apresentou PPD ao serem aplicados estímulos emparelhados com intervalo entre 25 a 50 ms e PPF com intervalos entre 100 e 400 ms, a via vCA1-mPFC apresentou apenas PPFs em todos os ITIs testados (de 50 a 400 ms). O PPF máximo nessa via foi obtido com ITI=50 ms, caindo gradativamente conforme o ITI era aumentado (Izaki *et al.*, 2002). É interessante salientar que foi reportado uma espécie de PPF registrado no mPFC induzido por estimulação emparelhada de vCA1 seguida de iCA1 (primeiro pulso em vCA1 e segundo pulso em iCA1: ITI=100 ms), mas não vice versa. Isso sugere que as duas rotas não só convergem para a mesma população de células corticais, como cooperam entre si no processo de indução de plasticidade sináptica de curto prazo no mPFC (Kawashima *et al.*, 2006).

1.3.3.2. Aspectos funcionais

De uma maneira geral, postula-se que a via CA1-mPFC seja responsável por (1) integrar diversos tipos de informações adquiridas e reprocessadas a cada momento, (2) processar memória de trabalho, (3) influenciar a consolidação de memórias declarativas de longo-prazo, (4) refinar a tomada de decisões e, por fim, (5) controlar comportamentos perseverantes (Floresco *et al.*, 1997; Laroche *et al.*, 2000; Floresco *et al.*, 2008).

Floresco et al., 1997, estudaram os efeitos da desconexão transiente da via vCA1-mPFC, por meio de microinjeções contralaterais de lidocaína no hipocampo e mPFC, sobre a memória espacial de trabalho avaliada em labirinto radial de oito braços (intervalo entre fase de treino e teste = 30 min). Consistentemente, (Wang e Cai, 2006) mostraram que infusões contralaterais de muscimol, um agonista de receptores de ácido gama-amino butírico-A (GABA-A), em vCA1 e no mPFC também produziam prejuízos de memória espacial de trabalho, dessa vez medido em labirinto em T (intervalo entre treino e teste = 0 a 60 s). Este procedimento de desconexão transiente da via vCA1-mPFC também mostrou-se eficaz em prejudicar a aquisição de comportamento operante não espacial de ratos (Izaki *et al.*, 2000). Alguns anos mais tarde, (Izaki *et al.*, 2008) tentaram dissociar os papéis das vias vCA1-mPFC e iCA1-mPFC quanto ao processamento de memória de trabalho de intervalos curtos (ordem de segundos). Para isso os autores desconectaram ambas as vias em grupos de animais distintos e avaliaram memória de trabalho com intervalos entre treino e teste mais curtos (de 4 a 16 s). Os resultados mostram que a integridade da via iCA1-mPFC é crítica para o processamento de memória de trabalho para intervalos curtos de tempo (Izaki *et al.*, 2008). Em contrapartida, a via vCA1-mPFC estaria mais envolvida em processamento de memória de trabalho de intervalos mais longos, da ordem de minutos (Floresco *et al.*, 1997). Por outro lado, (Churchwell e Kesner, 2011) obtiveram dados discrepantes dos acima descritos ao estudarem o papel da via iCA1-mPFC no processamento de memória de trabalho com intervalos longos (5 min) e curtos (10 s) por meio de inativações combinadas de iCA1 e do mPFC. Os autores mostraram que, em intervalos mais longos, iCA1 e mPFC interagem para que ocorra coordenação entre memórias retrospectivas e planejamento de comportamentos retrospectivos. Já em intervalos curtos, cada região é capaz de representar independentemente a informação espacial de maneira que seja suficiente para completar a

tarefa. Portanto, a dissociação funcional das rotas iCA1-mPFC e vCA1-mPFC ainda não está clara e necessita de estudos adicionais, preferencialmente com registros eletrofisiológicos simultâneos no hipocampo e mPFC durante tarefas de memória. Vale ressaltar que o estudo recente publicado por (Benchenane *et al.*, 2010), reportando aumento da coerência de fase na banda teta (4 – 12 Hz) entre hipocampo-mPFC durante o processamento de memória de trabalho, foi realizado em uma região de CA1 um pouco mais anterior que o usual (AP: - 5 mm vs. -5,8 a 6,2 mm; Izaki *et al.* 2008; Lopes-Aguiar *et al.*, 2013). Como discutido, a porção mais anterior do hipocampo não apresenta projeções diretas ao mPFC (Ferino *et al.*, 1987), o que torna difícil a interpretação dos resultados de Benchenane *et al.* (2010) em relação à possível dissociação funcional entre iCA1-mPFC e vCA1-mPFC.

1.4. Sistema colinérgico e plasticidade sináptica na via CA1-mPFC: implicações para o estudo da esquizofrenia

Uma das características mais recorrentes na esquizofrenia, juntamente com episódios de psicose, são os prejuízos em funções executivas (Manoach, 2003). Em muitos casos, estas disfunções são persistentes, incapacitantes e resistentes a tratamento. Estudos de neuroimagem por ressonância magnética funcional (fMRI) sugerem que os prejuízos de processamento de memória de trabalho em pacientes com esquizofrenia sejam resultado de uma incapacidade de determinados circuitos corticais apresentarem maior ativação ou desativação, dependendo da demanda cognitiva. Por exemplo, dados recentes indicam que, durante repouso, o córtex pré-frontal dorsolateral (DLPFC) de pacientes com esquizofrenia apresenta-se mais ativo quando comparado ao de sujeitos-controle. Por outro lado, durante o processamento de memória de trabalho, o DLPFC destes pacientes apresenta-se menos ativado (Pomarol-Clotet *et al.*, 2008; Whitfield-Gabrieli *et al.*, 2009). Além disso, foram

reportadas evidências sugerindo que pacientes com esquizofrenia possuem maior conectividade entre hipocampo e PFC durante repouso, comparado com sujeitos controle (Meyer-Lindenberg *et al.*, 2005).

De acordo com essas evidências clínicas, foi demonstrado que camundongos com deleção de calcineurina no prosencéfalo apresentam prejuízo de memória de trabalho e na bidirecionalidade da plasticidade sináptica hipocampal (Zeng *et al.*, 2001) e da transmissão sináptica no mPFC (Cottrell *et al.*, 2013). Consistentemente, estudos clínicos e experimentais reportaram diminuição na expressão da glicogênio sintase cinase-3 (GSK-3), uma enzima cujo estado de fosforilação apresenta-se afetado na esquizofrenia e em modelos animais de psicose (Beasley *et al.*, 2001; Nadri *et al.*, 2003; Kozlovsky *et al.*, 2004). Esta enzima está amplamente presente no tecido nervoso, além de fazer parte de cascatas de sinalização responsáveis por diversos mecanismos de plasticidade sináptica (Peineau *et al.*, 2008; Peineau *et al.*, 2009). Assim como a calcineurina, a atividade da GSK-3 é necessária para a conversão de LTP em LTD no hipocampo de roedores (Peineau *et al.*, 2007; Bradley *et al.*, 2012).

Nesse contexto, nosso laboratório mostrou que a atividade colinérgica muscarínica facilita tanto LTP, quanto LTD, na via CA1-mPFC (Lopes Aguiar *et al.*, 2008; Lopes-Aguiar *et al.*, 2013). Nossos resultados sugerem que a ativação de receptores muscarínicos colinérgicos por injeção do agonista muscarínico pilocarpina (PILO; 15 mg/Kg, i.p.) 20 min antes da aplicação de HFS, potencializa a manutenção da LTP cerca de 1,5 hora após a sua indução no mPFC. Em seguida, demonstramos que administração central de PILO (40 nmols, i.c.v.) antes de aplicação de LFS de 600 trens, converte uma depressão transiente (\approx 30 min) dos potenciais evocados corticais em uma LTD robusta e sustentada (\approx 180 min; ver **ANEXO 1**). Uma das possíveis implicações dos nossos achados é que a facilitação bidirecional da

plasticidade sináptica na via CA1-mPFC induzida por ativação muscarínica poderia explicar, pelo menos em parte, os efeitos antipsicóticos e pró-cognitivos de agonistas muscarínicos, que têm sido utilizados para a investigação de novos tratamentos em pacientes com esquizofrenia e em modelos animais de psicose (Bymaster *et al.*, 1999; Gomeza *et al.*, 1999; Lieberman *et al.*, 2008). Consistentemente, (Crook *et al.*, 2001) mostraram que pacientes com esquizofrenia apresentam disfunção de receptores muscarínicos do tipo M1 e M4 no mPFC. Esses achados foram corroborados em um estudo com modelos animais, que demonstrou que tratamento crônico com fenciclidina (PCP) também parece gerar efeito semelhante (Du Bois *et al.*, 2009). Ainda não se sabe se a LTD dependente de NMDARs da via CA1-mPFC descrita recentemente pelo nosso grupo (Lopes Aguiar *et al.*, 2013) também requer ativação de GSK-3 e calcineurina. Porém, a demonstração de que estas proteínas podem ser reguladas por antipsicóticos típicos (haloperidol) e atípicos (clozapina) no mPFC (Sutton e Rushlow, 2011), bem como nossos achados mais recentes sobre os efeitos modulatórios do lítio (Li+) sobre a facilitação muscarínica da LTP e LTD na via CA1-mPFC (Ruggiero *et al.* 2014. *Manuscrito em preparação*), reforçam a ideia de que a bidirecionalidade da plasticidade sináptica nesta região possa envolver tais cascatas intracelulares relevantes para o estudo da esquizofrenia (Roh *et al.*, 2007; Rushlow *et al.*, 2009).

Portanto, o estudo da plasticidade sináptica na via CA1-mPFC pode ser útil para a melhor compreensão dos mecanismos responsáveis pela (1) inabilidade dos pacientes com esquizofrenia de apresentar flexibilidade nos níveis de ativação e desativação do mPFC de acordo com a demanda cognitiva; e (2) pelos prejuízos de memória de trabalho e filtro sensorio-motor.

2. Introdução

2.1. Comorbidades psiquiátricas em Epilepsia do Lobo Temporal: Modelos animais e seus possíveis mecanismos subjacentes

A epilepsia é a condição neurológica grave que apresenta a maior prevalência no mundo (1% da população mundial; (Li e Sander, 2003; Ngugi *et al.*, 2010). Cerca de 6% dos pacientes epiléticos desenvolvem algum tipo de transtorno psiquiátrico. Essa condição limita as possibilidades de tratamento, correlaciona-se significativamente com ausência de resposta à terapia farmacológica com drogas antiepilépticas, pioram consideravelmente a qualidade de vida dos pacientes e seus familiares, além de impactar negativamente as funções executivas e aumentar o risco para suicídio (Gaitatzis *et al.*, 2004; Hitiris *et al.*, 2007). As comorbidades psiquiátricas mais comuns são os transtornos de humor (especialmente a depressão, em até 30% dos casos); seguidos por transtornos de ansiedade (10-25%); psicoses (2-7%) e transtornos de personalidade (1-2%) (Stefanello *et al.*, 2010).

O desenvolvimento de psicose - perturbação que envolve o início súbito de delírios, alucinações, discurso desorganizado ou comportamento amplamente desorganizado ou catatônico – ocorre em até 20% dos casos de epilepsia do lobo temporal (ELT) (Gaitatzis *et al.*, 2004; Tellez-Zenteno *et al.*, 2007). Esta comorbidade é geralmente classificada de acordo com sua relação temporal com as crises, sendo subdividida em ictais, peri-ictais e interictais. As psicoses peri-ictais ainda podem ser divididas em psicose pré-ictal (se manifesta imediatamente antes da crise) e pós-ictal (se manifesta logo após a crise), sendo o último mais comum em ELT (Kanemoto *et al.*, 2010). Os mecanismos subjacentes à relação entre a manifestação de psicose, prejuízos cognitivos e a severidade de crises em pacientes com ELT ainda são pouco compreendidos, o que torna os estudos com modelos animais imperativos.

A relação entre psicose e atividade ictal tem sido investigada experimentalmente por meio de (1) abrasamento elétrico de circuitos específicos (Ma e Leung, 2010); (2) protocolos de evocação de pós-descarga (AD, do inglês *afterdischarge*) única no hipocampo (Mccracken e Roberts, 2006); (3) estudos que utilizam desafio farmacológico com anfetamina ou meta-anfetamina em modelos de epilepsia do lobo temporal para verificar sensibilidade do sistema dopaminérgico (Cifelli e Grace, 2012); ou ainda (4) tratamentos agudos ou crônicos com antagonistas não-competitivos de receptores de NMDA (Corlett *et al.*, 2011).

Estudos com abrasamento por estimulação elétrica em circuitos específicos forneceram evidências sobre o envolvimento dopaminérgico em mecanismos possivelmente compartilhados entre epilepsia e psicose. O abrasamento da área tegmentar ventral (VTA), por exemplo, gera alterações emocionais e de interação social em gatos (Stevens e Livermore, 1978), além de potencializar a hiperlocomoção induzida por anfetamina ou meta-anfetamina em roedores (Watanabe *et al.*, 2004). Além disso, abrasamento hipocampal aumenta a densidade de receptores dopaminérgicos, assim como liberação de dopamina no NAcc de ratos (Csernansky *et al.*, 1988; Strecker e Moneta, 1994).

Estas alterações dopaminérgicas em circuitos mesolímbicos pós-ictais parecem envolver o hipocampo. Por exemplo, foi demonstrado que abrasamento elétrico (de 9 a 13 trens de 5 s a 60 Hz) no mPFC e NAcc produz hiperlocomoção, alterações de filtro sensorio motor e aumento aberrante de oscilações gama (30 a 80 Hz). Todas essas alterações são bloqueadas, se o hipocampo é previamente inativado por muscimol (Ma e Leung, 2010).

As alterações em circuitos límbico-corticais observadas em modelos experimentais de epilepsia parecem refletir as disfunções dopaminérgicas observadas em casos de comorbidades psiquiátricas observadas em pacientes com ELT (Leung *et al.*, 2000; Cifelli e Grace, 2012; Pittau *et al.*, 2012). Modelos de evocação de AD única no hipocampo por

estimulação elétrica são considerados úteis para o estudo de psicose pós-ictal, pois induzem hiperlocomoção, movimentos estereotipados e prejuízos sobre inibição do sobressalto acústico induzido por pré-pulso (PPI, do inglês *prepulse inhibition*) de maneira semelhante a modelos farmacológicos de psicose (Ma e Leung, 2004). Essa atividade locomotora excessiva no período pós-ictal parece ser mediada por receptores dopaminérgicos do subtipo D2 no NAcc e requer atividade intacta do pálido ventral, sugerindo que a via que conecta essas duas regiões seja crítica para expressão desse comportamento aberrante (Ma *et al.*, 1996). Além disso, o prejuízo de PPI gerado por AD apresenta-se associado a aumento da atividade do septo medial e de oscilações gama no hipocampo e mPFC. Essas alterações comportamentais e oscilatórias são provavelmente desencadeados por mecanismos envolvendo neurônios gabaérgicos, mas não de acetilcolina, no sistema septo-hipocampal (Ma e Leung, 1999).

Nesse sentido, estudos experimentais sobre sensibilização dopaminérgica induzida por crises têm sido úteis para elucidar a relação entre circuitos mesolímbicos, psicose e epilepsia (Cifelli e Grace, 2012). Por exemplo, foram reportadas evidências de que a atividade ictal eleva transientemente os níveis extracelulares de dopamina em diversas regiões encefálicas, incluindo hipocampo, estriado, NAcc e mPFC (Dazzi *et al.*, 1997). De fato, foi demonstrado recentemente que ratos submetidos a modelo de ELT por injeção de pilocarpina apresentam aumento significativo dos disparos espontâneos do VTA comparado aos controles (Cifelli e Grace, 2012). Postula-se que essa atividade populacional dos neurônios dopaminérgicos seja regulada pela via subículo ventral-NAcc-pálido ventral-VTA (Floresco *et al.*, 2009). Contudo, os mecanismos responsáveis pela hiperatividade hipocampal, capaz de modificar o tônus dopaminérgico em modelos de ELT, ainda não são bem compreendidos. Um importante aspecto dessa questão refere-se ao envolvimento dos

circuitos parahipocampais. O aumento da excitabilidade em pacientes com ELT, por exemplo, parece estar associado a pronunciada neurodegeneração na camada III do córtex entorrinal medial, que projeta diretamente para CA1 por meio da via temporoamônica (Du *et al.*, 1995). Este padrão de perda celular, está associado a maior excitabilidade hipocampal e parahipocampal e susceptibilidade a futuras crises e/ou descargas epileptiformes (Spencer e Spencer, 1994).

Portanto, uma hipótese a ser testada é de que a hiperexcitabilidade hipocampal seria um dos substratos biológicos compartilhados entre esquizofrenia e psicose associada a ELT. O aumento anormal da atividade em circuitos temporais em pacientes com ELT ou esquizofrenia seria capaz de produzir um estado de hiperfunção dopaminérgica, envolvendo as projeções do hipocampo ao NAcc como desencadeadoras desse processo (Mitchell *et al.*, 2000). Simultaneamente, a forte propagação dessa hiperatividade do hipocampo ao mPFC também causaria alterações de plasticidade sináptica de longo prazo que poderia estar subjacentes as disfunções executivas na esquizofrenia e ELT (Leung *et al.*, 2000; Ando *et al.*, 2004). Nesse contexto, são mandatórios experimentos que avaliem as alterações de plasticidade sináptica de circuitos límbico-corticais em diferentes modelos de psicose e ELT.

2.2. Modelos de psicose baseados na hipótese glutamatérgica da esquizofrenia

Os modelos de psicose gerados pela administração de PCP, cloridrato de cetamina racêmica (KET-R), cloridrato de cetamina-S+ (KET-S+) ou dizocilpina (MK-801) são baseados na hipótese glutamatérgica da esquizofrenia (Corlett *et al.*, 2011; Moghaddam e Javitt, 2012). Contudo, as alterações comportamentais que seguem ao tratamento agudo com antagonistas de NMDAR também parecem envolver, pelo menos secundariamente, alterações de circuitos dopaminérgicos (Moghaddam *et al.*, 1997; Manahan-Vaughan *et al.*,

2008). Os prejuízos gerados por KET-R em tarefas dependentes de PFC em humanos e roedores são mediados por receptores dopaminérgicos do tipo 2 (D2; (Verma e Moghaddam, 1996; Krystal *et al.*, 1999). Além disso, uma única dose de um desses antagonistas NMDARs gera um aumento preferencial dos níveis de dopamina no mPFC (Hondo *et al.*, 1994).

Os efeitos gerados por antagonistas de NMDAR parecem envolver a ativação de receptores não-NMDA (AMPA e cainato) (Moghaddam *et al.*, 1997; Kantrowitz e Javitt, 2012). Consistentemente, foi demonstrado que o pré-tratamento com antagonistas de receptores AMPA reduz os prejuízos de funções executivas e aumento de dopamina gerados por KET (Moghaddam *et al.*, 1997). As hipóteses mais aceitas para explicar tais efeitos postulam que: (1) NMDARs encontram-se localizados também nos terminais pré-sinápticos, sendo capazes de modular a liberação de glutamato (Brose *et al.*, 1994; Moghaddam e Javitt, 2012) e (2) antagonistas não-competitivos de NMDARs geram desinibição de neurônios piramidais corticais por meio da diminuição da atividade de interneurônios (Braun *et al.*, 2007; Homayoun e Moghaddam, 2007; McNally *et al.*, 2011). Além da possibilidade dos receptores NMDAR presentes nos interneurônios possuírem maior afinidade por KET, MK-801 e PCP, alguns subtipos de interneurônios possuem menor limiar para geração de potenciais de ação comparados às células piramidais (Csicsvari *et al.*, 1998). Esse estado de maior despolarização dos interneurônios permite que mais receptores NMDA, cujo bloqueio fisiológico de magnésio é cessado de acordo com alterações de voltagem da membrana, permaneçam ativos. Dessa forma, quando o sistema é exposto a um antagonista NMDA, existe um efeito preferencial sobre esses interneurônios, gerando um estado aberrante de inibição do tônus excitatório, ou seja, desinibição dos neurônios piramidais (Homayoun e Moghaddam, 2007; McNally *et al.*, 2011). Essa redução do impacto de receptores de GABA

sobre os neurônios piramidais levam, subseqüentemente, a uma situação instável em que ocorre um engajamento aberrante da população de células excitatórias, o que poderia ser interpretado como um aumento de ruído no processamento de informação (Jackson et al., 2004). Secundariamente, ocorre um aumento da liberação de glutamato pelas células piramidais, levando a um excesso de ativação de receptores AMPA nos terminais pós-sinápticos, especialmente do mPFC (Moghaddam *et al.*, 1997). Assim, de uma forma geral, esse processo de desinibição induzida por hipofunção de receptores NMDA pode comprometer os neurônios piramidais corticais em casos que sejam exigidas integração de novos estímulos, bem como, respostas subseqüentes de uma maneira coordenada para estações sub-corticais (Moghaddam e Javitt, 2012).

Jackson et al. (2004) observaram que injeção sistêmica de MK-801 (1) aumenta os disparos aleatórios e (2) diminui as salvas de disparos em aproximadamente 80% dos neurônios analisados no mPFC. Segundo os autores, a redução das salvas de disparos diminui a eficiência no processamento de informação nessa região, além de diminuir a regulação cortical das saídas comportamentais. Por outro lado, o aumento dos disparos aleatórios prejudica o filtro de informações irrelevantes, gerando saídas comportamentais anormais, como foi sugerido pelos autores após verificar que existe correlação significativa entre o número de comportamentos estereotipados e a atividade aleatória dos neurônios do mPFC. Além disso, foi observado que o mesmo tratamento com MK-801 também gera prejuízo do desempenho em PPI e memória de trabalho (Jackson *et al.*, 2004). Além disso, foi demonstrado que, ao contrário da injeção sistêmica, a microinfusão de PCP diretamente no mPFC não altera significativamente a frequência de disparos de seus neurônios (Suzuki *et al.*, 2002). Em contrapartida, a microinfusão de PCP diretamente no hipocampo ventral, produz aumento significativo da taxa de disparos no mPFC, acompanhado de

hiperlocomoção (Jodo *et al.*, 2005). Esses resultados, em conjunto, sugerem que a hiperativação da transmissão sináptica na via hipocampo-mPFC esteja envolvida na expressão das anormalidades comportamentais observadas em modelos de psicose experimental induzidos farmacologicamente por antagonismo não-competitivo de NMDA.

2.3. Disfunções da comunicação na via hipocampo-mPFC em modelos de psicose

Estudos eletrofisiológicos prévios forneceram evidências indiretas sobre o possível papel da via hipocampo-mPFC em modelos experimentais de psicose. Foram reportadas diversas evidências que correlacionam funções cognitivas com alterações nas oscilações gama no hipocampo, mPFC e circuitos associados (Chrobak e Buzsaki, 1998; Goto e O'donnell, 2001; Izaki e Akema, 2008). Essas oscilações estão relacionadas a funções altamente integradas, incluindo associação de informações (Headley e Weinberger, 2011), atenção (Womelsdorf e Fries, 2006) e memória de trabalho (Wang e Cai, 2006). O aumento das oscilações gama também pode ser observado no modelo AD hipocampal (Ma e Leung, 2010) e em ratos submetidos à injeção sistêmica de KET-R (Pinault, 2008). Entretanto, ainda são escassas as evidências sobre os possíveis efeitos da AD-hipocampal ou do tratamento de KET-R ou KET-S+ na plasticidade sináptica de curta e longa duração da via CA1-mPFC. Em nosso conhecimento, a comparação sistemática entre os efeitos eletrofisiológicos induzidos por AD e antagonistas de NMDAR sobre a via hipocampo-mPFC ainda não foi realizada sistematicamente, embora seja um passo crucial no sentido de melhor compreender os possíveis mecanismos comuns entre psicose associada a ELT e esquizofrenia.

Recentemente foram publicados trabalhos que investigaram a modulação de antagonistas de NMDARs na via hipocampo-mPFC. Kamiyama *et al.* (2011) estudaram os mecanismos dos efeitos de KET-R na via vCA1 -mPFC *in vivo*. Nesse trabalho, a administração

sistêmica de KET-R induziu um decaimento dos fPSPs basais no mPFC de ratos em livre movimento. Os autores também obtiveram resultados bastante semelhantes com animais anestesiados com uretana. Tal decaimento dos fPSPs apresentou-se associado a um prejuízo no filtro sensorio motor (Kamiyama *et al.*, 2011). No entanto, apesar de reportar os efeitos da KET-R sobre a neurotransmissão basal da via vCA1-mPFC, os autores não avaliaram os seus possíveis efeitos sobre a plasticidade sináptica de curta e longa-duração nessa via.

Concomitantemente ao trabalho de Kamiyama *et al.* (2011), as alterações de plasticidade sináptica de curta duração na via vCA1-mPFC foram investigadas por Kiss *et al.* (2011). Nesse trabalho foram realizados registros simultâneos de PPF e de LFPs em ratos anestesiados com uretana sob os efeitos de MK-801. Os autores reportaram que a administração sistêmica de MK-801 diminuiu as oscilações na banda de frequência delta-alta (2 - 4 Hz) e aumentou as oscilações em delta-baixa (0,5 – 2 Hz). Além disso, os autores observaram que o MK-801 é capaz de gerar prejuízo de plasticidade sináptica, medida por PPF na via vCA1-mPFC (Kiss, Hoffmann e Hajos, 2011). Em seguida, o mesmo grupo demonstrou que a microinfusão de MK-801 diretamente no tálamo médio-dorsal (TMD) é capaz de promover aumento de oscilações delta-baixa e diminuição de PPF na via vCA1-mPFC. Esses efeitos eletrofisiológicos foram bastante similares àqueles observados em experimentos adicionais com injeção sistêmica do mesmo fármaco. Por outro lado, os autores mostraram que a infusão intra-mPFC de MK-801 não é capaz de eliciar aumento de delta-baixa e redução de PPF (Kiss, Hoffmann, Scott, *et al.*, 2011). Os autores especulam que o sítio primário de ação do MK-801 não seria o córtex, mas sim múltiplos circuitos neuronais que projetam a ele, incluindo núcleos talâmicos. Tais alterações seriam capazes de mediar os prejuízos comportamentais e cognitivos observados em modelos de psicose experimental. Kiss *et al.* (2011b) ainda forneceram alguns dados que poderiam ser considerados

discrepantes de estudos anteriores (Homayoun e Moghaddam, 2007; Moghaddam e Javitt, 2012). Foram realizados experimentos utilizando registro multiuniário no mPFC após tratamento (sistêmico, intra-MD ou intra-mPFC) de MK-801 e mostraram diminuição global de atividade, associada a discreto aumento dos disparos em salvas. Os autores argumentaram que o fato dos experimentos terem sido conduzidos em animais anestesiados com uretana poderia modular os efeitos do MK-801 sobre a taxa de disparos do mPFC, quando comparado com literatura prévia (ver, por exemplo, dados mostrando aumento de disparos do mPFC após administração de MK-801 no trabalho de Jackson et al., (2004). Nessas condições experimentais, segundo Kiss et al (2011b), os interneurônios não se apresentam tão ativos quanto em animais em livre-movimento e, assim, o MK-801 afetaria, sem maiores distinções, neurônios piramidais e interneurônios. Portanto, uma hipótese a ser testada em estudos futuros seria a de que os antagonistas não-competitivos de receptores NMDA afetariam a atividade encefálica de maneira distinta, dependendo do estado comportamental e oscilatório do sujeito no momento do tratamento (Kiss et al., 2011b).

2.4. Novos alvos terapêuticos na psicose experimental

Em casos de psicose, além da intrínseca disfunção de receptores NMDA, também têm sido demonstrados distúrbios em diversos mecanismos modulatórios que estão se tornando, cada vez mais, alvos de estudos etiológicos e de intervenções terapêuticas (Moghaddam and Javitt, 2012). Dentre os mecanismos modulatórios, destacam-se a síntese e degradação de glicina e D-serina, que se ligam ao sítio modulatório de glicina no receptor NMDA (Javitt, 2008) e glutatona, que se liga ao sítio redox do mesmo receptor (Gysin *et al.*, 2007). Adicionalmente, inibidores endógenos de NMDA, como o ácido cinurênico, podem

ser chave para o desenvolvimento de fármacos que atuem em alvos secundários (Sathyaikumar *et al.*, 2011).

Contudo, uma preocupação importante a respeito da manipulação clínica dos níveis de neurotransmissão glutamatérgica diz respeito aos possíveis efeitos prejudiciais do tratamento crônico com agonistas ou antagonistas de seus receptores. Isso porque as sinapses glutamatérgicas são altamente dinâmicas, apresentando rápida resposta pós-sináptica e eficiente recaptção na fenda. Nesse sentido, uma ativação farmacológica sustentada de receptores glutamatérgicos poderia resultar, eventualmente, em neurotoxicidade, ou ainda, em respostas adaptativas, como endocitose de receptores AMPA e NMDA (Moghaddam e Javitt, 2012). Sendo assim, uma abordagem possível para evitar tais efeitos colaterais, seria utilizar fármacos capazes de modular a função dos receptores de uma maneira atividade-dependente, ou seja, aumentando ou reduzindo sua função de maneira transiente e em resposta a estímulos endógenos. Essa função é naturalmente exercida no encéfalo pelos moduladores alostéricos de receptores. Quando estes sítios alostéricos são ativados nos receptores, ocorre potencialização dos efeitos dos neurotransmissores. Em outras palavras, os moduladores alostéricos modulam a função do receptor apenas quando este é estimulado por um neurotransmissor naturalmente presente no encéfalo (Moghaddam and Javitt, 2012). Acredita-se, portanto, que os sítios de modulação alostérica dos receptores glutamatérgicos possam ser alvos ideais para o tratamento da esquizofrenia. Nesse sentido, dois tipos de modulação alostérica têm sido considerados em estudos de psicose experimental: (1) aqueles inerentes aos receptores NMDA e (2) aqueles inerentes aos receptores capazes de modular a neurotransmissão mediada por NMDA, como receptores do tipo AMPA, GABA-B e muscarínicos dos subtipos M1 e M4 (Bridges *et al.*, 2010).

Retomando os dados de Kiss et al (2011a) nesse contexto, é importante ressaltar que o aumento de oscilações lentas (delta baixa) e prejuízo da plasticidade de curta duração na via vCA1-mPFC, gerados por injeção sistêmica de MK-801, foram rapidamente revertidos após administração de modulador alostérico positivo de receptores AMPA (LY451395). Os autores argumentam que a atividade regular em delta-alta apresentada por ratos anestesiados com uretana, requer um tônus excitatório substancial, mediado pela atividade de receptores AMPA. Nessas condições experimentais, a injeção sistêmica de MK-801, gerou um estado de baixa atividade glutamatérgica no córtex, restaurado pelo modulador alostérico positivo de AMPA, LY451395. Contudo, estudos clínicos mostraram que esse tipo de fármaco não parece ser eficaz no tratamento dos sintomas positivos e déficits cognitivos observados na esquizofrenia (Goff *et al.*, 2008).

Outros pesquisadores têm utilizado como alvo os sítios modulatórios intrínsecos aos receptores NMDA. Inicialmente foram utilizados, em estudos clínicos, agonistas do sítio de glicina, como a própria glicina ou a D-serina; porém sem resultados conclusivos na clínica (Moghaddam and Javitt, 2012). A partir da década de 1990, foram propostos estudos com inibidores do transportador de glicina (GLiT). O objetivo, nesse caso, seria aumentar os níveis sinápticos de glicina, por meio do bloqueio de GLiT, que apresenta-se co-localizado com os receptores NMDA no terminal pós-sináptico (Javitt, 2008). Dessa forma, estudos pré-clínicos com roedores mostraram que a inibição de GLiT: reverte (1) a hiperatividade e (2) o excesso de liberação dopaminérgica, ambos induzidos por PCP (Javitt et al., 2004), (3) potencializa a atividade do mPFC *in vivo* (Chen et al., 2003) e (4) reverte os prejuízos de memória de trabalho induzidos por KET (Roberts et al., 2010). Em seguida, uma série de inibidores de alta afinidade para transportador de glicina foram desenvolvidos e também testados, com sucesso, em modelos (1) experimentais de psicose (Moghaddam and Javitt, 2012), (2)

pacientes acometidos por esquizofrenia (Alberati *et al.*, 2012) e, (3) em sujeitos controle submetidos a administração de KET (D'souza *et al.*, 2012).

É importante ressaltar que a clozapina, antipsicótico atípico, parece atuar também na modulação do sistema glutamatérgico (Homayoun and Moghaddam, 2007; Javitt, 2004). Homayoun & Moghaddam (2007) mostraram que a clozapina reduz efetivamente a hiperatividade cortical gerada por administração aguda de antagonistas de receptores NMDA. Além disso, ela também potencializa a transmissão de receptores NMDA, por meio de inibição de transportadores de glicina do tipo-A (Javitt, 2004). A clozapina também bloqueia os efeitos da PCP sobre reconhecimento social (Shimazaki *et al.*, 2010) e reverte o prejuízo em PPI gerado por MK-801 (Lipina *et al.*, 2005). Consistentemente, alguns estudos sugerem que a clozapina funcione, pelo menos em parte, como um agonista do sítio de glicina presente nos receptores NMDA (Moghaddam and Javitt, 2012). Além disso, foi demonstrado que ela é capaz de aumentar a magnitude da LTP induzida na via vCA1-mPFC, supostamente por meio de ativação de receptores dopaminérgicos do tipo D1 (Matsumoto *et al.*, 2008). Dessa forma, considerando as evidências obtidas sobre o papel dos moduladores alostéricos positivos, bem como, dos mecanismos subjacentes à ação da clozapina, é plausível supor que o aumento prévio da eficiência de receptores glutamatérgicos, por meio de estimulação elétrica de alta frequência indutora de LTP, também seria capaz de reverter/atenuar os efeitos induzidos por administração de antagonistas não-competitivos de receptores NMDA.

2. Objetivos

Considerando o exposto acima, o objetivo do presente trabalho foi (1) *caracterizar* os efeitos sobre a transmissão e plasticidade sináptica na via iCA1-mPFC induzidos por

antagonismo de receptores NMDA e por indução de AD-hipocampal e (2) *testar a hipótese* de que a indução prévia de LTP nessa via poderia atenuar ou modular as alterações eletrofisiológicas induzidas por KET-S+ ou AD.

3. Materiais e métodos

3.1. Sujeitos

Foram utilizados 74 ratos Wistar adultos machos com pesos entre 250 e 450 g, provenientes do Biotério Central da Universidade de São Paulo – USP/RP, sendo que 53 desses animais foram aproveitados como sujeitos experimentais.

Os ratos foram mantidos em caixas de polipropileno (40 x 33 x 18 cm; 3 animais por caixa) contendo raspas de madeira (maravalha) sobre o assoalho. Durante todo o período dos experimentos, os animais estiveram alojados em biotério com temperatura controlada ($25 \pm 2^\circ$ C) e submetidos a ciclo de 12 h de claro: 12 h de escuro com luzes acesas às 07h00min. Além disso, os ratos tiveram livre acesso à comida e água. Todos os protocolos experimentais foram aprovados pelo Comitê de Ética em Experimentação Animal da Faculdade de Medicina de Ribeirão Preto (CETEA - FMRP – USP; Processo: 193/2009).

3.2. Cirurgia estereotáxica para implante de eletrodos

Após injeção sistêmica de uretana (1,2 a 1,5 g/Kg i.p. em solução de NaCl 0,15 M a 50%), foi feita verificação do grau de anestesia por meio de pinçamento de cauda. Em seguida, foi realizada tricotomia do escalpo e fixação do animal em estereotáxico (KOPF; KOPF instruments; EUA). Posteriormente, foi feito procedimento de assepsia do escalpo com iodo e água oxigenada. Logo após, foi administrada injeção subcutânea de anestésico (lidocaína a 2% em solução de NaCl 0,15 M) no local da incisão. Os animais, então, foram

submetidos à incisão do escalpo para a exposição e limpeza da superfície do crânio. Tomando-se o bregma como referência ântero-posterior e médio-lateral, foram feitas três craniotomias (todas do lado esquerdo) segundo as coordenadas: [ântero-posterior (AP): - 4,7 mm; médio-lateral (ML): 4 mm; dorso-ventral (DV): - 2,5 a 2,8 mm para implante de eletrodo de registro na região intermediária de CA1 do hipocampo]; [AP: - 5,7 mm; ML + 4,4 mm; DV: - 2,5 a 2,8 mm para implante de eletrodo de estímulo em iCA1 do hipocampo] e [AP: + 3,0 mm; ML + 0,5 mm; DV: - 3,2 mm para o mPFC] (Paxinos and Watson, 2007).

Posteriormente, foi feito um quarto orifício localizado acima do córtex parietal e contralateral aos eletrodos, onde foi fixado no crânio um microparafuso com fio e conector para servir como terra e referência durante os registros. Os eletrodos foram feitos com fios de tungstênio revestidos por teflon (60 μ m de diâmetro; A-M Systems, Inc., EUA). Três eletrodos foram implantados: (1) monopolar de registro na região do mPFC; (2) bipolar (separação das pontas 0,5 mm) de estímulo na região CA1 do hipocampo posterior dorsal e (3) monopolar de registro pelo terceiro orifício localizado um pouco mais anterior que o eletrodo de estímulo. O eletrodo do mPFC foi o primeiro a ser implantado, sendo cimentado, logo após, com acrílico dental auto-polimerizável. Em seguida, o eletrodo de registro em CA1 foi implantado com a ajuda de áudio-monitor e visualização tempo-real dos LFPs. Quando o eletrodo de registro atingia a camada CA1, os LFPs apresentavam típico aparecimento de spikes e presença mais proeminente de oscilações teta (4-12 Hz). O eletrodo de estímulo foi posicionado corretamente na região CA1 por meio de aplicação de pulsos-teste com intensidade de 150 μ A, duração de 200 μ s e frequência de 0,05 Hz (1 pulso a cada 20 s) e registros dos fPSPs típicos (14 a 17 ms de latência para o primeiro pico negativo e amplitude > 0,2 mV) eliciados no mPFC (Romcy-Pereira et al. 2004; Lopes Aguiar et al., 2008). As coordenadas DV foram ajustadas de modo que fosse obtida a máxima amplitude dos fPSPs.

Os ratos foram mantidos sob controle da temperatura corporal ($37^{\circ} \pm 0,5^{\circ}\text{C}$) durante todo o experimento.

3.3. Aparato experimental

Todo aparato experimental foi isolado contra ruídos elétricos por uma gaiola de Faraday metálica (100 x 95 x 50 cm). Foi utilizado um estimulador digital (S88X; Grass Astro-Med[®], Inc; EUA) acoplado a uma unidade isoladora de estímulo corrente constante (PSIU6X; Grass Instruments; EUA) para geração de estímulos elétricos com frequência, duração e intensidade controlados. Foi utilizado também um conversor analógico-digital (Powerlab 16 bits, 4 canais; ADInstruments, Inc.; Austrália) que permitiu a digitalização do sinal biológico (taxa de amostragem = 10 kHz). Dois pré-amplificadores P55 A.C. da Grass Astro-Med[®], Inc; EUA, um para o canal do mPFC e outro para o hipocampo, foram utilizados para que os sinais eletrofisiológicos provindos de CA1 e mPFC fossem filtrados na banda de 1 Hz a 1 kHz e amplificado em 100 vezes. O conversor analógico-digital foi conectado (via USB) a um computador Pentium Core 2 Quad com o software LabChart 7.2 previamente instalado. Além disso, o Powerlab também foi conectado (via cabo de conexão BNC) ao estimulador S88X, afim de que o registro do sinal fosse sincronizado ao estímulo.

3.4. Curvas de entrada e saída e protocolos de estimulação

Para a construção das curvas de entrada e saída (E/S), foram aplicados pulsos quadrados monofásicos de 0,2 ms de duração em CA1 com intensidades crescentes. Em cada uma das nove intensidades escolhidas (60; 80; 100; 120; 150; 200; 300; 400; 500 μA) foram registrados e promediados três fPSPs no mPFC. Para cada animal, foi escolhida a intensidade de estímulo capaz de eliciar 70% da amplitude máxima dos fPSPs. Tal

intensidade foi utilizada para todas as etapas e protocolos de estimulação, com exceção da indução de AD, que sempre foi executada com 300 μ A (intensidade baseada em estudo-piloto realizado para definir a intensidade mínima capaz de eliciar AD com um único trem em todos os animais).

Os protocolos de estimulação utilizados estão ilustrados na **figura 1-c**. O PPF foi estudado por meio da aplicação de pares de pulsos monofásicos (duração de 200 μ s) em CA1 com concomitante registro dos fPSPs evocados no mPFC (fPSP1 e fPSP2). O intervalo inter-estímulos (ITI) em CA1 foi de ITI=80 ms, tipicamente capaz de gerar o maior PPF nessa via, juntamente com o ITI de 40 ms (Kiss et al., 2011a). A *indução de LTP* foi realizada por meio de aplicação de 2 estímulos em alta frequência (HFS), aos 30 e 60 min de registro. Cada HFS consistiu de duas séries de 10 trens (50 pulsos a 250 Hz; 200 ms de duração; a cada 10 s), separados por 10min (Jay and Burette, 1995). Para indução de *AD-hipocampal*, foi aplicado um único trem na região CA1: constituído de 200 pulsos (20 Hz; pulsos monofásicos de 1 ms de duração) com duração de 10 s. Para monitoramento dos efeitos oscilatórios de curto prazo da AD, foram monitorados LFPs no hipocampo e mPFC 1 min antes, durante e 1 min e 50 s após AD (Ma and Leung, 2010).

3.5. Desenho experimental

Os desenhos experimentais dos experimentos 1 e 2 estão resumidos na **figura 1-b**. Os sujeitos foram anestesiados com uretana e submetidos a implante de eletrodos na via CA1-mPFC e curva E/S. Em seguida, estímulos elétricos monofásicos duplos espaçados por 80 ms foram aplicados em CA1 para eliciar respostas basais (fPSP1) e respostas facilitadas por plasticidade pré-sináptica (fPSP2) no mPFC. O PPF foi calculado, posteriormente, pela razão entre as amplitudes de fPSP2 e fPSP1. No **experimento 1**, foram registrados respostas

no mPFC durante 90min para constituir uma linha de base antes da aplicação de (1) KET-S+ (12,5 mg/Kg i.p.) ou solução salina estéril 0,9% (SAL) e (2) AD-hipocampal ou Sham; constituindo os grupos KET-S+ (n=7), SAL (n=8), AD (n=7) e Sham (n=7), respectivamente. Em seguida os animais foram registrados por mais 120 min para monitoramento dos efeitos de KET-S+ ou AD. No **experimento 2**, foram registrados respostas evocadas no mPFC durante 30min para constituir uma linha de base antes da aplicação de dois HFS ou Sham (aos 30 e 60min de experimento) e administração/aplicação de KET-S+, AD ou SAL aos 90min; constituindo os grupos LTP-KET (n=9), LTP-AD (n=8) e LTP-SAL (n=6), respectivamente. Em seguida os animais foram registrados por mais 120 min para monitoramento dos efeitos de KET-S+. Em todos os grupos, foram registrados LFPs no hipocampo e mPFC ao longo de todo o experimento, simultaneamente aos registros de fPSPs. Ao final dos experimentos, os animais foram perfundidos para posterior avaliação de expressão do fator neurotrófico derivado do encéfalo (BDNF) no hipocampo e mPFC.

A KET-S+ foi escolhida por possuir quatro a cinco vezes maior afinidade pelos receptores NMDA (Oye *et al.*, 1992) e reproduzir melhor, em humanos, os positivos da esquizofrenia (Vollenweider *et al.*, 1997), comparada com a KET-R. Apesar do exposto acima, KET-R ainda é mais comumente utilizada em estudos de psicose experimental (Corlett *et al.*, 2007). Nesse sentido, tive a oportunidade de colaborar com o aluno de mestrado Matheus Teixeira Rossignoli (FAPESP #2011/04467-5) para investigar se esses dois sub-tipos de cetamina (KET-R e KET-S+) também influenciam de maneira distinta os padrões oscilatórios, eficiência basal e plasticidade sináptica de curta duração da via iCA1-mPFC. Os dados preliminares desse estudo foram apresentados no II Simpósio Internacional sobre Córtex pré-frontal que ocorreu em 2011 em Vitória, ES (**Anexo 2**).

3.6. Imunohistoquímica: método

Duas horas após injeção de KET-S+, AD-hipocampal ou seus respectivos controles, os animais receberam uma injeção adicional de uretana (1,5 g/Kg i.p.) e foram perfundidos com infusão transcardíaca de 200 mL de tampão fosfato salina (PBS) a 25°C, seguida por 400 mL de solução fixadora de paraformaldeído (PFA) 4% (p/v) em tampão fosfato (PB) a 4°C. Em seguida, os encéfalos foram removidos do crânio e imersos em PFA por 4 horas e depois em etanol 70% (v/v), por 1 dia. O encéfalo foi então desidratado, diafanizado e incluído em parafina. Os blocos de parafina foram cortados em seções com espessura de 8 µm nas coordenadas referentes ao mPFC, hipocampo anterior e hipocampo posterior dorsal. Os cortes foram colocados em lâminas previamente gelatinizadas para melhor aderência. Foram feitas imunohistoquímicas para detecção de BDNF, para acessar possíveis efeitos na plasticidade neuronal induzidos por KET ou AD. Segundo o protocolo de imunohistoquímica adaptado do nosso laboratório (Kandratavicius, Hallak, *et al.*, 2012), as seções foram submetidas ao bloqueio da peroxidase endógena com 4,5% (v/v) de H₂O₂ em PBS 50mM pH 7,4 e à recuperação antigênica por 10 minutos em microondas (Brastemp DES modelo BMU27ABHNA, em potência nominal máxima) com tampão citrato de sódio 10 mM pH 6. Foi utilizado para BDNF (diluição 1:30; Chemicon-Millipore, Billerica, MA, USA) diluído em tampão de bloqueio na concentração de 1:100. O anticorpo secundário biotilado utilizado para ambos primários foi o anticorpo produzido em porcos anti-IgG de coelho (#E0354, Dako®) na diluição de 1:200. A intensificação de sinal do complexo antígeno-anticorpo foi promovida pelo uso de um complexo avidina-biotina-peroxidase (Vectastain Elite ABC kit, #PK6100, Vector®) e a revelação com uso do cromógeno 3,3'-tetrahidrocloreto de diaminobenzidina (DAB, #34001, Pierce Biotechnology®). O tempo de revelação em solução de DAB foi de 10 min.

3.7. Imunohistoquímica: avaliação

Imagens das regiões de interesse foram coletadas por uma câmara de alta resolução AxioCamMR5 instalada a um microscópio Zeiss Axio Imager, foram convertidas em sinais digitais e alimentadas a um computador Windows usando o programa de análise de imagem AxioVision. A iluminação foi mantida uniforme e estável durante a coleta. As imagens foram transferidas para computador MacBook Pro e, com o programa ImageJ 1.45s [National Institutes of Health], foram convertidas para imagens de 8 bits e processadas pela ferramenta de limiar triangle. Com esta ferramenta, o software marca em vermelho pixels que possuam cor cinza igual ou superior ao limiar de marcação considerado positivo para a presença da proteína de interesse, calculando então a porcentagem de área imunopositiva em cada área amostral (**figura suplementar 1**). Mais detalhes sobre este procedimento podem ser vistos em rsbweb.nih.gov/ij/docs/examples/stained-sections/index.html.



Figura S1. Imagens representativas da quantificação das áreas imunopositivas. Após capturadas em RGB pela AxioCamMR5 [A], as imagens das regiões a serem avaliadas são convertidas em imagens de 8 bits em escala de cinza [B]. Após a conversão, pixels com valor de cinza considerados positivos para presença do antígeno de interesse são marcados em vermelho pela ferramenta Limiar [C], e calcula-se a área positiva em relação à área amostral total.

As regiões analisadas foram delimitadas seguindo-se as subdivisões apresentadas no atlas de coordenadas estereotáxicas (Paxinos e Watson, 2007): camada granular da fascia dentata, estrato piramidal de CA1 e córtex pré-frontal medial. Todas as avaliações histológicas foram realizadas por observador cego aos grupos analisados.

3.8. Análises de padrões oscilatórios

Ao longo de todo experimento registramos em CA1 e no mPFC, com o objetivo de monitorar a atividade oscilatória dessas regiões ao longo das várias manipulações experimentais. A coleta dos dados foi realizada em janelas de 19,5s para se adequar a frequência de coleta dos fPSPs (0,05 Hz) e ainda ter uma margem de 0,5s sem nenhum registro eletrofisiológico, permitindo que, se necessário, o experimento fosse interrompido sem que os dados da janela anterior fossem perdidos. Essas épocas de registros eletrofisiológicos continham nos primeiros 120 ms uma dupla de fPSPs evocados por estimulação pareada em CA1, espaçada por 80ms e, no tempo subsequente, LFPs espontâneos em CA1 e mPFC.

Todas as análises de padrões oscilatórios foram realizadas em Matlab (versão 2009b para Mac OS; The MathWorks, Natick, MA) por meio de códigos feitos sob demanda em nosso laboratório e de pacotes de análise de livre acesso. Os dados foram concatenados em uma matriz única e os 300 ms iniciais de cada época de 19,5 s contendo os fPSPs foram extraídos e concatenados em outra matriz para avaliação das amplitudes dos fPSPs e PPF. Em seguida, os dados de LFPs foram filtrados na banda de 0,5 a 500 Hz com a função *eegfilt* do pacote EEGLAB (<http://sccn.ucsd.edu/eeglab/>). Em seguida, os dados foram reamostrados de 10 para 1KHz (função *decimate* do Matlab) e as densidades espectrais de potência (PSDs) foram estimadas usando o método de p-Welch (Welch, 1967): promediação de 8 janelas por época com sobreposição de 50%. Foram calculadas as PSDs em cinco bandas de frequências diferentes em diferentes janelas temporais, a saber: delta (1 – 4 Hz); teta (4 – 12 Hz); beta (12 – 30 Hz); gama-baixa (30 – 55 Hz); gama-alta (65 – 100 Hz). Para comparar as mudanças das potenciais espectrais nas diferentes bandas de frequência ao longo do tempo foram realizados testes estatísticos intra-grupo com ANOVA de uma via de medidas

repetidas, seguida de teste *post-hoc* de Tukey, com nível de significância de $p < 0,05$. Para análises de correlações foi utilizada teste estatístico de Pearson.

As análises de comodulação entre amplitude dos envelopes de gama e fase de delta foram calculadas segundo (Tort *et al.*, 2010). Resumidamente, o índice de modulação ou MI (do inglês *modulation index*) é uma medida que expressa quão divergente de uma distribuição uniforme ideal é a distribuição real obtida pela distribuição da amplitude dos envelopes de uma frequência a ser modulada (neste caso, gama-alta) ao longo da fase de uma frequência moduladora (neste caso, delta) (**ver figura 10**).

3.9. Análise estatística dos potenciais evocados

Para os potenciais evocados no mPFC foi considerada a sua amplitude, ou seja, distância entre o ponto máximo do primeiro pico positivo e o ponto mínimo do primeiro pico negativo com latência de 14 a 17 ms. Em seguida, esses valores foram normalizados com relação à linha de base (primeiros 30 min de registro), definida como 100%. Foram utilizados os testes estatísticos de ANOVA de duas vias (ou uma via) de medidas repetidas e ANOVA simples de uma via, ambos seguidos do teste *post hoc* complementar de Tukey. O nível de significância foi de $p < 0,05$.

4. Resultados

Como descrito anteriormente, eletrodos monopolares de tungstênio foram implantados no hipocampo dorsal e na região pré-límbica (PL) do mPFC em animais anestesiados com uretana. Além disso, um eletrodo bipolar foi posicionado na região posterior dorsal de CA1 para eliciar fPSPs no mPFC (**figura 1-a**). O eletrodo de registro em CA1 foi implantado com a ajuda de áudio-monitor e visualização tempo-real dos LFPs.

Quando o eletrodo de registro atingia a camada CA1, os LFPs apresentavam típico aumento de espículas. Já o eletrodo de estímulo foi posicionado corretamente na região CA1 por meio de avaliação dos fPSPs obtidos no mPFC (Lopes-Aguiar et al., 2008; Lopes-Aguiar et al., 2013). As coordenadas DV foram ajustadas de modo que fosse obtida a máxima amplitude dos fPSPs. A figura 2 descreve as propriedades dos potenciais evocados na via CA1-mPFC em todos os animais incluídos nas análises do presente trabalho. Todos os animais estudados apresentaram fPSPs típicos da via CA1-mPFC, com curvas E/S semelhantes entre os grupos experimentais e controles (**figura 2-a**), amplitudes sempre superiores a 150 μ V (**figura 2-b**) e latência para o primeiro pico negativo entre 14 e 17 ms (**figura 2-c**), como descrito anteriormente (Laroche et al., 1990; Romcy-Pereira et al. 2004; Lopes-Aguiar et al., 2008). Além disso, o PPF (fPSP2/fPSP1) eliciado no mPFC após dupla de estímulos (ITI = 80 ms) em CA1, variou entre 2 e 3 (**figura 2-b**), também de maneira consistente com a literatura (Kiss et al., 2011a). Secções do mPFC e hipocampo marcadas por cresil-violeta foram avaliadas em microscópio e as sub-regiões de interesse foram fotografadas. Não foi executada lesão eletrolítica no final do experimento com o objetivo de poupar o tecido para análises subsequentes de imunohistoquímica, o que dificultou a visualização da posição final da ponta dos eletrodos. De qualquer forma, foi possível estimar o posicionamento dos eletrodos com base na lesão mecânica produzida pela sua inserção no tecido. A **figura 1-a** ilustra quais foram os subcampos no mPFC e hipocampo mais atingidos pelos eletrodos. Nenhum animal foi excluído nessa etapa da análise por apresentarem fPSPs homogêneos e dentro do esperado para a via iCA1-mPFC (ver introdução, **sessão 1.3.2** e também **figura 2**)

4.1. Indução de AD promove aumento de gama por curto-prazo no mPFC, mas não afeta padrões oscilatórios em longo-prazo

Modelos de evocação de AD única no hipocampo são considerados úteis para o estudo de psicose pós-ictal, pois induzem hiperlocomoção, movimentos estereotipados e prejuízo de filtro sensorio-motor, de maneira semelhante aos modelos farmacológicos de psicose (Ma e Leung, 2000). Essa atividade locomotora excessiva no período pós-ictal ocorre nos primeiros segundos após normalização dos LFPs e apresenta-se associada a aumento de oscilações gama (30 – 100 Hz) no mPFC e hipocampo (Ma and Leung, 2010; McCracken and Roberts, 2006).

A **figura 3** sintetiza os efeitos de curto prazo de AD sobre os padrões oscilatórios do mPFC de ratos anestesiados com uretana. Como mencionado nos métodos, no momento da indução de AD, a aplicação de pulsos-teste em CA1 foi cessada e um novo arquivo foi criado para registros contínuos de LFPs no hipocampo e mPFC por 180s, divididos em três janelas de 60s (janela 1: antes de AD; janela 2: estimulação + AD + LFPs com oscilações gama pós-AD; janela 3: LFPs não epileptiformes pós-AD). Como descrito anteriormente, o protocolo de estimulação elétrica utilizado (ver **métodos e figura 1-c**) foi capaz de gerar uma AD única em ambos, hipocampo e mPFC, seguida de aumento de oscilações gama-baixa (30 a 55 Hz) e gama-alta especificamente no mPFC [Comparações intra-grupo ao longo do tempo: Gama-baixa: $F(14,84)=4,07$, $p<0,0001$; Gama-alta: $F(14,84)=2,58$, $p<0,01$; ANOVA de uma via de medidas repetidas, **figura 3-d**]. Tal aumento no grupo AD foi rápido e robusto [gama-baixa: +200%, linha de base (-60s a -10s) vs. 40s: $p < 0,0001$; gama-alta: +110%, linha de base (-10s) vs. 40s: $p < 0,05$], voltando à linha de base após 30s a 40s (gama-baixa: 40s vs. 70 a 120s, $p < 0,0001$; gama-alta: 40s vs. 80 a 120s, $p < 0,05$). Não foram observadas diferenças de potência em delta, gama-baixa e gama-alta ao longo do tempo no grupo Sham. No grupo AD, a ANOVA de uma via de medidas repetidas indica que os valores de potência mudam ao longo do tempo [$F(6,84)=2,57$, $p < 0,01$], porém o teste post hoc de Tukey não apontou

especificamente onde tais diferenças se manifestam ($p > 0,05$ em todas as comparações intra-grupo). A figura **3-c** mostra também que, 80s após AD, ocorre forte redução da potência em todas as faixas de frequência a partir de 6Hz do hipocampo. A **3-e** mostra um espectograma de um animal representativo do grupo AD para ilustrar o mesmo fenômeno de aumento de gama no mPFC após AD, porém com destaque para sua magnitude e delimitação temporal.

4.2. KET S+ altera a dinâmica dos estados oscilatórios no hipocampo e córtex sob uretana

A **figura 4** traz um exemplo de traçados comprimidos de LFPs no mPFC e hipocampo obtidos de um mesmo animal durante o experimento 1 (duração: 210 min). Na **figura 4-b**, são mostrados espectogramas de potência em cinco bandas diferentes de frequência (delta, teta, beta, gama-baixa, gama alta) referentes aos seus respectivos traçados acima. Como descrito anteriormente (Clement *et al.*, 2008), os padrões oscilatórios do hipocampo e mPFC sob uretana apresentam diversos períodos de transição espontânea entre estados de sincronização (aumento de delta e queda ou ausência de alteração das potências em gama) e dessincronização (caracterizado por diminuição de oscilações lentas e aumento em gama). Porém, após tratamento com KET S+ (12,5 mg/Kg i.p.), ocorre aumento simultâneo das potências em delta e gama-alta no mPFC. No hipocampo, KET S+ exerce aumento significativo apenas em delta. Os gráficos e as estatísticas dos efeitos de induzidos por KET S+ estão sintetizados na **figura 5**.

Ao contrário de AD, o tratamento com KET S+ produz efeitos mais duradouros e de latência maior sobre os padrões oscilatórios do hipocampo e mPFC. Os gráficos apresentados na **figura 5-a** mostram as alterações de *curto prazo* produzidas por KET S+ no mPFC. Foram calculadas as médias da potência absoluta em três bandas de frequência

distintas (delta, gama-baixa e gama-alta) em janelas de 20 s, antes e depois de injeção de KET S+ ou SAL. A ANOVA de uma via de medidas repetidas mostrou que KET S+ promove aumento significativo das potências em delta [$F(6,210)=3,18$, $P < 0,0001$], gama-baixa [$F(6,210)=1,97$, $P < 0,01$] e gama-alta [$F(6,210)=4,66$, $P < 0,0001$]. Além disso, o teste *post hoc* de Tukey revelou que o aumento de gama-alta começa a ser significativo 420 s após injeção de KET S+ (420s vs. -120s; $p < 0,05$). Não foi possível definir em qual momento específico as potências em delta e gama-baixa aumentam ($p > 0,05$, teste de Tukey).

Os gráficos apresentados na **figura 5-b** mostram as alterações de *longo prazo* produzidas por KET S+ no mPFC e hipocampo. Foram calculadas as médias da potência absoluta em cinco bandas de frequência distintas (delta, teta, beta, gama-baixa e gama-alta) em janelas de 30 min, antes (-90, -60 e -30 min) e depois (30, 60, 90 e 120 min) de injeção de KET S+ ou SAL. A ANOVA de uma via de medidas repetidas mostrou que KET S+ promove aumento transiente de potência em delta aos 30 min [+50%, $F(6,36)=5,74$, $p < 0,001$; teste *post hoc* de Tukey: -30 vs. 30min, $p < 0,05$] associado a aumento sustentado de gama-alta de 30 a 120 min no mPFC [+60%, $F(6,36)=9,23$ $p < 0,0001$; teste *post hoc* de Tukey: -30 vs. 30, 60, 90 e 120 min, $p < 0,05$]. Nenhuma alteração foi observada no grupo SAL. KET S+ também promove aumento transiente de delta no hipocampo [+50%, $F(6,36)=3,82$, $p < 0,0001$; teste *post hoc* de Tukey: -30 vs. 30min, $p < 0,001$]. Os gráficos de densidade espectral de potência apresentados em **5-c** destacam de maneira mais clara o aumento simultâneo de delta e gama no mPFC, comparado com o aumento apenas de delta no hipocampo. A **figura 5d** traz exemplos de épocas de sincronização e dessincronização dos LFPs no mPFC antes e após KET-S+. Nos períodos sincronizados pós-KET-S+ é possível observar um maior acoplamento da amplitude dos envelopes de gama com a fase de delta (ver também **figuras 10 e 11**).

4.3. KET S+ e AD impactam a eficiência basal e a plasticidade pré-sináptica da via iCA1-mPFC *in vivo*

Todas as caracterizações eletrofisiológicas até aqui, foram realizadas nos grupos KET, SAL, Sham e AD. Este conjunto de dados, constitui o *experimento 1*. O objetivo desta etapa foi caracterizar e comparar os efeitos da injeção sistêmica de KET S+ e da indução de AD única no hipocampo sobre os padrões oscilatórios e comunicação da via iCA1-mPFC em animais anestesiados com uretana, já que estudos anteriores mostraram que ambos são capazes de gerar alterações comportamentais relevantes para o estudo das psicoses, como hiperlocomoção, estereotipias e prejuízo no filtro sensório-motor. A **figura 6** sintetiza os efeitos de KET S+ e AD sobre a transmissão e plasticidade sináptica de curta duração na via iCA1-mPFC *in vivo*. Nossos resultados indicam que a injeção sistêmica de KET S+ aumentou significativamente a amplitude do fPSP1 em dois momentos específicos, de 30 a 40 min e de 80 a 120 min pós-KET S+ [Interação tratamento x tempo: +10%, KET vs. SAL: $F(20, 260) = 1,88$, $p < 0,05$; ANOVA de duas vias de medidas repetidas e teste *post hoc* de Tukey, $p < 0,05$; **figura 6-a**] sem afetar de maneira significativa o fPSP2 da via iCA1-mPFC *in vivo* ($p > 0,05$). Em contrapartida, a indução de AD gera uma queda robusta de ambos, fPSP1 [Tratamento: -50%; Sham-AD vs. Sham-Sham: $F(1, 12) = 61,95$, $p < 0,001$, ANOVA de duas vias de medidas repetidas, **figura 6-b**] e fPSP2 [Tratamento: -60%; $F(1, 12) = 95,88$, $p < 0,001$] na mesma via. Além de robusto, esse efeito mostrou ser sustentado, mantendo a queda inicial dos fPSPs de 50 a 60% por, no mínimo, 2 horas em relação ao grupo controle (teste *post hoc* de Tukey para fPSP1 e fPSP2; $p < 0,05$). Embora KET-S+ e AD tenham efeitos bastante distintos sobre a eficiência basal da via iCA1-mPFC, ambos geram prejuízo sobre sua plasticidade pré-sináptica, medida por PPF [Tratamento: -15%; Sham-KET vs. Sham-SAL: $F(1, 13) = 39,34$, $p <$

0,001 e -13%; Sham-AD vs. Sham-Sham: PPF, $F(1, 12) = 6,31$, $p < 0.05$, ANOVA de duas vias de medidas repetidas; **figuras 6-a e 6-b**].

A figura 7 reporta as análises de correlação entre padrões oscilatórios e potenciais evocados na via iCA1-mPFC. Observamos que a eficiência basal da via iCA1-mPFC não correlaciona significativamente com a potência em delta no córtex (**figuras 7a e 7b**). Além disso, nossos resultados indicam que a magnitude das repostas basais evocadas no mPFC não correlaciona significativamente com a potência de gama-alta no grupo SAL (**figura 7-c**). Porém, no grupo KET observou-se correlação significativa ($r=0,62$; $p<0,0001$; **figura 7-d**). Quanto maior a potência em gama-alta cortical, maior a amplitude do fPSP1 na via iCA1-mPFC. Também verificamos que a magnitude do PPF na via iCA1-mPFC não correlaciona significativamente com a potência em delta no córtex (**figuras 7-e e 7-f**). O PPF também não correlaciona com a potência em gama-alta do mPFC no grupo SAL (**figura 7-g**). Porém, no grupo KET, observamos uma correlação significativa entre tais parâmetros ($r=-0,53$; $p<0,0001$; **figura 7-h**). Quanto maior a potência em gama-alta no córtex, menor o PPF na via iCA1-mPFC.

4.4. Indução prévia de LTP atenua os efeitos induzidos por KET S+ e AD na via CA1-mPFC

O *experimento 2* teve como objetivo testar se a indução prévia de LTP poderia atenuar os efeitos induzidos por KET S+ e AD na via iCA1-mPFC, já que estudos recentes têm demonstrado que o aumento da função dos receptores NMDA e AMPA por moduladores alostéricos positivos são capazes de reverter as alterações comportamentais e prejuízos cognitivos associados a modelo de psicose experimental. Nos gráficos apresentados na **figura 8** é possível observar que os três grupos (LTP-SAL, LTP-KET e LTP-AD) apresentam a mesma magnitude de LTP, tanto após o primeiro quanto o segundo HFS [Tratamento: $F(2,$

20) = 1,84; $p > 0,05$ – ANOVA de duas vias de medidas repetidas seguida de teste *post hoc* de Tukey: 10 a 90min; $p > 0,05$]. No grupo LTP-AD (**figura 8-c**), a aplicação de AD, assim como no experimento anterior (grupo Sham-AD; **figura 6-b**), gera decaimento da eficiência basal na via iCA1-mPFC, evidenciado por comparação intra-grupo [-75%; Tempo: $F(20, 400) = 3,69$; $p < 0,001$ – ANOVA seguida de teste *post hoc* de Tukey para grupo LTP-AD; 90min vs 100 – 140min; $p < 0,05$]. Entretanto, essa queda não mostrou ser tão robusta nem sustentada como no experimento anterior [fPSP1: LTP-AD vs. LTP-SAL; $p > 0,05$, **figura 8-c**]. Quando precedida por LTP, a administração de KET-S+ também não gerou o mesmo aumento significativo na amplitude dos fPSPs em relação ao seu respectivo controle (Interação tratamento x tempo: $F(40, 400) = 2,28$; $p < 0,05$ – ANOVA seguida de teste *post hoc* de Tukey, LTP-KET vs LTP-SAL; $p > 0,05$ de 90 a 210min).

Na figura 8 (abaixo), são mostradas evidências de que a indução de LTP, por si só, gera diminuição do PPF por 60 minutos [-25 a -15%; Tratamento: $F(1, 20) = 7,37$; $p < 0,05$; ANOVA de duas vias de medidas repetidas; teste *post hoc* de Tukey: -60 a 30min, $p < 0,05$; LTP-SAL vs. SAL]. Ao contrário do experimento anterior, nenhuma diferença foi observada entre os grupos tratados com LTP+KET, AD ou SAL [Tratamento: $F(2, 20) = 0,089$, $p = 0,9$; ANOVA de duas vias de medidas repetidas; **figuras 8b e 8c**]. Com o objetivo de tornar nossos achados mais claros, os valores médios de PPF em cada um dos blocos de 10 min dos grupos KET, LTP-KET, AD e LTP-AD foram subtraídos de seus respectivos controles (SAL, LTP-SAL, Sham, LTP-SAL) e plotados juntamente com os novos valores de erro padrão da média, após cálculo de sua propagação (**figura 8-d**). É possível notar que os grupos KET e AD possuem variação maior do que seus respectivos pares experimentais que receberam LTP prévia (LTP-KET e LTP-AD). Em outras palavras, KET-S+ e AD geram variação negativa dos PPFs na via CA1-mPFC apenas quando não são precedidos por LTP.

4.5. Modulação da LTP sobre as alterações induzidas por KET S+ nos padrões oscilatórios do mPFC

A **figura 9-a** sintetiza os achados referentes as análises densidade espectral de potência nos grupos: SAL, KET, AD, LTP-SAL, LTP-KET e LTP-AD. Na **figura 9-b** é possível observar que a indução prévia de LTP bloqueia o aumento na potência em delta do mPFC eliciada pela KET S+ [-50%, LTP-KET vs. KET; Interação tratamento x tempo: $F(6,84)=2,28$, $p < 0,05$; ANOVA de duas vias de medidas repetidas]. Além disso, o grupo LTP+KET apresenta menor magnitude em beta no mPFC após tratamento, comparado com o grupo KET [-40%, Tratamento: $F(6,84)=2,38$, $p < 0,05$; ANOVA de duas vias de medidas repetidas]. Curiosamente, a LTP não atenua o aumento de gama-alta no mPFC (LTP-KET vs. KET, $p > 0,05$. ANOVA), nem modula o aumento de delta no hipocampo ($p > 0,05$. ANOVA), induzidos por KET S+.

4.6. KET S+ aumenta a comodulação entre amplitude de gama-alta e fase de delta induzido no hipocampo e mPFC

A **figura 10** ilustra alguns dos principais achados em relação ao aumento de comodulação entre amplitude de gama-alta e fase de delta induzida por KET-S+ no experimento 1. Na **figura 10-a**, são apresentados exemplos de traçados de LFPs corticais, antes e depois de KET-S+, filtrados em delta (0,5 – 4 Hz; traçado azul) e em gama-alta (65 – 100 Hz; traçado preto). O traçado amarelo define os envelopes de gama-alta no LFP filtrado (65 – 100 Hz). A **figura 10-b** mostra a média da distribuição da amplitude de gama-alta pela fase de delta em janelas de 20° em um animal representativo, antes e depois de KET-S+. O MI é uma medida que expressa a divergência entre a distribuição da amplitude avaliada e

uma distribuição uniforme ideal (Tort et al., 2010). Portanto, ao compararmos o gráfico da esquerda (antes de KET-S+) com o da direita (pós-KET-S+), é possível observar que KET-S+ gera aumento de MI. O traçado amarelo representa o sinal filtrado em delta e as barras azuis são referentes à distribuição da amplitude de gama-alta ao longo da fase de delta. As linhas vermelhas, próximas aos picos dos traçados amarelos (delta), representam a faixa média de acoplamento entre amplitude de gama e fase de delta. Na **figura 10-c**, são apresentadas as médias dos MIs nos grupos KET e SAL calculados em janelas de 10 min para o mPFC (esquerda) e hipocampo (direita), ao longo de todo o experimento (210 min). É possível observar que KET aumenta em até três vezes o MI no mPFC e hipocampo por cerca de 60 minutos pós-injeção (as estatísticas estão demonstradas na **figura 11**).

4.7. Indução prévia de LTP atenua o aumento do MI induzido por KET S+ especificamente no mPFC

A **figura 11** sintetiza os principais resultados dos experimentos 1 e 2 quanto as avaliações de MI (amplitude gama-alta/fase de delta) no hipocampo e mPFC ao longo de todo o experimento. Foram realizadas comparações intra-grupo das médias dos MIs no mPFC e hipocampo, em diversas janelas de 30 min, antes e depois de KET S+ ou SAL. A ANOVA de uma via de medidas repetidas mostrou que KET S+ aumenta significativamente o MI no mPFC por 60 min pós-injeção [+200%; Tratamento: $F(6,36) = 9,02$; $p < 0,0001$, teste *post hoc* de Tukey, 30min e 60min vs. -30min (linha de base); $p < 0,05$; **figura 11-a**]. Nenhuma alteração significativa de MI foi observada no grupo SAL.

Em relação ao hipocampo, KET S+ também aumenta significativamente o MI por 60 min pós-injeção [+200%; ANOVA de uma via de medidas repetidas: Tratamento: $F(6,36) = 6,37$; $p < 0,0001$, teste *post hoc* de Tukey, 30min e 60min (pós-KET) vs. -30min (linha de

base); $p < 0,05$; **figura 11-b**]. Nenhuma alteração significativa de MI foi observada no grupo SAL. As **figuras 11-c,d,g,h** sintetizam os resultados obtidos nos grupos AD, Sham e LTP-AD. Nenhuma alteração significativa de MI foi observada nas comparações intra-grupos das médias no mPFC e hipocampo ($p > 0,05$; ANOVA de uma via de medidas repetidas). A **figura 11-e** resume os dados de MI no mPFC ao longo de todo experimento nos grupos LTP-KET e LTP-SAL. A ANOVA de uma via de medidas repetidas mostrou que a injeção KET S+, quando precedida por LTP, não produz aumento significativo do MI no mPFC ($p > 0,05$). Além disso, nenhuma alteração significativa de MI foi observada no grupo LTP-SAL, indicando que a LTP, por si só, não afeta o MI no mPFC ($p > 0,05$). Por outro lado, KET S+, precedido por LTP, é capaz de aumentar o MI no hipocampo por 30 min pós-injeção [+200%; Tratamento: $F(6,36) = 2,88$; $p < 0,05$, teste *post hoc* de Tukey, 30min (pós-KET) vs. -30min (linha de base); $p < 0,05$; **figura 11-f**]. Nenhuma alteração significativa de MI no hipocampo foi observada no grupo LTP-SAL. Para explorar mais detalhadamente a modulação da LTP sobre o aumento de MI induzido por KET S+, as médias dos MIs dos grupos KET e LTP-KET foram plotadas juntas e comparadas estatisticamente. A ANOVA de duas vias de medidas repetidas mostrou que as médias dos MIs no mPFC são significativamente diferentes entre os grupos KET e LTP-KET aos 30 e 60 min pós-KET S+ [-45%; Interação tratamento x tempo: $F(4,56) = 4,76$; $p < 0,01$, teste *post hoc* de Tukey, KET vs. LTP-KET: 30 e 60min; $p < 0,05$; **figura 11-i**]. Por outro lado, ambos os grupos exibiram aumento semelhante de MI no hipocampo, após injeção de KET ($p > 0,05$).

4.8. MI e potência de delta não exibem relação linear no mPFC e hipocampo

A **figura 12** mostra uma série de gráficos de dispersão da média dos MIs pela média da potência absoluta de delta no mPFC e hipocampo, para os grupos KET e LTP-KET, em

janelas de 20 s ao longo de todo o experimento (630 pontos). Os resultados mostram ausência de correlação linear entre tais variáveis ($p > 0,05$). Para avaliar qualitativamente a dinâmica temporal da relação entre MI e potência de delta, os 630 pontos foram plotados em escala de cores que reflete o momento do experimento. Por exemplo, pontos próximos ao branco são referentes ao início do experimento, pontos de cor laranja e vermelho estão próximos ao momento da injeção de KET-S+ e pontos escuros indicam o final do experimento. Abaixo dos gráficos de dispersão, foram plotados gráficos adicionais contendo apenas 7 pontos dos 630 plotados acima para ilustrar de forma mais clara como o aumento ou diminuição de MI não depende necessariamente de alteração na potência de delta. Por exemplo, na **figura 12-a**, o experimento é iniciado em -90 min com um valor médio de MI em torno de 0,01 e uma potência em delta em torno de 0,4 mV^2/Hz . Aos 15 min pós KET-S+ o MI sobe para mais de 0,04 e a potência em delta para cerca de 1,2 mV^2/Hz . Aos 60 min pós-KET, a potência em delta é ainda superior a 1 mV^2/Hz , porém o MI médio já caiu em cerca de 50%. Já na **figura 12-b**, a mesma dinâmica temporal não-linear também pode ser observada no mPFC dos animais do grupo LTP-KET. Note que aos 15 min pós-KET, a potência em delta é basicamente a mesma do início do experimento, porém o MI é cerca de 3 vezes maior. Nas **figuras 12-c e 12-d** podem ser observados exemplos da relação não-linear entre MI e potência de delta no hipocampo para os grupos KET e LTP-KET.

4.9. Resultados preliminares

4.9.1. Expressão de BDNF no hipocampo e mPFC

Ao final dos experimentos eletrofisiológicos, os animais foram perfundidos e os encéfalos preparados para procedimento padrão de imunohistoquímica (ver métodos). Nossos resultados indicam que: (1) KET S+ aumenta expressão de BDNF na camada granular

do giro denteado em ambos os hemisférios [+95%; ANOVA de duas vias simples; Tratamento: $F(1,17) = 11,95$; $p < 0,01$; **figura 13-a**]; (2) AD produz aumento na expressão de BDNF no mPFC [+100%; ANOVA de duas vias simples; Tratamento: $F(1,17) = 5,58$; $p < 0,05$; hemisfério contralateral à estimulação; **figura 13-b, à esquerda**] e diminuição bilateral em CA1 [-50%; ANOVA de duas vias simples; Tratamento: $F(1,24) = 18,57$; $p < 0,001$; **figura 13-b, centro**]; (3) LTP, por si só, é capaz de aumentar bilateralmente BDNF na camada granular do giro denteado [+140%; ANOVA de duas vias simples; Tratamento: $F(1,18) = 8,11$; $p = 0,01$; **figura 13-c, à direita**]. Nenhuma diferença foi observada entre os grupos que receberam LTP antes de KET S+ ou AD ($p > 0,05$; **figura 13-d**). Estão em andamento análises adicionais de imunohistoquímica para avaliar expressão de genes de expressão imediata (c-fos e zif-268), bem como, do receptor de BDNF, tirosina cinase B (TrKB).

5. Discussão

Transtornos psicóticos afetam até 20% dos pacientes acometidos por ELT e resultam de disfunções, ainda pouco compreendidas, presentes em vários níveis de organização neurobiológica. Em modelos animais, o desequilíbrio entre os sistemas excitatório e inibitório em circuito límbico-corticais gera disfunções secundárias no sistema dopaminérgico, levando a alterações comportamentais que se assemelham aos sintomas sintomas positivos e prejuízos cognitivos observados na esquizofrenia e psicose associada a ELT. A disfunção da plasticidade sináptica na via hipocampo-mPFC é apontado como um dos substratos biológicos envolvidos nesse processo.

Em resumo, nossos achados sugerem que a administração de KET-S+ promove aumento da eficiência basal da via iCA1-mPFC, enquanto a indução de AD gera uma queda, robusta e sustentada, da eficiência na mesma via. Apesar dos efeitos completamente

opostos sobre a eficiência da transmissão sináptica da via iCA1-mPFC, ambos os tratamentos promovem um importante prejuízo na plasticidade pré-sináptica da mesma via, medida por PPF. Do ponto de vista oscilatório, a KET-S+ promove, gradativamente (latência \cong 9 min) aumento transiente (duração \cong 30 min) de oscilações delta e sustentado de gama (\cong 120min) no mPFC. Já no hipocampo, a KET-S+ promove aumento de potência apenas na banda de frequência delta. A AD, por sua vez, afeta as oscilações do mPFC cerca de 35 a 40s depois de sua indução, gerando um pico transiente de gama-baixa e gama-alta. Ao contrário de KET-S+, a AD não exerce efeitos significativos nos padrões oscilatórios do mPFC a longo prazo. Além disso, observamos que o tratamento com KET S+ aumenta o MI calculado a partir da amplitude de gama-alta e fase de delta no hipocampo e mPFC. A indução prévia de LTP atenua as alterações da eficiência basal e de PPF na via CA1-mPFC produzidos por KET-S+ e AD. A LTP prévia também bloqueia o aumento de delta gerado por KET-S+ no mPFC, mas não o aumento de gama-alta. Por fim, observamos que a LTP bloqueia o aumento de MI no mPFC induzido por KET-S+, mas não modula tal efeito no hipocampo.

5.1. Efeitos da KET-S+ sobre a eficiência sináptica basal da via iCA1-mPFC de ratos anestesiados *in vivo*: possível compartilhamento de mecanismos com a LTP induzida por HFS

Uma das explicações para os efeitos produzidos por doses sub-anestésicas de antagonistas não competitivos de receptores NMDA (e.g. PCP, KET e MK-801) baseia-se na hipótese de eles são capazes de afetar preferencialmente a atividade de interneurônios (Jackson et al. 2004). Resumidamente, a administração sistêmica de PCP, KET ou MK-801 parece gerar um estado de desinibição local, que produz, por sua vez, aumento: (1) dos disparos de neurônios excitatórios, (2) das oscilações gama e (3) dos níveis extracelulares de

L-glutamato em redes límbico-corticais (Moghaddam and Javitt, 2012; Homayoun and Moghaddam, 2007). Tal efeito desorganiza o fluxo de informações em redes que envolvem tálamo, hipocampo, mPFC e NAcc, produzindo, secundariamente, aumento dos níveis extracelulares de dopamina no mPFC e NAcc, além de alterações comportamentais que se assemelham aos sintomas positivos da esquizofrenia, além de gerar prejuízos no filtro sensorio motor e na memória espacial de trabalho (Moghaddam and Javitt, 2012). Nossos resultados reforçam a hipótese da desinibição local, mostrando que ocorre aumento sustentado (por no mínimo 120 min) da eficiência basal na via iCA1-mPFC após administração sistêmica KET-S+. Tais achados estão de acordo com dados recentes publicados por (Blot *et al.*, 2013) que avaliaram os efeitos da injeção sistêmica de MK-801 na via vCA1-mPFC de ratos anestesiados com uretana. Os autores observaram que os fPSPs corticais apresentaram aumento de sua amplitude em cerca 10%, perdurando este efeito por, pelo menos, 120 min após tratamento. Tal aumento da eficácia sináptica induzida por MK-801 na via vCA1-mPFC foi bloqueado por infusão prévia intra-PFC de AP5, um antagonista de NMDARs capaz de bloquear LTP na mesma via. Além disso, o tratamento com MK-801 não é capaz de aumentar a eficiência sináptica da via vCA1-mPFC, se precedido por aplicação de HFS. Os autores especulam que possa existir compartilhamento de certos mecanismos celulares entre os efeitos induzidos por MK-801 e a LTP na via vCA1-mPFC. De acordo com essas evidências, nossos resultados mostram que a indução prévia de LTP também atenua o aumento da eficiência basal na via iCA1-mPFC produzidos por KET-S+ (ver também **sessão 5.10**).

5.2. Efeitos da KET-S+ sobre a plasticidade sináptica de curta duração da via iCA1-mPFC

A plasticidade sináptica de curta duração (medidos por PPF e PPD) é capaz de influenciar a transmissão sináptica de via em uma escala temporal muito curta (dezenas de milissegundos), alterando a probabilidade de disparos do neurônio pós-sináptico de acordo com a frequência de disparos do terminal pré-sináptico. Sugere-se que esta modalidade de plasticidade seja importante para o processamento de memórias de curta duração (Citri e Malenka, 2008). Embora esse tipo de plasticidade seja considerado importante para avaliar como as projeções hipocámpais influenciam as redes locais do mPFC, existem poucos trabalhos que investigaram PPF ou PPD em modelos animais de psicose. Kiss et al. (2011a) utilizaram ratos anestesiados com uretana para estudar os efeitos de tratamento agudo de MK-801 sistêmico sobre o PPF na via vCA1-mPFC. Os autores mostraram que MK-801 gerou diminuição de cerca 40 a 50% no PPF, voltando à linha base após cerca de 20 min. De acordo com os dados reportados por Blot et al. (2013), os autores também observaram aumento da eficiência basal da via vCA1-mPFC por, no mínimo, 60 min (Kiss et al., 2011a). O presente trabalho estende a caracterização das alterações de plasticidade cortical de curto prazo em modelos farmacológicos de psicose ao reportar que a KET-S+ gera diminuição sustentada do PPF na via iCA1-mPFC. Experimentos futuros que tenham como objetivo dissociar os mecanismos pré-sinápticos e pós-sinápticos induzidos por KET-S+ terão grande impacto para o avanço nesse campo do estudo experimental da psicose.

5.3. Mecanismos das oscilações gama na esquizofrenia e em modelos animais

Dados recentes indicam que, durante repouso, o córtex pré-frontal dorsolateral (DLPFC) de pacientes com esquizofrenia apresenta-se mais ativo quando comparado ao de sujeitos-controle. Por outro lado, durante o processamento de memória de trabalho, o DLPFC destes pacientes apresenta-se menos ativo (Pomarol-Clotet *et al.*, 2008; Whitfield-

Gabrieli *et al.*, 2009). Além disso, dados *post-mortem* sugerem que ocorra deficiência no sistema GABAérgico de pacientes acometidos por esquizofrenia. Esses estudos reportam redução da concentração cortical de GABA e da atividade da enzima glutamato descarboxilase (GAD-67), responsável pela síntese de GABA (Lisman *et al.*, 2008; Lisman, 2012). Essas alterações funcionais ocorrem principalmente nos interneurônios parvalbumina positivos (PV+; (Lewis e Moghaddam, 2006)). Os interneurônios PV+ do mPFC parecem ser cruciais para a regulação fina do balanço excitatório/inibitório local e, conseqüentemente, para o processamento de funções executivas. As células PV+ regulam os padrões de disparos de neurônios piramidais diretamente no cone axonal. A parvalbumina presente no ambiente intracelular dos interneurônios é particularmente importante nesse processo, pois o nível de atividade da célula modula sua expressão, além de ser capaz de atuar como tamponadora de cálcio (Ca²⁺) intracelular, diminuindo o período latente de deflagração do potencial de ação (Cellerino *et al.*, 1992; Philpot *et al.*, 1997). Isso facilita a ocorrência de disparos rápidos e repetitivos, gerando sincronia local (geralmente oscilações gama) ao interagirem com populações de neurônios piramidais (Somogyi e Klausberger, 2005; Fuchs *et al.*, 2007; Cardin *et al.*, 2009).

Foi reportado que pacientes com esquizofrenia apresentaram maior potência de oscilações gama durante estados basais ou de repouso, comparado com sujeitos controle. Por outro lado, o mesmo estudo reportou que tais pacientes exibiram menor capacidade de evocação de gama durante execução de tarefa de memória de trabalho, o que refletia em pior desempenho na tarefa, comparados com humanos saudáveis (Basar-Eroglu *et al.*, 2007). Portanto, o ritmo gama parece refletir processos distintos e ser gerado por diversos mecanismos. Por exemplo, o aumento de gama basal observado em pacientes com esquizofrenia, poderia ser meramente um reflexo do aumento desordenado da taxa de

disparo de neurônios piramidais, devido à disfunção de redes locais inibitórias (Buzsaki e Wang, 2012; Molina *et al.*, 2014). De fato, a ativação seletiva e sustentada de neurônios piramidais do mPFC com optogenética causa aumento das oscilações gama e prejuízo em interação social, medidos no mesmo conjunto de camundongos (Yizhar *et al.*, 2011). Por outro lado, as oscilações gama evocadas durante o processamento de trabalho poderiam ser explicadas pelo aumento da atividade de neurônios PV+ (Cardin *et al.* 2009). De acordo com os achados clínicos mencionados, (Carlen *et al.*, 2012) mostraram que a deleção global da subunidade NR1 dos NMDAR especificamente nos neurônios PV+ do encéfalo de camundongos é capaz de gerar prejuízos de memória espacial de trabalho, aumentar as oscilações gama basais e gerar um prejuízo na evocação de gama promovida por estimulação optogenética seletiva de interneurônios do córtex somatossensorial. Durante meu estágio de doutorado sanduíche, sob supervisão da Profa. Marie Carlén no Instituto Karolinska (Suécia), tive a oportunidade de colaborar para a ampliação do conhecimento nessa área, ao demonstrar que também é possível causar aumento de oscilações gama no mPFC, estrutura altamente relevante para o estudo da esquizofrenia e processamento de memória de trabalho. Para isso, realizamos estimulação optogenética seletiva das células corticais PV+ de camundongos anestesiados com uretana e registramos a reposta populacional das células do mPFC por meio de implante de sonda de silício de 32 canais ao lado do local do implante da fibra óptica (**ANEXO 3– figura 12**).

5.4. Efeitos de KET-S+ sobre as oscilações gama no hipocampo e mPFC

Como discutido anteriormente, o tratamento agudo com antagonistas de NMDAR em roedores é capaz de refletir uma parte importante dos sintomas observados na clínica, especialmente aqueles relacionados aos padrões oscilatórios aberrantes, prejuízos

cognitivos e de interação social (Moghaddam e Javitt, 2012). Como mencionado, escolhemos a KET-S+ por possuir quatro a cinco vezes maior afinidade pelos receptores NMDA (Oye *et al.*, 1992) e por reproduzir de maneira mais fidedigna os sintomas positivos da esquizofrenia ao ser aplicada em dose única em humanos saudáveis (Vollenweider *et al.*, 1997; Corlett *et al.*, 2007). No presente trabalho observamos que KET-S+ promove aumento sustentado de gama-alta (\cong 120 min) no mPFC. Esses dados estão consistentes com diversos estudos de eletrofisiologia *in vivo*, sugerindo que tratamento agudo sistêmico com doses sub-anestésicas de antagonistas não-competitivos de receptores NMDA são capazes de gerar aumento global da taxa de disparos de neurônios piramidais e diminuição de sua sincronia, refletindo em aumento de oscilações gama-alta e oscilações de alta frequência (HFO; > 100 Hz) (Pinault, 2008; Anver *et al.*, 2011; Wood *et al.*, 2012; Molina *et al.*, 2014). Contudo, não observamos aumento significativo de gama no hipocampo após KET-S+. Este resultado diverge de estudos anteriores realizados em animais acordados submetidos a tratamento com antagonistas de NMDAR (Caixeta *et al.*, 2013). Oscilações gama também podem ser geradas em circuitos locais do hipocampo, por meio da atividade síncrona entre interneurônios PV+ e neurônios piramidais (Csicsvari *et al.*, 2003). Embora exista um número importante de trabalhos eletrofisiológicos reportando os efeitos de antagonistas de NMDAR em regiões corticais e subcorticais de roedores em livre-movimento, ainda são insuficientes as evidências sobre os efeitos específicos de KET-S+ sobre os padrões oscilatórios hipocampais. Rossignoli *et al.* (2014) comparou os efeitos de diferentes antagonistas de NMDAR sobre os padrões oscilatórios e plasticidade sináptica da via iCA1-mPFC e, em seguida, testou se os efeitos produzidos por KET-S+ seriam mediados pelo sistema endocanabinóide em ratos anestesiados com uretana. Dentre outros achados, os autores reportaram resultados bastante similares ao presente trabalho em relação as alterações de

transmissão e plasticidade sináptica da via induzidas por KET-S+. Entretanto, também não foram observadas alterações significativas de oscilações gama nos LFPs registrados no hipocampo intermediário (Rossignoli, 2014). Em nosso conhecimento, ainda não foram publicados estudos sobre a caracterização dos efeitos de KET-S+ sobre os padrões oscilatórios do hipocampo intermediário em ratos anestesiados com uretana. Embora não tenhamos observado aumento de oscilações gama nessa região, a KET-S+ induziu prejuízo no PPF da via iCA1-mPFC, sugerindo que, de alguma forma, a população de neurônios hipocampais que projetam ao mPFC também foram afetados pelo tratamento. Além disso, observamos outras alterações eletrofisiológicas e de expressão de BDNF na camada granular do giro denteado do hipocampo no grupo KET, o que torna menos provável a explicação de que a KET-S+ possa não ter cruzado a barreira hemato-encefálica de maneira eficiente na região temporal.

Em conjunto com dados da literatura, nossos achados indicam que o tratamento sistêmico com KET-S+ (12,5 mg/Kg) gera um estado de hiperexcitabilidade cortical (evidenciado pelo aumento da potência dos LFPs na banda gama-alta), acompanhado de aumento de conectividade e prejuízo de plasticidade pré-sináptica na via iCA1-mPFC de ratos anestesiados com uretana. Portanto, o estudo dos efeitos de KET-S+ sistêmica em ratos anestesiados com uretana parece ser um modelo útil para investigar como alterações de conectividade entre circuitos límbico-corticais podem estar relacionados à manifestação de alterações eletrofisiológicas classicamente associadas aos sintomas positivos e prejuízos de memória de trabalho na esquizofrenia.

5.5. Alterações de ondas lentas na esquizofrenia e em modelos animais: efeitos de KET-S+ sobre oscilações delta no mPFC e hipocampo

Além de alterações em gama, pacientes com esquizofrenia não-medicados também parecem apresentar alterações das oscilações em delta e teta. (Schulman *et al.*, 2011) avaliaram os padrões de atividade encefálica de pacientes com esquizofrenia durante repouso por meio de registros de magneto-encefalograma (MEG). Os autores observaram um aumento de oscilações delta especificamente na região médio-ventral do PFC de pacientes com esquizofrenia, comparado com seus controles. Consistentemente, (Deakin *et al.*, 2008) reportaram dados de fMRI indicando que o tratamento agudo com KET-R em humanos controle reduz o metabolismo na mesma sub-região do PFC.

Experimentalmente, na maioria dos estudos reportados, a injeção sistêmica de antagonistas de NMDAR em roedores em livre-movimento produz aumento de oscilações delta em doses relativamente mais elevadas, mas ainda subanestésicas. Tal efeito é geralmente associado a ataxia, ao invés do aumento na locomoção geralmente descrito em modelos de psicose (Caixeta *et al.*, 2013). Por exemplo, (Zhang *et al.*, 2012) avaliaram os LFPs de CA1 e núcleo *reuniens* do tálamo (estrutura que projeta para CA1) de ratos acordados antes e após injeção sistêmica de KET-R. Os autores observaram que a dose de 50 mg/Kg foi capaz de produzir aumento da taxa de disparos e da potência em delta em ambas as regiões. A dose de 20 mg/Kg, entretanto, não foi capaz de gerar alterações nos padrões de ondas lentas de CA1 e tálamo, porém aumentou a potência em gama no hipocampo. Os autores ainda mostraram que o aumento de oscilações delta em CA1 parece envolver as projeções vindas do tálamo, evidenciado pelo: (1) aumento de coerência da potência em delta entre as duas regiões após KET-R; (2) redução dos efeitos produzidos por KET-R em CA1 quando o núcleo *reuniens* era simultaneamente inibido por injeção de muscimol; (3) aumento de oscilações delta em CA1 após infusão de KET-R diretamente no núcleo *reuniens* (Zhang *et al.*, 2012).

Registros agudos em roedores sob uretana são considerados úteis para modelar a dinâmica de atividade encefálica observada durante o sono e transtornos que envolvam alterações de ondas lentas. Clement et al., (2008) realizaram um estudo sistemático dos efeitos da uretana sobre os LFPs de regiões corticais e do hipocampo. Os autores mostraram que a uretana promove flutuações espontâneas nos padrões oscilatórios ao longo do tempo. Ou seja, animais anestesiados com uretana apresentam espontaneamente ciclos que se alternam entre estados de desativação colinérgica associado a ondas lentas e ativação colinérgica associada a ondas mais rápidas (principalmente teta no hipocampo e gama no córtex). Essas transições observadas nos LFPs hipocâmpais e corticais parecem não ocorrer devido à superficialização do nível de anestesia, pois complementos contínuos de uretana intravenosa não são capazes de suprimir tal fenômeno. No caso de modelos animais sob uretana, mesmo doses mais baixas de antagonistas de NMDAR são capazes de modular essa faixa de frequência de oscilação. Por exemplo, Kiss et al. (2011) realizaram registros simultâneos de PPF e de LFPs no vCA1 e mPFC de ratos anestesiados com uretana, antes e após injeção sistêmica MK-801. Os autores reportaram que MK-801 diminuiu as oscilações na banda de frequência delta-alta e aumentou as oscilações em delta-baixa (Kiss et al., 2011a). Em seguida, o mesmo grupo demonstrou que a microinfusão de MK-801, diretamente no TMD, ou ainda sua desativação por lidocaína, era capaz de gerar basicamente os mesmo efeitos eletrofisiológicos. É interessante notar que a infusão de MK-801 diretamente no mPFC não foi capaz de gerar alterações oscilatórias (Kiss et al., 2011b). Esses dados em conjunto, levaram os autores a propor que o sítio primário de ação do MK-801 não seria o córtex, mas sim múltiplos circuitos neuronais que projetam a ele, incluindo núcleos talâmicos, que seriam capazes de mediar as alterações comportamentais e cognitivas observadas nesse modelo de psicose experimental.

Portanto, nossos achados de que KET-S+ sistêmica gera aumento de oscilações delta em ambos, hipocampo e mPFC, estão consistentes com achados experimentais e clínicos e reforçam a ideia de que é possível modelar certos aspectos das disfunções de ondas lentas na esquizofrenia ao combinar uretana e tratamento agudo com doses subanestésicas de antagonistas de NMDAR. Adicionalmente, devido a grande semelhança entre nossos achados eletrofisiológicos e os obtidos por Kiss et al., (2011), especulamos que o tálamo seja o gerador das ondas delta produzidas por KET-S+ sistêmica. Tal estrutura parece impor os ritmos lentos no hipocampo, pela via núcleo reuniens-vCA1 (ou iCA1) e no mPFC, pela via TMD-mPFC. Contudo, em nosso conhecimento, ainda não foram reportados estudos com registros simultâneos no mPFC e hipocampo, acompanhados de tratamento sistêmico com algum antagonista de NMDAR e desativação seletiva do TMD ou núcleo *reuniens*. Tal procedimento seria importante para testar se as ondas lentas no mPFC poderiam ser geradas pela propagação de informação vindas de vCA1 e ou iCA1, ou se dependem essencialmente da geração talâmica.

5.6. As alterações eletrofisiológicas induzidas por KET-S+ geram as disfunções de eficiência basal e plasticidade pré-sináptica observadas?

No presente trabalho também testamos se existe correlação entre (1) oscilações delta e gama-alta e (2) eficiência e plasticidade pré-sináptica na via iCA1-mPFC. Embora KET-S+ tenha aumentado ambos, potência em delta e eficiência sináptica na via iCA1-mPFC, observamos que a amplitude do fPSP1 não correlaciona significativamente com a potência em delta no mPFC. Além disso, a potência em delta também não se correlaciona com o PPF, descartando a possibilidade da queda dos PPFs gerada por KET-S+ ser, na realidade, gerada secundariamente pelo aumento da probabilidade dos fPSPs evocados caírem no estado de

descida (*down state*) das ondas lentas corticais. Por outro lado, observamos que maiores valores de potência em gama-alta cortical coincide significativamente com maiores amplitudes do fPSP1 e menores PPFs na via iCA1-mPFC do grupo KET. Futuros experimentos que evoquem oscilações gama por diferentes estratégias optogenéticas e monitorem simultaneamente os fPSPs na via hipocampo-mPFC serão importantes para testar se o aumento desse padrão oscilatório causa alterações de amplitude dos fPSPs e PPFs nessa via.

5.8. Interação entre os efeitos oscilatórios induzidos por KET-S+

Os ritmos registrados no encéfalo interagem de diversas formas e, portanto, não podem ser estudados como processos independentes. A avaliação do acoplamento entre diferentes padrões oscilatórios parece ser importante para entender como o encéfalo processa: (1) informações sensoriais e de recompensa, (2) tomada de decisão, (3) memória de trabalho e (4) atenção (Canolty e Knight, 2010). Tipicamente, a fase de uma frequência oscilatória lenta modula a distribuição da amplitude de uma oscilação mais rápida (Jensen e Colgin, 2007). Contudo, embora represente uma potente ferramenta para avaliar estados oscilatórios durante processamento cognitivo, esse tipo de análise eletrofisiológica ainda é pouco explorado em investigações eletrofisiológicas em modelos animais de psicose ou de pacientes com esquizofrenia (Kirihara *et al.*, 2012; Kocsis *et al.*, 2013). Caixeta *et al.*, (2013) mostraram que tratamento agudo com KET-R sistêmica aumenta a comodulação teta-gama e teta-HFO no hipocampo, independente do aumento de potência em teta gerado pela hiperlocomoção associada ao tratamento em animais acordados.

Consistentemente, no presente trabalho, observamos que KET S+ produz aumento robusto do acoplamento fase entre fase de delta e amplitude de gama-alta no hipocampo e mPFC. Tal efeito mostrou-se independente da magnitude das potências em delta e gama-

alta. É importante notar que, sob uretana, as oscilações gama-alta do mPFC de ratos e camundongos encontram-se naturalmente posicionadas nos estados positivos (UP-states) das ondas lentas ((Massi *et al.*, 2012) ver também **ANEXO 3, figuras 3 e 4**). Massi *et al.* (2012) realizaram registros extracelulares de spikes e LFPs no mPFC, e posterior injeção justacelular para identificação das diferentes células registradas, em animais anestesiados com uretana. Os autores mostraram que, durante os estados positivos dominados por gama-alta, ocorria deslocamento dos disparos das células em cesto (basket-cells) PV+ para fases mais tardias das ondas lentas, onde as oscilações gama eram mais proeminentes. O autores especulam, portanto, que as células em cesto PV+ seriam as maiores geradoras das oscilações gama posicionadas no estados positivos das ondas lentas (Massi *et al.*, 2012). É interessante notar que foi possível observar flutuações espontâneas dos valores de MI, mesmo em registros de linha base ou em grupos controle que receberam injeção de SAL ao invés de KET-S+. Contudo, em nenhum dos registros, observamos uma flutuação espontânea de mesma magnitude (aumento de 4 vezes em relação à linha de base) induzida por KET-S+. Isso sugere que os efeitos de KET-S+ não poderiam ser explicados simplesmente por alteração do balanço excitatório/inibitório local do mPFC e hipocampo. É importante salientar que a disfunção dos NMDAR especificamente nas células PV+ parece não ser suficiente para alterar a relação temporal entre spikes e ondas lentas no mPFC de camundongos anestesiados com uretana (**ANEXO 3, figura 4**). Esses dados, em conjunto com a coincidência temporal observada no aumento de MI no hipocampo e mPFC (duração de 60 min; **figuras 10c, 11a e 11b**), sugerem que o tratamento agudo com KET-S+, em ratos anestesiados sob uretana, impõe oscilações delta no hipocampo e mPFC e aumenta o acoplamento entre fase de delta e amplitude de gama. Como mencionado anteriormente, está bem documentado que o aumento de oscilações delta no hipocampo e córtex induzido

por antagonistas de NMDAR envolve um maior controle do tálamo sobre essas estruturas (Kiss et al., 2011; Zhang et al., 2012). Porém, como reportado na **figura 12**, MI e potência em delta no mPFC e hipocampo não se correlacionam linearmente. Por exemplo, nos períodos pré-KET-S+, é possível observar diversos períodos no qual a potência em delta é relativamente alta, mas a comodulação é baixa. Isso sugere que os efeitos de KET-S+ sobre o MI do mPFC e CA1 não poderiam ser explicados apenas por uma imposição global gerada pelo tálamo sobre essas redes locais.

Uma hipótese plausível, é que o aumento de MI do mPFC e hipocampo seja um efeito secundário de um provável aumento dos níveis extracelulares de dopamina, gerado pela inibição de transportadores de dopamina induzido por KET-S+. Consistente com essa hipótese, foi demonstrado que injeção sistêmica de KET-R aumenta transientemente os níveis extracelulares de dopamina (por 60 min) no mPFC de ratos (Lorrain *et al.*, 2003). Importante notar que experimentos *in vitro* mostraram que a KET-S+ é cerca de oito vezes mais potente que a KET-R em sua capacidade de inibir transportadores de dopamina (Nishimura e Sato, 1999). Além disso, KET-S+ é capaz de aumentar os níveis de dopamina no estriado de humanos saudáveis (Vollenweider et al., 2000). Adicionalmente, a infusão local de agonista de receptor dopaminérgico D4 no mPFC de ratos é suficiente para promover aumento significativo de oscilações gama (Furth *et al.*, 2013; Kocsis *et al.*, 2013). Por fim, foi demonstrado que a infusão local de dopamina aumenta a coerência dos disparos de neurônios piramidais do mPFC de ratos anestesiados (Benchenane et al., 2010). Experimentos futuros com registros multiunitários simultaneamente no mPFC e iCA1 com inibição seletiva dos neurônios dopaminérgicos do VTA por optogenética, antes e depois de KET-S+, proporcionariam uma ótima oportunidade de testar nossa hipótese.

5.9. Efeitos da AD sobre os padrões oscilatórios e plasticidade sináptica da via iCA1-mPFC

Os experimentos de AD realizados no presente trabalho foram desenhados com base na hipótese de que a hiperexcitabilidade hipocampal seria um dos substratos biológicos comuns entre esquizofrenia e psicose associada a ELT. Queiroz et al. (2009) mostraram que crises recorrentes espontâneas afetam a plasticidade sináptica de curta duração no hipocampo de ratos submetidos a modelo de epilepsia induzido por cainato sistêmico. Mais especificamente, os autores avaliaram a conectividade e plasticidade sináptica de curta duração no giro denteado do hipocampo, antes, durante e após crises recorrentes espontâneas apresentados por ratos em fase crônica do modelo induzido por cainato sistêmico (2 a 5 meses depois da indução *status epilepticus*). Os seus principais achados foram: (1) aumento do PPD em períodos interictais; (2) queda das respostas evocadas no giro denteado cerca de 6 min antes do início da crise; (3) redução do PPD durante crises com durações longas (maior que 60 s), seguida de recuperação lenta (> 30 min) até atingir os níveis pré-ictais; (4) no momento da crise, foi observada forte queda das respostas evocadas no giro denteado associada a rápida volta da eficiência sináptica ao estado pré-ictal (Queiroz et al., 2009). Contudo, ainda não está claro de que maneira as alterações de excitabilidade e plasticidade sináptica observadas no hipocampo antes, durante e após uma crise, refletem na comunicação hipocampo-mPFC. No presente trabalho avaliamos se a aplicação de uma estimulação elétrica indutora de AD no hipocampo seria capaz de afetar a conectividade e padrões oscilatórios da via iCA1-mPFC. Nossos achados indicam que, mesmo sob uretana, a estimulação elétrica de 20 Hz por 10s em CA1 é capaz de elicir uma AD robusta de cerca de 15 s, que se propaga rapidamente ao mPFC e gera um pico transiente de oscilações gama-baixa e gama-alta cerca de 35 a 40 s após estimulação. Esses dados estão de acordo com o trabalho de Ma e Leung (2010), mostrando que os efeitos comportamentais e

eletrofisiológicos induzidos por abrasamento elétrico no mPFC e NAcc envolvem necessariamente, a comunicação com o hipocampo. Nesse estudo, os autores aplicaram de 9 a 13 trens de estimulação elétrica com duração de 5 s a 60 Hz no mPFC ou NAcc e observaram, após cerca de 60 s, que os animais estimulados apresentavam hiperlocomoção e aumento aberrante de oscilações gama (30 a 80 Hz) no mPFC. Essas alterações foram bloqueadas por inativação prévia do hipocampo. É possível, portanto, que as oscilações gama presentes no período ictal sejam geradas rapidamente por alças de comunicação entre córtex entorrinal, giro dentado, CA3, CA1 e mPFC (Csicsvari et al., 2003; Ma e Leung, 2010), refletindo em alterações de comunicação e plasticidade da via iCA1-mPFC.

Ao contrário de KET-S+, a AD não exerceu efeitos significativos nos padrões oscilatórios do mPFC e hipocampo em longo prazo. Além disso, ao invés de aumentar a eficiência da via iCA1-mPFC, a AD gerou uma forte depressão na amplitude dos fPSPs da via iCA1-mPFC. Tal efeito foi duradouro (no mínimo 120 min) o suficiente para ser considerado como semelhante a LTD. Adicionalmente, observamos que AD promoveu diminuição de PPF na mesma via, com magnitudes e cinéticas de efeito muito semelhantes aos efeitos induzidos por KET-S+. O fato de KET-S+ e AD promoverem reduções semelhantes na plasticidade pré-sináptica, mesmo com efeitos distintos nos potenciais evocados basais no mPFC, sugere que esses tratamentos possam ter atuado diferencialmente nos terminais pré e pós-sinápticos, alterando tanto a eficiência sináptica na via iCA1-mPFC quanto a excitabilidade local de redes intra-hipocámpais. Como mencionado na introdução, postula-se que o aumento anormal da atividade em circuitos temporais seja capaz de produzir um estado de hiperfunção dopaminérgica, envolvendo as projeções do hipocampo ao NAcc como desencadeadoras desse processo (Mitchell et al., 2000). Simultaneamente, a forte propagação dessa hiperatividade do hipocampo ao mPFC também causaria as disfunções

executivas frequentemente observadas em esquizofrenia e ELT (Ando et al., 2004; Leung et al., 2000, Kandratavicius et al., 2013).

Esses dados, em conjunto com os obtidos por tratamento com KET-S+, sugerem que os mecanismos subjacentes aos prejuízos persistentes de plasticidade sináptica de curta duração no hipocampo representam um alvo interessante a ser considerado na busca por substratos biológicos comuns entre prejuízos cognitivos, psicose associada a ELT e esquizofrenia. Além disso, a forte atenuação da influência das entradas excitatórias hipocampais sobre os neurônios do mPFC observada em animais submetidos a AD, representa uma oportunidade singular para testar algumas hipóteses formuladas no modelo proposto por (Lodge e Grace, 2007) e, em seguida, ampliá-lo com o intuito de integrar os achados recentes sobre as psicoses associadas a ELT (ver por exemplo, modelo adaptado por Kandratavicius et al., 2013), além de propor novas ideias para o desenvolvimento de terapias não-farmacológicas, (por exemplo, estimulação cerebral profunda na esquizofrenia; DBS, do inglês *deep brain stimulation*; (Ewing e Grace, 2013; Ewing e Winter, 2013; Perez et al., 2013).

5.10. Modulação da LTP sobre os efeitos induzidos por KET-S+ e AD: implicações para estudos de DBS em modelos de psicose

Por fim, testamos se a indução prévia de LTP poderia atenuar os efeitos induzidos por KET S+ e AD na via iCA1-mPFC, já que estudos recentes têm demonstrado que o aumento da função dos receptores NMDA e AMPA por moduladores alostéricos positivos são capazes de reverter as alterações comportamentais e prejuízos cognitivos associados a psicose experimental. Nossa suposição foi baseada na ideia de que a aplicação de HFS em CA1 seria capaz de melhorar a eficiência dos receptores AMPA e NMDA dos neurônios do mPFC, por

meio do aumento da influência excitatória dos neurônios vindos de CA1. Nossos achados sugerem que, de fato, a indução prévia de LTP atenua (ou bloqueia em alguns casos) alguns dos efeitos eletrofisiológicos induzidos por KET-S+ e AD.

Um dos resultados mais intrigantes do presente trabalho foi obtido da avaliação da plasticidade de curta-duração na via iCA1-mPFC. Como mencionado, observamos redução significativa do PPF induzida por ambos, KET-S+ e AD. Em seguida, observamos que a indução de LTP prévia foi capaz de bloquear completamente as alterações da eficiência basal e de PPF na via CA1-mPFC produzidos por KET-S+ e AD. Isso sugere que a aplicação de HFS em CA1 também influenciou redes intra-hipocâmpais, que, mesmo sob efeito de KET-S+ ou em período pós-ictal (efeito de AD), foram capazes de apresentar o mesmo nível de plasticidade pré-sináptica dos controles, evidenciado pela ausência de diferença das médias de PPF entre os grupos AD, Sham, KET e SAL. Considerando que a integridade do PPF está associado a qualidade do processamento e filtro de informações sensoriais (Citri e Malenka, 2008), uma das nossas previsões seria de que a aplicação de HFS no hipocampo atenuaria o prejuízo de PPI induzido por KET. Consistentemente, Ewing e Grace (2013) testaram se a aplicação de DBS no hipocampo ventral seria capaz de atenuar os prejuízos nos potenciais evocados por estimulação acústica observados em ratos submetidos a modelo de esquizofrenia induzido durante o desenvolvimento. Os autores mostraram que DBS (20 min, 130 Hz, pulsos monofásicos de 0,1 ms) no hipocampo ventral praticamente aboliu as respostas do hipocampo aos estímulos acústicos, porém restaurou os prejuízos observados nas regiões infra-límbicas do mPFC e do TMD (Ewing e Grace, 2013). Os autores argumentam que a aparente desativação do hipocampo ventral gerado por DBS pode ter atenuado o estado hiperdopaminérgico usualmente apresentado por este modelo (Gill *et al.*, 2011). Tal

“normalização” do sistema dopaminérgico poderia estar subjacente à restauração do processamento acústico na região infra-límbica do mPFC e TMD.

Além da avaliação de PPF, mostramos também que a indução de LTP prévia também bloqueia o aumento de delta gerado por KET-S+ no mPFC, mas não o aumento de gama-alta. Além disso, a LTP não foi capaz de alterar o aumento de delta no hipocampo observado nos animais tratados com KET-S+. Em nosso conhecimento, a ideia de que a aplicação de HFS no hipocampo seja capaz de modular padrões oscilatórios no mPFC é relativamente nova. Uma hipótese a ser testada seria a de que os efeitos modulatórios induzidos pela aplicação prévia de LTP nas oscilações corticais, durante os efeitos de KET-S+, poderiam ser explicados por uma melhor regulação do tônus dopaminérgico associado a melhora da eficiência de receptores NMDA presentes nos interneurônios do mPFC (Lavin e Grace, 2001). Consistentemente, foram reportadas evidências de que populações semelhantes de CA1 projetam ao mPFC e NAcc (Thierry et al., 2000); e que a aplicação de HFS em CA1 gera aumento dos níveis extracelulares de dopamina no mPFC (Gurden *et al.*, 2000). Como mencionado, KET-S+ produz uma série de alterações eletrofisiológicas que não são necessariamente interdependentes. Uma das explicações para o aumento de delta induzido por KET-S+ seria um excessivo engajamento talâmico, capaz de gerar um estado de sincronização global. O fato da aplicação de HFS em CA1 modular especificamente o aumento das oscilações delta no mPFC induzido por KET-S+ torna o cenário um pouco mais complicado, já que o hipocampo não projeta diretamente ao tálamo. Uma possibilidade a ser investigada é de que a aplicação de HFS em CA1 tenha fortalecido preferencialmente as conexões entre neurônios excitatórios hipocámpais e interneurônios do mPFC, tornando a rede local mais organizada e resistente as oscilações lentas impostas possivelmente pelo tálamo durante efeito de KET-S+. De fato, parece ser plausível considerar que ocorra tal

ativação preferencial de interneurônios do mPFC, já que foram reportadas evidências de aumento transiente de oscilações gama-baixa no mPFC após a aplicação de HFS em iCA1 (Izaki e Akema, 2008). Experimentos que avaliem simultaneamente potenciais evocados na via TMD-mPFC e CA1-mPFC, antes e após aplicação de HFS em CA1, de animais controle e tratados com KET-S+, serão importantes para testar essa hipótese.

Por fim, observamos que a LTP bloqueia o aumento de MI no mPFC induzido por KET-S+, mas não modula tal efeito no hipocampo. Interessante notar que, de acordo com a **figura 12b**, a diminuição do MI do mPFC no grupo LTP-KET não pode ser explicada simplesmente pela diminuição da potência em delta mencionada anteriormente. Como mencionado, uma explicação possível para o aumento aberrante de MI induzido por KET-S+ envolveria a forte capacidade desse fármaco em inibir o funcionamento dos transportadores de dopamina. Assim, o aumento extracelular de dopamina no mPFC e redes associadas aumentaria a precisão temporal dos disparos corticais, refletindo em maior acoplamento entre a fase de delta e amplitude de gama-alta. Assim como proposto anteriormente, sugerimos que o aumento da eficiência da comunicação entre hipocampo e mPFC possa gerar, de alguma forma, um estado de resistência a um provável excesso de ativação dopaminérgica gerado por KET-S+. Em nosso conhecimento, não existem estudos que tenham tentado dissociar as alterações da dinâmica de populações de neurônios piramidais e interneurônios do córtex induzidas por LTP. Uma ideia interessante seria inibir seletivamente os neurônios piramidais do mPFC com optogenética durante todo o procedimento de aplicação de HFS em CA1. Isso garantiria que as conexões entre neurônios de iCA1 e interneurônios do mPFC fossem, de fato, priorizadas.

6. Conclusão

Nossos achados indicam que o tratamento sistêmico com KET-S+ (relevante para o estudo da esquizofrenia) e a indução de AD no hipocampo (relevante para o estudo da psicose pós-ictal) produzem alterações complexas sobre a conectividade, plasticidade sináptica e padrões oscilatórios na via iCA1-mPFC *in vivo*. A prevenção de boa parte desses efeitos eletrofisiológicos, por meio de indução de LTP, dá suporte a ideia de que o DBS aplicado no hipocampo seria capaz de atenuar os prejuízos de processamento cognitivo em modelos animais de esquizofrenia. Esperamos que tais resultados possam ser traduzidos futuramente para a clínica, colaborando, portanto, para o desenvolvimento de tratamentos não-farmacológicos que visem a prevenção ou atenuação dos prejuízos cognitivos associados a transtornos psiquiátricos e/ou comorbidades psiquiátricas associadas a ELT.

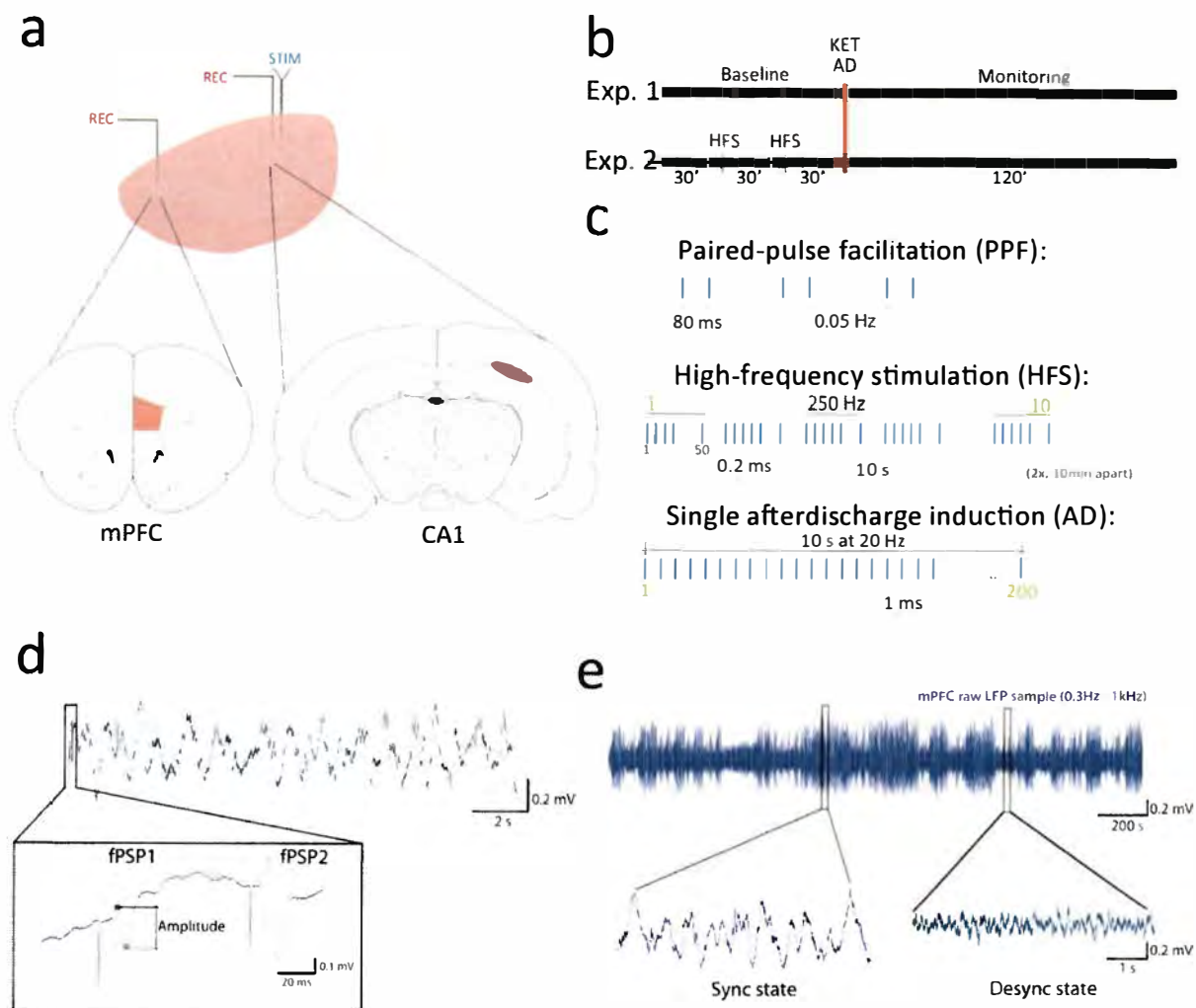


Figura 1. Medidas eletrofisiológicas, estímulos elétricos e paradigmas experimentais. (a) LFPs foram obtidos por meio de eletrodos monopolares de tungstênio implantados no hipocampo (CA1) e na região pré-límbica (PL) do mPFC em animais anestesiados com uretana. Além disso, um eletrodo bipolar foi posicionado na região posterior dorsal de CA1 hipocampal para elicitar fPSPs no mPFC. (b) *Paradigmas experimentais*. No experimento 1, foram registradas respostas no mPFC a cada 20 s para linha de base (90 min) antes da aplicação de (1) KET-S(+) (12,5 mg/Kg i.p.) ou veículo e (2) AD-hipocampal ou Sham, formando os grupos KET (n=7), SAL (n=8), AD (n=7) e Sham (n=7). Em seguida os animais foram registrados por mais 120 min para monitoramento. No experimento 2, foram registradas respostas evocadas no mPFC durante 30 min para constituir uma linha de base antes da aplicação de dois HFS ou Sham (aos 30 e 60 min de experimento) e administração/aplicação de KET, AD ou SAL aos 90 min, formando os grupos LTP-KET (n=9), LTP-AD (n=8) e LTP-SAL (n=6). Subsequentemente, os animais foram monitorados por 120 min adicionais. Em todos os grupos, foram registrados LFPs no hipocampo e mPFC ao longo de todo o experimento, simultaneamente aos registros de fPSPs evocados. (c) *Paradigmas de estimulação elétrica*. Durante todo o experimento, foi realizado a aplicação de pares de pulsos em CA1 com concomitante registro dos fPSPs evocados no mPFC a cada 20 s. O intervalo inter-estímulos (ITI) em CA1 foi de 80 ms, tipicamente capaz de gerar o maior PPF nessa via (Kiss et al., 2011). A eficiência basal da via CA1-mPFC foi avaliada pela amplitude

do fPSP1 e a plasticidade pré-sináptica ou PPF foi avaliada pela razão entre as amplitudes de fPSP2 e fPSP1. A LTP foi induzida por meio de aplicação de HFS: duas séries de 10 trens (50 pulsos a 250 Hz; 200 ms de duração; a cada 10 s), separados por 10min (Jay e Burette, 1995). Para evocação de AD-hipocampal única, foi aplicado um trem na região CA1: 200 pulsos (20Hz; pulsos monofásicos de 1ms) com duração de 10 s. **(d)** O sinal analógico vindo do animal foi amplificado, filtrado, digitalizado e dividido em épocas de 19,5 s. Estes períodos de registros englobam, nos primeiros 120 ms, uma dupla de fPSPs evocados por estimulação pareada em CA1 (ITI = 80ms) e, no tempo subsequente, LFPs espontâneos em CA1 e mPFC. Para análises oscilatórias, os primeiros 300 ms foram removidos. **(e)** Exemplo de LFP (0.3Hz – 1 kHz) coletado no mPFC de um animal anestesiado com uretana. Como descrito por trabalhos anteriores, em roedores anestesiados com uretana, é possível observar transições espontâneas de estados sincronizados (ondas lentas e de alta amplitude) para estados dessincronizados (oscilações mais rápidas e de baixa amplitude).

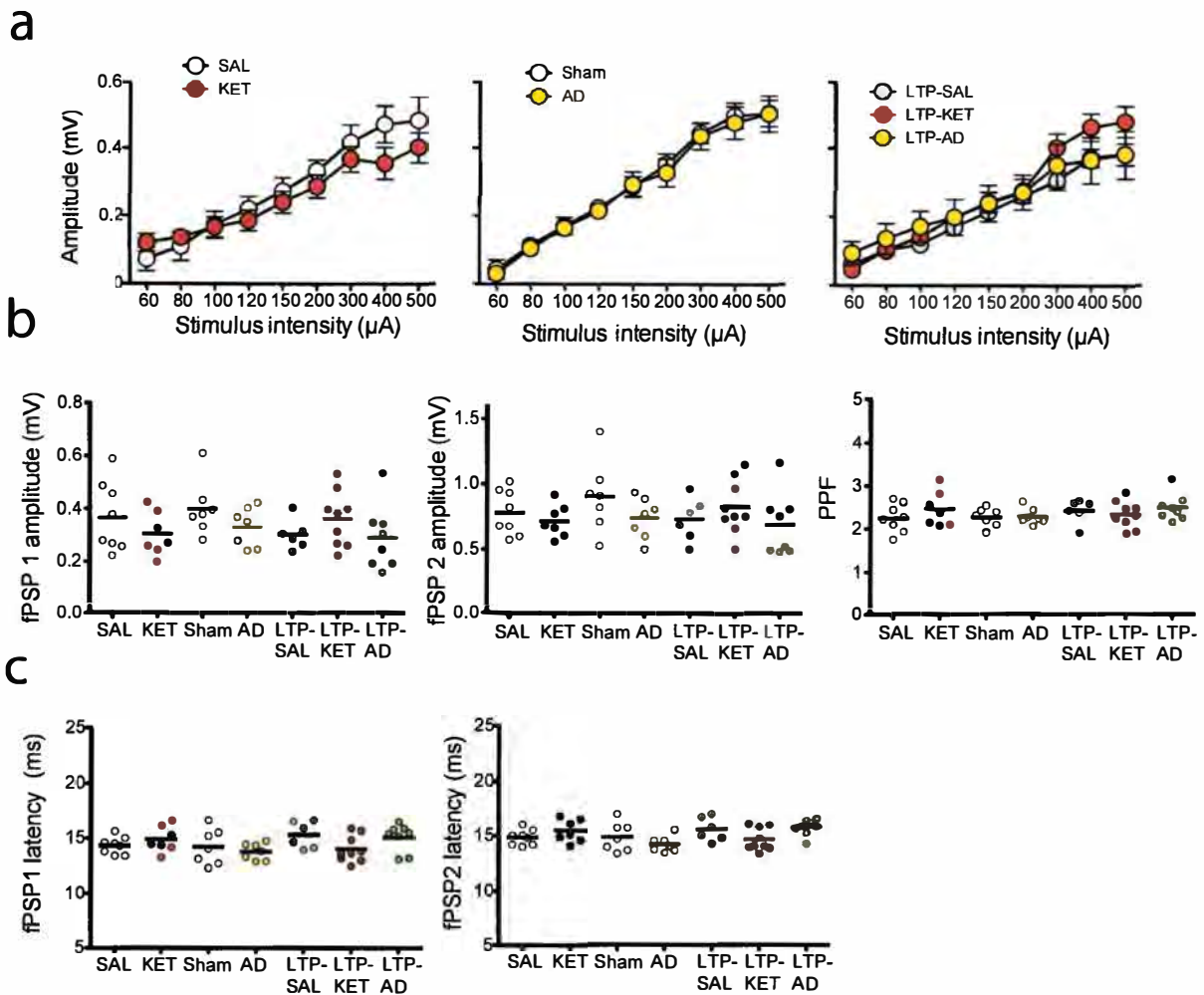


Figura 2. Propriedades dos potenciais evocados na via CA1-mPFC *in vivo*. (a) *Curvas de entrada e saída (E/S)*. Estímulos monofásicos de 0,2 ms de duração foram aplicados em CA1 em intensidades crescentes (60, 80, 100, 120, 150, 200, 300, 400, 500 μA) e os seus respectivos fPSPs evocados no mPFC foram simultaneamente registrados. A intensidade de estímulo escolhida para todos os experimentos foi de 70% da amplitude máxima dos fPSPs. Não foram obtidas diferenças entre os grupos, quando comparadas as suas curvas E/S. (b,c) Todos os animais incluídos nas análises apresentaram fPSPs típicos da via CA1-mPFC com amplitude do fPSP1 sempre acima de 150 μV e latência do primeiro pico negativo entre 14 e 17 ms (Lopes Aguiar et al., 2008; Lopes-Aguiar et al, 2013). Além disso, o PPF (fPSP2/fPSP1) eliciado no mPFC após estímulo pareado de 80 ms no hipocampo, variou entre 2 e 3, também de maneira consistente com a literatura (Kiss et al., 2011). Não foram observadas diferenças entre as médias das amplitudes, PPF e latências dos grupos incluídos nos experimentos 1 e 2. Dados expressos como média \pm erro padrão (a) ou média + dispersão dos valores (b, c). ANOVA simples de uma via; $p > 0,05$.

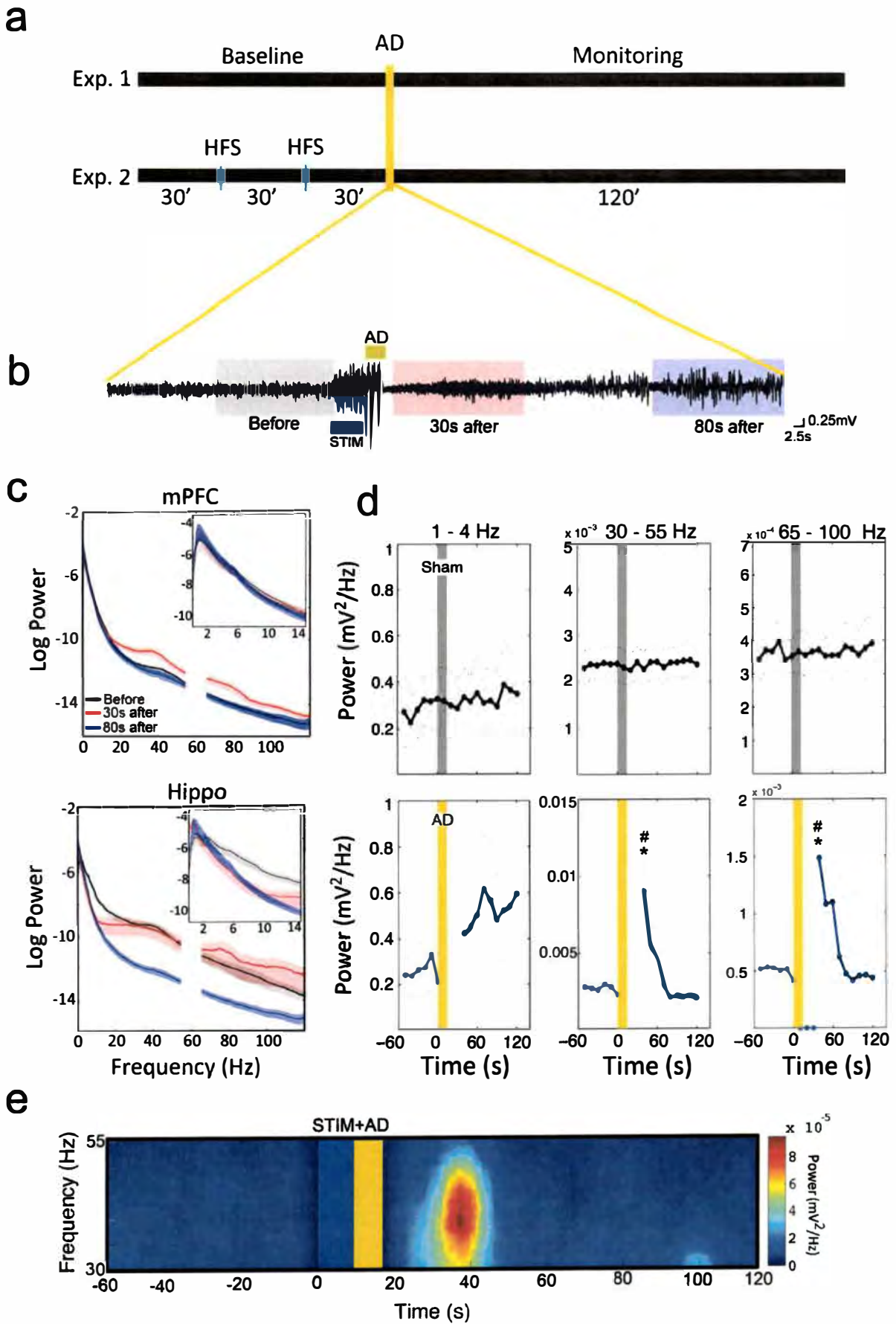
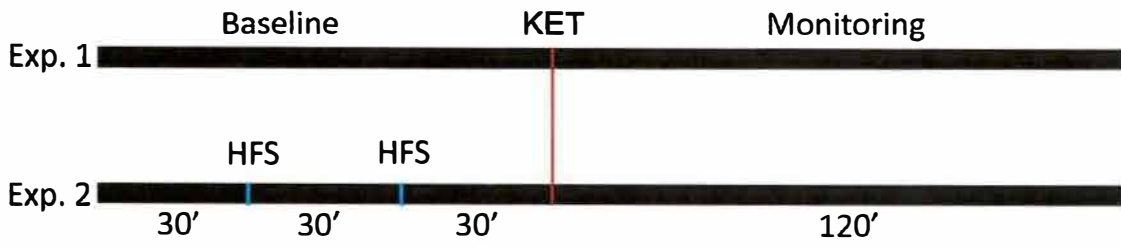


Figura 3. Efeitos de curto prazo induzidos por AD. (a) Paradigma experimental destacando o momento de indução da AD. (b) Para avaliação dos efeitos oscilatórios de curto prazo da AD, foram monitorados LFPs no hipocampo e mPFC 1min antes, durante e 1 min após estímulo (Ma and Leung, 2010). O protocolo de estímulo utilizado foi capaz de eliciar uma única pós-descarga, seguida de aumento de oscilações gama (30 a 100 Hz). (c) Densidade espectral de potência média para LFPs registrados no mPFC e CA1 em três momentos distintos: antes, 30 s e 80 s após AD. *Acima*, é possível observar que, no mPFC, ocorre aumento de potência nas bandas de gama-baixa (30 a 55 Hz) e alta (65 – 100 Hz) apenas para época referente aos 30s após AD. *Abaixo*, mostra redução global da potência espectral média do hipocampo, 80s após AD. (d) Análise da potência absoluta média por banda de frequência ao longo de todo o registro em torno de AD ou Sham (60 s antes e 120 s depois) revela um aumento rápido e transiente induzido por AD nas bandas gama-baixa e alta. Os 10 s de estimulação e os 20 s subsequentes que continham a AD foram removidos das análises. (e) Exemplo de espectrograma na faixa de frequência de 30 a 55 Hz ao longo de todo o registro de LFPs em torno de AD, evidenciando um aumento rápido e bem delimitado no tempo de oscilações gama. Dados expressos como média \pm erro padrão. * $p < 0,05$ (comparação com a linha de base). # $p < 0,05$ (comparação com o período tardio de registro: 120 s). ANOVA de uma via medidas repetidas com teste post hoc de Tukey.

a



b

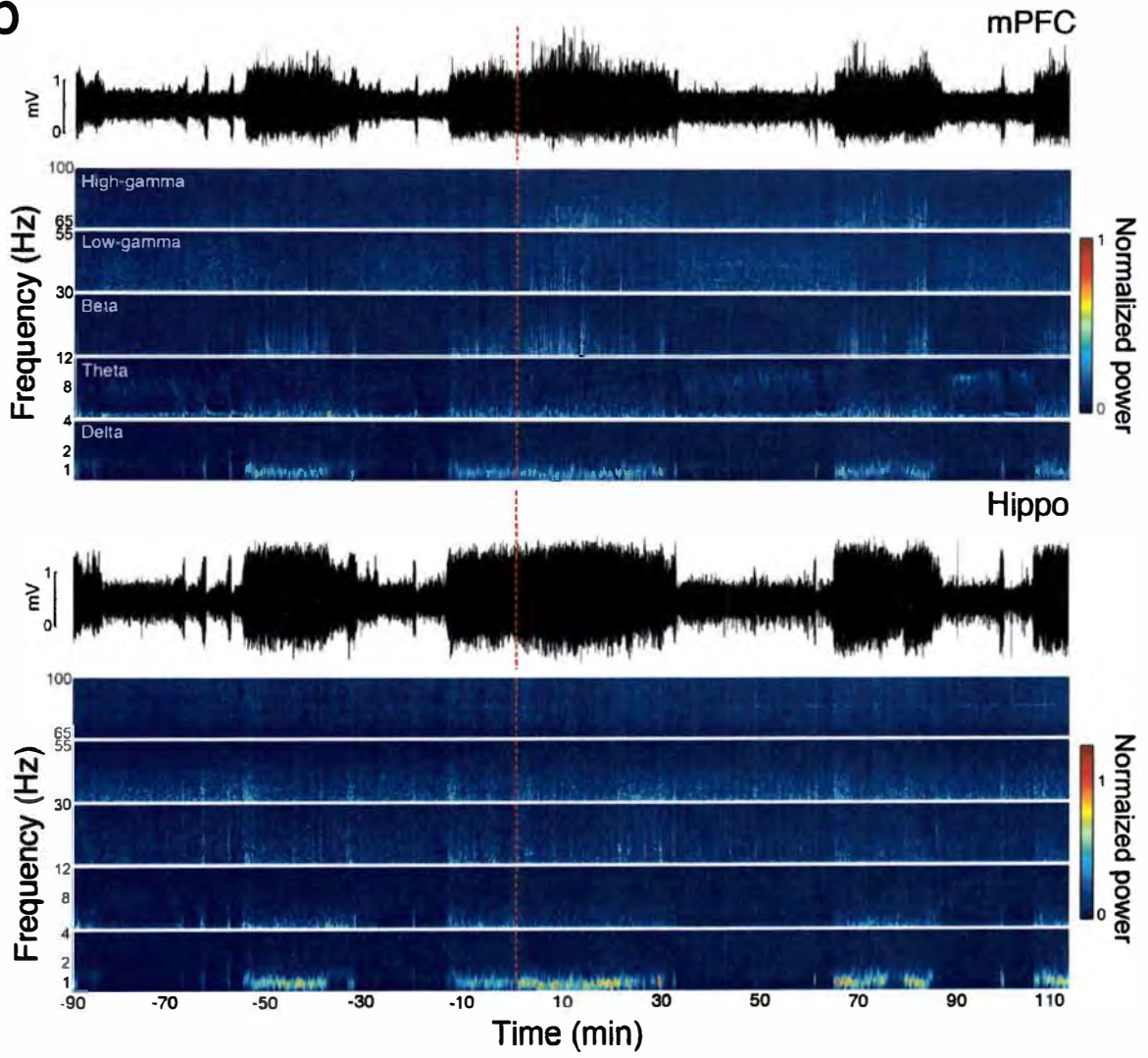


Figura 4. Alteração da dinâmica dos estados oscilatórios no hipocampo e córtex sob uretana induzido por KET S+. (a) Em ambos os experimentos, foram registrados simultaneamente LFPs em CA1 e no mPFC durante 90 min antes e 120 min depois de injeção de KET S+ (12,5 mg/kg, i.p.). (b) *Acima*, exemplos de traçados comprimidos de LFPs no mPFC e hipocampo obtidos de um mesmo animal durante o experimento 1 (duração: 210 min). *Abaixo*, espectogramas de potência em cinco bandas diferentes de frequência (delta, teta, beta, gama-baixa, gama alta) referentes aos seus respectivos traçados. Durante a linha de base, os padrões oscilatórios apresentam diversos períodos de transição espontânea entre estados de sincronização (aumento de delta e queda ou ausência de alteração das potências em gama) e dessincronização (caracterizado por diminuição de oscilações lentas e aumento em gama). Note que ocorre aumento simultâneo de delta e gama-alta após KET no mPFC, evento raramente observado durante os registros de linha de base. No hipocampo, a KET promove aumento mais pronunciado em delta nos primeiros 30 min pós-tratamento.

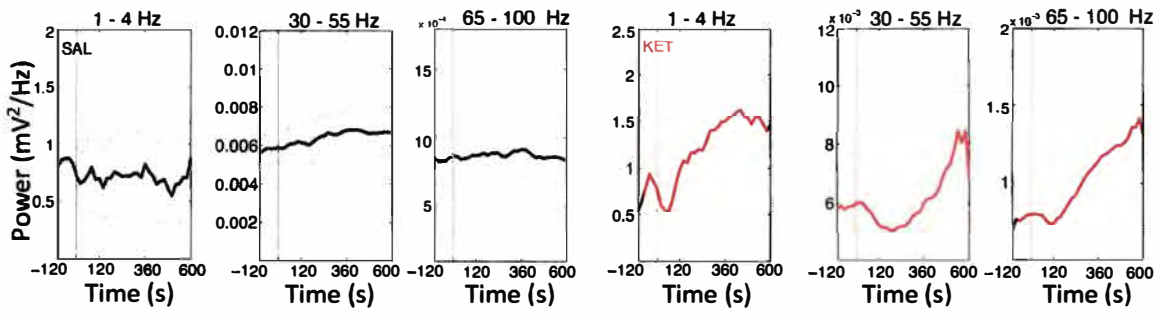
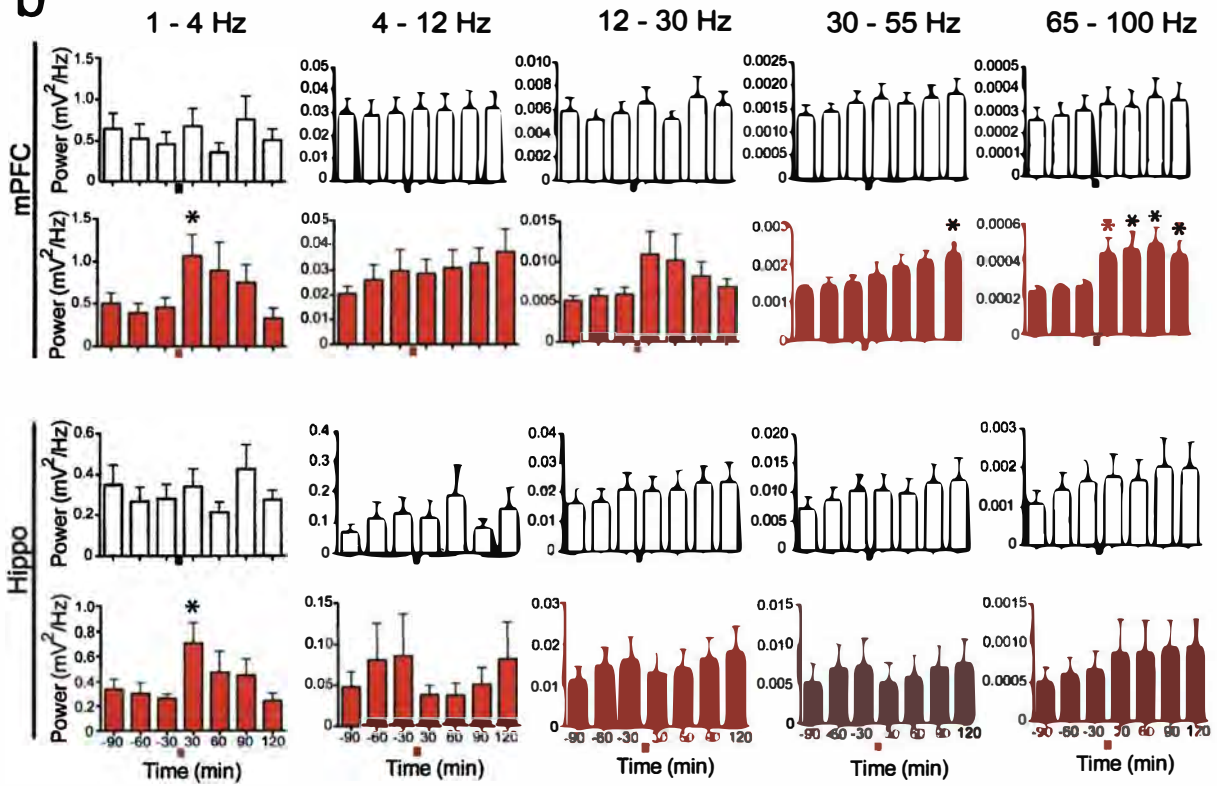
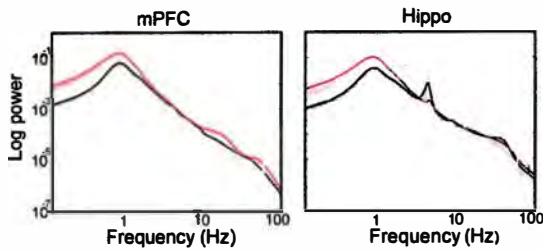
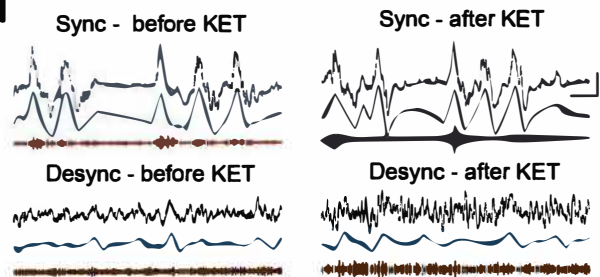
a**b****c****d**

Figura 5. Efeitos de KET sobre os padrões oscilatórios no hipocampo e mPFC. (a) Alterações de curto prazo. Média da potência absoluta em três bandas de frequência distintas (delta, gama-baixa e gama-alta) calculada em torno de injeção de SAL (esquerda) e KET S+ (direita) 120 s antes e 600 s depois do tratamento. KET promove aumento sustentado das potências em delta, gama-baixa e gama-alta cerca de 400 s após injeção. Nenhuma alteração foi observada no grupo SAL. **(b) Alterações de longo prazo.** Média da potência absoluta em blocos de 30 min ao longo de todo o experimento para as bandas delta, teta, beta, gama-baixa e gama-alta. *Acima*, KET S+ promove aumento transiente de potência em delta aos 30 min associado a aumento sustentado de gama-alta de 30 a 120 min no mPFC (blocos pós-tratamento comparados com a linha de base). Nenhuma alteração foi observada no grupo SAL. *Abaixo*, KET S+ promove aumento transiente de delta no hipocampo (aos 30min). **(c)** Densidade espectral de potência para o mPFC e hipocampo antes (linhas pretas) e 30min após KET S+ (linhas vermelhas). **(d)** Exemplos de traçados representativos de LFPs (linhas pretas: 0,3 Hz – 1 kHz), de traçados filtrados em delta-baixa (linhas azuis: 0,5 Hz - 1 Hz) e em gama-alta (linhas vermelhas: 65 Hz – 100 Hz) em épocas de sincronização e dessincronização dos LFPs no mPFC antes e após KET. Nos períodos sincronizados pós-KET também é possível observar um maior acoplamento da amplitude dos envelopes de gama com a fase de delta (ver também figura 10). Dados expressos como média \pm erro padrão. * $p < 0,05$ na comparação com os últimos 30 min de linha de base (- 30 min). Barras pretas abaixo do eixo x representam o momento da injeção de SAL e barras vermelhas de KET S+.

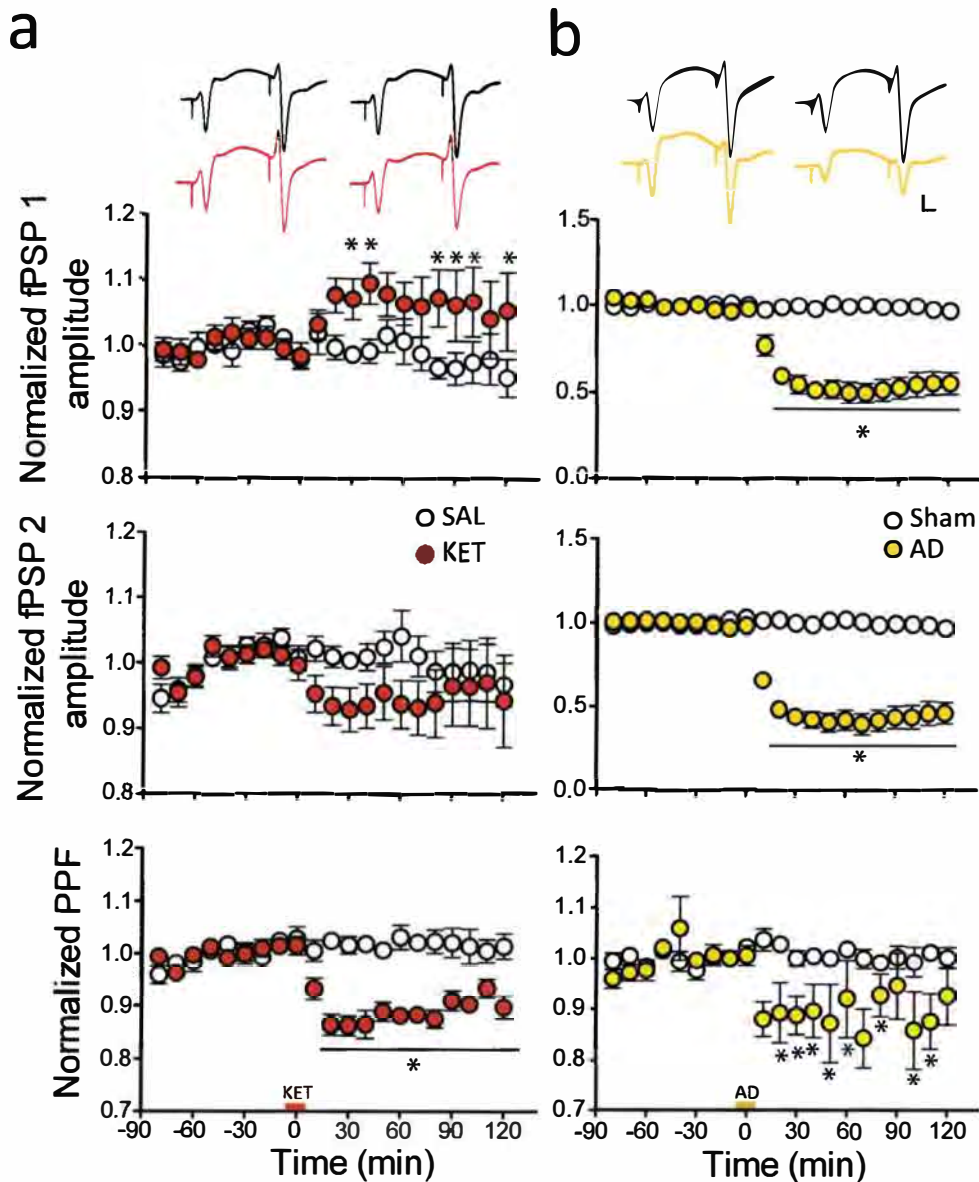


Figura 6. Efeitos de KET S+ e AD sobre a eficiência basal e plasticidade pré-sináptica da via CA1-mPFC. (a) KET S+ aumenta significativamente a amplitude do fPSP1 e reduz o PPF, sem afetar de maneira significativa o fPSP2 da via CA1-mPFC *in vivo*. (b) Indução de AD gera uma queda robusta de ambos, fPSP1 e fPSP2 na via CA1-mPFC. Além de robusto, esse efeito mostrou ser sustentado, mantendo a queda inicial dos fPSPs de 50 a 60% por, no mínimo, 2 horas. Assim como a KET S+, a indução de AD também gerou prejuízo de PPF. Os dados foram organizados em blocos de 10min e normalizados pela média da linha de base. Dados expressos como média \pm erro padrão. * $p < 0,05$ em relação ao grupo controle (ANOVA de duas vias medidas repetidas, seguido de teste *post hoc* de Tukey). Parte superior da figura, exemplos de fPSPs representativos para ilustrar os efeitos de KET e AD.

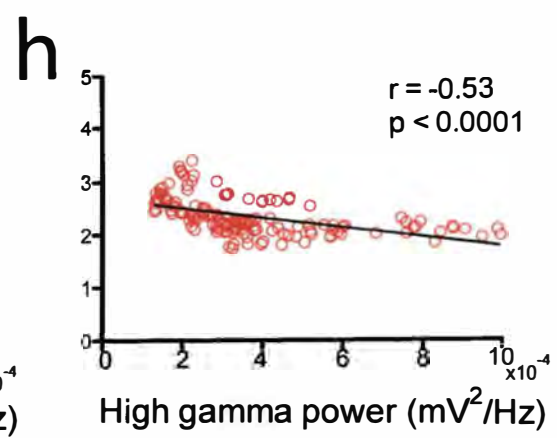
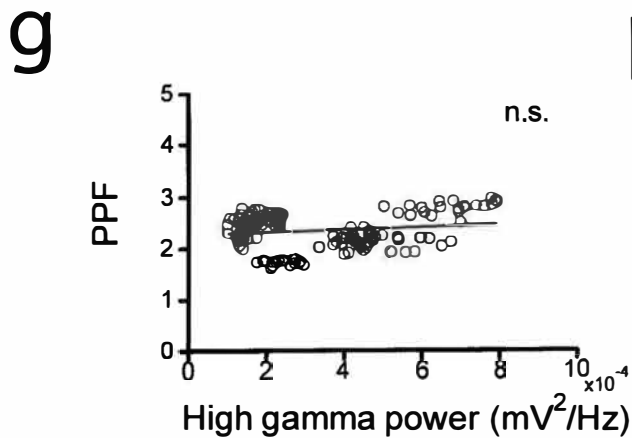
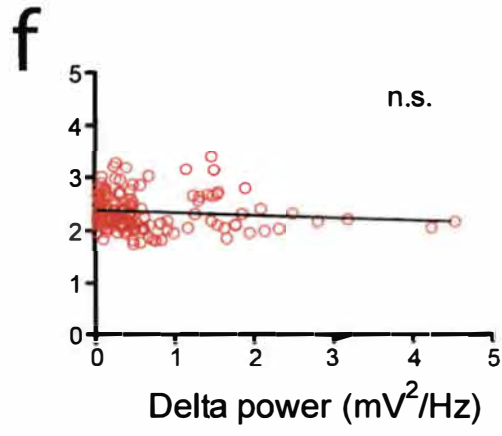
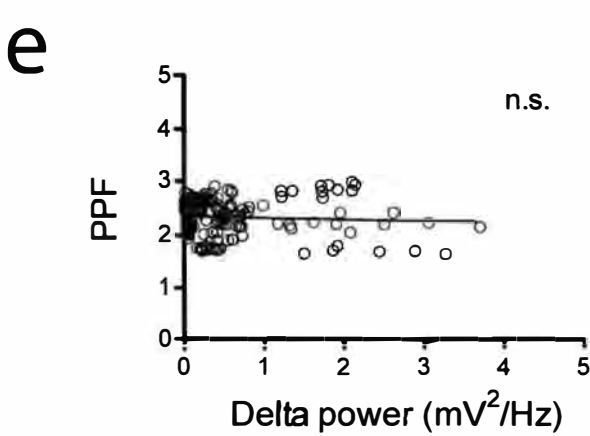
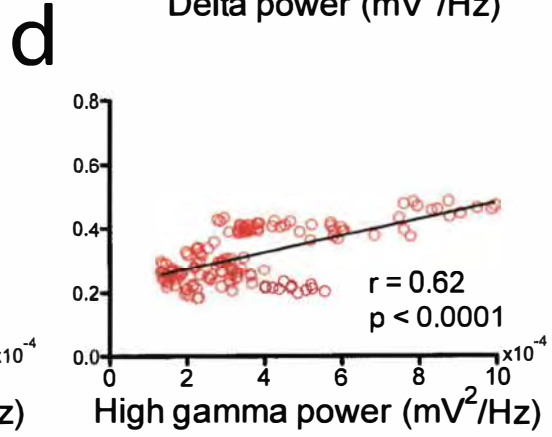
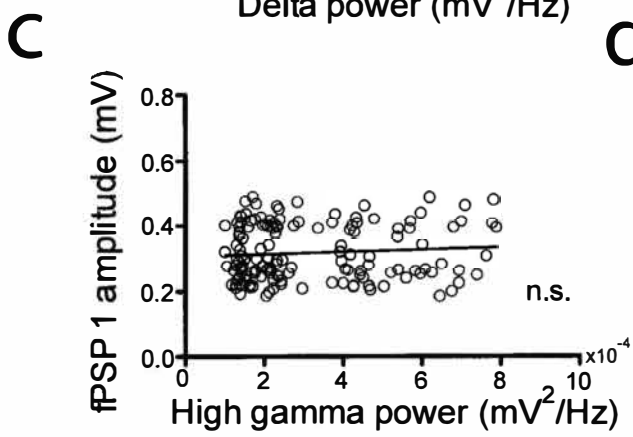
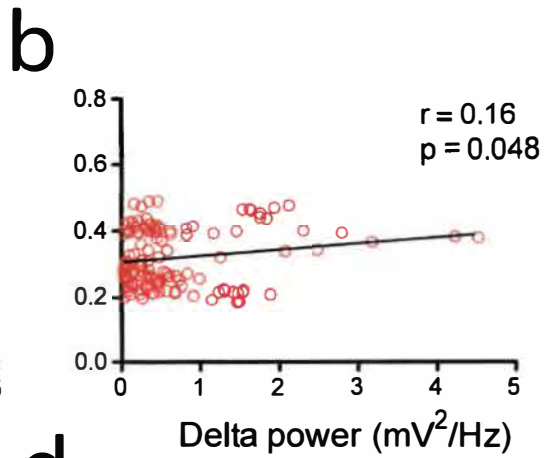
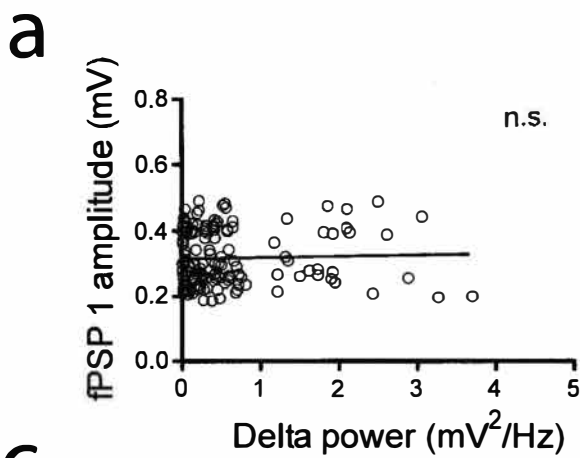


Figura 7. Correlações entre padrões oscilatórios e potenciais evocados na via CA1-mPFC. (a, b) Eficiência basal da via CA1-mPFC não correlaciona significativamente com a potência em delta no córtex. **(c, d)** Magnitude das repostas basais evocadas no mPFC não correlaciona significativamente com a potência de gama-alta no grupo SAL. Porém, no grupo KET observou-se correlação significativa ($r=0,62$; $p<0,0001$). Quanto maior a potência em gama-alta cortical, maior a amplitude do fPSP1 na via CA1-mPFC. **(e, f)** PPF não correlaciona significativamente com a potência em delta no córtex. **(g, h)** PPF não correlaciona com potência em gama alta cortical no grupo SAL, porém, no grupo KET observou-se correlação significativa entre tais parâmetros ($r=-0,53$; $p<0,0001$). Quanto maior a potência em gama-alta no córtex, menor o PPF na via CA1-mPFC.

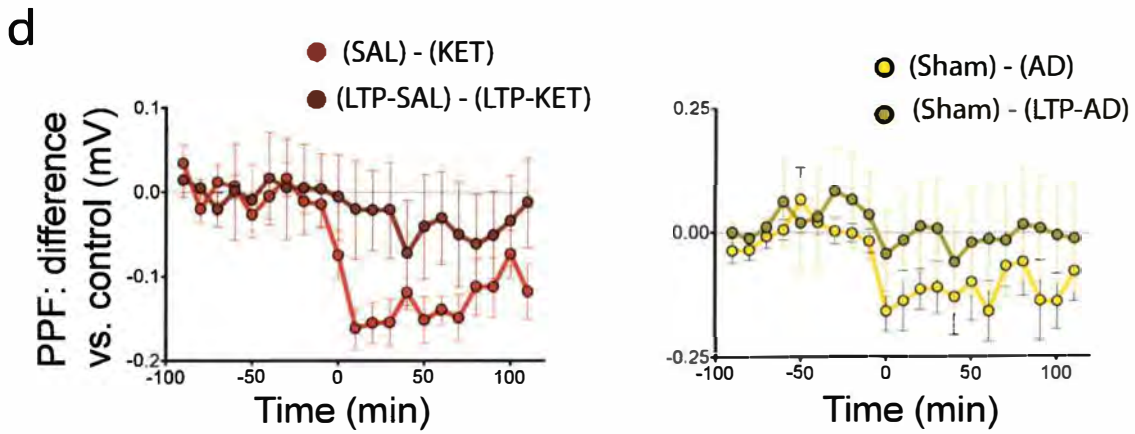
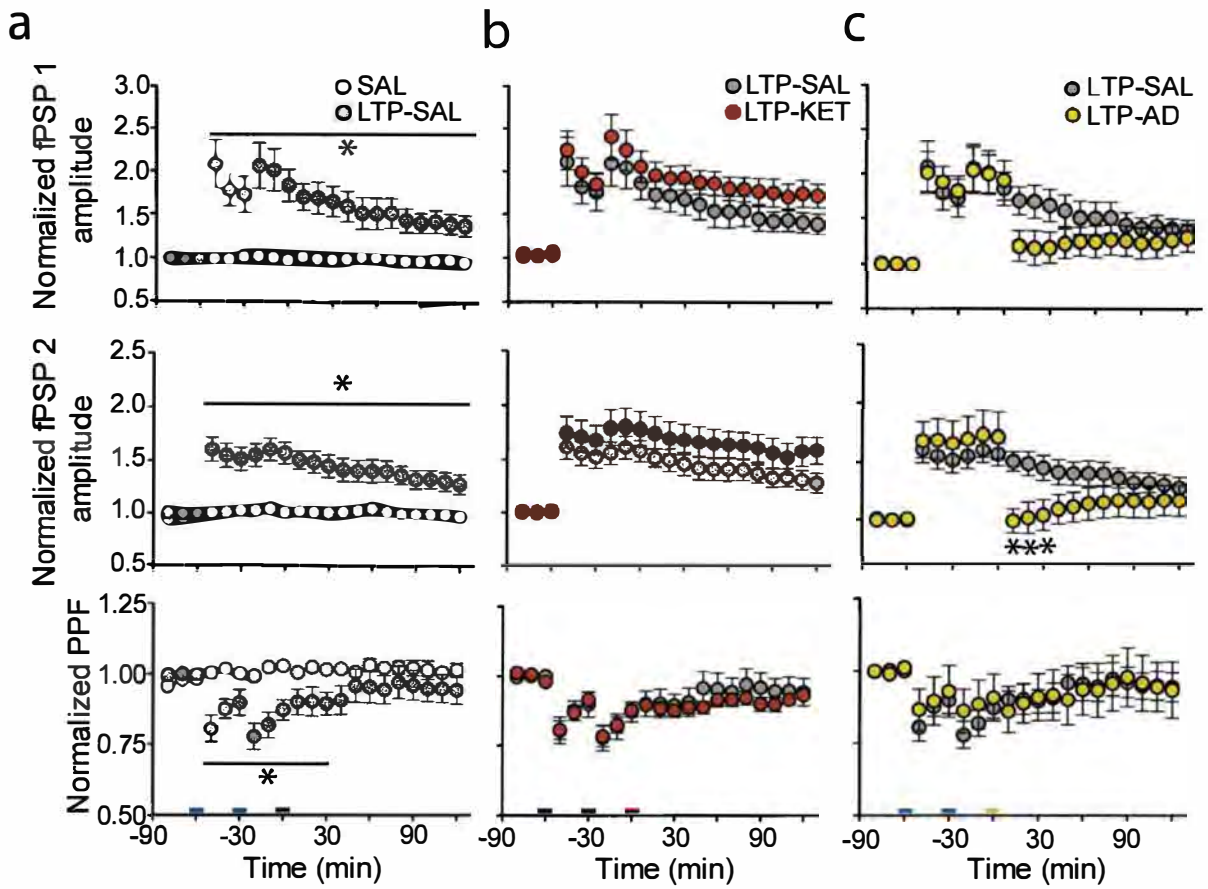


Figura 8. Efeitos da indução prévia de LTP sobre os efeitos de KET e AD na via CA1-mPFC. (a) Dupla aplicação de estimulação de alta frequência em CA1 (intervalo entre protocolos: 30 min) promove LTP robusta e sustentada (por no mínimo 120 minutos). Tal efeito mostrou-se associado a uma diminuição transiente do PPF por 60 minutos. (b) Injeção de KET não altera significativamente os potenciais evocados e o PPF na via CA1-mPFC quando precedido de LTP. (c) A indução de AD promove queda transiente dos potenciais evocados basais, mas não afeta o PPF quando precedido de LTP. (d) *Esquerda*, comparação entre os grupos KET e LTP-KET quanto à diferença de PPF em relação ao seu respectivo grupo controle sugere que a LTP module os efeitos de KET sobre o PPF. *Direita*, comparação entre os grupos AD e LTP-AD quanto à diferença de PPF em relação ao seu respectivo grupo controle sugere que a LTP também module os efeitos de AD sobre o PPF. Dados expressos como média \pm erro padrão. * $p < 0,05$ em relação ao grupo controle (ANOVA de duas vias medidas repetidas, seguido de teste *post hoc* de Tukey).

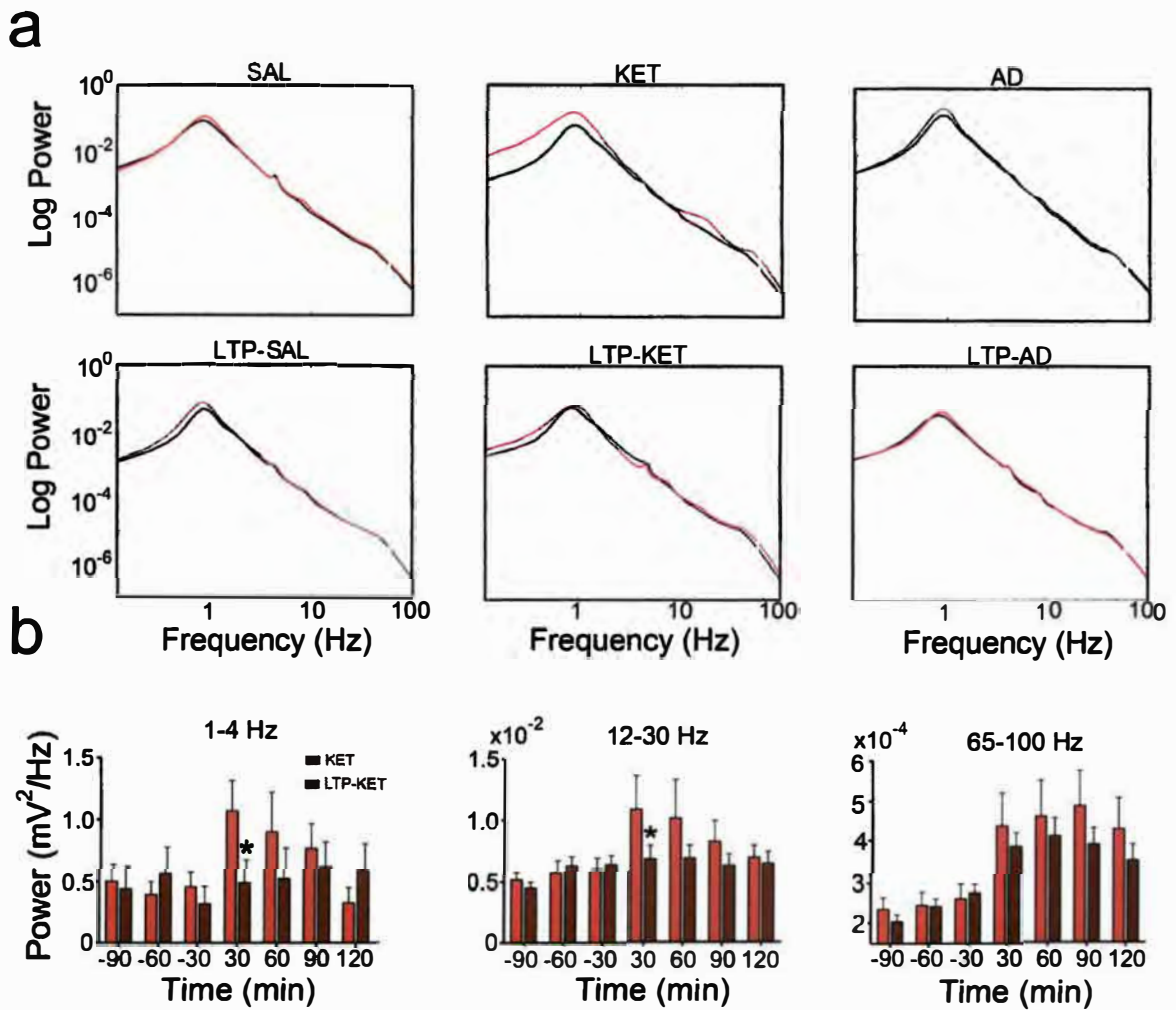


Figura 9. Modulação da LTP sobre as alterações induzidas por KET S+ nos padrões oscilatórios do mPFC. (a) Densidade espectral de potência calculada 30 minutos antes (traçado preto) de KET, SAL ou AD e 30 minutos depois (traçado vermelho) de KET, SAL ou AD. **(b)** Análise da potência absoluta em blocos de 30 minutos indica que a LTP bloqueia o aumento de delta e beta induzidos por KET S+. Note que a LTP não atenua o aumento de gama-alta induzido por KET S+ no mPFC. Dados expressos como média \pm erro padrão. * $p < 0,05$ em relação ao grupo controle (ANOVA de uma via medidas repetidas, seguido de teste *post hoc* de Tukey).

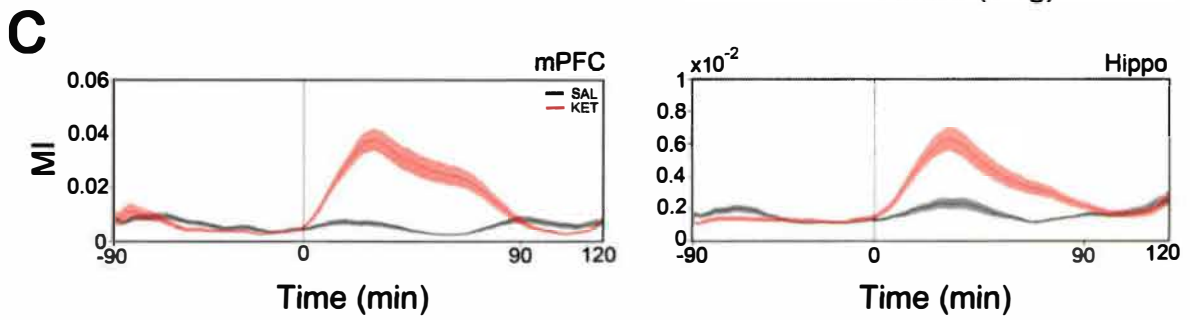
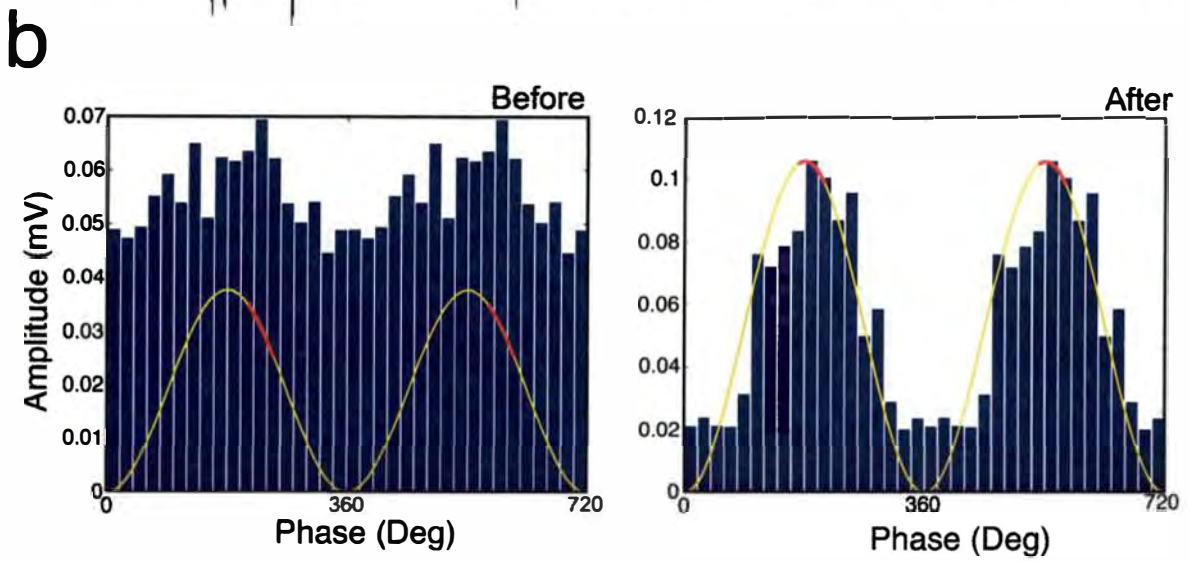
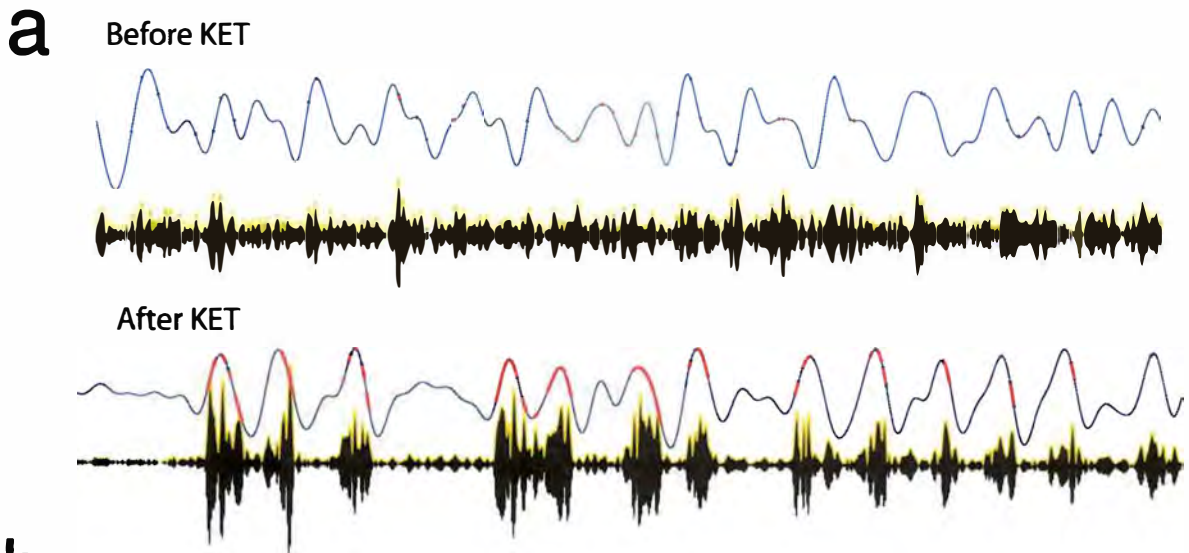


Figura 10. KET S+ aumenta a comodulação entre amplitude de gama-alta e fase de delta induzido no hipocampo e mPFC. (a) Exemplos de traçados de LFPs corticais, antes e depois de KET, filtrados em delta (0,5 – 4 Hz; traçado azul) e em gama-alta (65 – 100 Hz; traçado preto). Traçado amarelo define os envelopes de gama-alta no LFP filtrado (65 – 100 Hz). **(b)** Média da distribuição da amplitude de gama-alta pela fase de delta em janelas de 20° em um animal representativo, antes e depois de KET. O MI é uma medida que expressa a divergência entre a distribuição da amplitude avaliada e uma distribuição uniforme ideal (Tort et al., 2010). Portanto, ao compararmos o gráfico da esquerda (antes de KET) com o da direita (pós-KET), é possível observar que KET gera aumento de MI. O traçado amarelo representa o sinal filtrado em delta e as barras azuis são referentes à distribuição da amplitude de gama-alta ao longo da fase de delta. As linhas vermelhas, próximas aos picos dos traçados amarelos (delta), representam a faixa média de acoplamento amplitude-fase. **(c)** Média dos MIs nos grupos KET e SAL calculados em janelas de 10 min para o mPFC (esquerda) e hipocampo (direita), ao longo de todo o experimento (210 min). É possível observar que KET aumenta em até três vezes o MI no mPFC e hipocampo por cerca de 60 minutos pós-injeção (ver análises estatísticas na figura 11).

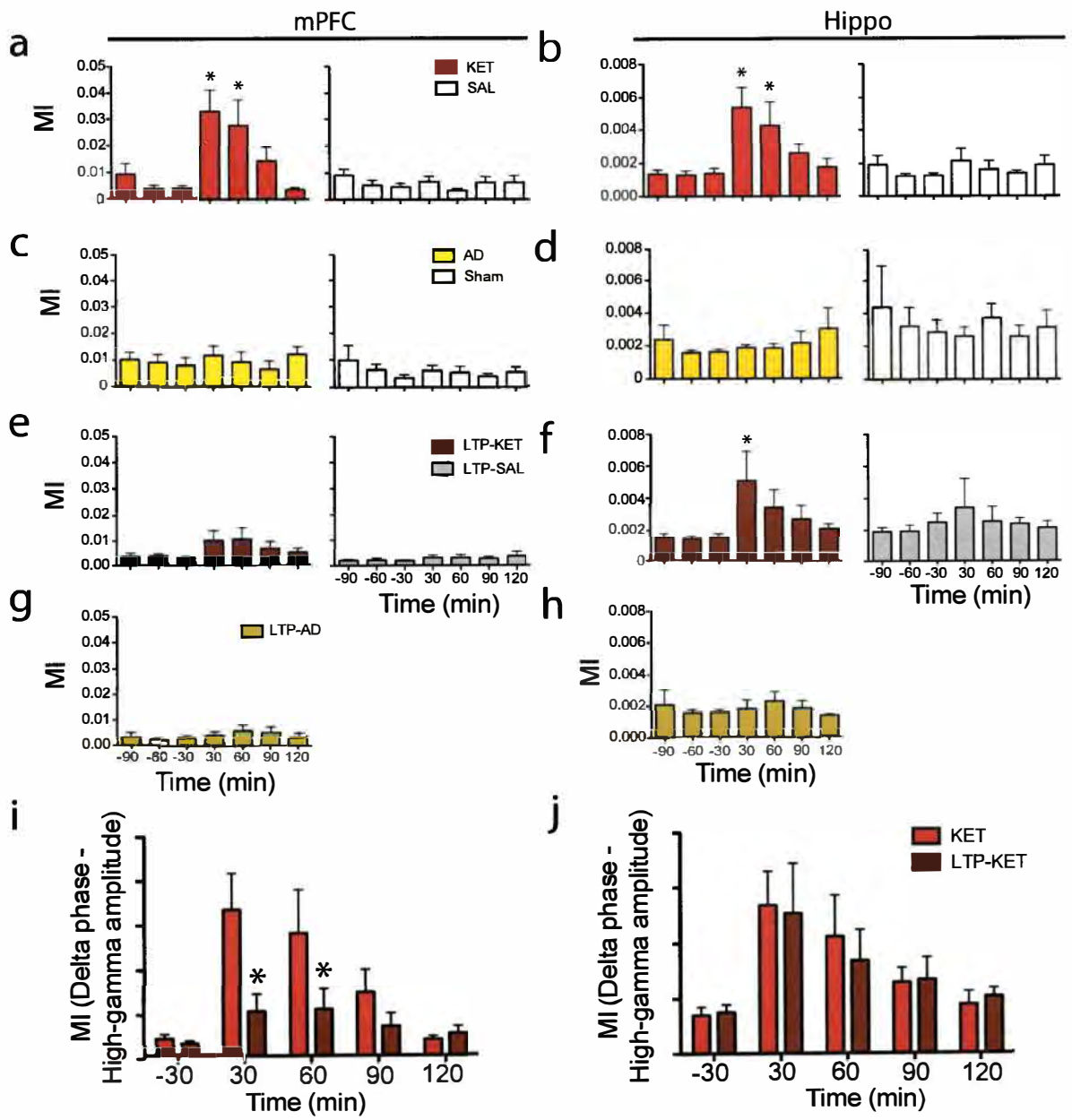


Figura 11. Indução prévia de LTP atenua o aumento do MI induzido por KET S+ especificamente no mPFC. (a) Comparações intra-grupo das médias dos MIs no *mPFC* em janelas de 30 min antes e depois de KET S+ ou SAL. *Esquerda*, KET S+ aumenta significativamente o MI por 60 min pós-injeção. *Direita*, nenhuma alteração significativa de MI foi observada no grupo SAL. (b) Comparações intra-grupo das médias dos MIs no *hipocampo*. *Esquerda*, KET S+ aumenta significativamente o MI por 60 min pós-injeção. *Direita*, nenhuma alteração significativa de MI foi observada no grupo SAL. (c, d) Nenhuma alteração significativa de MI foi observada nos grupos AD e Sham no mPFC e hipocampo. (e) *Esquerda*, KET S+ não produz aumento significativo do MI no mPFC quando precedida por LTP. *Direita*, nenhuma alteração significativa de MI foi observada no grupo LTP-SAL. (f) *Esquerda*, KET S+, precedido por LTP, aumenta significativamente o MI no hipocampo por 30 min pós-injeção. *Direita*, nenhuma alteração significativa de MI foi observada no grupo LTP-SAL. (g, h) Nenhuma alteração significativa de MI foi observada no grupo LTP-AD no mPFC e hipocampo. (i, f) MIs dos grupos KET e LTP-KET plotados juntos para evidenciar a modulação diferencial da LTP sobre o aumento do MI induzido por KET S+. As médias dos MIs no mPFC, 30 e 60 min pós-injeção, são significativamente maiores no grupo KET, comparado ao grupo LTP-KET. Por outro lado, ambos os grupos exibiram aumento semelhante de MI no hipocampo, após injeção de KET. Dados expressos como média \pm erro padrão. * $p < 0,05$ em relação aos últimos 30 min de linha de base (ANOVA de uma via medidas repetidas ou de duas vias medidas repetidas, seguidos de teste *post hoc* de Tukey).

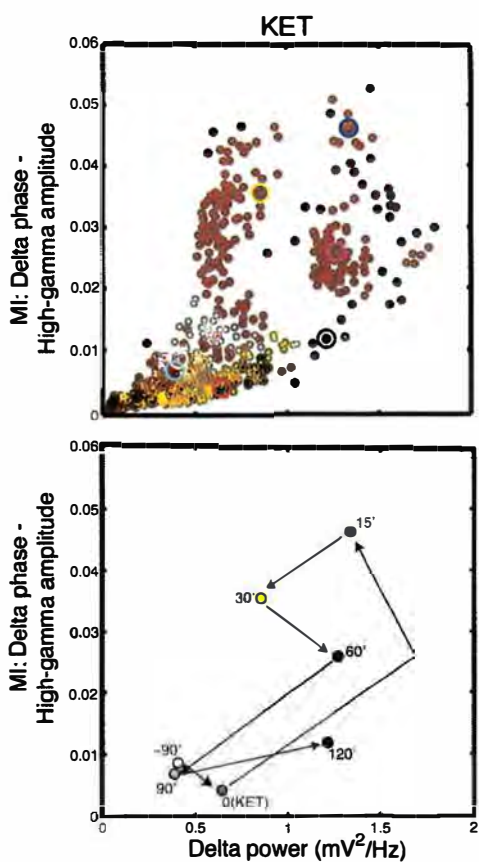
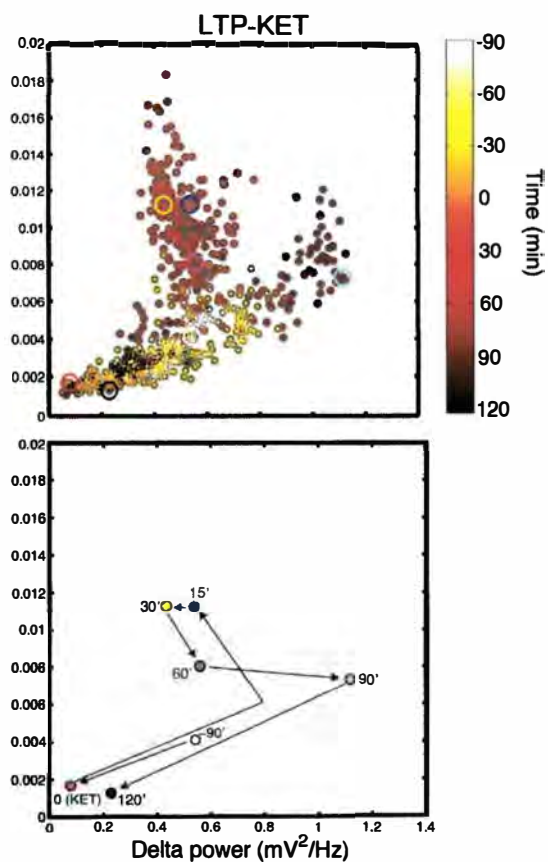
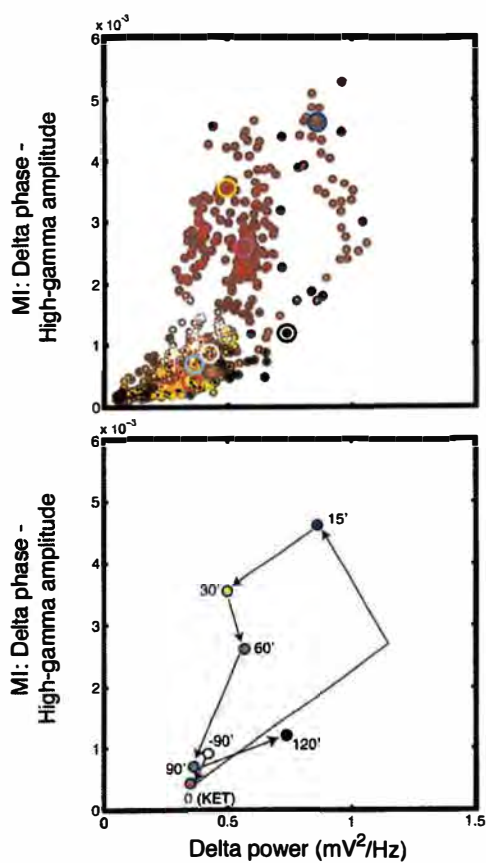
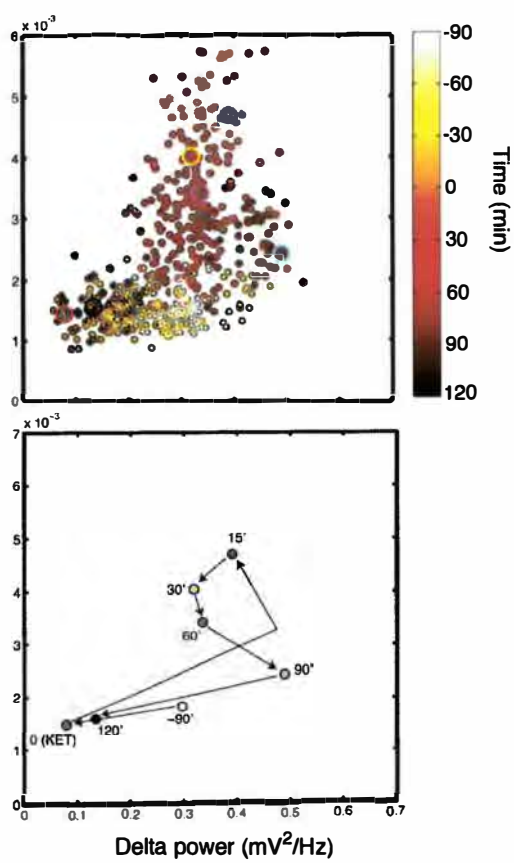
a**mPFC****b****c****Hippo****d**

Figura 12. Exemplo de relação não-linear entre MI e potência de delta no mPFC e hipocampo antes e após KET S+. **(a)** *Acima*, gráfico de dispersão da média dos MIs pela média da potência absoluta de delta no mPFC em janelas de 20 s ao longo de todo o experimento (630 pontos) mostra ausência de correlação linear entre tais variáveis. A escala de cor dos pontos permite observar a dinâmica temporal da relação entre MI e potência de delta. Pontos próximos ao branco são referentes ao início do experimento, pontos de cor laranja e vermelho estão próximos ao momento da injeção de KET S+ e pontos escuros indicam o final do experimento. *Abaixo*, gráfico contendo apenas 7 pontos dos 630 plotados acima para ilustrar de forma mais clara como o aumento ou diminuição de MI não depende necessariamente de alteração na potência de delta, especialmente em períodos pós-KET. Por exemplo, o experimento é iniciado em -90 min com um valor médio de MI em torno de 0,01 e uma potência em delta em torno de 0,4 mV²/Hz. Aos 15 min pós KET S+ o MI sobe para mais de 0,04 e a potência em delta para cerca de 1,2 mV²/Hz. Aos 60 min pós-KET, a potência em delta é ainda superior a 1 mV²/Hz, porém o MI médio já caiu em cerca de 50%. **(b)** A mesma dinâmica temporal não-linear também pode ser observada no mPFC dos animais do grupo LTP-KET. Por exemplo, aos 15 min pós-KET, a potência em delta é basicamente a mesma do início do experimento, porém o MI é cerca de 3 vezes maior. **(c, d)** Exemplos da relação não-linear entre MI e potência de delta no hipocampo para os grupos KET e LTP-KET.

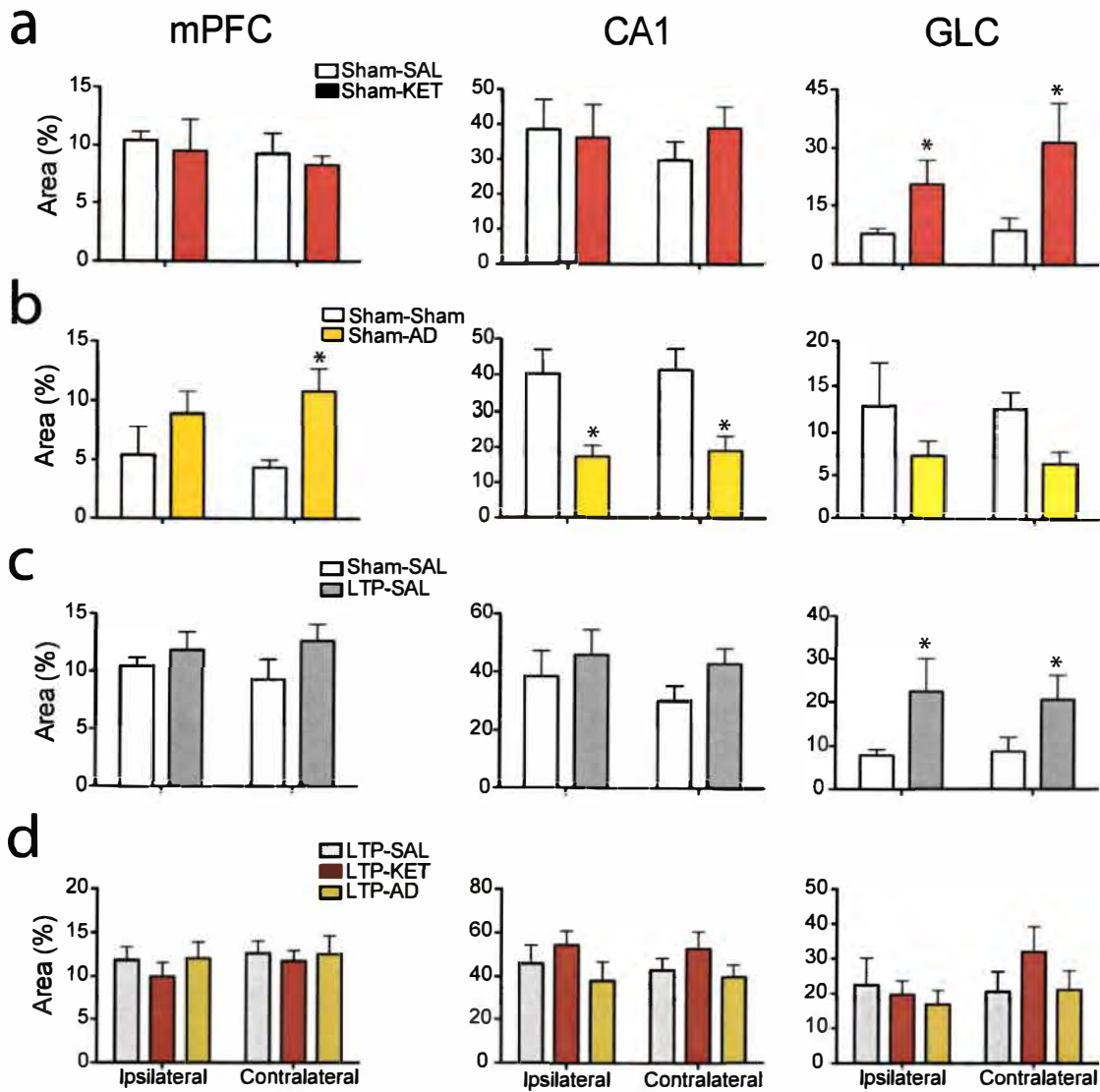


Figura 13. Análise imunohistoquímica de BDNF no hipocampo e mPFC. (a) KET S+ aumenta expressão de BDNF na camada granular do giro denteado em ambos os hemisférios. **(b)** AD produz aumento na expressão de BDNF no mPFC (apenas no hemisfério contralateral à estimulação) e diminuição bilateral em CA1. **(c)** Indução de LTP, por si só, é capaz de aumentar bilateralmente BDNF na camada granular do giro denteado. **(d)** Nenhuma diferença foi observada entre os grupos que receberam LTP antes de KET S+ ou AD. Dados expressos como média \pm erro padrão. * $p < 0,05$ em relação ao grupo controle (ANOVA simples de uma via, seguido de teste *post hoc* de Tukey).

Referências bibliográficas

ALBERATI, D. et al. Glycine reuptake inhibitor RG1678: a pharmacologic characterization of an investigational agent for the treatment of schizophrenia. **Neuropharmacology**, v. 62, n. 2, p. 1152-61, Feb 2012. ISSN 1873-7064 (Electronic)

0028-3908 (Linking). Disponível em: < <http://www.ncbi.nlm.nih.gov/pubmed/22138164> >.

ANDO, N. et al. Enhancement of central dopaminergic activity in the kainate model of temporal lobe epilepsy: implication for the mechanism of epileptic psychosis.

Neuropsychopharmacology, v. 29, n. 7, p. 1251-8, Jul 2004. ISSN 0893-133X (Print)

0006-3223 (Linking). Disponível em: < <http://www.ncbi.nlm.nih.gov/pubmed/15039765> >.

ANVER, H. et al. NMDA receptor hypofunction phase couples independent gamma-oscillations in the rat visual cortex. **Neuropsychopharmacology**, v. 36, n. 2, p. 519-28, Jan 2011. ISSN 1740-634X (Electronic)

0006-3223 (Linking). Disponível em: < <http://www.ncbi.nlm.nih.gov/pubmed/20962769> >.

BASAR-EROGLU, C. et al. Working memory related gamma oscillations in schizophrenia patients. **Int J Psychophysiol**, v. 64, n. 1, p. 39-45, Apr 2007. ISSN 0167-8760 (Print)

0167-8760 (Linking). Disponível em: < <http://www.ncbi.nlm.nih.gov/pubmed/16962192> >.

BEASLEY, C. et al. Glycogen synthase kinase-3beta immunoreactivity is reduced in the prefrontal cortex in schizophrenia. **Neurosci Lett**, v. 302, n. 2-3, p. 117-20, Apr 20 2001. ISSN 0304-3940 (Print)

0304-3940 (Linking). Disponível em: < <http://www.ncbi.nlm.nih.gov/pubmed/11290401> >.

BENCHENANE, K. et al. Coherent theta oscillations and reorganization of spike timing in the hippocampal- prefrontal network upon learning. **Neuron**, v. 66, n. 6, p. 921-36, Jun 24 2010. ISSN 1097-4199 (Electronic)

0896-6273 (Linking). Disponível em: < <http://www.ncbi.nlm.nih.gov/pubmed/20620877> >.

BLISS, T. V.; COLLINGRIDGE, G. L. A synaptic model of memory: long-term potentiation in the hippocampus. **Nature**, v. 361, n. 6407, p. 31-9, Jan 7 1993. ISSN 0028-0836 (Print)

0028-0836 (Linking). Disponível em: < <http://www.ncbi.nlm.nih.gov/pubmed/8421494> >.

BLISS, T. V.; LOMO, T. Long-lasting potentiation of synaptic transmission in the dentate area of the anaesthetized rabbit following stimulation of the perforant path. **J Physiol**, v. 232, n. 2, p. 331-56, Jul 1973. ISSN 0022-3751 (Print)

0022-3751 (Linking). Disponível em: < <http://www.ncbi.nlm.nih.gov/pubmed/4727084> >.

BLOT, K. et al. Modulation of Hippocampus-Prefrontal Cortex Synaptic Transmission and Disruption of Executive Cognitive Functions by MK-801. **Cereb Cortex**, Dec 4 2013. ISSN 1460-2199 (Electronic)

1047-3211 (Linking). Disponível em: < <http://www.ncbi.nlm.nih.gov/pubmed/24304584> >.

BRADLEY, C. A. et al. A pivotal role of GSK-3 in synaptic plasticity. **Front Mol Neurosci**, v. 5, p. 13, 2012. ISSN 1662-5099 (Electronic)

1662-5099 (Linking). Disponível em: < <http://www.ncbi.nlm.nih.gov/pubmed/22363262> >.

BRAUN, I. et al. Alterations of hippocampal and prefrontal GABAergic interneurons in an animal model of psychosis induced by NMDA receptor antagonism. **Schizophr Res**, v. 97, n. 1-3, p. 254-63, Dec 2007. ISSN 0920-9964 (Print). Disponível em: < <http://www.ncbi.nlm.nih.gov/pubmed/17601703> >.

BRIDGES, T. M. et al. The antipsychotic potential of muscarinic allosteric modulation. **Drug News Perspect**, v. 23, n. 4, p. 229-40, May 2010. ISSN 0214-0934 (Print)

0214-0934 (Linking). Disponível em: < <http://www.ncbi.nlm.nih.gov/pubmed/20520852> >.

BROSE, N. et al. Differential assembly of coexpressed glutamate receptor subunits in neurons of rat cerebral cortex. **J Biol Chem**, v. 269, n. 24, p. 16780-4, Jun 17 1994. ISSN 0021-9258 (Print)

0021-9258 (Linking). Disponível em: < <http://www.ncbi.nlm.nih.gov/pubmed/8207001> >.

BUZSAKI, G.; WANG, X. J. Mechanisms of gamma oscillations. **Annu Rev Neurosci**, v. 35, p. 203-25, 2012. ISSN 1545-4126 (Electronic)

0147-006X (Linking). Disponível em: < <http://www.ncbi.nlm.nih.gov/pubmed/22443509> >.

BYMASTER, F. P. et al. Potential role of muscarinic receptors in schizophrenia. **Life Sci**, v. 64, n. 6-7, p. 527-34, 1999. ISSN 0024-3205 (Print)

0024-3205 (Linking). Disponível em: < <http://www.ncbi.nlm.nih.gov/pubmed/10069519> >.

CAIXETA, F. V. et al. Ketamine alters oscillatory coupling in the hippocampus. **Sci Rep**, v. 3, p. 2348, 2013. ISSN 2045-2322 (Electronic)

2045-2322 (Linking). Disponível em: < <http://www.ncbi.nlm.nih.gov/pubmed/23907109> >.

CANOLTY, R. T.; KNIGHT, R. T. The functional role of cross-frequency coupling. **Trends Cogn Sci**, v. 14, n. 11, p. 506-15, Nov 2010. ISSN 1879-307X (Electronic)

1364-6613 (Linking). Disponível em: < <http://www.ncbi.nlm.nih.gov/pubmed/20932795> >.

CARDIN, J. A. et al. Driving fast-spiking cells induces gamma rhythm and controls sensory responses. **Nature**, v. 459, n. 7247, p. 663-7, Jun 4 2009. ISSN 1476-4687 (Electronic)

0028-0836 (Linking). Disponível em: < <http://www.ncbi.nlm.nih.gov/pubmed/19396156> >.

CARLEN, M. et al. A critical role for NMDA receptors in parvalbumin interneurons for gamma rhythm induction and behavior. **Mol Psychiatry**, v. 17, n. 5, p. 537-48, May 2012. ISSN 1476-5578 (Electronic)

1359-4184 (Linking). Disponível em: < <http://www.ncbi.nlm.nih.gov/pubmed/21468034> >.

CELLERINO, A. et al. Parvalbumin immunoreactivity: a reliable marker for the effects of monocular deprivation in the rat visual cortex. **Neuroscience**, v. 51, n. 4, p. 749-53, Dec 1992. ISSN 0306-4522 (Print)

0306-4522 (Linking). Disponível em: < <http://www.ncbi.nlm.nih.gov/pubmed/1488119> >.

CERQUEIRA, J. J. et al. The prefrontal cortex as a key target of the maladaptive response to stress. **J Neurosci**, v. 27, n. 11, p. 2781-7, Mar 14 2007. ISSN 1529-2401 (Electronic)

0270-6474 (Linking). Disponível em: < <http://www.ncbi.nlm.nih.gov/pubmed/17360899> >.

CHEN, L.; MUHLHAUSER, M.; YANG, C. R. Glycine transporter-1 blockade potentiates NMDA-mediated responses in rat prefrontal cortical neurons in vitro and in vivo. **J Neurophysiol**, v. 89, n. 2, p. 691-703, Feb 2003. ISSN 0022-3077 (Print)

0022-3077 (Linking). Disponível em: < <http://www.ncbi.nlm.nih.gov/pubmed/12574447> >.

CHROBAK, J. J.; BUZSAKI, G. Gamma oscillations in the entorhinal cortex of the freely behaving rat. **J Neurosci**, v. 18, n. 1, p. 388-98, Jan 1 1998. ISSN 0270-6474 (Print)

0270-6474 (Linking). Disponível em: < <http://www.ncbi.nlm.nih.gov/pubmed/9412515> >.

CHURCHWELL, J. C.; KESNER, R. P. Hippocampal-prefrontal dynamics in spatial working memory: interactions and independent parallel processing. **Behav Brain Res**, v. 225, n. 2, p. 389-95, Dec 1 2011. ISSN 1872-7549 (Electronic)

0166-4328 (Linking). Disponível em: < <http://www.ncbi.nlm.nih.gov/pubmed/21839780> >.

CIFELLI, P.; GRACE, A. A. Pilocarpine-induced temporal lobe epilepsy in the rat is associated with increased dopamine neuron activity. **Int J Neuropsychopharmacol**, v. 15, n. 7, p. 957-64, Aug 2012. ISSN 1469-5111 (Electronic)

1461-1457 (Linking). Disponível em: < <http://www.ncbi.nlm.nih.gov/pubmed/21745437> >.

CITRI, A.; MALENKA, R. C. Synaptic plasticity: multiple forms, functions, and mechanisms. **Neuropsychopharmacology**, v. 33, n. 1, p. 18-41, Jan 2008. ISSN 0893-133X (Print)

0006-3223 (Linking). Disponível em: < <http://www.ncbi.nlm.nih.gov/pubmed/17728696> >.

CLEMENT, E. A. et al. Cyclic and sleep-like spontaneous alternations of brain state under urethane anaesthesia. **PLoS One**, v. 3, n. 4, p. e2004, 2008. ISSN 1932-6203 (Electronic)

1932-6203 (Linking). Disponível em: < <http://www.ncbi.nlm.nih.gov/pubmed/18414674> >.

COLLINGRIDGE, G. L. et al. Long-term depression in the CNS. **Nat Rev Neurosci**, v. 11, n. 7, p. 459-73, Jul 2010. ISSN 1471-0048 (Electronic)

1471-003X (Linking). Disponível em: < <http://www.ncbi.nlm.nih.gov/pubmed/20559335> >.

CORLETT, P. R.; HONEY, G. D.; FLETCHER, P. C. From prediction error to psychosis: ketamine as a pharmacological model of delusions. **J Psychopharmacol**, v. 21, n. 3, p. 238-52, May 2007. ISSN 0269-8811 (Print)

0269-8811 (Linking). Disponível em: < <http://www.ncbi.nlm.nih.gov/pubmed/17591652> >.

CORLETT, P. R. et al. Glutamatergic model psychoses: prediction error, learning, and inference. **Neuropsychopharmacology**, v. 36, n. 1, p. 294-315, Jan 2011. ISSN 1740-634X (Electronic)

0006-3223 (Linking). Disponível em: < <http://www.ncbi.nlm.nih.gov/pubmed/20861831> >.

COTTRELL, J. R. et al. Working memory impairment in calcineurin knock-out mice is associated with alterations in synaptic vesicle cycling and disruption of high-frequency synaptic and network activity in prefrontal cortex. **J Neurosci**, v. 33, n. 27, p. 10938-49, Jul 3 2013. ISSN 1529-2401 (Electronic)

0270-6474 (Linking). Disponível em: < <http://www.ncbi.nlm.nih.gov/pubmed/23825400> >.

CROOK, J. M. et al. Low muscarinic receptor binding in prefrontal cortex from subjects with schizophrenia: a study of Brodmann's areas 8, 9, 10, and 46 and the effects of neuroleptic drug treatment. **Am J Psychiatry**, v. 158, n. 6, p. 918-25, Jun 2001. ISSN 0002-953X (Print)

0002-953X (Linking). Disponível em: < <http://www.ncbi.nlm.nih.gov/pubmed/11384900> >.

CSERNANSKY, J. G. et al. Mesolimbic dopaminergic supersensitivity following electrical kindling of the amygdala. **Biol Psychiatry**, v. 23, n. 3, p. 285-94, Feb 1 1988. ISSN 0006-3223 (Print)

0006-3223 (Linking). Disponível em: < <http://www.ncbi.nlm.nih.gov/pubmed/2962647> >.

CSICSVARI, J. et al. Reliability and state dependence of pyramidal cell-interneuron synapses in the hippocampus: an ensemble approach in the behaving rat. **Neuron**, v. 21, n. 1, p. 179-89, Jul 1998. ISSN 0896-6273 (Print)

0896-6273 (Linking). Disponível em: < <http://www.ncbi.nlm.nih.gov/pubmed/9697862> >.

CSICSVARI, J. et al. Mechanisms of gamma oscillations in the hippocampus of the behaving rat. **Neuron**, v. 37, n. 2, p. 311-22, Jan 23 2003. ISSN 0896-6273 (Print)

0896-6273 (Linking). Disponível em: < <http://www.ncbi.nlm.nih.gov/pubmed/12546825> >.

D'SOUZA, D. C. et al. Glycine transporter inhibitor attenuates the psychotomimetic effects of ketamine in healthy males: preliminary evidence. **Neuropsychopharmacology**, v. 37, n. 4, p. 1036-46, Mar 2012. ISSN 1740-634X (Electronic)

0006-3223 (Linking). Disponível em: < <http://www.ncbi.nlm.nih.gov/pubmed/22113087> >.

DALLEY, J. W.; CARDINAL, R. N.; ROBBINS, T. W. Prefrontal executive and cognitive functions in rodents: neural and neurochemical substrates. **Neurosci Biobehav Rev**, v. 28, n. 7, p. 771-84, Nov 2004. ISSN 0149-7634 (Print)

0149-7634 (Linking). Disponível em: < <http://www.ncbi.nlm.nih.gov/pubmed/15555683> >.

DAMASIO, A. R. Time-locked multiregional retroactivation: a systems-level proposal for the neural substrates of recall and recognition. **Cognition**, v. 33, n. 1-2, p. 25-62, Nov 1989. ISSN 0010-0277 (Print)

0010-0277 (Linking). Disponível em: < <http://www.ncbi.nlm.nih.gov/pubmed/2691184> >.

DAZZI, L. et al. Enhancement of basal and pentylentetrazol (PTZ)-stimulated dopamine release in the brain of freely moving rats by PTZ-induced kindling. **Synapse**, v. 26, n. 4, p. 351-8, Aug 1997. ISSN 0887-4476 (Print)

0887-4476 (Linking). Disponível em: < <http://www.ncbi.nlm.nih.gov/pubmed/9215594> >.

DEAKIN, J. F. et al. Glutamate and the neural basis of the subjective effects of ketamine: a pharmaco-magnetic resonance imaging study. **Arch Gen Psychiatry**, v. 65, n. 2, p. 154-64, Feb 2008. ISSN 1538-3636 (Electronic)

0003-990X (Linking). Disponível em: < <http://www.ncbi.nlm.nih.gov/pubmed/18250253> >.

DEGENETAIS, E. et al. Synaptic influence of hippocampus on pyramidal cells of the rat prefrontal cortex: an in vivo intracellular recording study. **Cereb Cortex**, v. 13, n. 7, p. 782-92, Jul 2003. ISSN 1047-3211 (Print)

1047-3211 (Linking). Disponível em: < <http://www.ncbi.nlm.nih.gov/pubmed/12816894> >.

DREVETS, W. C. et al. Subgenual prefrontal cortex abnormalities in mood disorders. **Nature**, v. 386, n. 6627, p. 824-7, Apr 24 1997. ISSN 0028-0836 (Print)

0028-0836 (Linking). Disponível em: < <http://www.ncbi.nlm.nih.gov/pubmed/9126739> >.

DU BOIS, T. M. et al. Perinatal PCP treatment alters the developmental expression of prefrontal and hippocampal muscarinic receptors. **Prog Neuropsychopharmacol Biol Psychiatry**, v. 33, n. 1, p. 37-40, Feb 1 2009. ISSN 0278-5846 (Print)

0278-5846 (Linking). Disponível em: < <http://www.ncbi.nlm.nih.gov/pubmed/18940225> >.

DU, F. et al. Preferential neuronal loss in layer III of the medial entorhinal cortex in rat models of temporal lobe epilepsy. **J Neurosci**, v. 15, n. 10, p. 6301-13, Oct 1995. ISSN 0270-6474 (Print)

0270-6474 (Linking). Disponível em: < <http://www.ncbi.nlm.nih.gov/pubmed/7472396> >.

EWING, S. G.; GRACE, A. A. Deep brain stimulation of the ventral hippocampus restores deficits in processing of auditory evoked potentials in a rodent developmental disruption model of schizophrenia. **Schizophr Res**, v. 143, n. 2-3, p. 377-83, Feb 2013. ISSN 1573-2509 (Electronic). Disponível em: < <http://www.ncbi.nlm.nih.gov/pubmed/23269227> >.

EWING, S. G.; WINTER, C. The ventral portion of the CA1 region of the hippocampus and the prefrontal cortex as candidate regions for neuromodulation in schizophrenia. **Med Hypotheses**, v. 80, n. 6, p. 827-32, Jun 2013. ISSN 1532-2777 (Electronic)

0306-9877 (Linking). Disponível em: < <http://www.ncbi.nlm.nih.gov/pubmed/23583328> >.

FERINO, F.; THIERRY, A. M.; GLOWINSKI, J. Anatomical and electrophysiological evidence for a direct projection from Ammon's horn to the medial prefrontal cortex in the rat. **Exp Brain Res**, v. 65, n. 2, p. 421-6, 1987. ISSN 0014-4819 (Print)

0014-4819 (Linking). Disponível em: < <http://www.ncbi.nlm.nih.gov/pubmed/3556468> >.

FLORESCO, S. B.; BLOCK, A. E.; TSE, M. T. Inactivation of the medial prefrontal cortex of the rat impairs strategy set-shifting, but not reversal learning, using a novel, automated procedure. **Behav Brain Res**, v. 190, n. 1, p. 85-96, Jun 26 2008. ISSN 0166-4328 (Print)

0166-4328 (Linking). Disponível em: < <http://www.ncbi.nlm.nih.gov/pubmed/18359099> >.

FLORESCO, S. B.; SEAMANS, J. K.; PHILLIPS, A. G. Selective roles for hippocampal, prefrontal cortical, and ventral striatal circuits in radial-arm maze tasks with or without a delay. **J Neurosci**, v. 17, n. 5, p. 1880-90, Mar 1 1997. ISSN 0270-6474 (Print)

0270-6474 (Linking). Disponível em: < <http://www.ncbi.nlm.nih.gov/pubmed/9030646> >.

FLORESCO, S. B.; ZHANG, Y.; ENOMOTO, T. Neural circuits subserving behavioral flexibility and their relevance to schizophrenia. **Behav Brain Res**, v. 204, n. 2, p. 396-409, Dec 7 2009. ISSN 1872-7549 (Electronic)

0166-4328 (Linking). Disponível em: < <http://www.ncbi.nlm.nih.gov/pubmed/19110006> >.

FUCHS, E. C. et al. Recruitment of parvalbumin-positive interneurons determines hippocampal function and associated behavior. **Neuron**, v. 53, n. 4, p. 591-604, Feb 15 2007. ISSN 1097-4199 (Electronic)

0896-6273 (Linking). Disponível em: < <http://www.ncbi.nlm.nih.gov/pubmed/17296559> >.

FURTH, K. E. et al. Dopamine, cognitive function, and gamma oscillations: role of D4 receptors. **Front Cell Neurosci**, v. 7, p. 102, 2013. ISSN 1662-5102 (Electronic)

1662-5102 (Linking). Disponível em: < <http://www.ncbi.nlm.nih.gov/pubmed/23847468> >.

GAITATZIS, A. et al. The epidemiology of the comorbidity of epilepsy in the general population. **Epilepsia**, v. 45, n. 12, p. 1613-22, Dec 2004. ISSN 0013-9580 (Print)

0013-9580 (Linking). Disponível em: < <http://www.ncbi.nlm.nih.gov/pubmed/15571520> >.

GILL, K. M. et al. A novel alpha5GABA(A)R-positive allosteric modulator reverses hyperactivation of the dopamine system in the MAM model of schizophrenia. **Neuropsychopharmacology**, v. 36, n. 9, p. 1903-11, Aug 2011. ISSN 1740-634X (Electronic)

0006-3223 (Linking). Disponível em: < <http://www.ncbi.nlm.nih.gov/pubmed/21562483> >.

GODSIL, B. P. et al. The hippocampal-prefrontal pathway: the weak link in psychiatric disorders? **Eur Neuropsychopharmacol**, v. 23, n. 10, p. 1165-81, Oct 2013. ISSN 1873-7862 (Electronic)

0924-977X (Linking). Disponível em: < <http://www.ncbi.nlm.nih.gov/pubmed/23332457> >.

GOFF, D. C. et al. A placebo-controlled add-on trial of the Ampakine, CX516, for cognitive deficits in schizophrenia. **Neuropsychopharmacology**, v. 33, n. 3, p. 465-72, Feb 2008. ISSN 0893-133X (Print)

0006-3223 (Linking). Disponível em: < <http://www.ncbi.nlm.nih.gov/pubmed/17487227> >.

GOLDMAN-RAKIC, P. S. Anatomical and functional circuits in prefrontal cortex of nonhuman primates. Relevance to epilepsy. **Adv Neurol**, v. 66, p. 51-63; discussion 63-5, 1995a. ISSN 0091-3952 (Print)

0091-3952 (Linking). Disponível em: < <http://www.ncbi.nlm.nih.gov/pubmed/7771311> >.

_____. Cellular basis of working memory. **Neuron**, v. 14, n. 3, p. 477-85, Mar 1995b. ISSN 0896-6273 (Print)

0896-6273 (Linking). Disponível em: < <http://www.ncbi.nlm.nih.gov/pubmed/7695894> >.

_____. Regional and cellular fractionation of working memory. **Proc Natl Acad Sci U S A**, v. 93, n. 24, p. 13473-80, Nov 26 1996. ISSN 0027-8424 (Print)

0027-8424 (Linking). Disponível em: < <http://www.ncbi.nlm.nih.gov/pubmed/8942959> >.

GOMEZA, J. et al. Pronounced pharmacologic deficits in M2 muscarinic acetylcholine receptor knockout mice. **Proc Natl Acad Sci U S A**, v. 96, n. 4, p. 1692-7, Feb 16 1999. ISSN 0027-8424 (Print)

0027-8424 (Linking). Disponível em: < <http://www.ncbi.nlm.nih.gov/pubmed/9990086> >.

GOTO, Y.; O'DONNELL, P. Synchronous activity in the hippocampus and nucleus accumbens in vivo. **J Neurosci**, v. 21, n. 4, p. RC131, Feb 15 2001. ISSN 1529-2401 (Electronic)

0270-6474 (Linking). Disponível em: < <http://www.ncbi.nlm.nih.gov/pubmed/11160416> >.

GOTO, Y.; YANG, C. R.; OTANI, S. Functional and dysfunctional synaptic plasticity in prefrontal cortex: roles in psychiatric disorders. **Biol Psychiatry**, v. 67, n. 3, p. 199-207, Feb 1 2010. ISSN 1873-2402 (Electronic)

0006-3223 (Linking). Disponível em: < <http://www.ncbi.nlm.nih.gov/pubmed/19833323> >.

GURDEN, H.; TAKITA, M.; JAY, T. M. Essential role of D1 but not D2 receptors in the NMDA receptor-dependent long-term potentiation at hippocampal-prefrontal cortex synapses in vivo. **J Neurosci**, v. 20, n. 22, p. RC106, Nov 15 2000. ISSN 1529-2401 (Electronic)

0270-6474 (Linking). Disponível em: < <http://www.ncbi.nlm.nih.gov/pubmed/11069975> >.

GYSIN, R. et al. Impaired glutathione synthesis in schizophrenia: convergent genetic and functional evidence. **Proc Natl Acad Sci U S A**, v. 104, n. 42, p. 16621-6, Oct 16 2007. ISSN 0027-8424 (Print)

0027-8424 (Linking). Disponível em: < <http://www.ncbi.nlm.nih.gov/pubmed/17921251> >.

HEADLEY, D. B.; WEINBERGER, N. M. Gamma-band activation predicts both associative memory and cortical plasticity. **J Neurosci**, v. 31, n. 36, p. 12748-58, Sep 7 2011. ISSN 1529-2401 (Electronic)

0270-6474 (Linking). Disponível em: < <http://www.ncbi.nlm.nih.gov/pubmed/21900554> >.

HEBB, D. O. **The organization of behavior**. Mahwah Lawrence Erlbaum Associates, 1949.

HITIRIS, N. et al. Mortality in epilepsy. **Epilepsy Behav**, v. 10, n. 3, p. 363-76, May 2007. ISSN 1525-5050 (Print)

1525-5050 (Linking). Disponível em: < <http://www.ncbi.nlm.nih.gov/pubmed/17337248> >.

HOMAYOUN, H.; MOGHADDAM, B. NMDA receptor hypofunction produces opposite effects on prefrontal cortex interneurons and pyramidal neurons. **J Neurosci**, v. 27, n. 43, p. 11496-500, Oct 24 2007. ISSN 1529-2401 (Electronic)

0270-6474 (Linking). Disponível em: < <http://www.ncbi.nlm.nih.gov/pubmed/17959792> >.

HONDO, H. et al. Effect of phencyclidine on dopamine release in the rat prefrontal cortex; an in vivo microdialysis study. **Brain Res**, v. 633, n. 1-2, p. 337-42, Jan 7 1994. ISSN 0006-8993 (Print)

0006-8993 (Linking). Disponível em: < <http://www.ncbi.nlm.nih.gov/pubmed/8137168> >.

ISHIKAWA, A. et al. Essential role of D1 but not D2 receptors in methamphetamine-induced impairment of long-term potentiation in hippocampal-prefrontal cortex pathway. **Eur J Neurosci**, v. 22, n. 7, p. 1713-9, Oct 2005. ISSN 0953-816X (Print)

0953-816X (Linking). Disponível em: < <http://www.ncbi.nlm.nih.gov/pubmed/16197511> >.

IZAKI, Y.; AKEMA, T. Gamma-band power elevation of prefrontal local field potential after posterior dorsal hippocampus-prefrontal long-term potentiation induction in anesthetized rats. **Exp Brain Res**, v. 184, n. 2, p. 249-53, Jan 2008. ISSN 1432-1106 (Electronic)

0014-4819 (Linking). Disponível em: < <http://www.ncbi.nlm.nih.gov/pubmed/17828391> >.

IZAKI, Y.; HORI, K.; NOMURA, M. Disturbance of rat lever-press learning by hippocampo-prefrontal disconnection. **Brain Res**, v. 860, n. 1-2, p. 199-202, Mar 31 2000. ISSN 0006-8993 (Print)

0006-8993 (Linking). Disponível em: < <http://www.ncbi.nlm.nih.gov/pubmed/10727644> >.

IZAKI, Y.; TAKITA, M.; AKEMA, T. Specific role of the posterior dorsal hippocampus-prefrontal cortex in short-term working memory. **Eur J Neurosci**, v. 27, n. 11, p. 3029-34, Jun 2008. ISSN 1460-9568 (Electronic)

0953-816X (Linking). Disponível em: < <http://www.ncbi.nlm.nih.gov/pubmed/18540879> >.

IZAKI, Y.; TAKITA, M.; NOMURA, M. Local properties of CA1 region in hippocampo-prefrontal synaptic plasticity in rats. **Neuroreport**, v. 13, n. 4, p. 469-72, Mar 25 2002. ISSN 0959-4965 (Print)

0959-4965 (Linking). Disponível em: < <http://www.ncbi.nlm.nih.gov/pubmed/11930163> >.

IZAKI, Y. et al. Differences between paired-pulse facilitation and long-term potentiation in the dorsal and ventral hippocampal CA1-prefrontal pathways of rats. **Brain Res**, v. 992, n. 1, p. 142-5, Nov 28 2003. ISSN 0006-8993 (Print)

0006-8993 (Linking). Disponível em: < <http://www.ncbi.nlm.nih.gov/pubmed/14604783> >.

JACKSON, M. E.; HOMAYOUN, H.; MOGHADDAM, B. NMDA receptor hypofunction produces concomitant firing rate potentiation and burst activity reduction in the prefrontal cortex. **Proc Natl Acad Sci U S A**, v. 101, n. 22, p. 8467-72, Jun 1 2004. ISSN 0027-8424 (Print)

0027-8424 (Linking). Disponível em: < <http://www.ncbi.nlm.nih.gov/pubmed/15159546> >.

JAVITT, D. C. Glutamate as a therapeutic target in psychiatric disorders. **Mol Psychiatry**, v. 9, n. 11, p. 984-97, 979, Nov 2004. ISSN 1359-4184 (Print)

1359-4184 (Linking). Disponível em: < <http://www.ncbi.nlm.nih.gov/pubmed/15278097> >.

_____. Glycine transport inhibitors and the treatment of schizophrenia. **Biol Psychiatry**, v. 63, n. 1, p. 6-8, Jan 1 2008. ISSN 1873-2402 (Electronic)

0006-3223 (Linking). Disponível em: < <http://www.ncbi.nlm.nih.gov/pubmed/18082555> >.

JAY, T. M.; BURETTE, F.; LAROCHE, S. NMDA receptor-dependent long-term potentiation in the hippocampal afferent fibre system to the prefrontal cortex in the rat. **Eur J Neurosci**, v. 7, n. 2, p. 247-50, Feb 1 1995. ISSN 0953-816X (Print)

0953-816X (Linking). Disponível em: < <http://www.ncbi.nlm.nih.gov/pubmed/7757261> >.

_____. Plasticity of the hippocampal-prefrontal cortex synapses. **J Physiol Paris**, v. 90, n. 5-6, p. 361-6, 1996. ISSN 0928-4257 (Print)

0928-4257 (Linking). Disponível em: < <http://www.ncbi.nlm.nih.gov/pubmed/9089514> >.

JAY, T. M. et al. Plasticity at hippocampal to prefrontal cortex synapses is impaired by loss of dopamine and stress: importance for psychiatric diseases. **Neurotox Res**, v. 6, n. 3, p. 233-44, 2004. ISSN 1029-8428 (Print)

1029-8428 (Linking). Disponível em: < <http://www.ncbi.nlm.nih.gov/pubmed/15325962> >.

JENSEN, O.; COLGIN, L. L. Cross-frequency coupling between neuronal oscillations. **Trends Cogn Sci**, v. 11, n. 7, p. 267-9, Jul 2007. ISSN 1364-6613 (Print)

1364-6613 (Linking). Disponível em: < <http://www.ncbi.nlm.nih.gov/pubmed/17548233> >.

JO, J. et al. Experience-dependent modification of mechanisms of long-term depression. **Nat Neurosci**, v. 9, n. 2, p. 170-2, Feb 2006. ISSN 1097-6256 (Print)

1097-6256 (Linking). Disponível em: < <http://www.ncbi.nlm.nih.gov/pubmed/16429132> >.

JODO, E. et al. Activation of medial prefrontal cortex by phencyclidine is mediated via a hippocampo-prefrontal pathway. **Cereb Cortex**, v. 15, n. 5, p. 663-9, May 2005. ISSN 1047-3211 (Print)

1047-3211 (Linking). Disponível em: < <http://www.ncbi.nlm.nih.gov/pubmed/15342431> >.

KAMIYAMA, H. et al. Mechanisms underlying ketamine-induced synaptic depression in rat hippocampus-medial prefrontal cortex pathway. **Neuroscience**, v. 177, p. 159-69, Mar 17 2011. ISSN 1873-7544 (Electronic)

0306-4522 (Linking). Disponível em: < <http://www.ncbi.nlm.nih.gov/pubmed/21163337> >.

KANDRATAVICIUS, L. et al. Differential aberrant sprouting in temporal lobe epilepsy with psychiatric co-morbidities. **Psychiatry Res**, v. 195, n. 3, p. 144-50, Feb 28 2012. ISSN 0165-1781 (Print)

0165-1781 (Linking). Disponível em: < <http://www.ncbi.nlm.nih.gov/pubmed/21741094> >.

KANDRATAVICIUS, L. et al. Psychiatric comorbidities in temporal lobe epilepsy: possible relationships between psychotic disorders and involvement of limbic circuits. **Rev Bras Psiquiatr**, v. 34, n. 4, p. 454-66, Dec 2012. ISSN 1809-452X (Electronic)

1516-4446 (Linking). Disponível em: < <http://www.ncbi.nlm.nih.gov/pubmed/23429818> >.

KANEMOTO, K.; TADOKORO, Y.; OSHIMA, T. Violence and postictal psychosis: a comparison of postictal psychosis, interictal psychosis, and postictal confusion. **Epilepsy Behav**, v. 19, n. 2, p. 162-6, Oct 2010. ISSN 1525-5069 (Electronic)

1525-5050 (Linking). Disponível em: < <http://www.ncbi.nlm.nih.gov/pubmed/20727827> >.

KANTROWITZ, J.; JAVITT, D. C. Glutamatergic transmission in schizophrenia: from basic research to clinical practice. **Curr Opin Psychiatry**, v. 25, n. 2, p. 96-102, Mar 2012. ISSN 1473-6578 (Electronic)

0951-7367 (Linking). Disponível em: < <http://www.ncbi.nlm.nih.gov/pubmed/22297716> >.

KAWASHIMA, H. et al. Cooperativity between hippocampal-prefrontal short-term plasticity through associative long-term potentiation. **Brain Res**, v. 1109, n. 1, p. 37-44, Sep 13 2006. ISSN 0006-8993 (Print)

0006-8993 (Linking). Disponível em: < <http://www.ncbi.nlm.nih.gov/pubmed/16859647> >.

KEIFER, J.; ZHENG, Z. AMPA receptor trafficking and learning. **Eur J Neurosci**, v. 32, n. 2, p. 269-77, Jul 2010. ISSN 1460-9568 (Electronic)

0953-816X (Linking). Disponível em: < <http://www.ncbi.nlm.nih.gov/pubmed/20646058> >.

KIRIHARA, K. et al. Hierarchical organization of gamma and theta oscillatory dynamics in schizophrenia. **Biol Psychiatry**, v. 71, n. 10, p. 873-80, May 15 2012. ISSN 1873-2402 (Electronic)

0006-3223 (Linking). Disponível em: < <http://www.ncbi.nlm.nih.gov/pubmed/22361076> >.

KISS, T.; HOFFMANN, W. E.; HAJOS, M. Delta oscillation and short-term plasticity in the rat medial prefrontal cortex: modelling NMDA hypofunction of schizophrenia. **Int J Neuropsychopharmacol**, v. 14, n. 1, p. 29-42, Feb 2011. ISSN 1469-5111 (Electronic)

1461-1457 (Linking). Disponível em: < <http://www.ncbi.nlm.nih.gov/pubmed/20334724> >.

KISS, T. et al. Role of Thalamic Projection in NMDA Receptor-Induced Disruption of Cortical Slow Oscillation and Short-Term Plasticity. **Front Psychiatry**, v. 2, p. 14, 2011. ISSN 1664-0640 (Electronic)

1664-0640 (Linking). Disponível em: < <http://www.ncbi.nlm.nih.gov/pubmed/21556284> >.

KOCSIS, B. et al. Impact of ketamine on neuronal network dynamics: translational modeling of schizophrenia-relevant deficits. **CNS Neurosci Ther**, v. 19, n. 6, p. 437-47, Jun 2013. ISSN 1755-5949 (Electronic)

1755-5930 (Linking). Disponível em: < <http://www.ncbi.nlm.nih.gov/pubmed/23611295> >.

KOZLOVSKY, N. et al. Reduced GSK-3beta mRNA levels in postmortem dorsolateral prefrontal cortex of schizophrenic patients. **J Neural Transm**, v. 111, n. 12, p. 1583-92, Dec 2004. ISSN 0300-9564 (Print)

0300-9564 (Linking). Disponível em: < <http://www.ncbi.nlm.nih.gov/pubmed/15565492> >.

KRYSTAL, J. H. et al. NMDA agonists and antagonists as probes of glutamatergic dysfunction and pharmacotherapies in neuropsychiatric disorders. **Harv Rev Psychiatry**, v. 7, n. 3, p. 125-43, Sep-Oct 1999. ISSN 1067-3229 (Print)

1067-3229 (Linking). Disponível em: < <http://www.ncbi.nlm.nih.gov/pubmed/10483932> >.

LAROCHE, S.; DAVIS, S.; JAY, T. M. Plasticity at hippocampal to prefrontal cortex synapses: dual roles in working memory and consolidation. **Hippocampus**, v. 10, n. 4, p. 438-46, 2000. ISSN 1050-9631 (Print)

1050-9631 (Linking). Disponível em: < <http://www.ncbi.nlm.nih.gov/pubmed/10985283> >.

LAROCHE, S.; JAY, T. M.; THIERRY, A. M. Long-term potentiation in the prefrontal cortex following stimulation of the hippocampal CA1/subicular region. **Neurosci Lett**, v. 114, n. 2, p. 184-90, Jul 3 1990. ISSN 0304-3940 (Print)

0304-3940 (Linking). Disponível em: < <http://www.ncbi.nlm.nih.gov/pubmed/2395531> >.

LAVIN, A.; GRACE, A. A. Stimulation of D1-type dopamine receptors enhances excitability in prefrontal cortical pyramidal neurons in a state-dependent manner. **Neuroscience**, v. 104, n. 2, p. 335-46, 2001. ISSN 0306-4522 (Print)

0306-4522 (Linking). Disponível em: < <http://www.ncbi.nlm.nih.gov/pubmed/11377838> >.

LEUNG, L. S.; MA, J.; MCLACHLAN, R. S. Behaviors induced or disrupted by complex partial seizures. **Neurosci Biobehav Rev**, v. 24, n. 7, p. 763-75, Sep 2000. ISSN 0149-7634 (Print)

0149-7634 (Linking). Disponível em: < <http://www.ncbi.nlm.nih.gov/pubmed/10974356> >.

LEWIS, D. A.; MOGHADDAM, B. Cognitive dysfunction in schizophrenia: convergence of gamma-aminobutyric acid and glutamate alterations. **Arch Neurol**, v. 63, n. 10, p. 1372-6, Oct 2006. ISSN 0003-9942 (Print)

0003-9942 (Linking). Disponível em: < <http://www.ncbi.nlm.nih.gov/pubmed/17030651> >.

LI, L. M.; SANDER, J. W. [National demonstration project on epilepsy in Brazil]. **Arq Neuropsiquiatr**, v. 61, n. 1, p. 153-6, Mar 2003. ISSN 0004-282X (Print)

0004-282X (Linking). Disponível em: < <http://www.ncbi.nlm.nih.gov/pubmed/12715043> >.

LIEBERMAN, J. A.; JAVITCH, J. A.; MOORE, H. Cholinergic agonists as novel treatments for schizophrenia: the promise of rational drug development for psychiatry. **Am J Psychiatry**, v. 165, n. 8, p. 931-6, Aug 2008. ISSN 1535-7228 (Electronic)

0002-953X (Linking). Disponível em: < <http://www.ncbi.nlm.nih.gov/pubmed/18676593> >.

LIPINA, T. et al. Modulators of the glycine site on NMDA receptors, D-serine and ALX 5407, display similar beneficial effects to clozapine in mouse models of schizophrenia. **Psychopharmacology (Berl)**, v. 179, n. 1, p. 54-67, Apr 2005. ISSN 0033-3158 (Print)

0033-3158 (Linking). Disponível em: < <http://www.ncbi.nlm.nih.gov/pubmed/15759151> >.

LISMAN, J. Excitation, inhibition, local oscillations, or large-scale loops: what causes the symptoms of schizophrenia? **Curr Opin Neurobiol**, v. 22, n. 3, p. 537-44, Jun 2012. ISSN 1873-6882 (Electronic)

0959-4388 (Linking). Disponível em: < <http://www.ncbi.nlm.nih.gov/pubmed/22079494> >.

LISMAN, J. E. et al. Circuit-based framework for understanding neurotransmitter and risk gene interactions in schizophrenia. **Trends Neurosci**, v. 31, n. 5, p. 234-42, May 2008. ISSN 0166-2236 (Print)

0166-2236 (Linking). Disponível em: < <http://www.ncbi.nlm.nih.gov/pubmed/18395805> >.

LODGE, D. J.; GRACE, A. A. Aberrant hippocampal activity underlies the dopamine dysregulation in an animal model of schizophrenia. **J Neurosci**, v. 27, n. 42, p. 11424-30, Oct 17 2007. ISSN 1529-2401 (Electronic)

0270-6474 (Linking). Disponível em: < <http://www.ncbi.nlm.nih.gov/pubmed/17942737> >.

LOPES AGUIAR, C. et al. Muscarinic acetylcholine neurotransmission enhances the late-phase of long-term potentiation in the hippocampal-prefrontal cortex pathway of rats in vivo: a possible involvement of monoaminergic systems. **Neuroscience**, v. 153, n. 4, p. 1309-19, Jun 2 2008. ISSN 0306-4522 (Print)

0306-4522 (Linking). Disponível em: < <http://www.ncbi.nlm.nih.gov/pubmed/18455317> >.

LOPES-AGUIAR, C. et al. NMDA receptor blockade impairs the muscarinic conversion of sub-threshold transient depression into long-lasting LTD in the hippocampus-prefrontal cortex pathway in vivo: correlation with gamma oscillations. **Neuropharmacology**, v. 65, p. 143-55, Feb 2013. ISSN 1873-7064 (Electronic)

0028-3908 (Linking). Disponível em: < <http://www.ncbi.nlm.nih.gov/pubmed/23022398> >.

LORRAIN, D. S. et al. Effects of ketamine and N-methyl-D-aspartate on glutamate and dopamine release in the rat prefrontal cortex: modulation by a group II selective metabotropic glutamate receptor agonist LY379268. **Neuroscience**, v. 117, n. 3, p. 697-706, 2003. ISSN 0306-4522 (Print)

0306-4522 (Linking). Disponível em: < <http://www.ncbi.nlm.nih.gov/pubmed/12617973> >.

LYNCH, M. A. Long-term potentiation and memory. **Physiol Rev**, v. 84, n. 1, p. 87-136, Jan 2004. ISSN 0031-9333 (Print)

0031-9333 (Linking). Disponível em: < <http://www.ncbi.nlm.nih.gov/pubmed/14715912> >.

MA, J.; BRUDZYNSKI, S. M.; LEUNG, L. W. Involvement of the nucleus accumbens-ventral pallidal pathway in postictal behavior induced by a hippocampal afterdischarge in rats. **Brain Res**, v. 739, n. 1-2, p. 26-35, Nov 11 1996. ISSN 0006-8993 (Print)

0006-8993 (Linking). Disponível em: < <http://www.ncbi.nlm.nih.gov/pubmed/8955921> >.

MA, J.; LEUNG, L. S. Schizophrenia-like behavioral changes after partial hippocampal kindling. **Brain Res**, v. 997, n. 1, p. 111-8, Jan 30 2004. ISSN 0006-8993 (Print)

0006-8993 (Linking). Disponível em: < <http://www.ncbi.nlm.nih.gov/pubmed/14715156> >.

_____. Kindled seizure in the prefrontal cortex activated behavioral hyperactivity and increase in accumbens gamma oscillations through the hippocampus. **Behav Brain Res**, v. 206, n. 1, p. 68-77, Jan 5 2010. ISSN 1872-7549 (Electronic)

0166-4328 (Linking). Disponível em: < <http://www.ncbi.nlm.nih.gov/pubmed/19744527> >.

MA, J.; LEUNG, L. W. Medial septum mediates the increase in post-ictal behaviors and hippocampal gamma waves after an electrically induced seizure. **Brain Res**, v. 833, n. 1, p. 51-7, Jun 26 1999. ISSN 0006-8993 (Print)

0006-8993 (Linking). Disponível em: < <http://www.ncbi.nlm.nih.gov/pubmed/10375676> >.

MALENKA, R. C.; BEAR, M. F. LTP and LTD: an embarrassment of riches. **Neuron**, v. 44, n. 1, p. 5-21, Sep 30 2004. ISSN 0896-6273 (Print)

0896-6273 (Linking). Disponível em: < <http://www.ncbi.nlm.nih.gov/pubmed/15450156> >.

MANAHAN-VAUGHAN, D. et al. A single application of MK801 causes symptoms of acute psychosis, deficits in spatial memory, and impairment of synaptic plasticity in rats. **Hippocampus**, v. 18, n. 2, p. 125-34, 2008. ISSN 1098-1063 (Electronic)

1050-9631 (Linking). Disponível em: < <http://www.ncbi.nlm.nih.gov/pubmed/17924525> >.

MANOACH, D. S. Prefrontal cortex dysfunction during working memory performance in schizophrenia: reconciling discrepant findings. **Schizophr Res**, v. 60, n. 2-3, p. 285-98, Apr 1 2003. ISSN 0920-9964 (Print). Disponível em: < <http://www.ncbi.nlm.nih.gov/pubmed/12591590> >.

MASSEY, P. V.; BASHIR, Z. I. Long-term depression: multiple forms and implications for brain function. **Trends Neurosci**, v. 30, n. 4, p. 176-84, Apr 2007. ISSN 0166-2236 (Print)

0166-2236 (Linking). Disponível em: < <http://www.ncbi.nlm.nih.gov/pubmed/17335914> >.

MASSI, L. et al. Temporal dynamics of parvalbumin-expressing axo-axonic and basket cells in the rat medial prefrontal cortex in vivo. **J Neurosci**, v. 32, n. 46, p. 16496-502, Nov 14 2012. ISSN 1529-2401 (Electronic)

0270-6474 (Linking). Disponível em: < <http://www.ncbi.nlm.nih.gov/pubmed/23152631> >.

MATSUMOTO, M. et al. Characterization of clozapine-induced changes in synaptic plasticity in the hippocampal-mPFC pathway of anesthetized rats. **Brain Res**, v. 1195, p. 50-5, Feb 21 2008. ISSN 0006-8993 (Print)

0006-8993 (Linking). Disponível em: < <http://www.ncbi.nlm.nih.gov/pubmed/18201687> >.

MCCRACKEN, C. B.; ROBERTS, D. C. A single evoked afterdischarge produces rapid time-dependent changes in connexin36 protein expression in adult rat dorsal hippocampus. **Neurosci Lett**, v. 405, n. 1-2, p. 84-8, Sep 11 2006. ISSN 0304-3940 (Print)

0304-3940 (Linking). Disponível em: < <http://www.ncbi.nlm.nih.gov/pubmed/16859830> >.

MCNALLY, J. M. et al. Complex receptor mediation of acute ketamine application on in vitro gamma oscillations in mouse prefrontal cortex: modeling gamma band oscillation abnormalities in schizophrenia. **Neuroscience**, v. 199, p. 51-63, Dec 29 2011. ISSN 1873-7544 (Electronic)

0306-4522 (Linking). Disponível em: < <http://www.ncbi.nlm.nih.gov/pubmed/22027237> >.

MEYER-LINDENBERG, A. S. et al. Regionally specific disturbance of dorsolateral prefrontal-hippocampal functional connectivity in schizophrenia. **Arch Gen Psychiatry**, v. 62, n. 4, p. 379-86, Apr 2005. ISSN 0003-990X (Print)

0003-990X (Linking). Disponível em: < <http://www.ncbi.nlm.nih.gov/pubmed/15809405> >.

MITCHELL, S. N. et al. Activation of the retrohippocampal region in the rat causes dopamine release in the nucleus accumbens: disruption by fornix section. **Eur J Pharmacol**, v. 407, n. 1-2, p. 131-8, Oct 27 2000. ISSN 0014-2999 (Print)

0014-2999 (Linking). Disponível em: < <http://www.ncbi.nlm.nih.gov/pubmed/11050300> >.

MOGHADDAM, B. et al. Activation of glutamatergic neurotransmission by ketamine: a novel step in the pathway from NMDA receptor blockade to dopaminergic and cognitive disruptions associated with the prefrontal cortex. **J Neurosci**, v. 17, n. 8, p. 2921-7, Apr 15 1997. ISSN 0270-6474 (Print)

0270-6474 (Linking). Disponível em: < <http://www.ncbi.nlm.nih.gov/pubmed/9092613> >.

MOGHADDAM, B.; JAVITT, D. From revolution to evolution: the glutamate hypothesis of schizophrenia and its implication for treatment. **Neuropsychopharmacology**, v. 37, n. 1, p. 4-15, Jan 2012. ISSN 1740-634X (Electronic)

0006-3223 (Linking). Disponível em: < <http://www.ncbi.nlm.nih.gov/pubmed/21956446> >.

MOLINA, L. A.; SKELIN, I.; GRUBER, A. J. Acute NMDA receptor antagonism disrupts synchronization of action potential firing in rat prefrontal cortex. **PLoS One**, v. 9, n. 1, p. e85842, 2014. ISSN 1932-6203 (Electronic)

1932-6203 (Linking). Disponível em: < <http://www.ncbi.nlm.nih.gov/pubmed/24465743> >.

NADRI, C.; KOZLOVSKY, N.; AGAM, G. [Schizophrenia, neurodevelopment and glycogen synthase kinase-3]. **Harefuah**, v. 142, n. 8-9, p. 636-42, 644, Sep 2003. ISSN 0017-7768 (Print)

0017-7768 (Linking). Disponível em: < <http://www.ncbi.nlm.nih.gov/pubmed/14518171> >.

NGUGI, A. K. et al. Estimation of the burden of active and life-time epilepsy: a meta-analytic approach. **Epilepsia**, v. 51, n. 5, p. 883-90, May 2010. ISSN 1528-1167 (Electronic)

0013-9580 (Linking). Disponível em: < <http://www.ncbi.nlm.nih.gov/pubmed/20067507> >.

NICOLL, R. A.; ROCHE, K. W. Long-term potentiation: peeling the onion. **Neuropharmacology**, v. 74, p. 18-22, Nov 2013. ISSN 1873-7064 (Electronic)

0028-3908 (Linking). Disponível em: < <http://www.ncbi.nlm.nih.gov/pubmed/23439383> >.

NISHIMURA, M.; SATO, K. Ketamine stereoselectively inhibits rat dopamine transporter. **Neurosci Lett**, v. 274, n. 2, p. 131-4, Oct 22 1999. ISSN 0304-3940 (Print)

0304-3940 (Linking). Disponível em: < <http://www.ncbi.nlm.nih.gov/pubmed/10553955> >.

OYE, I.; PAULSEN, O.; MAURSET, A. Effects of ketamine on sensory perception: evidence for a role of N-methyl-D-aspartate receptors. **J Pharmacol Exp Ther**, v. 260, n. 3, p. 1209-13, Mar 1992. ISSN 0022-3565 (Print)

0022-3565 (Linking). Disponível em: < <http://www.ncbi.nlm.nih.gov/pubmed/1312163> >.

PAXINOS, G.; WATSON, C. **The rat brain in stereotaxic coordinates**. 6th. Amsterdam ; Boston ;; Academic Press/Elsevier, 2007. ISBN 9780125476126 (spiral binding)

0125476124 (spiral binding)

9780123737212 (CD-ROM)

0123737214 (CD-ROM). Disponível em: < Publisher description

<http://www.loc.gov/catdir/enhancements/fy0745/2006937142-d.html> >.

PEINEAU, S. et al. The role of GSK-3 in synaptic plasticity. **Br J Pharmacol**, v. 153 Suppl 1, p. S428-37, Mar 2008. ISSN 0007-1188 (Print)

0007-1188 (Linking). Disponível em: < <http://www.ncbi.nlm.nih.gov/pubmed/18311157> >.

PEINEAU, S. et al. A systematic investigation of the protein kinases involved in NMDA receptor-dependent LTD: evidence for a role of GSK-3 but not other serine/threonine kinases. **Mol Brain**, v. 2, p. 22, 2009. ISSN 1756-6606 (Electronic)

1756-6606 (Linking). Disponível em: < <http://www.ncbi.nlm.nih.gov/pubmed/19583853> >.

PEINEAU, S. et al. LTP inhibits LTD in the hippocampus via regulation of GSK3beta. **Neuron**, v. 53, n. 5, p. 703-17, Mar 1 2007. ISSN 0896-6273 (Print)

0896-6273 (Linking). Disponível em: < <http://www.ncbi.nlm.nih.gov/pubmed/17329210> >.

PEREZ, S. M. et al. Hippocampal deep brain stimulation reverses physiological and behavioural deficits in a rodent model of schizophrenia. **Int J Neuropsychopharmacol**, v. 16, n. 6, p. 1331-9, Jul 2013. ISSN 1469-5111 (Electronic)

1461-1457 (Linking). Disponível em: < <http://www.ncbi.nlm.nih.gov/pubmed/23190686> >.

PHILPOT, B. D.; LIM, J. H.; BRUNJES, P. C. Activity-dependent regulation of calcium-binding proteins in the developing rat olfactory bulb. **J Comp Neurol**, v. 387, n. 1, p. 12-26, Oct 13 1997. ISSN 0021-9967 (Print)

0021-9967 (Linking). Disponível em: < <http://www.ncbi.nlm.nih.gov/pubmed/9331168> >.

PINAULT, D. N-methyl d-aspartate receptor antagonists ketamine and MK-801 induce wake-related aberrant gamma oscillations in the rat neocortex. **Biol Psychiatry**, v. 63, n. 8, p. 730-5, Apr 15 2008. ISSN 1873-2402 (Electronic)

0006-3223 (Linking). Disponível em: < <http://www.ncbi.nlm.nih.gov/pubmed/18022604> >.

PITTAU, F. et al. Patterns of altered functional connectivity in mesial temporal lobe epilepsy. **Epilepsia**, v. 53, n. 6, p. 1013-23, Jun 2012. ISSN 1528-1167 (Electronic)

0013-9580 (Linking). Disponível em: < <http://www.ncbi.nlm.nih.gov/pubmed/22578020> >.

POMAROL-CLOTET, E. et al. Failure to deactivate in the prefrontal cortex in schizophrenia: dysfunction of the default mode network? **Psychol Med**, v. 38, n. 8, p. 1185-93, Aug 2008. ISSN 0033-2917 (Print)

0033-2917 (Linking). Disponível em: < <http://www.ncbi.nlm.nih.gov/pubmed/18507885> >.

QUEIROZ, C. M. et al. Dynamics of evoked local field potentials in the hippocampus of epileptic rats with spontaneous seizures. **J Neurophysiol**, v. 101, n. 3, p. 1588-97, Mar 2009. ISSN 0022-3077 (Print)

0022-3077 (Linking). Disponível em: < <http://www.ncbi.nlm.nih.gov/pubmed/18842951> >.

ROBERTS, B. M. et al. Glycine transporter inhibition reverses ketamine-induced working memory deficits. **Neuroreport**, v. 21, n. 5, p. 390-4, Mar 31 2010. ISSN 1473-558X (Electronic)

0959-4965 (Linking). Disponível em: < <http://www.ncbi.nlm.nih.gov/pubmed/20186106> >.

ROH, M. S. et al. Haloperidol and clozapine differentially regulate signals upstream of glycogen synthase kinase 3 in the rat frontal cortex. **Exp Mol Med**, v. 39, n. 3, p. 353-60, Jun 30 2007. ISSN 1226-3613 (Print)

1226-3613 (Linking). Disponível em: < <http://www.ncbi.nlm.nih.gov/pubmed/17603289> >.

ROSSIGNOLI, M. T. **Estudo dos efeitos de antagonistas de receptor NMDA sobre a transmissão e plasticidade pré-sináptica na via CA1-CPFM e sua modulação pelo sistema endocanabinóide em ratos anestesiados in vivo** 2014. (Dissertação de mestrado). Faculdade de Medicina de Ribeirão Preto, Universidade de São Paulo

RUSHLOW, W. J. et al. Antipsychotics affect multiple calcium calmodulin dependent proteins. **Neuroscience**, v. 161, n. 3, p. 877-86, Jul 7 2009. ISSN 1873-7544 (Electronic)

0306-4522 (Linking). Disponível em: < <http://www.ncbi.nlm.nih.gov/pubmed/19289156> >.

SATHYASAIKUMAR, K. V. et al. Impaired kynurenine pathway metabolism in the prefrontal cortex of individuals with schizophrenia. **Schizophr Bull**, v. 37, n. 6, p. 1147-56, Nov 2011. ISSN 1745-1701 (Electronic)

0586-7614 (Linking). Disponível em: < <http://www.ncbi.nlm.nih.gov/pubmed/21036897> >.

SCHULMAN, J. J. et al. Imaging of thalamocortical dysrhythmia in neuropsychiatry. **Front Hum Neurosci**, v. 5, p. 69, 2011. ISSN 1662-5161 (Electronic)

1662-5161 (Linking). Disponível em: < <http://www.ncbi.nlm.nih.gov/pubmed/21863138> >.

SHIMAZAKI, T.; KAKU, A.; CHAKI, S. D-Serine and a glycine transporter-1 inhibitor enhance social memory in rats. **Psychopharmacology (Berl)**, v. 209, n. 3, p. 263-70, Apr 2010. ISSN 1432-2072 (Electronic)

0033-3158 (Linking). Disponível em: < <http://www.ncbi.nlm.nih.gov/pubmed/20198471> >.

SOMOGYI, P.; KLAUSBERGER, T. Defined types of cortical interneurone structure space and spike timing in the hippocampus. **J Physiol**, v. 562, n. Pt 1, p. 9-26, Jan 1 2005. ISSN 0022-3751 (Print)

0022-3751 (Linking). Disponível em: < <http://www.ncbi.nlm.nih.gov/pubmed/15539390> >.

SPENCER, S. S.; SPENCER, D. D. Entorhinal-hippocampal interactions in medial temporal lobe epilepsy. **Epilepsia**, v. 35, n. 4, p. 721-7, Jul-Aug 1994. ISSN 0013-9580 (Print)

0013-9580 (Linking). Disponível em: < <http://www.ncbi.nlm.nih.gov/pubmed/8082614> >.

SQUIRE, L. R.; STARK, C. E.; CLARK, R. E. The medial temporal lobe. **Annu Rev Neurosci**, v. 27, p. 279-306, 2004. ISSN 0147-006X (Print)

0147-006X (Linking). Disponível em: < <http://www.ncbi.nlm.nih.gov/pubmed/15217334> >.

STEFANELLO, S. et al. Psychiatric comorbidity and suicidal behavior in epilepsy: a community-based case-control study. **Epilepsia**, v. 51, n. 7, p. 1120-5, Jul 2010. ISSN 1528-1167 (Electronic)

0013-9580 (Linking). Disponível em: < <http://www.ncbi.nlm.nih.gov/pubmed/19889019> >.

STEVENS, J. R.; LIVERMORE, A., JR. Kindling of the mesolimbic dopamine system: animal model of psychosis. **Neurology**, v. 28, n. 1, p. 36-46, Jan 1978. ISSN 0028-3878 (Print)

0028-3878 (Linking). Disponível em: < <http://www.ncbi.nlm.nih.gov/pubmed/563537> >.

STRECKER, R. E.; MONETA, M. E. Electrical stimulation of the kindled hippocampus briefly increases extracellular dopamine in the nucleus accumbens. **Neurosci Lett**, v. 176, n. 2, p. 173-7, Aug 1 1994. ISSN 0304-3940 (Print)

0304-3940 (Linking). Disponível em: < <http://www.ncbi.nlm.nih.gov/pubmed/7830940> >.

SUTTON, L. P.; RUSHLOW, W. J. The effects of neuropsychiatric drugs on glycogen synthase kinase-3 signaling. **Neuroscience**, v. 199, p. 116-24, Dec 29 2011. ISSN 1873-7544 (Electronic)

0306-4522 (Linking). Disponível em: < <http://www.ncbi.nlm.nih.gov/pubmed/22001305> >.

SUZUKI, Y. et al. Acute administration of phencyclidine induces tonic activation of medial prefrontal cortex neurons in freely moving rats. **Neuroscience**, v. 114, n. 3, p. 769-79, 2002. ISSN 0306-4522 (Print)

0306-4522 (Linking). Disponível em: < <http://www.ncbi.nlm.nih.gov/pubmed/12220577> >.

TAKITA, M.; FUJIWARA, S. E.; IZAKI, Y. Functional structure of the intermediate and ventral hippocampo-prefrontal pathway in the prefrontal convergent system. **J Physiol Paris**, v. 107, n. 6, p. 441-7, Dec 2013. ISSN 1769-7115 (Electronic)

0928-4257 (Linking). Disponível em: < <http://www.ncbi.nlm.nih.gov/pubmed/23719128> >.

TAKITA, M. et al. Induction of stable long-term depression in vivo in the hippocampal-prefrontal cortex pathway. **Eur J Neurosci**, v. 11, n. 11, p. 4145-8, Nov 1999. ISSN 0953-816X (Print)

0953-816X (Linking). Disponível em: < <http://www.ncbi.nlm.nih.gov/pubmed/10583503> >.

TAKITA, M. et al. Synaptic plasticity dynamics in the hippocampal-prefrontal pathway in vivo. **Neuroreport**, v. 21, n. 1, p. 68-72, Jan 6 2010. ISSN 1473-558X (Electronic)

0959-4965 (Linking). Disponível em: < <http://www.ncbi.nlm.nih.gov/pubmed/19996810> >.

TELLEZ-ZENTENO, J. F. et al. Psychiatric comorbidity in epilepsy: a population-based analysis. **Epilepsia**, v. 48, n. 12, p. 2336-44, Dec 2007. ISSN 0013-9580 (Print)

0013-9580 (Linking). Disponível em: < <http://www.ncbi.nlm.nih.gov/pubmed/17662062> >.

TIERNEY, P. L. et al. Influence of the hippocampus on interneurons of the rat prefrontal cortex. **Eur J Neurosci**, v. 20, n. 2, p. 514-24, Jul 2004. ISSN 0953-816X (Print)

0953-816X (Linking). Disponível em: < <http://www.ncbi.nlm.nih.gov/pubmed/15233760> >.

TORT, A. B. et al. Measuring phase-amplitude coupling between neuronal oscillations of different frequencies. **J Neurophysiol**, v. 104, n. 2, p. 1195-210, Aug 2010. ISSN 1522-1598 (Electronic)

0022-3077 (Linking). Disponível em: < <http://www.ncbi.nlm.nih.gov/pubmed/20463205> >.

VERMA, A.; MOGHADDAM, B. NMDA receptor antagonists impair prefrontal cortex function as assessed via spatial delayed alternation performance in rats: modulation by dopamine. **J Neurosci**, v. 16, n. 1, p. 373-9, Jan 1996. ISSN 0270-6474 (Print)

0270-6474 (Linking). Disponível em: < <http://www.ncbi.nlm.nih.gov/pubmed/8613804> >.

VERTES, R. P. Interactions among the medial prefrontal cortex, hippocampus and midline thalamus in emotional and cognitive processing in the rat. **Neuroscience**, v. 142, n. 1, p. 1-20, Sep 29 2006. ISSN 0306-4522 (Print)

0306-4522 (Linking). Disponível em: < <http://www.ncbi.nlm.nih.gov/pubmed/16887277> >.

VOLLENWEIDER, F. X. et al. Differential psychopathology and patterns of cerebral glucose utilisation produced by (S)- and (R)-ketamine in healthy volunteers using positron emission tomography (PET). **Eur Neuropsychopharmacol**, v. 7, n. 1, p. 25-38, Feb 1997. ISSN 0924-977X (Print)

0924-977X (Linking). Disponível em: < <http://www.ncbi.nlm.nih.gov/pubmed/9088882> >.

WANG, G. W.; CAI, J. X. Disconnection of the hippocampal-prefrontal cortical circuits impairs spatial working memory performance in rats. **Behav Brain Res**, v. 175, n. 2, p. 329-36, Dec 15 2006. ISSN 0166-4328 (Print)

0166-4328 (Linking). Disponível em: < <http://www.ncbi.nlm.nih.gov/pubmed/17045348> >.

WANG, J. H.; KELLY, P. T. The balance between postsynaptic Ca(2+)-dependent protein kinase and phosphatase activities controlling synaptic strength. **Learn Mem**, v. 3, n. 2-3, p. 170-81, Sep-Oct 1996. ISSN 1072-0502 (Print)

1072-0502 (Linking). Disponível em: < <http://www.ncbi.nlm.nih.gov/pubmed/10456087> >.

WATANABE, T. et al. Kindling of the ventral tegmental area induces supersensitivity in the central dopamine system. **Brain Res**, v. 1003, n. 1-2, p. 194-8, Apr 2 2004. ISSN 0006-8993 (Print)

0006-8993 (Linking). Disponível em: < <http://www.ncbi.nlm.nih.gov/pubmed/15019580> >.

WELCH, P. D. The use of fast fourier transform for the stimation of power spectra: a method based on time averaging over short, modified periodograms. **IEEE Trans Audio and Eletroacoust**, v. 15, p. 70-73, 1967.

WHITFIELD-GABRIELI, S. et al. Hyperactivity and hyperconnectivity of the default network in schizophrenia and in first-degree relatives of persons with schizophrenia. **Proc Natl Acad Sci U S A**, v. 106, n. 4, p. 1279-84, Jan 27 2009. ISSN 1091-6490 (Electronic)

0027-8424 (Linking). Disponível em: < <http://www.ncbi.nlm.nih.gov/pubmed/19164577> >.

WOMELSDORF, T.; FRIES, P. Neuronal coherence during selective attentional processing and sensory-motor integration. **J Physiol Paris**, v. 100, n. 4, p. 182-93, Oct 2006. ISSN 0928-4257 (Print)

0928-4257 (Linking). Disponível em: < <http://www.ncbi.nlm.nih.gov/pubmed/17317118> >.

WOOD, J.; KIM, Y.; MOGHADDAM, B. Disruption of prefrontal cortex large scale neuronal activity by different classes of psychotomimetic drugs. **J Neurosci**, v. 32, n. 9, p. 3022-31, Feb 29 2012. ISSN 1529-2401 (Electronic)

0270-6474 (Linking). Disponível em: < <http://www.ncbi.nlm.nih.gov/pubmed/22378875> >.

YIZHAR, O. et al. Neocortical excitation/inhibition balance in information processing and social dysfunction. **Nature**, v. 477, n. 7363, p. 171-8, Sep 8 2011. ISSN 1476-4687 (Electronic)

0028-0836 (Linking). Disponível em: < <http://www.ncbi.nlm.nih.gov/pubmed/21796121> >.

ZENG, H. et al. Forebrain-specific calcineurin knockout selectively impairs bidirectional synaptic plasticity and working/episodic-like memory. **Cell**, v. 107, n. 5, p. 617-29, Nov 30 2001. ISSN 0092-8674 (Print)

0092-8674 (Linking). Disponível em: < <http://www.ncbi.nlm.nih.gov/pubmed/11733061> >.

ZHANG, Y. et al. NMDAR antagonist action in thalamus imposes delta oscillations on the hippocampus. **J Neurophysiol**, v. 107, n. 11, p. 3181-9, Jun 2012. ISSN 1522-1598 (Electronic)

0022-3077 (Linking). Disponível em: < <http://www.ncbi.nlm.nih.gov/pubmed/22423006> >.

ZHONG, P. et al. Serotonin facilitates long-term depression induction in prefrontal cortex via p38 MAPK/Rab5-mediated enhancement of AMPA receptor internalization. **J Physiol**, v. 586, n. Pt 18, p. 4465-79, Sep 15 2008. ISSN 1469-7793 (Electronic)

0022-3751 (Linking). Disponível em: < <http://www.ncbi.nlm.nih.gov/pubmed/18653660> >.

ANEXO 1



Contents lists available at SciVerse ScienceDirect

Neuropharmacology

journal homepage: www.elsevier.com/locate/neuropharm



Texto removido. Contém direitos autorais.

ANEXO 2

Comparative analysis of Ketamine S(+) and Ketamine racemate effects on hyperlocomotion and short-term synaptic plasticity disruption in the hippocampal-medial prefrontal cortex pathway *in vivo*

Rossignoli, M.T.¹; Lopes-Aguiar, C.¹; Bueno-Júnior, L.S.¹; Ruggiero, R.N.¹; Esteves, I. M.; Romcy-Pereira, R.N.² and Leite, J.P.¹

¹Dept. of Neuroscience and Behavioral Sciences, Ribeirão Preto School of Medicine, University of São Paulo, Ribeirão Preto – SP, Brazil.

²Brain Institute, Federal University of Rio Grande do Norte, Natal – RN, Brazil.

E-mails: rossignoli.mt@gmail.com; rnrpereira@gmail.com; jpleite@fmrp.usp.br



Introduction

Psychosis are frequently associated to cognitive dysfunction, such as disruption of working memory that recruits hippocampal-frontocortical circuits and is specially affected by GABA-glutamate imbalance. Subanesthetic doses of ketamine racemate (KET) or its optical isomer ketamine S(+) (KET S+) are used as experimental model of psychosis-based on hypofunction of NMDA receptor. Although less studied experimentally, KET S+ has a higher affinity for NMDA receptors and can better reproduce the psychotic-like symptoms than KET. These distinct effects of ketamine isomeric forms on NMDA receptors have been poorly understood.

Objective: to investigate the effects of KET and KET S+ on locomotor activity and presynaptic plasticity in the hippocampus CA1-medial prefrontal cortex (mPFC) pathway of rats *in vivo*.

Methods

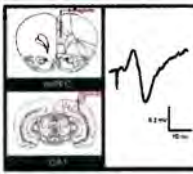
Animals: Male Wistar adults (300g-450g).

Non-competitive NMDA receptors antagonist Ketamine: KET, ketamine racemate; 12,5 mg/Kg i.p., in sterile saline (NaCl, 0.15M); KET S+, S(+)-Ketamine; 12,5mg/Kg, i.p., in sterile saline (NaCl, 0.15M).

Behavioral test: intact animals were placed in the open field for habituation and baseline (10min) and received KET, KET S+ or vehicle (VEH). After injections, locomotor behavior was recorded for 30 min.



Surgery: new groups of naive rats anesthetized with urethane (1–1.5g/Kg, i.p., in saline) under body control at 37 ± 0.5°C. Implantation of bipolar stimulation electrode in CA1 and recording electrodes in dorsal hippocampus and mPFC (teflon-coated tungsten wire; 60µm diameter).



Experimental design: new groups of naive urethane-anesthetized rats underwent stereotaxic surgery for electrode implants and subsequent recording of field post-synaptic potential (fPSPs) evoked by paired-pulse stimuli (inter-pulse interval=80ms) in CA1. After 90 min of baseline recordings, animals were treated with KET, KET S+ or VEH and monitored for additional 120min. fPSPs were digitized at 10KHz after band-pass filtering (0.3-3KHz) and quantified using LabChart software. In all experiments, the statistical analysis was performed using two-way ANOVA for repeated measures and Bonferroni post-hoc test.



Results

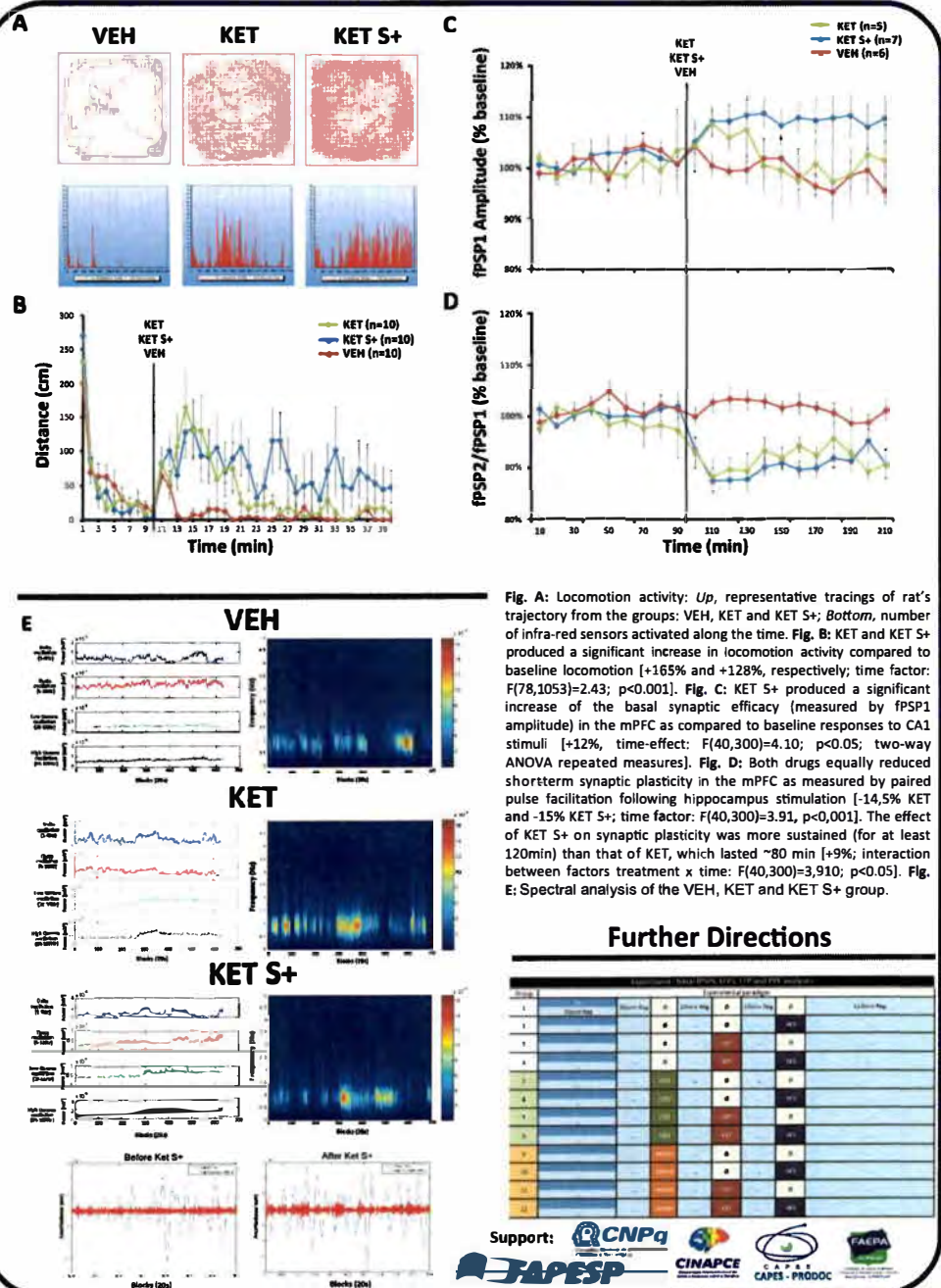


Fig. A: Locomotion activity: *Up*, representative tracings of rat's trajectory from the groups: VEH, KET and KET S+; *Bottom*, number of infra-red sensors activated along the time. **Fig. B:** KET and KET S+ produced a significant increase in locomotion activity compared to baseline locomotion [+165% and +128%, respectively; time factor: $F(78,1053)=2.43$; $p<0.001$]. **Fig. C:** KET S+ produced a significant increase of the basal synaptic efficacy (measured by fPSP1 amplitude) in the mPFC as compared to baseline responses to CA1 stimuli [+12%, time-effect: $F(40,300)=4.10$; $p<0.05$; two-way ANOVA repeated measures]. **Fig. D:** Both drugs equally reduced short-term synaptic plasticity in the mPFC as measured by paired pulse facilitation following hippocampus stimulation [-14,5% KET and -15% KET S+; time factor: $F(40,300)=3.91$, $p<0.001$]. The effect of KET S+ on synaptic plasticity was more sustained (for at least 120min) than that of KET, which lasted ~80 min [+9%; interaction between factors treatment x time: $F(40,300)=3.910$; $p<0.05$]. **Fig. E:** Spectral analysis of the VEH, KET and KET S+ group.

Further Directions

Group	Baseline	Baseline	Baseline	Baseline	Baseline	Baseline	Baseline	Baseline	Baseline
1									
2									
3									
4									
5									
6									
7									
8									
9									
10									



ANEXO 3

Scientific report

Grant: # 2012/07107-2 (Research Internships Abroad program)

São Paulo Research Foundation (FAPESP)

Title of the project: Episodic-like memory and oscillatory patterns in the hippocampus and medial prefrontal cortex of adult rats subjected to early-life seizures

Author: Cleiton Lopes Aguiar¹ (doctoral scholarship #2009/54410-0)

Supervisor of the doctoral scholarship: João Pereira Leite¹

Supervisor of the internship abroad: Marie Carlén²

¹Department of Neuroscience and Behavioral Sciences, Ribeirão Preto School of Medicine, University of São Paulo, Brazil

²Department of Neuroscience, Karolinska Institutet, Stockholm, Sweden

Table of Contents

1. Background	3
2. Original project summary	4
3. Scientific report summary	4
4. Introduction	5
4.1. Interneuron dysfunction as a shared biological substrate in epilepsy and schizophrenia	
4.2. Carlén's laboratory research background	
5. Initial project adjustments	7
6. Overall and specific objectives	8
6.1. Research objectives	
7. Subjects, materials and general methodologies	10
7.1. Subjects	
7.2. Viral injection	
7.3. Viral constructs and Cre-dependent gene expression	
8. Experiment I: Specific methods and preliminary findings	12
8.1. Electrophysiology and optical stimulation	
8.2. Spike sorting	
8.3. Examining gamma oscillations and spike-timing in the mPFC during urethane-induced UP- and-DOWN states	
8.4. Optogenetics: contextualization and strategies to detect and remove light-artifacts	
8.5. Optogenetics validation: Detection of light-induced inhibition and activation	
8.6. Examining the role of NMDARs in cortical PV+ cells during evoked gamma oscillations by optogenetics	
8.7. Classification of units in putative FS and RS cells: waveforms, interspike interval histograms and optogenetic effects	
9. Experiment II: Rationale, specific methods and preliminary findings	20
10. Concluding remarks and acknowledgements	23
11. References	24
12. Figure legends	26
14. Table 1: summary of all acute recordings	31
15. Table 2: library of all sorted units	35
16. Figures	38

1. Background

Our research group, heading by Prof. João Pereira Leite (University of São Paulo – Brazil), has been profoundly interested in the underlying mechanisms of epileptogenesis, cognitive deficits and psychiatric comorbidities in temporal lobe epilepsy in both clinical (Kandratavicius et al. 2014, 2013 Mathern et al. 1997) and experimental (Lopes-Aguiar et al., 2013, Bueno-Junior et al., 2012; Lopes-Aguiar et al., 2008; Leite et al., 1990) perspectives. The original project was designed to extend our knowledge in this field by examining the relationship between oscillatory activity in hippocampus and mPFC and cognition in a model of developmental seizure. We expected to take advantage of the Morris's group expertise in behavior in order to refine our strategies towards a better comprehension of cognitive deficits in epilepsy. However, I have had to change my supervisor of the internship abroad due to problems with tuition fees, which was raised on very strict rules imposed by the United Kingdom Border Agency and on a policy of the University of Edinburgh based on charging in a very expensive way non-European students. Generally speaking, one of the most important differences between doing an internship abroad in UK compared to Sweden is that the first one does not allow PhD students develop their internship as a visiting researcher. Thus, they obligate us to enroll in a graduate program and, consequently, to pay Tuition Fees. In my case, even with guarantee of salaries from FAPESP, I was charged in around 15 thousand pounds for a year of internship. Profs. Leite, Morris and I have exhausted the possibilities to solve this situation and decided to decline from the fellowship, after months of e-mails exchange. However, as I had already changed a lot of my PhD schedule to go abroad, I considered changing the foreign supervisor, instead of just declining the fellowship. Fortunately, I did receive an immediate positive reply after an e-mail sent to Prof. Marie Carlén, at Karolinska Institutet.

Although Prof. Carlén is not mainly focused on epilepsy, Prof. Leite and I agreed her research focus was still fitting very well to the main objective of the project, namely: probing causal links between oscillatory patterns and cognition. Indeed, Prof. Carlén has been using cutting-edge tools in neuroscience to investigate the role of parvalbumin positive (PV+) interneurons in cognition and behavior during normal and pathological conditions, which is increasingly becoming a key topic in epilepsy as well. For instance, it has been shown that fast spiking (FS) interneurons control seizure propagation in the cortex (Schwaller et al. 2004) and that the absence of cortical PV+ facilitates hypersynchrony in the hippocampus (Cammarota et al. 2013). Therefore, we decided to move towards an integration of the original project with her scientific interests and, therefore, perform a new project. This document reports my

scientific research performed during an internship abroad from January to December of 2013 under Prof. Marie Carlén supervision at Karolinska Institutet.

2. Original project summary

Several clinical and experimental studies have provided convincing evidence showing that early-life seizure (ELS) events trigger late spontaneous seizures and/or cognitive deficits; however, the underlying mechanism of such late changes remains unclear. Neuronal cell loss and mossy fibre sprouting may be absent in the presence of later seizures and cognitive deficits. On the other hand, inflammatory process associated to microglia over-activation, besides plasticity-related events at a molecular/cellular level, usually occurs not only in the hippocampus but probably also in extra-limbic circuits. One possibility to probe neuronal plasticity on the network level *in vivo* is quantifying oscillatory activity patterns of local field potentials (LFPs). Therefore, further studies are required using freely moving electrophysiological recordings throughout an animal's life and attendant memory tasks in order to dissociate different phases and facets of the episodic-like memory processing. In this sense, the event arena paradigm represents an opportunity to investigate the effect of ELS into adulthood, specifically with respect to (1) the temporal dynamics of systems memory consolidation, and (2) the hippocampus/medial prefrontal cortex (mPFC) encoding responsible for enabling relevant new paired associates (PA; flavour/place) to be assimilated into an original schema. Therefore, the aim of the present project is, in adult animals previously subjected to ELS, to investigate the relationship between oscillatory activity in hippocampus and mPFC with the cognitive performance of an episodic-like memory task. In particular, we aim to verify whether the inhibition of ELS-associated inflammation process by minocycline treatment attenuates the later oscillatory effects, likewise later learning ability impairments in the event-arena. Rats will be subjected to ELS induction by Li-PILO at P12 and seven additional daily injections of minocycline. Control groups will be treated only with its drugs vehicles. Forty-eight days after ELS, electrodes in the mPFC and in CA1 of the hippocampus will be stereotaxically implanted under anaesthesia. Rats will be subjected to the event arena task, LFPs will be recorded daily using a telemetry system and eventual cellular loss and changes in microglia will be examined.

3. Scientific report summary

Perturbed excitatory-inhibitory balance occurs in multiple psychiatric and neurological conditions and might be a critical link between schizophrenia positive and negative symptoms, aberrant neural oscillatory activity, cognitive deficits and psychiatric comorbidities in epilepsy. Adult rats previously subjected to early-life seizures (ELS) display (1) enhancement of basal gamma oscillations, (2) down-regulation of NR1 and NR2B sub-units of NMDA receptors in the hippocampus, (3) reduction of parvalbumin (PV) immunoreactivity in the hippocampus and (4) impairment in short-term but not spatial memory. Thus, supported by prior findings, we assumed that the mice lacking the NMDAR subunit NR1 selectively in PV-expressing cells (PV-Cre-NR1f/f) is a suitable model to probe the mechanisms of excitatory/inhibitory disturbances and its impact in cognition and cortical processing. Recently, Carlén's group showed that loss of NMDAR-mediated drive of PV interneurons results in cognitive deficits and changes in network activities highly relevant to schizophrenia symptomatology. Importantly, BDNF also has been associated with the pathophysiology of schizophrenia. It has been shown that BDNF receptor (trkB)-signaling in PV interneurons is

critical for network synchronization in the gamma-band in hippocampus, but the role of *trkB* signaling in neuronal network activities at large is unknown. Therefore, in the *experiment I*, we aimed to investigate the role of NMDAR specifically in PV+ neurons during basal and optogenetically-evoked gamma oscillations in the mPFC. In the *experiment II*, we sought to probe the importance of *trkB* signaling specifically in PV+ interneurons in normal cognitive and emotional processes. PV-Cre or PV-Cre-NR1f/f mice were injected with the following vectors: AAV2-DIO-ChR2-mCherry (*Exp.I*), AAV5-DIO-TrkB.T1-mCherry (*Exp.II*) or AAV5-DIO-EYFP (*control*). Four to twelve weeks later, the animals were submitted to electrophysiological recordings with light-stimulation under urethane (*Exp.I*) or to behavioral battery (*Exp.II*). Our preliminary findings suggest that deletion of NR1 subunit in the PV+ cells is associated to higher power in theta and a trend towards higher power in beta and low-gamma in the mPFC. Also, we successfully demonstrated that photostimulation for activation of ChR2-expressing PV+ neurons also imposes transitory decrease in the firing rate of nearby neurons and preferentially enhances gamma oscillations in the mPFC. Finally, BDNF-TrkB signaling disruption specifically in PV+ interneurons of mPFC seems to be sufficient to perturb emotional processing in mice.

4. Introduction

4.1. Interneuron dysfunction as a shared biological substrate in epilepsy and schizophrenia

Cognitive deficits and psychiatry comorbidities are potential major sources of disability in children and adults with epilepsy (for a review, see Lin et al. 2012). Several clinical studies have provided evidence that early-life seizure (ELS) events trigger late spontaneous seizures and cognitive deficits, and seem to increase the risk for development of psychiatry comorbidities. For instance, a history of both febrile seizures and epilepsy is associated with a 2-fold higher risk of schizophrenia as compared with people with no such history (Vestergaard et al. 2005). Experimental studies have shown that adult rodents previously subjected to ELS exhibit: (1) enhancement of basal gamma oscillations and disruption of theta (4 – 10Hz) and gamma (30 – 80 Hz) coherence between CA1 subfield of hippocampus and medial prefrontal cortex (mPFC) (Kleen et al. 2011), (2) down-regulation of NR1 and NR2B sub-units of N-methyl-D-aspartate receptor (NMDAR) in the hippocampus (Saghyan et al. 2008), (3) reduction of parvalbumin (PV) immunoreactivity in the hippocampus (Gill et al. 2010), (4) impairment in short-term but not spatial memory (Cornejo et al. 2010) and finally, (5) a long-lasting auditory gating deficit (Tsai et al. 2012).

All of the above findings on different levels involve major players and processes important to the excitatory/inhibitory (E/I) balance in the brain. Improper inhibition, and hence a perturbed excitatory-inhibitory balance, exists in multiple psychiatric conditions, including autism, Angelman's, Down's, Rett's and Fragile X syndrome, respectively, among others (Marín, 2012). In essence, the *linkage of interneuron dysfunction to cognitive impairment* is starting to be appreciated. It is therefore critical to better understand the

interplay between excitation and inhibition in order to link seizures, aberrant neural oscillatory activity, cognitive deficits and psychiatric comorbidities in epilepsy.

4.2. Carlén's laboratory research background

The disruption of the E/I balance in the brain by acute treatment with non-competitive NMDAR antagonists (e.g. MK-801, ketamine and phencyclidine) is considered a useful pharmacological model of schizophrenia as administration of this class of drugs reproduces both positive and negative as well as cognitive symptoms displayed in the disorder (e.g. stereotyped behaviors, working memory deficits, sensory motor gating disruption as well as emotional and social impairments (for a review, Moghaddam and Javitt 2012). The NMDAR antagonists are suggested to cause opposite effects on GABAergic inhibitory interneurons versus pyramidal excitatory neurons. In accordance with this idea, it has been demonstrated that systemic injection of MK-801 impacts the activity in the medial prefrontal cortex (mPFC) by enhancing the firing rate of pyramidal neurons while decreasing the activity of putative fast-spiking (FS) interneurons (Homayoun and Moghaddam 2007). NMDARs antagonists also trigger aberrant gamma oscillations associated to stereotypy and hyperlocomotion, depending on the dose. Besides, long-term dysfunctions induced by NMDAR antagonists (hours to days after treatment) on sensory motor gating disruption, social interaction, emotional memory and working memory have been correlated to disruption of gamma oscillations (Moghaddam and Javitt 2012).

Gamma oscillations are strongly related to cognitive processing in mammals. As mentioned before, its impairment is mainly raised on E/I unbalance and have been considered a hallmark of the Schizophrenia's pathophysiology. For instance, psychotic episodes are usually associated with aberrant enhancement of gamma oscillations. On the other hand, negative and/or cognitive deficits are correlated with its reduced elicitation (Basar-Eroglu et al. 2007; Hanslmayr et al. 2012). A number of studies with pharmacological models of schizophrenia have been successfully reproducing some of these oscillatory abnormalities (Rotaru et al. 2012). However, is still poorly understood how specific sub-types of interneurons could be involved in these gamma-related dysfunctions (Nakazawa et al. 2012).

When induced by driving cortical FS cells with optogenetics, gamma oscillations promote higher neocortical signal transmission (Sohal et al. 2009) and improve sensorial processing in PV-Cre mice (Cardin et al. 2010). In both studies, cell type selectivity was obtained using Cre-dependent expression of the light-activated channel Channelrhodopsin-2 (ChR2). Carlén et al. (2012) addressed the hypothesis of NMDAR hypofunction in schizophrenia by studying mice lacking the NMDAR subunit NR1 selectively in PV-expressing

cells (PV-Cre/NR1f/f transgenic mice: PV-Cre-NR1f/f mice). In summary, these animals displayed: (1) enhanced baseline cortical gamma oscillations, (2) decreased induction of gamma by optogenetic drive of PV interneurons or (3) by systemic administration of the NMDAR antagonist MK-801, and (4) selective working memory impairments for short intervals. According to the authors, these findings could reflect a general decrease in excitability of PV interneurons caused by diminished glutamatergic drive. One of the many questions that remains to be addressed is whether the mPFC of PV-Cre-NR1f/f mice, a region critically involved in psychiatry disorders, also display similar impairments in the dynamics of basal and optogenetically-evoked gamma oscillations, as previously demonstrated in the barrel cortex by Carlén et al. (2012).

5. Initial project adjustments

Therefore, during my internship abroad we decided:

(A) **Replace the ELS model by the transgenic PV-Cre-NR1f/f mice.** Adult rodents previously subjected to ELS display (1) enhancement of basal gamma oscillations (Kleen et al. 2011), (2) down-regulation of NR1 and NR2B sub-units of NMDA receptors in the hippocampus (Saghyan et al. 2008), (3) reduction of parvalbumin (PV) immunoreactivity in the hippocampus (Gill et al. 2010) and (4) impairment in short-term but not spatial memory (Cornejo et al. 2010). Thus, supported by prior findings (Korotkova et al., 2010, Carlén et al. 2012), we assumed the PV-Cre-NR1f/f mouse is a suitable model in this context of probing mechanisms of excitatory/inhibitory disturbances and its impact in cognition (see also session 3.2). We also have investigated behavior and electrophysiological alterations of PV-Cre-NR1f/f mice compared with its littermates (NR1f/f mice) during normal conditions and under ketamine S+ intraperitoneal injection (12.5 mg/Kg in sterile saline 0.9%). I received the ketamine from Prof. Leite's laboratory in order to perform experiments with exactly the same drug and dose I used during my prior experiments in Brazil. Therefore, we hopefully will be able to connect both results, from Leite's and Carlen's groups. The data analysis is still ongoing and will be part of my PhD thesis.

(B) **Replace the chronic electrophysiological recordings of local field potentials in ELS rats by acute recordings with silicon probes associated to optogenetic stimulation in PV-Cre and PV-Cre-NR1f/f mice.** We aimed to investigate the role of NMDAR specifically in PV+ neurons during basal and evoked gamma oscillations in the mPFC. Performing these experiments was a unique opportunity to improve my skills in unit recordings and data analysis, besides stay in touch with the state-of-the-art optogenetic tools. Furthermore, it worked as a concrete first step towards setting up optogenetics at Leite's group – USP-

RP/Brazil, in collaboration with my co-supervisor Prof. Rodrigo Romcy-Pereira – Brain Institute – Natal/Brazil. For this, at the end of my internship abroad, I have acquired a system for optical stimulation (Plexon LED system) with my technical reserve and took advantage of the expertise of my colleagues in the laboratory of Prof. Carlén to learn how to set up and handle the system during electrophysiological experiments. Therefore, during the development of my PhD project in Brazil (FAPESP #2009/54410-0), I will be able to set up this system at Prof. Leite's laboratory, where they have already obtained an acquisition system for multiunit recordings from the same company (Plexon Inc.).

(C) Supplement the project with a new set of experiments to probe the specific role of the brain-derived neurotrophic factor (BDNF)/ tyrosine receptor kinase B (trkB) signaling in PV+ cells during emotional and cognitive processes. The BDNF is preferentially secreted from glutamatergic neurons while its receptor trkB is expressed in both glutamatergic and GABA-ergic neurons. Among the cortical GABA-ergic neurons, the PV interneurons express trkB abundantly (Cellerino et al. 1996). Importantly, BDNF/trkB signaling disruptions has been associated with the pathophysiology of schizophrenia (Wong et al. 2013) and it has been shown that trkB-signaling in PV interneurons is critical for network synchronization in the gamma-band in hippocampus (Zheng et al. 2011), which make it a very attractive target to probe the relationship between cognitive deficits and brain oscillations abnormalities. **Therefore, we aimed to investigate the importance of trkB signaling specifically in PV+ interneurons in normal cortical circuit functions and cognition.** The methods and some preliminary findings regarding this project are described below. This project has been implemented in collaboration with Nicolas Guyon, a PhD student from Carlén's lab. As reported below, we quickly achieved a promising body of data in the first set of animals we studied, which opened new perspectives to further investigate the relationship between BDNF signaling, PV neurons, behavior and (possibly) gamma oscillations in normal and in pathological conditions. We recently submitted an abstract to 9th FENS (Federation of European Neuroscience Societies) Forum of Neuroscience 2014 with our preliminary data (please find attached).

6. Overall and specific objectives

Our overall objective is to examine how different E/I balance disruptions impact cognition and neural activity in mPFC. Particularly, we aimed to further investigate the specific role of PV+ interneurons and its NMDA and trkB receptors in cognition and mPFC activity. To perturb the brain excitatory/inhibitory balance we took advantage of transgenic animals (PV-Cre and PV-Cre-NR1f/f mice), optogenetics and electrophysiological approach (FS interneurons

driving in the mPFC by optogenetics and spike recordings with silicon probes) and a viral-vector-based strategy to disrupt BDNF/trkB signaling. Cognition will be explored by studying: (1) social interaction, (2) locomotion, (3) recognition memory and (4) working memory.

6.1 Research objectives

Experiment I: Investigation of UP-and-DOWN state and gamma oscillations in the medial prefrontal cortex of urethane-anesthetized mice lacking NMDA receptors in parvalbumin neurons

(I) In order to test (1) whether the UP-and-DOWN state and synchrony between LFPs and spikes require intact function of NMDAR on PV-interneurons and (2) whether the previously described enhancement of basal theta and gamma oscillations in barrel cortex (Carlén et al, 2012) and hippocampus (Korotkova et al., 2010) also can be found in the mPFC, we performed inter-groups comparisons for cortical LFPs and spike-timing during baseline (light-off) of PV-Cre and PV-Cre-NR1f/f mice.

(II) In order to check for potential light-induced artifacts in the LFPs, we performed intra-group comparisons for cortical LFPs and spike-timing immediately before and during optical stimulation in the mPFC of control subjects (PV-Cre animals injected with AAV5-EF1a-DIO-EYFP in the mPFC);

(III) In order to check for evoked gamma oscillations and modulation of spikes firing rate in the mPFC, we performed intra-group comparisons for cortical LFPs and spikes immediately before and during optical stimulation in the mPFC of PV-Cre and PV-Cre-NR1f/f experimental subjects (PV-Cre animals injected with AAV2-EF1a-DIO-ChR2-mCherry in the mPFC);

Experimental approach II: Study of the role of BDNF-trkB signaling in cortical parvalbumin interneurons during cognitive and emotional processes

Research objectives:

(I) To investigate behavioral alterations induced by BDNF-trkB signaling disruption in the medial prefrontal cortex PV+ cells of mice, we performed inter-group comparisons (between groups injected with AAV5-DIO-trkb.T1-mCherry or AAV5-DIO-EYFP) for social aggression, novel object recognition, elevated plus maze, open field and fear conditioning.

7. Subjects, materials and general methodologies

7.1. Subjects

All procedures and experiments were approved by the local animal ethics committees of Stockholm North and Karolinska Institutet in Sweden. To generate mice lacking NMDAR specifically in PV interneurons (PV-Cre-NR1f/f mice) PV-Cre⁺ knock-in mice were crossed to mice carrying 'floxed' NR1 alleles (Carlén et al. 2012). The *experiment I* was executed in adult PV-Cre^{+/+}NR1f/f (females; n=3) and PV-Cre +/- mice: females (n=14) and males (n=9) of 15–20 weeks age. We also performed two pilot experiments with an adult male Galanin-Cre (Gal-Cre) mouse and an adult male C57BL/6N mouse. The table 1 summarizes the use of the animals along the validation and execution of the experiment I. In the *experiment II* we studied male adults C57BL/6N mice (n=10) to set up and validate the behavior tasks and then performed the main experiments with adult male PV-Cre +/- mice (n=8) of 15–20 weeks age. For the resident-intruder test, we also used male juvenile (3-4 weeks) PV-Cre +/- mice as an intruder and the abovementioned adult PV-Cre mice as the resident. C57BL/6N mice were purchased from Charles River and habituated to the new environment for a minimum of 1 week before any experimental manipulation. PV-Cre^{+/+}NR1f/f and NR1f/f mice were bred at the Karolinska Institute, Sweden.

Animals were housed in groups (3–5 mice/cage) using Makrolon type III cages, under standardized conditions with a 12-hour light-dark cycle (light 7:00am), stable temperature (20±1°C) and humidity (40 to 50%) with access to food and water ad libitum.

7.2. Viral injection

Initially, the micropipette (graduated borosilicate glass capillary; Wiretrol I, Drummond; Calibrated micropipette, 10µl size, Fisher Scientific) was filled with mineral oil and fixed into the Quintessential Stereotaxic Injector (Stoelting, Wood Dale, IL). Then, we filled the tip of the micropipette with 6µL of desired virus (titer ~ 10¹²) dyed with *Fast Green* 2.5% (Electron Microscopy Sciences). The animal was anesthetized initially with isoflurane administered in an induction chamber or small container with isoflurane vaporizer with O₂ at ~0.5 to 1 L/min. Then, the animal was placed in the stereotaxic apparatus with the nose in the anesthesia head-holder with isoflurane at 2% on a heating blanket (37 °C) in a bio-safety cabinet class 2 with sterile surgical environment. The animal's reflexes were tested and the isoflurane level was reduced to 1 or 1.5% over the course of the surgery. The animal was treated with analgesic buprenorphine (0.2 mg/kg) before the incision and the eyes were covered with eye lubricant (Viscotears, Novartis). The scalp was shaved with hair trimmers and lidocaine 1% was injected subcutaneously. Using a fresh scalpel blade, a single incision

through the skin was made. The connective tissue around the skull was gently removed as needed for clear viewing of the bregma.

The craniotomies and targeting was performed using the following stereotaxic coordinates: (A) Experiment I: AP: 1.8mm, ML: +0.3mm, DV: -1.4mm (prelimbic mPFC; unilateral); (B) Experiment II: AP: 1.8mm, ML: ± 0.3 mm, DV: -1.6mm (infralimbic mPFC; unilateral). During the craniotomy, we stopped when the drill bit reached the bottom of the skull. The total diameter of the burr hole was rarely larger than the diameter of the drill bit (around 100 μ m). Then, using a syringe needle, we removed the remaining skull so that the dura could be seen through a stereomicroscope and carefully opened. Sterile saline 0.9% was regularly applied over the skull while drilling to remove bone dust and control heat generation. Subsequently, the pipette was lowered until the tip touches the exposed dura. This point was set as the 'zero' in the DV axis. Then, the pipette tip was lowered through the dura until the target (prelimbic region of the mPFC). Then, 0.4 μ L/hemisphere of the virus of interest was injected at a rate of 0.1 μ L/min. When the injection was completed, we kept the glass pipette inside the brain for additional 10 minutes before beginning to retract it. Using the *Fast Green* as a marker we were able to ensure that the correct volume of virus was expelled through the pipette. At the end of the procedure, the edges of the skin were pulled together and we applied small amounts of cyanoacrylate glue (Vetbond Tissue Adhesive, Henry Schein) to seal. The animal was monitored until be completely recovered from the anesthesia.

7.3. Viral constructs and Cre-dependent gene expression

In the Experiment I we performed unilateral injections of the vector AAV2-DIO-ChR2-mCherry, which gives Cre-dependent and cell-type-specific expression of light-activated channels *in vivo*. The viral vector AAV2-DIO-ChR2-mCherry carries an inverted version of ChR2 fused to the fluorescent marker mCherry. This strategy prevents ChR2 from being expressed in the absence of Cre. In the presence of Cre, ChR2-mCherry is inverted into the sense direction and expressed from the EF-1a (EEF1A1) promoter (**fig. 1e**; Cardin et al. 2009, Carlén et al. 2010). In the Experiment 2 we performed bilateral injections of the vector AAV5-DIO-TrkB.T1-mCherry. Control animals for both experiments received a vector carrying only the fluorescent marker EYFP: AAV5-DIO-EYFP.

Four to twelve weeks after virus injection, mice were transcardially perfused with phosphate-buffered saline (PBS, pH 7.4) followed by 4% formaldehyde in PB, and brains were post-fixed overnight at 4°C. Free floating sections (40 μ m) were cut using a vibratome (Leica VT100) and mounted on glass slides and coverslipped for virus expressing examination. PV staining was performed in two animals (one each experiment) to evaluate the cell-type

specific expression of ChR2-mCherry and TrkB.T1-Cherry. For this, 40µm sections were incubated with blocking solution (10% donkey serum in TBS 1x with 0.3% Triton) for 1 h at room temperature, and then incubated at room temperature over night with primary antibody (PV25 rabbit: rabbit polyclonal anti-PV (PV25, Swant) at a dilution of 1:1000) diluted in blocking solution. Next, we stained the sections with secondary antibody (Alexa Fluor® 488 anti rabbit (1:500); Jackson Immuno Research) after extensive washing in PBS. Images were captured with a fluorescent microscope (Leica DM6000B) at 10 or 20x magnification.

The **figure 1** illustrates a strong label with mCherry suggesting robust expression of ChR2 in three animals from the PV-Cre group (**fig.1a**, first row of images) and three animals from the PV-Cre-Nr1f/f group (**fig.1b**, second row of images) with a 10x zoom sample to demonstrate a proper transfection regarding spread and number of cell bodies labeled with mCherry (**fig.1d**). The previously described high cell-specificity of ChR2 expression conferred by the DIO construct can be observed in the in the **fig.1f**, where immunohistochemistry confirmed that more than 95% of mCherry labeled cells expressed PV. We observed a good gene expression in the PV-Cre animals injected with the control virus (**fig.1c**, first two images in the third row). The same pattern of expression can be observed in the PV-Cre animals bilaterally injected with the vector AAV5-DIO-TrkB.T1-mCherry (**fig.2a**) or its controls (**fig.2b**). Immunohistochemistry from one representative animal also indicate high cell-specificity of the TrkB.T1-mCherry expression (**fig.2c**).

8. Experiment I: Specific methods and preliminary findings

8.1. Electrophysiology and optical stimulation

Six to twelve weeks after the virus injection, the subjects were anesthetized with urethane (1.1g/Kg in sterile saline 0.9%, i.p.) and fixed in the stereotaxic apparatus with the nose in the anesthesia head-holder (isoflurane at 0.25%) on a heating blanket with feedback loop able to maintain the body temperature at $37\pm 0.5^{\circ}\text{C}$ (Harvard Apparatus). Using the initial burr hole and the above-described coordinates we made a new craniotomy over the mPFC, large enough to allow positioning of both optical fiber and silicon probe (*A4x2-tet-5mm-150-200-312-A32 Neuronexus*; **fig. 3b**), which was coupled to an adapter for connecting 32 channel headstage preamplifier; Neuralynx;). Then, dura was carefully removed, avoiding brain tissue damage and excessive bleeding, which usually worsens the spike recordings quality and reduces laser light transmission. Small amounts of saline 0.9% were continuously dropped on the craniotomy in order to prevent brain surface dryness. An additional craniotomy was made over the parietal cortex to fix a ground-screw, which was used as a reference as well. Then, we carefully positioned the silicon probe in the mPFC with real-time electrophysiological

monitoring for additional 30min to allow the brain tissue to recover and to optimize the number of cells recorded per tetrode. The recordings were performed using a Neuralynx Cheetah 64 system. Electrical signals were divided, pre-amplified (1000x) and filtered for local field potentials (LFPs) and single unit activity. The biological signal was sampled at 32 kHz and band-pass filtered between 600–6,000 Hz to record spikes and between 0.5–100 Hz to record LFPs (**fig.3c**).

We next positioned an unjacketed optical fiber (200 μ m core diameter; numerical aperture: 0.22; ThorLabs) 1mm above the recording site using an oblique insertion (10 to 15 degrees of slope; 0.3mm below the brain surface). This strategy seems to be effective in attenuating photoelectric artifacts by reducing the contacts exposure to the light (**fig. 1a**; Carlén et al. 2010). Optical stimulation was generated by a 473nm laser source (100mW; CNI Lasers) or LED system (20mW; Plexon Inc.) triggered through a data acquisition board (National Instruments BNC-2110) controlled by a program custom-made in LabView, by Kim Hoseok (Marie Carlén's post-doc). During the experiment, a broad range of light-stimulation frequencies (8, 16, 24, 32, 40, 48, 60, 80 and 90 Hz) was applied three times randomly in bouts of 3s of 1-ms pulses width with 20mW power in pilot experiments (ongoing data analysis) and 5mW in the main experiment (**presented data**). Laser power was measured before each experiment by a compact power meter console with digital 4" LCD (ThorLabs).

8.2. Spike sorting

Spikes were manually sorted into individual units (presumptive neurons) off-line based on analysis of peak amplitude, waveform energy and principal components using MClust program (A.D. Redish; <http://redishlab.neuroscience.umn.edu/MClust/MClust.html>). Cluster quality was evaluated by the isolation distance (Harris et al., 2001) and L-ratio (Schmitzer-Torbert et al., 2005). Clusters with isolation distance <12 or L-ratio >0.3 were excluded. Autocorrelation and interspike interval (ISI) histograms charts were inspected for all putative cells. In cases in which the autocorrelation showed absolute refractory period violations (spike counts at periods <1.2ms), we improved cluster separation, otherwise, the cluster was excluded (**figs. 3d and 6a-c**). The cells were entitled according to the number of the animal studied (Acute 1 to 22), number of the tetrode (TT1 to TT8) and number of the cluster sorted in a tetrode. For instance, the **figure 6a** brings information from *Ac21-TT4-C3* (Animal Ac21, tetrode 4, cluster 3). The supplementary **table S1** summarizes basic information regarding all the 133 presumptive neurons sorted from animals Ac12 to Ac22.

8.3. Examining gamma oscillations and spike-timing in the mPFC during urethane-induced UP-and-DOWN states

Slow oscillations with UP-and-DOWN-states and nested spindle or gamma oscillations are a hallmark of the sleeping brain (Buzsáki, 2006). Urethane-anesthetized rats and mice display spontaneous forebrain state alternations between deactivated patterns resembling slow wave sleep (SWS) and activated patterns resembling rapid eye movement (REM; Pagliardini et al. 2013). At the first electrophysiological recordings, our main concern was reducing 50Hz electrical noise and standardizing the urethane anesthesia level regarding stability of UP-and-DOWN states and mortality rate. After pilot experiments (see animals 1 to 11; **table 1**) we achieved very stable LFPs recordings with clear UP-and-DOWN states associated with low mortality rate (9%). For this, we reduced the urethane dose from 1.25 to 1.0 g/Kg and combined isoflurane (0.25%) along the experiment, according to Lee et al. (2012). Even from samples of our raw data read in the Neuroexplorer (Nex Technologies) it is noticeable how aligned the sorted spikes are to the LFPs UP-states. The **fig.3e** conveys a 40s-epoch recording of a PV-Cre mouse showing the firing activity of five sorted putative neurons and 4 channels of LFPs (one each shank). As a first step towards evaluating the comodulation between delta phase and gamma amplitude, the raw LFPs data were imported to the Matlab (Mathworks) and down-sampled (decimation to 1KHz). Then, a 10s-epoch of LFP was band-pass filtered in (55-120 Hz) and plotted together with the raw LFP tracing with Matlab custom-made scripts written in collaboration with Kim Hoseok (**fig.4a**).

Furthermore, to extend our evaluation of the urethane-induced UP-and-DOWN states, we performed additional analysis using the Neuroexplorer, with collaboration of Calvin Young (Carlén's lab post doc). First, for each channel, spike-triggered average field was calculated as the mean of the raw LFP segments (6 channels, different tetrodes) in -2 to +2s windows surrounding the spike. Second, we calculated spike-field coherence spectrum to determine specific potential frequency ranges of entrainment. Determining spike-LFP relationships when both signals are recorded from the same probe can give misleading results due to incomplete removal of spikes from the LFP signal. The spike-triggered average field exemplified in the **fig.4b** shows that it is possible to avoid this in future analysis by assessing LFPs from nearby contacts, which, in this case, seemed to yield very similar results. Anyway, because the silicon probe was inserted coronally (**fig.3a**), we aim to further investigate possible asymmetry in the spikes-LFPs relationship depending on the measured cortical layer. For the present LFPs analysis, we evaluated the channel 12 (tetrode 3) of all animals. Regarding the spikes, we sorted putative cells from all tetrodes.

Next, we tested whether this relationship between LFPs and spikes during UP-and-DOWN states requires intact NMDAR in PV+ cells. Our preliminary findings indicate that deletion of NR1 subunit in the PV cells did not affect spike-LFP synchrony during urethane-

induced UP-and-DOWN states under urethane. Both groups displayed high synchronous relationship between spikes and LFPs (average lag between UP state and spike incidence: PV-Cre group: -5.4 ± 8.3 ms; PV-Cre-NR1f/f group: $-2,5 \pm 6.6$ ms; Student t-test $p > 0.05$; **figs.5b-c**) with preferential entrainment to low-delta range of frequency (0.5 to 1 Hz; **fig.5d**).

Basket cells are a major generator of both spindle and gamma oscillations during UP-states (Massi et al., 2012). However, the role of NMDAR in PV cells in the nested gamma oscillations during urethane-induced UP-and-DOWN states is still poorly understood. Here, we addressed this question by **assessing the oscillatory patterns of urethane-anesthetized PV-Cre-NR1f/f mice and its controls (PV-Cre) in the mPFC**. For this, after 10min from the last optical stimulus, we imported our data into the Neuroexplorer, selected the 100s-epoch with the most stable UP-and-DOWN states and calculated the average relative power spectral density (PSD%) and logPSD ($PSD = 10 * \log_{10}(\text{raw-spectrum})$) for all animals in both groups (PV-Cre, $n=5$ and PV-Cre-NR1f/f, $n=3$). Then, the PSDs of following bands of frequency were averaged using Matlab and statistically compared between groups: delta (0.5 – 4 Hz), theta (6 – 10 Hz), beta (12 – 24 Hz), low-gamma (30 – 48 Hz) and high-gamma (52 – 80 Hz). Our preliminary results indicate that PV-Cre-NR1f/f group displayed LFPs with higher power in theta (+78%, $p=0.03$, Student t-test; **fig.5g**) and a trend towards higher power in beta and low-gamma ($p=0.07$ and $p=0.09$, respectively; **figs.5h-i**). These findings are in agreement with prior studies showing an enhancement of basal theta and gamma oscillations in barrel cortex of animals under isoflurane (Carlén et al, 2012) and in the hippocampus in awake animals (Korotkova et al., 2010).

8.4. Optogenetics: contextualization and strategies to detect and remove light-artifacts

Optogenetics can be defined as the combination of genetic and optical methods to achieve gain or loss of function of well-defined events in specific cells of living tissue (Deisseroth, 2011). A number of very impacting optogenetic studies have provided unprecedented insights on the dissection of circuits involved in cognition and psychiatric disorders (Kvitsiani et al, 2013, Deisseroth 2014). In our scientific context, optogenetics is a particularly interesting tool because provides opportunities to establish causal links between PV+ cells, gamma oscillations and cortical information flow (Cardin et al. 2009, Carlén et al. 2012; Hamilton et a. 2013; Lee et al., 2014). Nevertheless, there are still technical issues to overcome in optogenetics. One of the problems of using electrophysiological recordings coupled to optogenetics is direct interaction between light and metal electrodes when immersed in brain tissue (or saline). This phenomenon causes light-induced electrical artifacts that could be a confounding factor during LFP and spike recordings. These artifacts are most

likely due to a photovoltaic effect (also referred to as photogalvanic or Becquerel effect). Becquerel demonstrated that exposing metal electrodes, such as platinum, gold, and silver, to sunlight produced very small electric current when these metals were in electrolyte (Han 2012). Initiatives are ongoing to develop “light-proof” electrodes but it is still an issue in optogenetics. Classically, light-induced artifact usually distorts LFP, but not spike waveforms. However, when laser light is applied with duration of less than a couple of milliseconds per pulse, it may produce artifact waveforms comparable to spike waveforms (Han. 2012). In contrast, slow voltage fluctuations in the LFP usually appear as an exponential charging and discharging, with duration of approximately twice the length of the light stimulus (see the topic “Light-artifacts” in <http://www.openoptogenetics.org/>). Carlén et al. 2010 showed that artifacts in the LFP recorded by the metal electrode can be eliminated by changing the angle of the electrode so that the shaft does not intersect the laser beam.

In our case, we used standard silicon probes with electrode sites made with iridium, likewise able to display Becquerel effect. Here, in order to avoid breaking the silicon probe, we have decided perform a 10 to 15 degrees oblique insertion of the optical fiber instead. As illustrated in the **fig. 6**, this approach did not work for high-power optical stimulations (> 20 mW) but worked satisfactorily for protocols with lower power (around 5 mW), at least using the raw LFP tracings observation as a criterion. Regarding spikes, we had a couple of intriguing examples of artifact waveforms very similar to spikes. One of the cases is depicted in the **figure 7d** (waveform *Ac12-TT2-C4*, see also supplementary **table S1**). This cluster was sorted from a PV-Cre mouse injected with ChR2-mCherry and its consistency was tolerable: Isolation Distance (15.7) and L-ratio (0.24). However, in the cluster-checking output file provided by MClust, a poor signal-to-noise ratio between the sites of the tetrode was observed. Basically, all the sites recorded the same voltage amplitude variation along the time. Thus, fortunately, this cluster produced by light-artifacts could be easily removed from our recordings at the spike-sorting phase of data analysis. Though, we also documented two additional cases from the animal *Ac13* (PV-Cre mouse injected with control virus; clusters *Ac13-TT3-C2* and *Ac13-TT4-C2*) that was much more delicate. The output files provided by the MClust indicated that the Isolation Distance and L-ratio were appropriate and the signal-to-noise ratio between the tetrode sites was tolerable (see also **supplementary figures S1 and S2**). Importantly, we observed that these “spikes” were excessively time-locked to light-stimulation and, although these “units” were originated from two distinct tetrodes (TT3 and TT4), its latencies to the first spike after the stimulus onset were exactly the same (latency = 2.4 ms). Besides, nonetheless we stimulated with a broad range of frequencies (8 - 90 Hz), their firing rate was most of the times not entrained to the stimulation frequency and never higher than 20 Hz (data not shown). Finally, the waveforms and interspike interval histograms

of these “cells” do not resemble FS cells (**supplementary figs. S1 and S2**). Indeed, in the k-means cluster analysis based on the spike width and peak-to-trough ratio, these “units” were classified in the regular spiking cells cluster (**fig.13**). More details about this waveforms classification were addressed in the **session 7.8**. Therefore, at least for our case, the examination of (1) spike latencies to stimulus onset; (2) event-related firing rate histogram and (3) waveforms was sufficient to detect and remove “spike-like” waveforms induced by light artifacts.

8.5. Optogenetics validation: Detection of light-induced inhibition and activation

Photostimulation for activation of ChR2-expressing PV+ neurons imposes transitory decrease in the firing rate of nearby neurons in barrel cortex (Cardin et al., 2009) and mPFC (Kvitsiani et al., 2013). To search for optogenetic effects, we imported our sorted spikes and timestamps to Neuroexplorer and manually extracted the very first event from all of the 3s-train of stimulation (9 frequencies, 3 cycles, n = 27 trains). Then, we generated peri-event histograms and rasters for all the cells sorted. The **fig. 8** provides our most remarkable evidence of optogenetic effect in a PV-Cre animal injected with ChR-mCherry submitted to 27 trials of 3s-trains of stimulation (1ms pulses at 8, 16, 24, 32, 48, 60, 80 and 90 Hz; 5mW). Inhibition of firing activity was evident in 5 of 7 putative RS cells (**fig.8a-e**) and associated to robust activation of a putative FS cell (cell *Ac18-TT8-C1*; **fig.8f**). Waveform evaluation of the light-activated putative FS showed good signal-to-noise ratio between the tetrode sites. In the **fig.8g** a larger peri-event spike histogram of the same unit shows that the *Ac18-TT8-C1* response to light is not stereotyped (did not fire only in the same frequency of stimulation). Importantly, the *Ac18-TT8-C1* cell had a reasonable latency to first spike after light onset = 3.05 ms (**fig.9a**; Carlén et al. 2012) and displayed an average waveform consistent with a putative FS cell (**fig.13a**). Also, further analysis indicated that the *Ac18-TT8-C1* cell was unable to follow the pulses of light stimulation with good reliability in frequencies above 60Hz (**figs.9f-k**). Because ChR2 desensitizes in continuous light to a smaller steady-state conductance (Nagel et al. 2003), we speculate that ChR2 displayed the same phenomenon during 3s-trains of light-pulses at or above 60Hz.

Intriguingly, the putative FS cell *Ac18-TT8-C1* was completely silent during light-off periods. This intriguing phenomenon of “silent at rest, active under stimulation” has been previously described in FS interneurons from neostriatum of rats *in vitro* (Koo and Tepper, 2002), in some corticocortical neurons of rabbits (Swadlow, 2003) and in FS cells in the neocortex of anesthetized rats (Puig et al., 2008). However, it remains poorly understood. At the end of the experiment, we took advantage of the same experimental session to stimulate

the mPFC with single 50ms-pulses of light at 0.5Hz (5mW) and evaluate if the cell *Ac18-TT8-C1* displayed excessive time locking to the events. The **supplementary figure S3** contrasts a reasonable event-related activation pattern of *Ac18-TT8-C1* (**fig.S3a**) with a very unusual event-related responses from a presumed light-artifact (*Ac12-TT4-C3*; **fig.S4b**). Interestingly, the *AC18-TT8-C1* displayed persistence of firing activity up to 20ms after light cessation, which is in agreement to the literature data (Cardin et al. 2009; Kvitsiani et al., 2013).

Finally, we also observed a number of examples of robust light-induced inhibition of putative cortical RS cells in PV-Cre-NR1f/f mice expressing ChR2-mCherry (**fig.10**). Some units from PV-Cre mice expressing ChR2-mCherry were just partially inhibited by light (**fig. 11a-d**). Importantly, we did not observe any case of inhibition of RS cells in PV-Cre mice injected with control virus (AAV5-DIO-EYFP; **fig11e-h**).

8.6. Examining the role of NMDARs in cortical PV+ cells during evoked gamma oscillations by optogenetics

After gathering evidence that optogenetics was indeed working satisfactorily in our experiments, we aimed to investigate the role of NMDAR specifically in PV+ neurons during basal and optogenetically-evoked gamma oscillations in the mPFC. For this, we studied PV-Cre and PV-Cre-NR1f/f mice injected with ChR-mCherry or control virus submitted to 27 trials of 3s-trains of blue light stimulation (1ms pulses at 8, 16, 24, 32, 48, 60, 80 and 90 Hz; 5mW). For each light stimulation frequency, we measured PSDs% in an 8Hz band centered [-4; +4] on the frequency of interest. Power ratio was calculated by dividing the relative power in a frequency band during light stimulation by the relative power calculated from a 3s-epoch extracted immediately before each train (baseline).

Our preliminary results indicated that light pulses in the mPFC seem to produce LFP power enhancement preferentially in the gamma range. Stimulation of FS cells at 8 Hz in the PV-Cre and PV-Cre-NR1f/f mice had no effect on LFP power at 4-12 Hz (centered at 8Hz). However, stimulation at 40 Hz caused a significant increase in 36-44 Hz (centered at 40Hz) LFP power (PV-Cre/ChR2: $P=0.054$ - **Fig. 12c**; PV-Cre-NR1f/f/ChR2: $P=0.03$ - **fig.12d**). In contrast, stimulation in the mPFC of PV-Cre mice transfected with control virus did not cause significant increase of LFP power neither at 8Hz nor at 40 Hz. The number of subjects is still not sufficient to perform statistics with the power ratio evaluation. However, it suggests a poorer optogenetic-induced gamma evocation in PV-Cre-NR1f/f mice (**fig.12e**), according to Carlén et al. (2012). We are currently collecting more data with collaboration of Nicolas Guyon (Carléns' PhD student) in order to improve the power of our analysis and conclude the present work.

Lastly, it is worth to mention that, during recent analysis, we noticed some trials with power enhancement in the control animals. In all cases, we observed artifacts induced by light-stimulation at or above 80 Hz. Thus, in the future, we strongly suggest a careful approach to rule-out possible light-artifacts in the LFPs. Anyway, as can be observed in the **fig.12e**, no power enhancement was observed up to 60Hz, which is our range of interest.

8.7. Classification of units in putative FS and RS cells: waveforms, interspike interval histograms and optogenetic effects

Spike waveforms were characterized, as shown in the **fig.13a (right-bottom portion)**, by importing the raw data of the waveforms into the Matlab, and then, by calculating (1) the ratio between the amplitude of the initial peak (p) to the following trough (v) and (2) the duration of the spike at half height (w). Hoseok Kim has collaborated at this step with custom-made scripts in Matlab. Then, we plotted a scatter with the above-mentioned parameters for all sorted units ($n=8$ animals; 133 units; see also **table 2**) and performed k-means clustering (a method of vector quantization) in order to partition the population of waveforms between clusters of FS and RS putative cells. FS and RS clusters were significantly different in both mean spike width (FS = 0.21 ± 0.01 ms, $n = 34$; RS = 0.30 ± 0.008 ms; $n = 99$; unpaired t-test, $p < 0.0001$) and peak/trough ratio (FS = 1.5 ± 0.07 , $n=34$; RS = 3.2 ± 0.047 , $n=99$; unpaired t-test, $p < 0.0001$).

To validate our classification, we took advantage of our findings on optogenetics (inhibition or activation by light) and light-artifacts to label some cells in the scatter plotting (**fig.13a**). Consistently, all the light-inhibited cells (orange dots) were included in the RS-like waveform cluster (black dots), except the *Ac19-TT2-C1* cell. Although this cell might not be a FS cell because its interspike interval histogram displayed a jitter distribution (**fig.13e**), quite different from the spike-timing of the putative FS cell *Ac21-TT5-C1*, which displayed a burst pattern of activity along the experiment (**fig.13d**). The **figures 13b and 13c** bring additional examples of interspike jitter distribution in the interval histograms of cells classified as putative RS cells. Lastly, we also labeled the waveforms presumably generated by light-induced artifacts (red dots). As mentioned before, this strategy can be useful to help in the fine detection of light-artifacts. For instance, for our kind of optogenetic manipulation, it is suspicious when a “cell”, which was classified in the RS cluster, display activation by light. That was the case of the “cells” we labeled, namely: *Ac12TT2-C4*, *Ac12TT4-C3*, *Ac13TT3-C2* and *Ac13TT4-C2*. Also, it is possible taking advantage of this approach to tag and, then, to probe functionality of different cell subtypes, as described recently (Kvitsiani et al., 2013; Pi et al., 2013; Kepecs and Fishell, 2014).

9. Experiment II: Rationale, specific methods and preliminary findings

BDNF and its full-length trkB receptor seem to be reduced in schizophrenia (Weickert et al., 2003; Hashimoto et al., 2005). One of the most important truncated isoforms of trkB is **trkB-T1**, which acts as a dominant-negative receptor by forming inactive heterodimers with TrkB, **preventing BDNF signaling**. Both trkB and trkB.T1 are naturally co-expressed in neurons (principal and interneurons) and glia. Therefore, the efficiency of **BDNF signaling in a cell** has been proposed **to be contingent on its relative levels of the TrkB and TrkB.T1 isoforms** (Armanini et al., 1995). Interestingly, the full-length trkB-TK1:truncated trkB ratio has been found significantly decreased in schizophrenia both on the mRNA and protein level (Wong et al. 2013). Besides, the synchronization in gamma range was dramatically reduced in the hippocampal area CA1 of mutant mice, in which the trkB gene has been selectively ablated in PV+ interneurons (Zheng et al. 2011). Here, we aimed **to investigate the importance of trkB signaling specifically in PV+ interneurons in normal cortical circuit functions, cognition and emotional processing**. For this, Yang Xuan, a PhD student supervised by Profs. Carlén and Meletis, has cloned TrkB.t1-mCherry into an adeno-associated viral (AAV) DIO vector to render Cre-dependent expression.

As described before, adult males PV-Cre mice were anesthetized and submitted to bilateral injection in the infralimbic mPFC of AAV5-DIO-TrkB.T1-mCherry. Control animals received AAV5-DIO-EYFP. Aggressive behavior was probed before and after microinjections to rule out possible effects induced by the surgical procedure. Then, a behavior battery was performed, in collaboration with Nicolas Guyon, from the 6th to the 81th day after surgery, namely: resident-intruder test, novel object recognition, elevated plus maze, open field and extinction of non-contextual fear (**fig.14a**). Animals were perfused and the trkB.t1 expression was confirmed by examination of 40µm mPFC coronal sections for the presence of mCherry-fluorescence (**see session 6.2. and fig.2**).

In the **aggressive behavior test** (or resident-intruder paradigm), a single adult male mouse (resident) was allowed to freely explore his own home cage (36cmX18cmX12cm) alone, inside the experimental room for one minute. Then, a juvenile male mouse (3-4 week old) was introduced in the opposite corner of the cage for additional 4 minutes. The cage top was replaced by a transparent acrylic piece to record the session with video camera. Subsequently, a blind experimenter scored social interaction, latency to first attack and total time spent in aggressive behaviour.

Recognition memory was probed by the **novel object recognition test**. In this test, a mouse was initially placed in an arena (58cmX33cmX30) and allowed to explore for 10 min

(habituation). Following habituation, two identical objects were fixed in the arena and the animal was placed in the arena for 5-min (sample phase). After 10min from the sample phase, we replaced one of the objects by a novel one with similar size, but different shape and color/brightness; and the same animal was placed again in the arena for additional 5 min to explore the familiar and the novel objects (10min-test). After 24h, we kept the familiar object from the sample phase and replaced the novel from the 10min-test by a third one (totally different from the first two objects). Then, the animal was allowed to freely-explore the objects for 5 min (24h-test). The positions of the objects, including the one replaced, were counterbalanced across animals. We used triplicates of objects in order to never repeat the familiar object across the sessions. The sessions were video recorded and, subsequently, a blind experimenter scored exploration time for each object to calculate the discrimination index.

Anxiety was probed in the **elevated plus maze**, which is a plus-shaped maze elevated 73.5 cm above the floor. It consists of two closed arms with 15-cm high opaque walls and two open arms (40cmX7cm). Each mouse was placed in the center (5 x 5 cm) of the maze facing one of the closed arms. During the 5-min test period, the movement of the mouse was recorded and tracked by Viewer (Biobserv), which was able to calculate the times spent in closed arms, center and open arms. The maze was cleaned with 70% ethanol and wiped with paper towels between each trial.

Locomotion activity was probed in the **open field** test. Briefly, each individual mouse was placed near the wall-side of a 46cmX46cmX30cm arena, and the movement of the mouse was monitored for 60 min (TSE/ActiMot2). The total distance traveled and time in center (imaginary square with 25% of the open-field area) were measured. The open field arena was cleaned with 70% ethanol and wiped with paper towels between each trial.

Non-contextual fear memory was probed by the following protocol. Initially, we used a rectangular shape chamber with transparent acrylic walls (21x21x40cm). The floor consisted of stainless steel bars that could be electrified to deliver a mild shock. The chamber was situated inside a sound-attenuating box with a ventilating fan (TSE multi-conditioning system). The conditioned stimulus (CS) was a 5 kHz sine wave with duration of 30s and an intensity of 70 dB. The unconditioned stimulus (US) was a 0.7 mA footshock, 0.5s in duration, which co-terminated with the tone during the conditioning phase. Between sessions, floor trays and shock bars were cleaned with ethanol 70% and the chamber walls were wiped with a paper towels. Behavior was recorded with digital video cameras. On day 1, mice were habituated to the chamber for 150s (without tone and shock), followed by 3 CS+US trials (tone paired with shock; inter-trial interval (ITI) = 40 ± 4 s) and one resting trial (60s, without tone and/or shock). On day 2, all animals were submitted to habituation in a new chamber

(circular shape, dark acrylic, diameter = 20cm x high = 40 cm) during 150s and received 15 extinction tones (without shock) with an ITI of 5s, besides a resting trial of 60s. On day 3, at the same chamber, all subjects received 15 additional extinction trials (only CS; ITI = 40 ± 4s) to test for extinction of non-contextual fear. To analyze freezing, we first performed a manual quantification from one animal and compared with the manual quantification from TSE-Multiconditioning software. Linear correlation analysis revealed a significant and robust association between manual and automatic quantification, which gave us more conviction to keep using the software to assess freezing (Number of XY Pairs: 66; Pearson $r = 0.8994$; 95% confidence interval: 0.8403 to 0.9374; P value (two-tailed) < 0.0001; R squared = 0.8090; **fig.15b**).

Our preliminary data shows consistent viral expression in PV-expressing neurons in prelimbic and infralimbic aspects of the mPFC (**fig.2**). Mice injected with *trkB.t1* seem to display normal aggressiveness ($p < 0.05$; Two way ANOVA RM; **fig.14b**), recognition memory ($p < 0.05$; non-paired Student t-test; **fig.14c**) and locomotion ($p > 0.05$; Two way ANOVA RM; **fig.14d**). However, they did display disturbances in behaviors related to fear and anxiety. More specifically, acquisition in auditory fear conditioning is highly deficient in *TrkB* animals compared to controls (-68%; Treatment x time interaction effect; $F(9,54) = 2.5$; $p = 0.017$; Two way ANOVA RM; **fig.15c**), leading to a poorer non-contextual fear memory retrieval 24h after acquisition (-43%; Treatment effect; $F(1,12) = 9.0$; $p = 0.024$; Two way ANOVA RM; **fig.15d**) but not after 48h (**fig.15e**). Besides, we observed higher anxiety-related behaviors in *TrkB.T1* expressing mice, when compared to controls relative to time spent in the open arms in the elevated plus maze test (-23%; $p = 0.03$; non-paired Student t-test; **fig. 14e**) and to time spent at center of the open field in the first 3min (-42,8%; $p = 0.02$; Student t-test; **fig.14d-top-right inset**). Our findings point to a role of BDNF-*trkB* signaling in the mPFC PV+ interneurons in emotional processing. Further studies are required to try dissecting cognitive and emotional deficits related to BDNF-*trkB* disruption in PV+ cells of the mPFC. In this sense, Nicolas Guyon is currently running more experiments with the same experimental design, in order to improve our statistics and better decide the next steps. I will collaborate in the data analysis and design of new experiments to complement a future scientific manuscript for publication.

10. Concluding remarks and acknowledgements

Perturbed excitatory-inhibitory balance occurs in multiple psychiatric and neurological conditions and might be a critical link between schizophrenia symptoms, aberrant neural oscillatory activity, cognitive deficits and psychiatric comorbidities in epilepsy. Causal links between brain information processing at micro-circuitries wired by a constellation of different

sub-types of cells and cognitive impairment is a big challenge, which starts to be effectively addressed with the advent of optogenetics. The present data is just the start of a big story to be written within this theoretical framework. We still have an immense amount of data to be examined from additional experiments I performed a few weeks before leaving. As mentioned before, even the presented data are still in process of data analysis and we prefer to be cautious with the interpretation of our preliminary results. Anyway, below we highlighted our main findings/achievements:

(1) Deletion of NR1 subunit in the PV+ cells did not affect spike-LFP synchrony during urethane-induced UP-and-DOWN states under urethane;

(2) PV-Cre-NR1f/f mice displayed LFPs with higher power in theta and a trend towards higher power in beta and low-gamma in the mPFC. These findings are in agreement with prior studies showing an enhancement of basal theta and gamma oscillations in barrel cortex of animals under isoflurane (Carlén et al, 2012) and in the hippocampus in awake animals (Korotkova et al., 2010);

(3) Light-induced artifacts do represent a challenge in neuroscience and deserves more attention to avoid misinterpretations of electrophysiological data. Here, we successfully removed artifacts in LFPs by reducing laser power from 20 to 5mW and by using an oblique insertion of the optical fiber. Also, at least for our cases, the examination of (a) spike latencies to stimulus onset; (b) event-related firing rate histogram and (c) waveforms was sufficient to detect and remove “spike-like” waveforms induced by light artifacts;

(4) Photostimulation for activation of ChR2-expressing PV+ neurons also imposes transitory decrease in the firing rate of nearby neurons and enhancement of gamma oscillations in the mPFC;

(5) It seems feasible taking advantage of optogenetics to tag cell subtypes in a scatter plot based on spike waveforms. This strategy can be useful for improve light-artifact detection, but also, to study different cell subtypes in a specific circuits.

(6) BDNF-TrkB signaling disruption specifically in PV+ interneurons of mPFC seems to be sufficient to perturb emotional processing in mice.

During my internship abroad at Carlén’s lab (Karolinska Institutet) I had the great opportunity to participate in a laboratory extremely diverse culturally but at the same time cohesive in a sense of curiosity and enthusiasm in looking for the cutting-edge of tools and concepts in neuroscience. From Carlén’s group I have learned very important principles of optogenetics and electrophysiology, but also made genuine friends. I thank all researchers/friends of Carlén’s and Meletis’ labs and particularly I acknowledge:

Marie Carlén, for the inestimable support and great vision of science;

Calvin Young, for the extremely valuable discussions on neuroscience and for helping me in the experimental design and data analysis of electrophysiological experiments;

Débora Masini, for tutoring me during virus injections and perfusions procedures during the first months of my internship, when I was not familiar with procedures in mice at all;

Kim Hoseok, for the collaboration to set up the acute recordings system, to perform the experiments and to develop scripts in Matlab for our data analysis;

Nicolas Guyon, for the great collaboration in many levels of my internship experiments. Undoubtedly, his participation pushed forward the execution of the project and now it represents a possibility to successfully conclude the experiments for publication;

Konstantinos Meletis and *Yang Xuan*, for collaborating in the TrkB-T1 project;

Laura Pozzi and *Iskra Pollak Dorocic* for giving tutorials on stainings, microscope and brain sectioning;

Daniel Furth and *Daniel Kaping* for helping with the 32 channels silicon probe mapping and configuration file of Neuralynx;

João Pereira Leite and *Rodrigo Romcy-Pereira*, for providing valuable discussions and advises by Skype;

São Paulo Research Foundation (*FAPESP*) for the financial support (#2009/54410-0 and #2012/07107-2).

11. References

- Armanini MP, McMahon SB, Sutherland J, Shelton DL, Phillips HS. **Eur J Neurosci.** 1995 Jun 1;7(6):1403-9.
- Basar-Eroglu C, Brand A, Hildebrandt H, Karolina Kedzior K, Mathes B, Schmiedt, C. **Int J Psychophysiol.** 2007 Apr;64(1):39-45.
- Bueno-Junior LS, Lopes-Aguiar C, Ruggiero RN, Romcy-Pereira RN, Leite JP. **PLoS One.** 2012;7(10):e47484.
- Buzsáki G (2006) **Rhythms of the brain.** New York: Oxford University Press.
- Cammarota M, Losi G, Chiavegato A, Zonta M, Carmignoto G. **J Physiol.** 2013 Feb 15;591(Pt 4):807-22.
- Cardin JA1, Carlén M, Meletis K, Knoblich U, Zhang F, Deisseroth K, Tsai LH, Moore CI. **Nature.** 2009 Jun 4;459(7247):663-7.
- Carlén M1, Meletis K, Siegle JH, Cardin JA, Futai K, Vierling-Claassen D, Rühlmann C, Jones SR, Deisseroth K, Sheng M, Moore CI, Tsai LH. **Mol Psychiatry.** 2012 May;17(5):537-48.
- Cellerino A, Maffei L, Domenici L. **Eur J Neurosci.** 1996 Jun;8(6):1190-7.
- Cornejo BJ, Mesches MH, Benke TA. **Epilepsy Behav.** 2008 Nov;13(4):585-92.
- Deisseroth K. **Nat Methods.** 2011 Jan;8(1):26-9.
- Gill DA, Ramsay SL, Tasker RA. **Brain Res.** 2010 May 17;1331:114-23.
- Goldstein B, Friedman LK. **Eur J Neurosci.** 2010 Dec;32(11):1897-911.
- Hamilton LS, Sohl-Dickstein J, Huth AG, Carels VM, Deisseroth K, Bao S. **Neuron.** 2013 Nov 20;80(4):1066-76.

Hanslmayr S, Backes H, Straub S, Popov T, Langguth B, Hajak G, Bäuml KH, Landgrebe M. **Hum Brain Mapp.** 2013 Sep;34(9):2266-75.

Harvey A. Swadlow. *Cerebral Cortex* Jan 2003;13:25–32; 1047–3211

Hashimoto T, Bergen SE, Nguyen QL, Xu B, Monteggia LM, Pierri JN, Sun Z, Sampson AR. **J Neurosci.** 2005 Jan 12;25(2):372-83.

Homayoun H, Moghaddam B. **J Neurosci.** 2007 Oct 24;27(43):11496-500.

Kandratavicius L, Hallak JE, Leite JP. **Epilepsy Behav.** 2014 Feb 5.

Kandratavicius L, Rosa-Neto P, Monteiro MR, Guiot MC, Assirati JA Jr, Carlotti CG Jr, Kobayashi E, Leite JP. **Hippocampus.** 2013 Dec;23(12):1212-30.

Kepecs A, Fishell G. **Nature.** 2014 Jan 16;505(7483):318-26.

Kleen JK, Wu EX, Holmes GL, Scott RC, Lenck-Santini PP. **J Neurosci.** 2011 Oct 26;31(43):15397-406.

Korotkova T1, Fuchs EC, Ponomarenko A, von Engelhardt J, Monyer H. **Neuron.** 2010 Nov 4;68(3):557-69.

Kvitsiani D, Ranade S, Hangya B, Taniguchi H, Huang JZ, Kepecs A. **Nature.** 2013 Jun 20;498(7454):363-6

Lee AT, Gee SM, Vogt D, Patel T, Rubenstein JL, Sohal VS. **Neuron.** 2014 Jan 8;81(1):61-8

Leite JP, Bortolotto ZA, Cavalheiro EA. **Neurosci Biobehav Rev.** 1990 Winter;14(4):511-7.

Lin JJ, Mula M, Hermann BP. **Lancet.** 2012 Sep 29;380(9848):1180-92.

Lopes Aguiar C, Romcy-Pereira RN, Escorsim Szawka R, Galvis-Alonso OY, Anselmo-Franci JA, Pereira Leite J. **Neuroscience.** 2008 Jun 2;153(4):1309-19.

Lopes-Aguiar C, Bueno-Junior LS, Ruggiero RN, Romcy-Pereira RN, Leite JP. **Neuropharmacology.** 2013 Feb;65:143-55.

Marín O. **Nat Rev Neurosci.** 2012 Jan 18;13(2):107-20.

Massi L, Lagler M, Hartwich K, Borhegyi Z, Somogyi P, Klausberger T. **J Neurosci.** 2012 Nov 14;32(46):16496-502.

Mathern GW, Pretorius JK, Kornblum HI, Mendoza D, Lozada A, Leite JP, Chimelli LM, Fried I, Sakamoto AC, Assirati JA, Lévesque MF, Adelson PD, Peacock WJ. **Brain.** 1997 Nov;120 (Pt 11):1937-59.

Moghaddam B1, Javitt D. **Neuropsychopharmacology.** 2012 Jan;37(1):4-15.

Nagel G, Szellas T, Huhn W, Kateriya S, Adeishvili N, Berthold P, Ollig D, Hegemann P, Bamberg E. **Proc Natl Acad Sci U S A.** 2003 Nov 25;100(24):13940-5

Nakazawa K1, Zsiros V, Jiang Z, Nakao K, Kolata S, Zhang S, Belforte JE. **Neuropharmacology.** 2012 Mar;62(3):1574-83.

Pagliardini S, Gosgnach S, Dickson CT. **PLoS One.** 2013 Jul 30;8(7):e70411.

Pi HJ, Hangya B, Kvitsiani D, Sanders JI, Huang ZJ. **Nature.** 2013 Nov 28;503(7477):521-4.

Puig, MV, Ushimaru, M and Kawaguchi, Y. **Proc Natl Acad Sci U S A.** 2008 Jun 17 105(24).

Rotaru DC1, Lewis DA, Gonzalez-Burgos G. **Rev Neurosci.** 2012 Jan 9;23(1):97-109.

Schwaller B, Tetko IV, Tandon P, Silveira DC, Vreugdenhil M, Henzi T, Potier MC, Celio MR, Villa AE. **Mol Cell Neurosci.** 2004 Apr;25(4):650-63.

Sohal VS1, Zhang F, Yizhar O, Deisseroth K. **Nature.** 2009 Jun 4;459(7247):698-702.

Tibor Koo's and James M. Tepper. **The Journal of Neuroscience,** January 15, 2002, 22(2):529–535.

Tsai ML1, Crutchley M, Boyce R, Ma J, Boon F, Cain DP, Leung LS. *Physiol Behav.* 2012 Jun 25;106(4):534-41.

Vestergaard M, Pedersen CB, Christensen J, Madsen KM, Olsen J, Mortensen PB. **Schizophr Res.** 2005 Mar 1;73(2-3):343-9.

Weickert CS, Hyde TM, Lipska BK, Herman MM, Weinberger DR, Kleinman JE. *Mol Psychiatry*. 2003 Jun;8(6):592-610.

Wong J, Rothmond DA, Webster MJ, Weickert CS. *Schizophr Bull*. 2013 Jan;39(1):130-40.

Xue Han. *ACS Chem. Neurosci*. 2012, 3, 577–584.

Zheng K, An JJ, Yang F, Xu W, Xu ZQ, Wu J, Hökfelt TG, Fisahn A, Xu B, Lu B. *Proc Natl Acad Sci U S A*. 2011 Oct 11;108(41):17201-6.

12. Figure legends

Figure 1. Cre-dependent expression of the light-activated ChR2. (a) When injected unilaterally into the mPFC of adult PV-Cre mice, the viral vector AAV2-DIO-ChR2-mCherry provided robust expression of ChR2 in PV+ interneurons; (b) The same pattern of expression can be observed in PV-Cre-NR1f/f mice; (c) Besides, the injection of the control vector AAV5-DIO-EYFP provided robust expression of the EYFP fluorophore as well; (d) 10X magnification of a section from a AAV2-DIO-ChR2-mCherry injected PV-Cre mouse showing a good of cell bodies transfected in prelimbic area of mPFC; (e) The adeno-associated viral vector AAV-DIO-ChR2-mCherry carries an inverted version of ChR2 fused to the fluorescent markers mCherry. This strategy prevents ChR2 from being expressed in the absence of Cre. The loxP variants loxP and lox2272 flanking ChR2-mCherry are incompatible and cannot recombine with each other (lee et al., 1998), leading to a stochastic recombination of either variant (Livet et al., 2007) in the presence of Cre. Because both loxP variants both loxP variants are constitutes of lox pairs facing each other, recombination results in inversion of ChR2-mCherry into the sense orientation. As a consequence of the first recombination event, the second unrecombined loxP variant now is constituted of two directly oriented lox sites and will therefore excise one of the lox sites of the first loxP variant, an event that prevents further recombination. This strategy eliminates possible misexpression of ChR2 due to leakiness of the commonly used translational stop cassettes and targets recombination and expression of ChR2-mCherry exclusively to Cre expressing cells (from Cardin et al. 2009); (f) Staining for PV+ in a mPFC section from a transfected PV-Cre mouse with AAV2-DIO-ChR2-mCherry conveys examples of cells expressing ChR2-mCherry which showed detectable levels of PV (white arrows).

Figure 2. Cre-dependent expression of the truncated trkb receptor (Trkb.T1). (a) When injected bilaterally targeting the infralimbic tmPFC of adult PV-Cre mice, the viral vector AAV2-DIO-TrkB.T1-mCherry provided robust expression of TrkB.T1 in PV+ interneurons; (b) Besides, the injection of the control vector AAV5-DIO-EYFP provided robust expression of the EYFP fluorophore as well; (c) image with higher magnitude showing cell-specific expression of TrkB.t1-mCherry with good co-localization with the PV+ staining (white arrows).

Figure 3. Acute recordings in the mPFC associated to optogenetics. (a) Schematic representation of the mPFC, the positioning of the silicon probe and the oblique insertion of the optical fiber (10–15 degrees of slope) to attenuate light-artifacts. (b) Basic configuration of the silicon probe used in our experiments: *A4x2-tet-5mm-150-200-312-A32*; Neuronexus. (c) A screenshot from the software Cheetah 64 during recordings of LFPs and spikes in the mPFC of a urethane-anesthetized mouse. (d) Example of sorted putative cells using MClust.

(e) Raw data of LFPs and sorted spikes imported and displayed in Neuroexplorer. It is remarkable the synchrony between spikes and UP-and-DOWN states in the LFPs in the mPFC.

Figure 4. Gamma oscillations and spike-timing in the mPFC during urethane-induced UP-and-DOWN states. (a) A 10s-epoch of LFP was band-pass filtered in (55-120 Hz) and plotted together with the raw LFP tracing to illustrate gamma nested to UP-states; (b) Spike-triggered average field for six LFPs channels (different tetrodes) surrounding the spikes of a sorted unit from TT8 seemed to yield similar results. The colormap represents the LFPs amplitude in each trial of 4s-window (-2, +2).

Figure 5. Relationship between LFPs and spikes during UP-and-DOWN states in PV-Cre and PV-Cre-NR1f/f. (a) Raw data displayed in Neuroexplorer illustrating an impressive proportion of cells aligned to the UP-states of a 10s-epoch LFP recorded in the mPFC of a PV-Cre-NR1-f/f mouse under urethane. One of these periods is highlighted by yellow rectangle. (b) Average of the temporal correlation between spike and LFPs in the PV-Cre (n=27 cells; grey) and PV-Cre-NR1f/f (n=54 cells; red) groups indicate that the lack of NR1 subunit in PV neurons did not disrupt synchrony spike-LFP during cortical UP-and-DOWN states. (c) Scatter plot with the time lag between spike and LFPs of all cells sorted for both groups. (d) Spectral coherence analysis between LFPs and spikes indicates a very specific frequency range of entrainment (0.5 – 1Hz) for both groups. (e) To assess possible alterations in basal oscillatory patterns in the mPFC of urethane-anesthetized PV-Cre-NR1f/f mice a 100s-epoch with the most stable UP-and-DOWN states was evaluated regarding its power spectrum. The average relative power spectral density suggests higher power at frequencies from theta to low gamma in PV-Cre-NR1f/f animals. Indeed, statistical analysis indicate that PV-Cre-NR1f/f group displayed LFPs with higher power in (g) theta and a trend towards higher power in (h) beta and (i) low-gamma. No differences were observed in (f) delta and (j) high-gamma ranges of frequency. * Statistical significant: $p=0.03$; Student t-test. Data are shown as mean \pm s.e.m.

Figure 6. Elimination of light-induced artifacts in LFPs recordings. (a) Direct exposure of metal electrodes to the laser beam causes large electrical artifacts. This example was taken from recordings in the mPFC not transduced with AAV2-DIO-ChR2-mCherry. Although we were already using an oblique insertion of the optical fiber in relation to the silicon probe, it is possible to see that 1ms light-pulses applied at 20mW power caused a large and repeated artifact in the LFP recording (lower black trace). The artifact started at the onset of each light pulse and usually lasted more than the light pulse width. (b) Another sample of LFP during light stimulation. Now, a PV-Cre animal transfected with control virus AAV-DIO-EYFP displayed a cleaner LFP tracing when the laser power was reduced from 20 to 5mW. Artifacts in the metal sites of the silicon probe recordings were indeed eliminated by changing the angle of the fiber, associated to reduction in the power as can be illustrated in (c) and (d).

Figure 7. Checking clusters to detect light-artifacts. (a) *Ac21-TT4-C3* is a sorted unit from a PV-Cre-NR1f/f mouse transfected with ChR2-mCherry. It shows good signal-to-noise ratio between the tetrode sites (top), excellent parameters of cluster quality (bottom; L-Ratio and Isolation Distance) and dispersed ISI (middle), indicating irregular firing. (b) *Ac22-TT1-C2* is a sorted unit from a PV-Cre-NR1f/f mouse transfected with ChR2-mCherry as well. It shows a good signal-to-noise ratio between the tetrode sites, worse parameters of cluster quality

(thought still acceptable) and a more concentrated ISI, indicating a better spike timing. **(c)** *Ac22-TT1-C2* is a sorted unit from a PV-Cre mouse transfected with ChR2-mCherry. It shows a good signal-to-noise ratio between the tetrode sites, remarkable parameters of cluster quality and an unusual ISI due to light-activation in specific frequencies. For instance, the peak of firing near to 30ms might be related to 32Hz stimulation ($F=1/0.03125s$) and the other ones, near to 20 and 25ms, might be caused by 40 and 48Hz stimulation. Importantly, it is possible to see firing activity in intermediate frequencies, suggesting spontaneous firing between light-pulses and/or trains. **(d)** Likewise the prior cluster, *Ac12-TT2-C4* is a sorted unit from a PV-Cre mouse transfected with ChR2-mCherry. It displays a poor signal-to-noise ratio between the tetrode sites, worse parameters of cluster quality (thought still acceptable) and a very unusual ISI, with peaks excessively locked to the frequencies of stimulation. Therefore, this waveform is a candidate to be considered as a light-artifact.

Figure 8. Optogenetics validation: Example of light-induced inhibition and activation in a PV-Cre mouse. A PV-Cre animal injected with ChR-mCherry was submitted to 27 trials of 3s-trains of stimulation (1ms pulses at 8, 16, 24, 32, 48, 60, 80 and 90 Hz; 5mW). **(a-e)** Perievent raster and histogram of five different cells are shown to exemplify firing activity suppression during light stimulation. **(f)** Perievent raster and time histogram of a putative FS cell showing a robust activation during light stimulation. **(g)** Shows the waveforms and a larger perievent raster and time histogram of the same unit displayed in **f**.

Figure 9. Putative FS cell displayed a rapid firing-rate increase followed by a decrease until a steady state under light-stimulation. **(a)** The event-related spike responses of the cell *Ac18-TT8-C1* (above) display a biologically reasonable latency (3.05ms) to the stimulus (below); **(b)** Spike counting trial-by-trial during 3s of light stimulation highlights the rapid firing-rate increase followed by a decrease until a steady state under light-stimulation. Colormap is the number of spikes per bin. Then, the same data were grouped in bins of 1s and the trials were sorted according to the frequency of stimulation. Stimulation frequencies up to 16Hz were able to entrain the cell to firing around the same frequency. In this case, the entrainment lasted the whole period of optical stimulation (**c-d**). However, in higher frequencies, the same cell failed to follow the stimulation frequency (**e-h**). This was particularly more evident in frequencies above 60Hz (**i-k**).

Figure 10. Optogenetics validation: Example of light-induced inhibition in a PV-Cre-NR1f/f mouse. A PV-Cre-NR1f/f animal injected with ChR-mCherry was submitted to 27 trials of 3s-trains of stimulation (1ms pulses at 8, 16, 24, 32, 48, 60, 80 and 90 Hz; 5mW). Perievent raster and histogram of two different cells from the same animal are shown to exemplify firing activity suppression during light stimulation.

Figure 11. Optogenetics validation: Examples of partial light-induced inhibition and of absence of light-effect in control animals **(a-c)** Perievent raster and time histogram of three different cells from a PV-Cre ChR2 expressing mouse are shown to exemplify partial firing activity suppression during light stimulation; **(d)** Perievent raster and time histogram of one cell from the same mouse to exemplify no firing activity suppression during light stimulation; **(e-h)** Perievent raster and time histograms of four cells (two each control virus injected mouse) to exemplify no firing activity modulation during light stimulation.

Figure 12. Role of NMDARs in cortical PV+ cells during evoked gamma oscillations by optogenetics. (a) Single-unit recordings during optogenetic activation of a FS–PV+ interneuron. The protocol of stimuli consisted in 27 trials of 3s-trains of blue light stimulation (1ms pulses at 8, 16, 24, 32, 48, 60, 80 and 90 Hz; 5mW). The reliability of the FS cell in following the light stimulus is illustrated in figure 9. *Left side*: PSD% from a representative trial of (b) one PV-Cre mouse transfected with control virus, (c) one PV-Cre mouse transfected with ChR2-mCherry and (d) one PV-Cre-NR1f/f mouse transfected with ChR2-mCherry. (b-d: *Right side*): Average of PSDs (%) centered at 8Hz (4 to 12 Hz) and at 40 Hz (36 to 44 Hz) in three trials of 8 and 40Hz optical stimulation trains each. (b) No significant differences were observed when compared average of trials before and during light. (c) PV-Cre and (d) PV-Cre-NR1f/f mice both expressing ChR2, seem to produce LFP power enhancement preferentially in the gamma range when submitted to light pulses in the mPFC. In both groups, stimulation of FS cells at 8 Hz had no effect on LFP power at 4-12 Hz (centered at 8Hz). However, stimulation at 40 Hz did cause a significant increase LFP power at 36-44Hz. (e) The number of subjects is still not sufficient to perform statistics with the power ratio evaluation. However, it suggests a poorer optogenetic-induced gamma evocation in PV-Cre-NR1f/f mice (fig.12e), according to Carlén et al. (2012). * p = 0.039; # p = 0.054; baseline vs stimulation trial; paired Student t-test. Data are shown as mean ± s.e.m.

Figure 13. Classification of units in putative FS and RS cells. (a) **Right-bottom corner**: First, for each waveform, we calculated (1) the ratio between the amplitude of the initial peak (p) to the following trough (v) and (2) the duration of the spike at half height (w). Then, we plotted a scatter with the above-mentioned parameters for all sorted units (**main chart**; n=8 animals; 133 units) and performed k-means clustering to partition the population of waveforms between clusters of FS and RS putative cells. Consistently, 9/10 of the light-inhibited cells (orange dots) were included in the RS-like waveform cluster (black dots). Lastly, we also labeled the waveforms presumably generated by light-induced artifacts (red dots). As mentioned before, this strategy can be useful to help in the fine detection of light-artifacts. (b-e) Examples of ISI histogram distribution of cells classified as putative RS cells with random firing pattern revealed as dispersed ISIs (b,c and e) and one classified as putative FS cell, with ISI histogram revealing burst-firing pattern (d).

Figure 14. BDNF-TrkB signaling disruption specifically in PV+ interneurons of mPFC exacerbates anxiety-like behaviors without impacts social behavior, recognition memory, and locomotion. (a) Experimental design. Adult males PV-Cre mice were anesthetized and submitted to bilateral injection in the infralimbic mPFC of AAV5-DIO-TrkB.T1-mCherry. Control animals received AAV5-DIO-EYFP. Aggressive behavior was probed one day before and after microinjections to rule out possible effects induced by the surgical procedure. Then, a behavior battery was performed from the 6th to the 81th day after surgery, namely: resident-intruder test, novel object recognition, elevated plus maze, open field and extinction of non-contextual fear. Animals were perfused and the trkB.t1 expression was confirmed by examination of 40µm mPFC coronal sections for the presence of mCherry-fluorescence. (b) Resident-intruder test. *Top*: Evaluation of the amount of time an adult male mouse (resident) spent sniffing a juvenile mouse (intruder) in 5 sessions over 7 weeks after virus injection. *Middle*: Assessment of the amount of time spent by the resident in offensive episodes (defined as an attack that included either biting or wrestling; Ogawa et al., 1999) towards the intruder. *Bottom*: Quantification of the latency to the first attack. No significant

differences were observed between groups in all comparisons ($p > 0.05$; ANOVA Two way RM). **(c)** Novel object recognition test. *Bottom*: Following habituation, two identical objects were fixed in the arena and the animal was placed in the arena for 5-min (sample phase). After 10min from the sample phase, we replaced one of the objects by a novel one with similar size, but different shape and color/brightness; and the same animal was placed again in the arena for additional 5 min to explore the familiar and the novel objects (10min-test). After 24h, we kept the familiar object from the sample phase and replaced the novel from the 10min-test by a third one (totally different from the first two objects). Then, the animal was allowed to freely-explore the objects for 5 min (24h-test). Preference (%) was calculated as follows: $((\text{time spent exploring the novel object}) / (\text{the total time of object exploration})) * 100$. No significant differences were observed between groups in both 10min test (top) and 24h test (middle) ($p > 0.05$; non-paired Student t-test). **(d)** Open field. Briefly, each subject was placed near the wall-side of an arena, and the movement of the mouse was monitored for 60 min (TSE/ActiMot2). The total distance traveled and time in center (imaginary square with 25% of the open-field area) were measured. No significant differences were observed between groups ($p > 0.05$; ANOVA Two way RM). However, *trkB.T1* mice spent lesser time at center (central portion encompassing 25% of the arena) of the open field in the first 3min of test ($p < 0.05$; non-paired Student t-test). **(e)** Elevated plus maze. Consistent with the results obtained from the time spent in the center of the open field, *trkB.T1* animals displayed a reduced amount of time spent in the open arms as well ($p < 0.05$; non-paired Student t-test). * Statistical significant: $p < 0.05$; Student t-test. Data are shown as mean \pm s.e.m.

Figure 15. BDNF-TrkB signaling disruption specifically in PV+ interneurons of mPFC impairs acquisition of non-contextual fear memory. **(a)** Experimental design: On day 1, mice were habituated to the chamber for 150s (without tone and shock), followed by 3 CS+US trials (tone paired with shock; inter-trial interval (ITI) = 40 ± 4 s) and one resting trial (60s, without tone and/or shock). On day 2, all animals were submitted to habituation in a new chamber (circular shape, dark acrylic, diameter = 20cm x high = 40 cm) during 150s and received 15 extinction tones (without shock) with an ITI of 5s, besides a resting trial of 60s. On day 3, at the same chamber, all subjects received 15 additional extinction trials (only CS; ITI = 40 ± 4 s) to test for extinction of non-contextual fear. **(b)** To check the consistency of the automatic freezing behavior by the TSE-Multiconditioning software, we performed a correlation between manual versus automatic quantifications from the same animal. Linear correlation analysis revealed a significant and robust association between manual and automatic quantification, which gave us more conviction to keep using the software to assess freezing (Number of XY Pairs: 66; Pearson $r = 0.8994$; 95% confidence interval: 0.8403 to 0.9374; P value (two-tailed) < 0.0001 ; R squared = 0.8090). **(c)** During the conditioning phase (day 1), *TrkB.T1* mice displayed significant reduction of freezing behavior during the pause that followed the second presentation of the CS, besides during the third presentation of CS and its subsequent pause. **(d)** On the day 2, the fear memory retrieval elicited by CS was poorer in the *TrkB.T1* group compared to control animals. **(e)** On the day 3, no significant differences were observed between groups.). * Statistical significant: $p < 0.05$; Two way ANOVA RM. Data are shown as mean \pm s.e.m.

Figure S1. Cluster checking file of unit Ac13-TT3-C2 generated by MClust after sorting

Figure S2. Cluster checking file of unit Ac13-TT4-C2 generated by MClust after sorting

Figure S3. Peri-stimulation raster and time histogram during 150 trials of 50ms light-pulse of a putative FS cell *Ac18-TT8-C1* (a) and a waveform produced by light-artifact, *Ac12-TT4-C3* (b). Interestingly, the *Ac18-TT8-C1* displayed persistence of firing activity up to 20ms after light cessation, contrasting with *Ac12-TT4-C3*, which displayed an extremely time-locked response related to the event.

Table 1. Summary of all acute recordings

Subject	Genotype Gender	Virus	Ac. Rec (Date)	Aims	Conclusions
System test #1	PV-Cre female	DIO-ChR2- mCherry (10 weeks before acute recordings)	04 Sep 2013	Set up the acquisition system and laser controlling; Check LFPs under urethane; Remove electrical noise; Characterize light-induced spikes and/or artifacts	- Good virus expression - Low electrical noise - Occurrence of light-artifacts in the LFPs - Laser power 20mw
System test #2	Gal-Cre male	Non-injected	26 Sep 2013	Improve urethane induced UP-DOWN state	Animal died before the recordings get started;
Acute #1	PV-Cre male	DIO-ChR2- mCherry (11 weeks before acute recordings)	01 Oct 2013	Evaluate LFPs and spikes under urethane; Remove electrical noise; Characterize light-induced spikes and/or artifacts; Set up laser power and protocols of stimulation;	- Good virus expression - No optogenetic effect - Low electrical noise - Occurrence of light-artifacts in the LFPs - Laser power 20mw
Acute #2	PV-Cre male	DIO-ChR2- mCherry (11 weeks before acute recordings)	08 Oct 2013	Characterize light-induced spikes and/or artifacts; Set up laser power and protocols of stimulation;	- Good virus expression - No optogenetic effect - Low electrical noise - Occurrence of light-artifacts in the LFPs - Laser power 20mw
System test #2	C57BL/6N male	Non-injected	09 Oct 2013	Remove electrical noise; Fix some problems with grounding;	- Problems with the ground connected to the silicon probe adaptor; - High-frequency noise (>3KHz) was coming from the laser source (only when the ground has some problem);
Acute #3	PV-Cre male	DIO-ChR2- mCherry (12 weeks before acute recordings)	15 Oct 2013	Characterize light-induced spikes and/or artifacts; Improve the optical fiber position;	- Good virus expression; - Good number of cells per tetrode; - No optogenetic effect; - Low electrical noise; - Occurrence of light-artifacts in the LFPs; - Laser power 20mw;
Acute #4	PV-Cre male	DIO-ChR2- mCherry (12 weeks before acute recordings)	17 Oct 2013	Test new stimulation protocols; Evaluate whether is possible improve or perturb the synchrony during UP-DOWN state by driving PV-cells in different frequencies;	- Good virus expression; - Good number of cells per tetrode; - Occurrence of light-artifacts in the LFPs; - Laser power 20mw; - Data analysis is in progress;
Acute #5	PV-Cre male	DIO-ChR2- mCherry (12 weeks before acute recordings)	22 Oct 2013	Evaluate whether is possible improve or perturb the synchrony during UP-DOWN state by driving PV-cells in different frequencies;	- Good virus expression; - Good number of cells per tetrode; - Reduced light-artifacts in the LFPs; - Laser power 20mw;

					<ul style="list-style-type: none"> - Better control of the optical fiber position; - Data analysis is in progress; - Good virus expression; - Good number of cells per tetrode; - Putative fast spiking cell driven by light (TT4). - Interpretation of this data is still difficult due to LFP contamination by light; (cont.) - Laser power 20mw; - Data analysis is in progress;
Acute #6	PV-Cre male	DIO-ChR2-mCherry (12 weeks before acute recordings)	23 Oct 2013	Evaluate whether is possible improve or perturb the synchrony during UP-DOWN state by driving PV-cells in different frequencies;	
(cont.) Acute #6					
Acute #7	PV-Cre male	DIO-ChR2-mCherry (13 weeks before acute recordings)	29 Oct 2013	Evaluate whether is possible improve or perturb the synchrony during UP-DOWN state by driving PV-cells in different frequencies;	<ul style="list-style-type: none"> - Good virus expression; - No good recordings; - After first set of stimulation animal died;
Acute #8	PV-Cre male	DIO-ChR2-mCherry (13 weeks before acute recordings)	30 Oct 2013	Evaluate whether is possible improve or perturb the synchrony during UP-DOWN state by driving PV-cells in different frequencies;	<ul style="list-style-type: none"> - Good virus expression; - Good number of cells per tetrode; - Strong inhibition of putative regular spiking cells (TT3); - Laser power 20mw; - Data analysis is in progress;
Acute #9	PV-Cre male	DIO-ChR2-mCherry (13 weeks before acute recordings)	01 Nov 2013	Evaluate whether is possible improve or perturb the synchrony during UP-DOWN state by driving PV-cells in different frequencies;	<ul style="list-style-type: none"> - Good virus expression; - Excessive bleeding from the craniotomy over the medial prefrontal cortex; - No cells recorded; - Interruption of the surgery; - Animal died before recordings get started;
Acute #10	PV-Cre female	Control DIO-EYFP (6 weeks before acute recordings)	12 Nov 2013	Investigate UP-and-DOWN state and gamma oscillations in the medial prefrontal cortex of urethane-anesthetized PV-Cre mice	
Acute #11	PV-Cre female	Control DIO-EYFP (6 weeks before acute recordings)	13 Nov 2013	Investigate UP-and-DOWN state and gamma oscillations in the medial prefrontal cortex of urethane-anesthetized PV-Cre mice;	<ul style="list-style-type: none"> - Animal died before recordings get started; - Females are probably more sensitive to urethane than males;
Acute #12	PV-Cre female	DIO-ChR2-mCherry (7 weeks before acute recordings)	21 Nov 2013	Investigate UP-and-DOWN state and gamma oscillations in the medial prefrontal cortex of urethane-anesthetized PV-Cre mice;	<ul style="list-style-type: none"> - Good virus expression; - Good number of cells per tetrode in the mPFC; - Use of isoflurane 0.05% associated to urethane (1 mg/Kg instead of 1.25 mg/Kg); - No light artifact in the LFPs; - Partial inhibition of putative regular spiking cells: - Laser power 5mw; - Preliminary data is shown in the present report;
Acute #13	PV-Cre female	Control DIO-EYFP (6 weeks)	22 Nov 2013	Investigate UP-and-DOWN state and gamma oscillations in the medial prefrontal cortex	<ul style="list-style-type: none"> - Good virus expression; - Good number of cells per tetrode in the mPFC;

		before acute recordings)		of urethane-anesthetized PV-Cre mice;	<ul style="list-style-type: none"> - Use of isoflurane 0.05% associated to urethane; - No light artifact in the LFPs; - Laser power 5mw; - Preliminary data is shown in the present report;
Acute #14	PV-Cre female	DIO-ChR2-mCherry (8 weeks before acute recordings)	25 Nov 2013	Investigate UP-and-DOWN state and gamma oscillations in the medial prefrontal cortex of urethane-anesthetized PV-Cre mice;	<ul style="list-style-type: none"> - Good virus expression; - Good number of cells per tetrode in the mPFC; - Use of isoflurane 0.05% associated to urethane; - No light artifact in the LFPs; - Laser power 5mw; - Data is not shown (no optogenetic effect); - Good virus expression; - Animal died before recordings get started;
Acute #15	PV-Cre female	Control DIO-EYFP (6 weeks before acute recordings)	26 Nov 2013	Investigate UP-and-DOWN state and gamma oscillations in the medial prefrontal cortex of urethane-anesthetized PV-Cre mice;	<ul style="list-style-type: none"> - Good virus expression; - Good number of cells per tetrode in the mPFC; - Use of isoflurane 0.05% associated to urethane; - No light artifact in the LFPs; - Laser power 5mw; - Preliminary data is shown in the present report;
Acute #16	PV-Cre female	Control DIO-EYFP (6 weeks before acute recordings)	01 Dec 2013	Investigate UP-and-DOWN state and gamma oscillations in the medial prefrontal cortex of urethane-anesthetized PV-Cre mice;	<ul style="list-style-type: none"> - Good virus expression; - Good number of cells per tetrode in the mPFC; - Use of isoflurane 0.05% associated to urethane; - No light artifact in the LFPs; - Laser power 5mw; - Preliminary data is shown in the present report;
Acute #17	PV-Cre female	DIO-ChR2-mCherry (8 weeks before acute recordings)	10 Dec 2013	Investigate UP-and-DOWN state and gamma oscillations in the medial prefrontal cortex of urethane-anesthetized PV-Cre mice;	<ul style="list-style-type: none"> - Good virus expression; - Animal died before recordings get started;
Acute #18	PV-Cre female	DIO-ChR2-mCherry (8 weeks before acute recordings)	14 Dec 2013	Investigate UP-and-DOWN state and gamma oscillations in the medial prefrontal cortex of urethane-anesthetized PV-Cre mice;	<ul style="list-style-type: none"> - Excellent data; - Good virus expression; - Good number of cells <i>per</i> tetrode in the mPFC; - Use of isoflurane 0.05% associated to urethane; - No light artifact in the LFPs; - Inhibition of putative regular spiking cells: - Very clear activation of putative fast spiking cell (TT8); - Laser power 5mw; - Preliminary data is shown in the present report;
(cont.)					
Acute #19	PV-Cre female	DIO-ChR2-mCherry (8 weeks before acute recordings)	16 Dec 2013	Investigate UP-and-DOWN state and gamma oscillations in the medial prefrontal cortex of urethane-anesthetized PV-Cre mice;	<ul style="list-style-type: none"> - Good virus expression; - Good number of cells <i>per</i> tetrode in the mPFC; - Use of isoflurane 0.05% associated to urethane; - No light artifact in the LFPs; - Inhibition of putative regular spiking cells: - Laser power 5mw;

Acute #20	NR1-PV-Cre female	DIO-ChR2-mCherry (7 weeks before acute recordings)	19 Dec 2013	Investigate UP-and-DOWN state and gamma oscillations in the medial prefrontal cortex of urethane-anesthetized mice lacking NMDA receptors in parvalbumin neurons	<ul style="list-style-type: none"> - Preliminary data is shown in the present report; - Good virus expression; - Great number of cells per tetraode in the mPFC; - Use of isoflurane 0.05% associated to urethane; - No light artifact in the LFPs; - Partial inhibition of putative regular spiking cells; - Laser power 5mw; - Preliminary data is shown in the present report;
Acute #21	NR1-PV-Cre female	DIO-ChR2-mCherry (7 weeks before acute recordings)	20 dec 2013	Investigate UP-and-DOWN state and gamma oscillations in the medial prefrontal cortex of urethane-anesthetized mice lacking NMDA receptors in parvalbumin neurons;	<ul style="list-style-type: none"> - Good virus expression; - Great number of cells per tetraode in the mPFC; - Use of isoflurane 0.05% associated to urethane; - No light artifact in the LFPs; - Very clear inhibition of some putative regular spiking cells; - Laser power 5mw; - Preliminary data is shown in the present report;
Acute #22 (cont.)	NR1-PV-Cre female	DIO-ChR2-mCherry (7 weeks before acute recordings)	21 Dec 2013	Investigate UP-and-DOWN state and gamma oscillations in the medial prefrontal cortex of urethane-anesthetized mice lacking NMDA receptors in parvalbumin neurons;	<ul style="list-style-type: none"> - Good virus expression; - Great number of cells per tetraode in the mPFC; - Use of isoflurane 0.05% associated to urethane; - No light artifact in the LFPs; - Partial inhibition of putative regular spiking cells; - Laser power 5mw; - Preliminary data is shown in the present report;

Table 2. Library of all sorted units

Cell ID	Width	Peak-trough ratio	Cluster - Kmeans
<i>Ac12TT1-C1</i>	0,31	3,1	RS
<i>Ac12TT1-C2</i>	0,16	3,0	RS
<i>Ac12TT1-C3</i>	0,28	3,1	RS
<i>Ac12TT1-C4</i>	0,28	3,0	RS
<i>Ac12TT2-C1</i>	0,31	3,1	RS
<i>Ac12TT2-C3</i>	0,31	2,7	RS

Ac12TT2-C4	0,13	2,9	RS
Ac12TT3-C1	0,28	2,6	RS
Ac12TT3-C2	0,13	3,6	RS
Ac12TT3-C3	0,28	3,4	RS
Ac12TT3-C4	0,28	2,5	RS
Ac12TT3-C5	0,31	2,6	RS
Ac12TT3-C6	0,31	2,8	RS
Ac12TT3-C7	0,28	3,1	RS
Ac12TT4-C1	0,31	3,0	RS
Ac12TT4-C2	0,31	3,5	RS
Ac12TT4-C3	0,13	2,8	RS
Ac12TT5-C1	0,31	2,9	RS
Ac12TT6-C1	0,28	3,2	RS
Ac13TT1-C1	0,31	3,2	RS
Ac13TT2-C2	0,31	3,4	RS
Ac13TT2-C3	0,31	3,8	RS
Ac13TT3-C1	0,31	3,8	RS
Ac13TT3-C2	0,41	3,8	RS
Ac13TT3-C3	0,31	3,5	RS
Ac13TT4-C1	0,31	2,6	RS
Ac13TT4-C2	0,41	3,5	RS
Ac13TT5-C1	0,28	4,4	RS
Ac13TT5-C3	0,31	4,1	RS
Ac16TT1-C4	0,19	3,4	RS
Ac16TT1-C5	0,59	3,5	RS
Ac18TT5-C1	0,28	2,9	RS
Ac18TT5-C2	0,31	2,8	RS
Ac18TT5-C3	0,19	2,8	RS
Ac18TT6-C1	0,28	2,9	RS
Ac18TT6-C2	0,28	3,2	RS
Ac18TT6-C3	0,31	2,9	RS
Ac20TT1-C1	0,41	3,1	RS
Ac20TT1-C2	0,41	2,7	RS
Ac20TT1-C3	0,31	2,7	RS
Ac20TT2-C2	0,28	2,6	RS
Ac20TT3-C1	0,28	2,6	RS
Ac20TT3-C2	0,34	3,1	RS
Ac20TT3-C3	0,41	3,4	RS
Ac20TT4-C2	0,28	3,2	RS
Ac20TT4-C3	0,28	3,3	RS
Ac20TT4-C4	0,31	3,1	RS
Ac20TT4-C5	0,31	3,6	RS
Ac20TT5-C1	0,28	3,5	RS
Ac20TT5-C2	0,28	2,6	RS
Ac20TT5-C3	0,41	3,2	RS
Ac20TT5-C4	0,41	3,4	RS
Ac20TT6-C1	0,28	3,1	RS
Ac20TT6-C2	0,44	3,3	RS

Ac20TT6-C3	0,38	2,7	RS
Ac20TT6-C4	0,31	2,8	RS
Ac20TT7-C2	0,31	3,1	RS
Ac20TT8-C1	0,34	2,5	RS
Ac20TT8-C2	0,16	3,1	RS
Ac20TT8-C3	0,16	3,2	RS
Ac20TT8-C5	0,31	2,9	RS
Ac20TT8-C6	0,34	2,8	RS
Ac21TT3-C1	0,44	2,9	RS
Ac21TT3-C2	0,41	3,6	RS
Ac21TT4-C1	0,31	3,8	RS
Ac21TT4-C2	0,28	3,5	RS
Ac21TT5-C3	0,28	2,5	RS
Ac21TT5-C4	0,31	3,6	RS
Ac21TT5-C5	0,28	2,6	RS
Ac21TT6-C1	0,28	3,0	RS
Ac21TT6-C2	0,28	3,7	RS
Ac21TT6-C3	0,41	3,2	RS
Ac21TT6-C5	0,31	2,5	RS
Ac21TT7-C1	0,19	2,6	RS
Ac21TT7-C2	0,31	3,2	RS
Ac21TT7-C3	0,31	4,2	RS
Ac21TT7-C4	0,28	4,3	RS
Ac21TT7-C5	0,13	3,9	RS
Ac21TT7-C6	0,19	3,8	RS
Ac21TT7-C7	0,31	3,0	RS
Ac21TT8-C3	0,22	4,2	RS
Ac21TT8-C4	0,28	3,4	RS
Ac21TT8-C5	0,44	4,2	RS
Ac22TT1-C3	0,31	3,8	RS
Ac22TT1-C4	0,41	3,3	RS
Ac22TT2-C1	0,19	3,0	RS
Ac22TT3-C1	0,16	3,2	RS
Ac22TT3-C2	0,16	4,3	RS
Ac22TT3-C3	0,31	3,4	RS
Ac22TT3-C4	0,38	3,2	RS
Ac22TT4-C2	0,44	2,5	RS
Ac22TT4-C3	0,41	3,4	RS
Ac22TT5-C2	0,44	3,0	RS
Ac22TT5-C3	0,34	2,9	RS
Ac22TT6-C1	0,31	3,5	RS
Ac22TT6-C2	0,31	3,0	RS
Ac22TT6-C3	0,31	3,5	RS
Ac22TT7-C1	0,31	4,1	RS
Ac22TT7-C2	0,31	3,3	RS
Ac12TT2-C2	0,25	1,9	FS
Ac12TT7-C2	0,13	2,0	FS
Ac13TT1-C2	0,25	1,1	FS

Ac13TT2-C1	0,25	1,7	FS
Ac13TT3-C4	0,22	1,6	FS
Ac13TT4-C3	0,28	1,0	FS
Ac13TT5-C2	0,31	1,3	FS
Ac16TT1-C1	0,28	2,3	FS
Ac16TT1-C2	0,16	1,6	FS
Ac16TT1-C3	0,16	1,7	FS
Ac18TT5-C4	0,19	1,9	FS
Ac18TT8-C1	0,19	0,9	FS
Ac19TT1-C1	0,28	1,1	FS
Ac19TT1-C2	0,16	1,2	FS
Ac19TT1-C3	0,22	1,0	FS
Ac19TT2-C1	0,19	1,0	FS
Ac19TT3-C1	0,16	1,9	FS
Ac20TT2-C1	0,16	1,8	FS
Ac20TT4-C1	0,25	0,9	FS
Ac20TT6-C5	0,28	1,9	FS
Ac20TT7-C1	0,28	1,9	FS
Ac20TT8-C4	0,16	1,8	FS
Ac21TT4-C3	0,25	1,0	FS
Ac21TT5-C1	0,22	0,8	FS
Ac21TT5-C2	0,19	1,7	FS
Ac21TT6-C4	0,16	1,1	FS
Ac21TT8-C1	0,13	2,0	FS
Ac21TT8-C2	0,13	2,3	FS
Ac22TT1-C1	0,31	1,9	FS
Ac22TT1-C2	0,25	1,9	FS
Ac22TT4-C1	0,22	2,2	FS
Ac22TT5-C1	0,22	1,0	FS
Ac22TT7-C3	0,19	1,9	FS
Ac22TT8-C1	0,16	1,5	FS

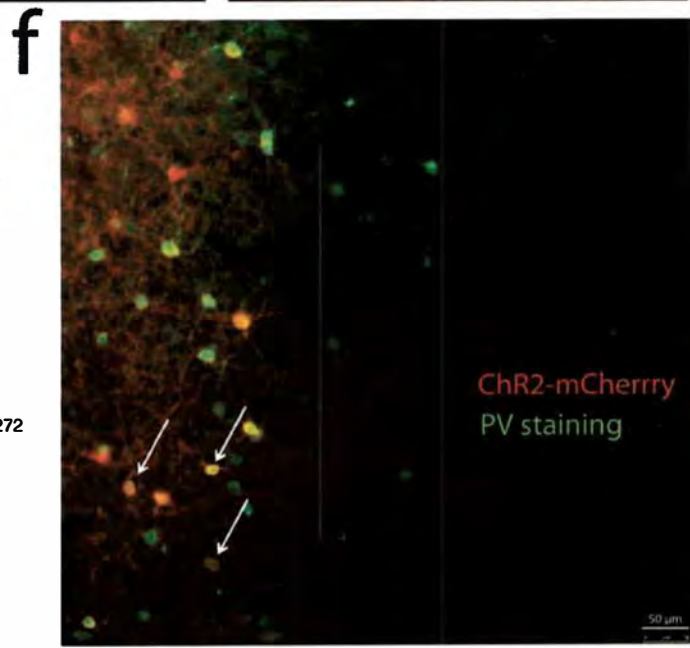
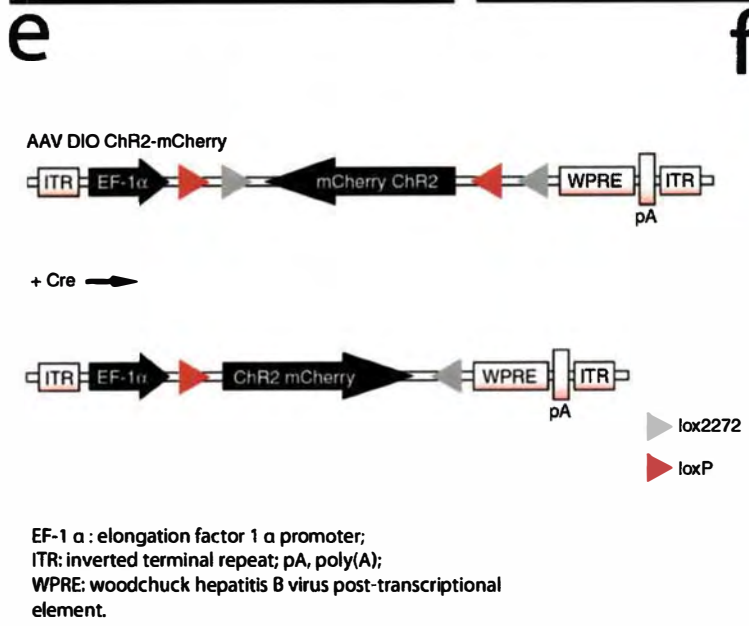
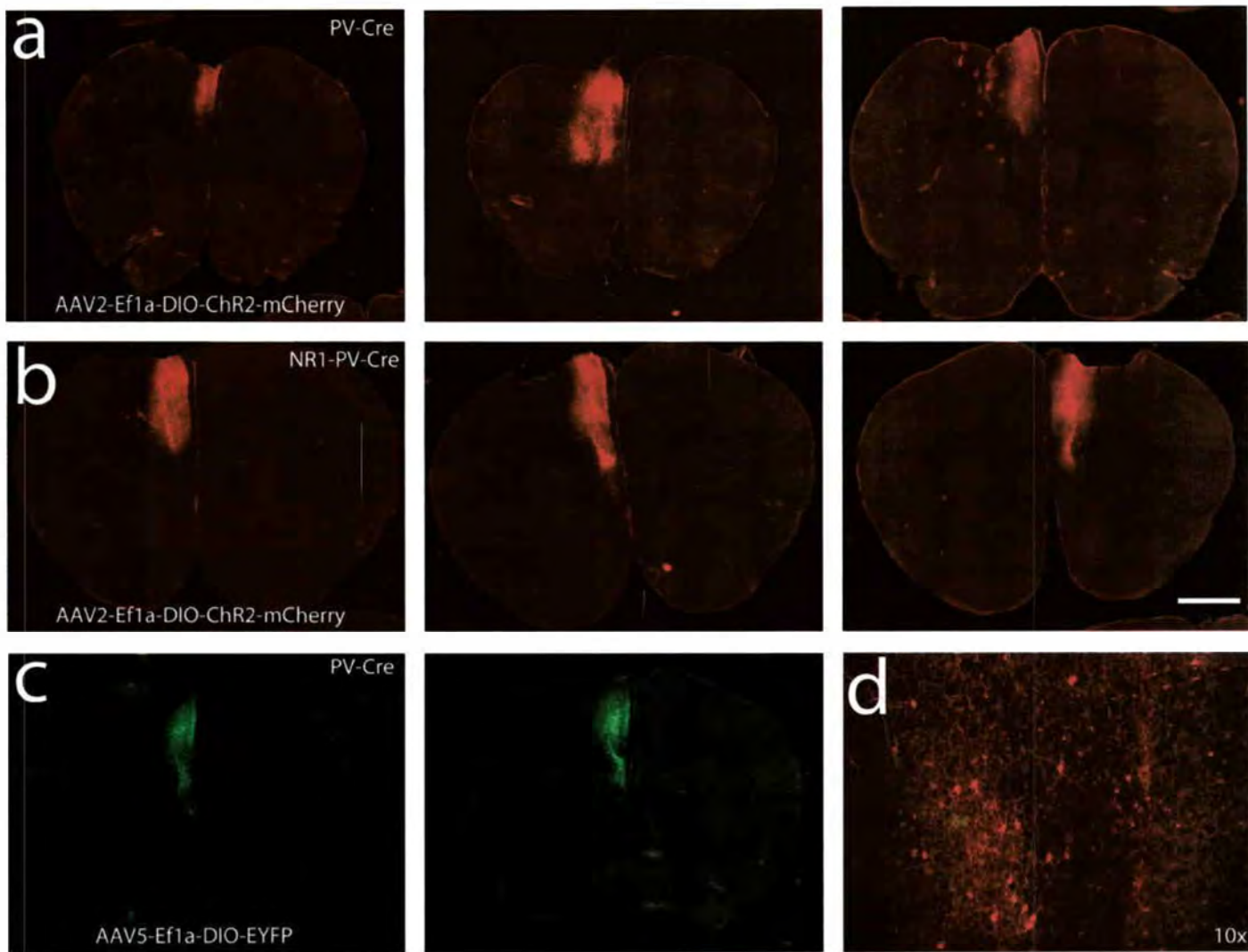


Figure 1. Cre-dependent expression of the light-activated ChR2. (a) When injected unilaterally into the mPFC of adult PV-Cre mice, the viral vector AAV2-DIO-ChR2-mCherry provided robust expression of ChR2 in PV+ interneurons; (b) The same pattern of expression can be observed in PV-Cre-NR1f/f mice; (c) Besides, the injection of the control vector AAV5-DIO-EYFP provided robust expression of the EYFP fluorophore as well; (d) 10X magnification of a section from a AAV2-DIO-ChR2-mCherry injected PV-Cre mouse showing a good of cell bodies transfected in prelimbic area of mPFC; (e) The adeno-associated viral vector AAV-DIO-ChR2-mCherry carries an inverted version of ChR2 fused to the fluorescent markers mCherry. This strategy prevents ChR2 from being expressed in the absence of Cre. The loxP variants loxP and lox2272 flanking ChR2-mCherry are incompatible and cannot recombine with each other (Lee et al., 1998), leading to a stochastic recombination of either variant (Livet et al., 2007) in the presence of Cre. Because both loxP variants both loxP variants are constitutes of lox pairs facing each other, recombination results in inversion of ChR2-mCherry into the sense orientation. As a consequence of the first recombination event, the second unrecombined loxP variant now is constituted of two directly oriented lox sites and will therefore excise one of the lox sites of the first loxP variant, an event that prevents further recombination. This strategy eliminates possible misexpression of ChR2 due to leakiness of the commonly used translational stop cassettes and targets recombination and expression of ChR2-mCherry exclusively to Cre expressing cells (from Cardin et al. 2009); (f) Staining for PV+ in a mPFC section from a transfected PV-Cre mouse with AAV2-DIO-ChR2-mCherry conveys examples of cells expressing ChR2-mCherry which showed detectable levels of PV (white arrows).

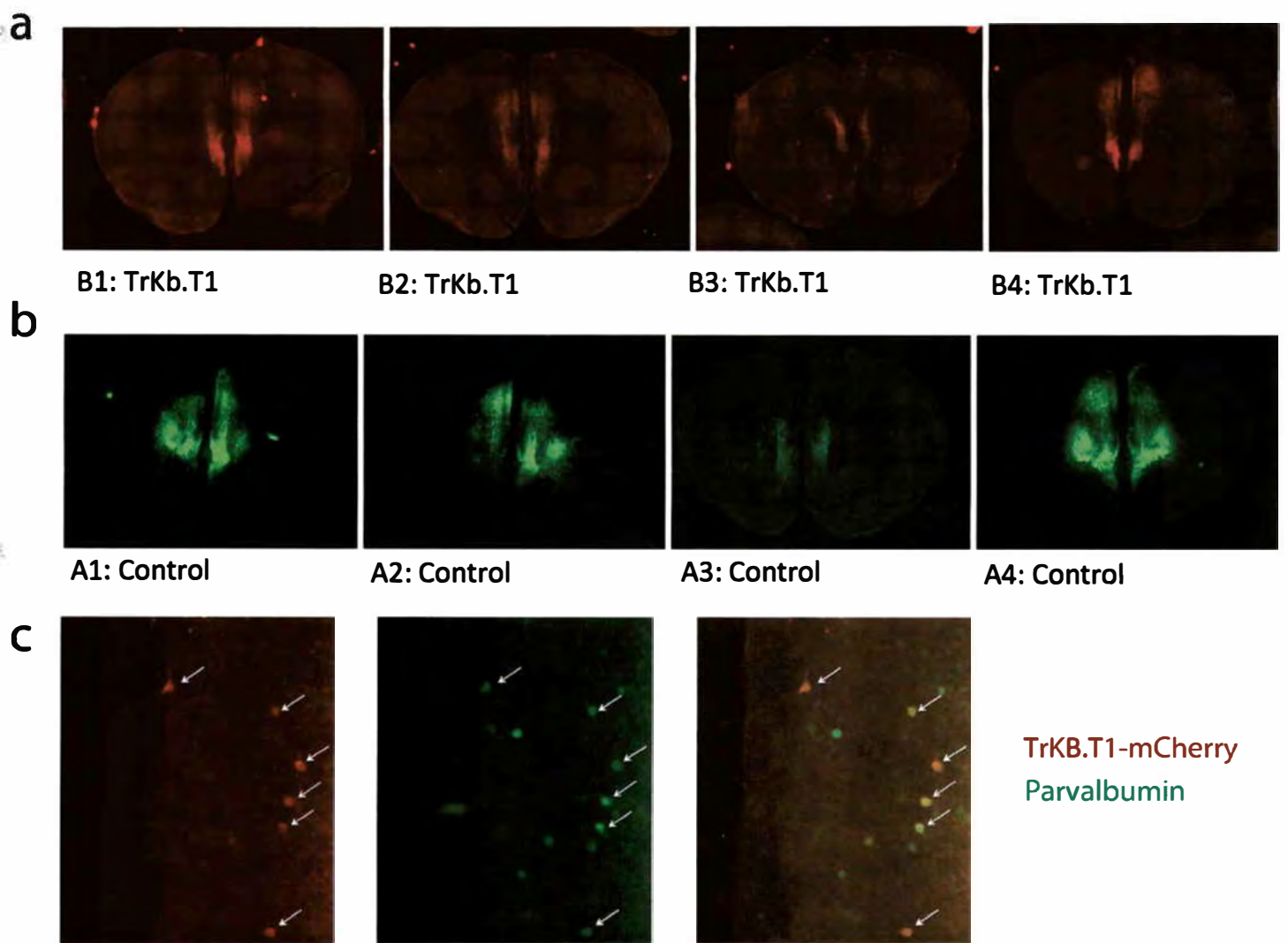


Figure 2. Cre-dependent expression of the truncated trkb receptor (Trkb.T1). (a) When injected bilaterally targeting the infralimbic tmPFC of adult PV-Cre mice, the viral vector AAV2-DIO-TrkB.T1-mCherry provided robust expression of TrkB.T1 in PV+ interneurons; (b) Besides, the injection of the control vector AAV5-DIO-EYFP provided robust expression of the EYFP fluorophore as well; (c) image with higher magnitude showing cell-specific expression of TrkB.t1-mCherry with good co-localization with the PV+ staining (white arrows).

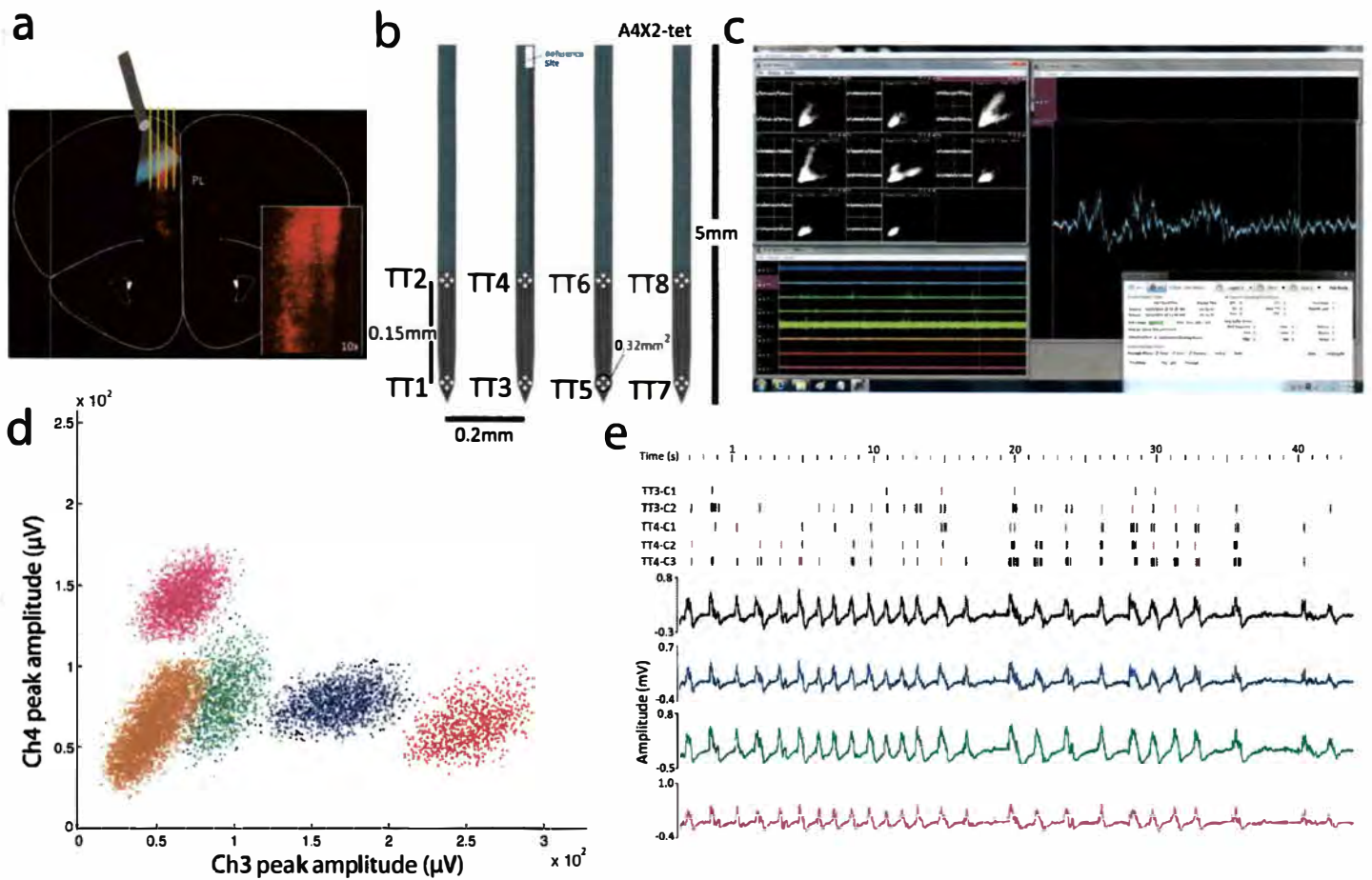


Figure 3. Acute recordings in the mPFC associated to optogenetics. (a) Schematic representation of the mPFC, the positioning of the silicon probe and the oblique insertion of the optical fiber (10–15 degrees of slope) to attenuate light-artifacts. (b) Basic configuration of the silicon probe used in our experiments: A4x2-tet-5mm-150-200-312-A32; Neuronex. (c) A screenshot from the software Cheetah 64 during recordings of LFPs and spikes in the mPFC of a urethane-anesthetized mouse. (d) Example of sorted putative cells using MClust. (e) Raw data of LFPs and sorted spikes imported and displayed in Neuroexplorer. It is remarkable the synchrony between spikes and UP-and-DOWN states in the LFPs in the mPFC.

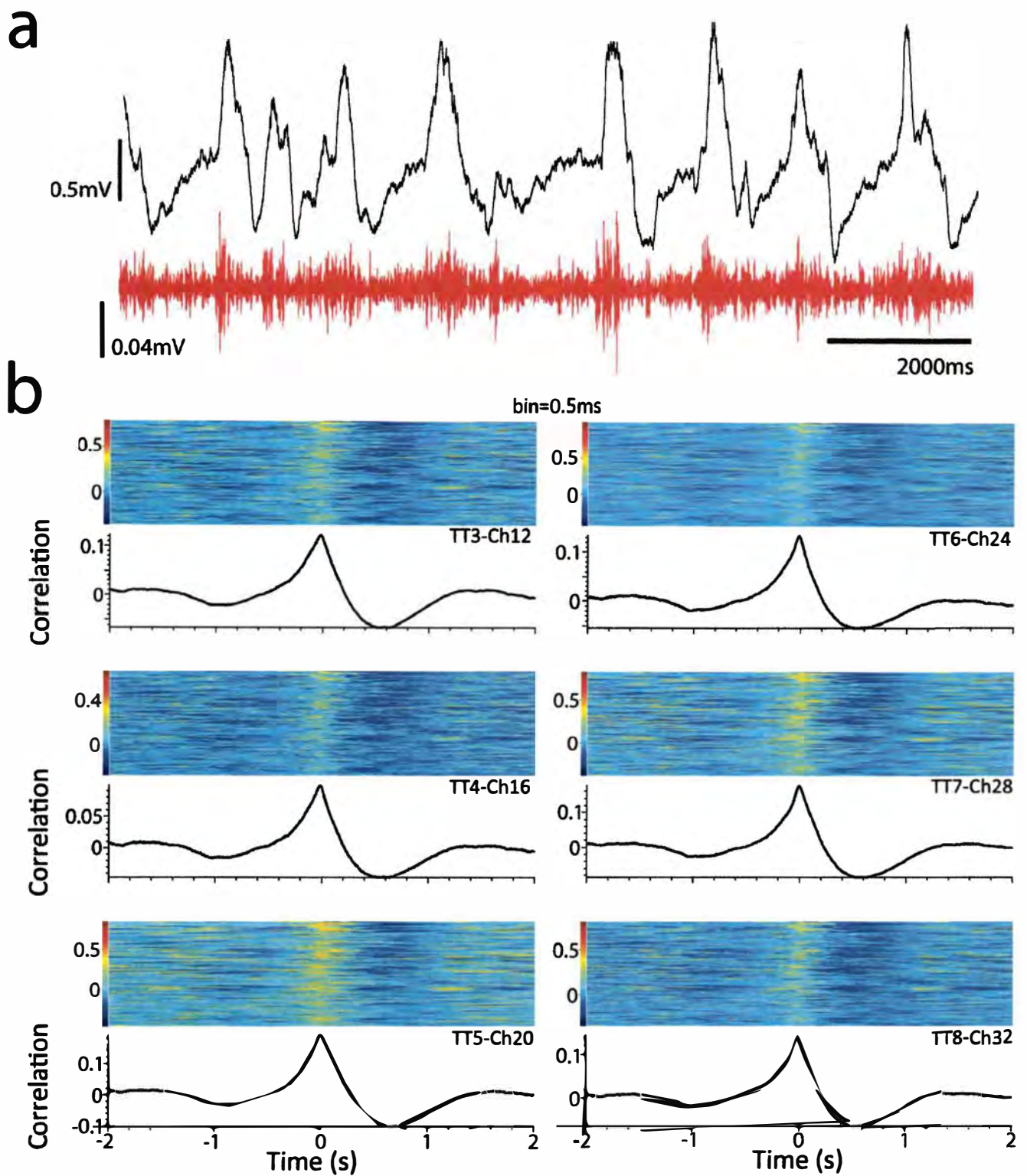
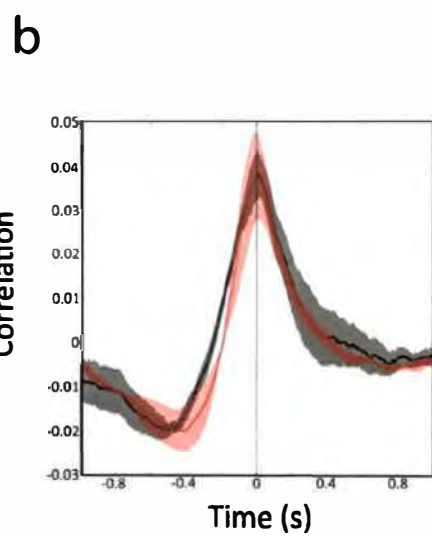
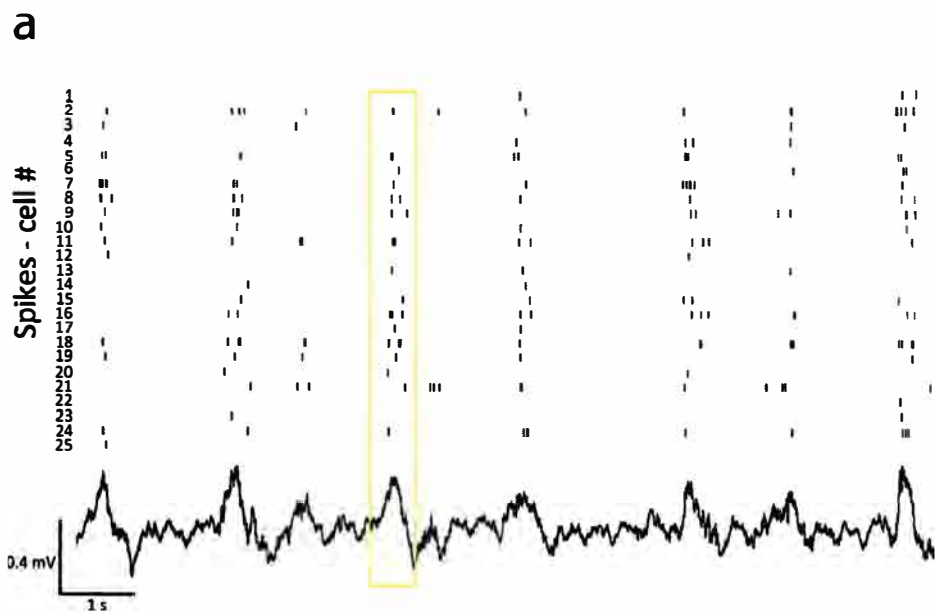


Figure 4. Gamma oscillations and spike-timing in the mPFC during urethane-induced UP-and-DOWN states. (a) A 10s-epoch of LFP was band-pass filtered in (55-120 Hz) and plotted together with the raw LFP tracing to illustrate gamma nested to UP-states; **(b)** Spike-triggered average field for six LFPs channels (different tetrodes) surrounding the spikes of a sorted unit from TT8 seemed to yield similar results. The colormap represents the LFPs amplitude in each trial of 4s-window (-2, +2).



— PV-Cre (n=5)
— NR1-PV-Cre (n=3)

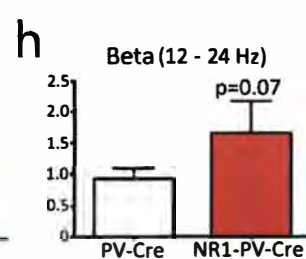
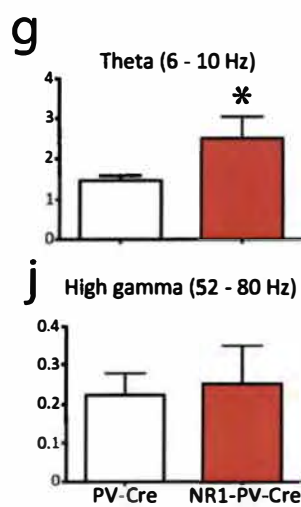
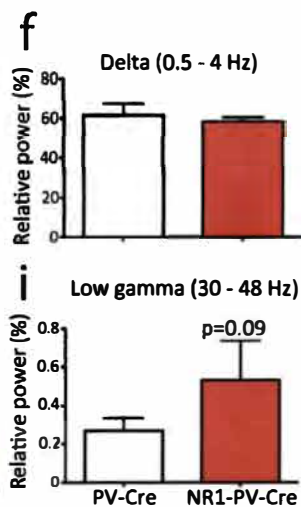
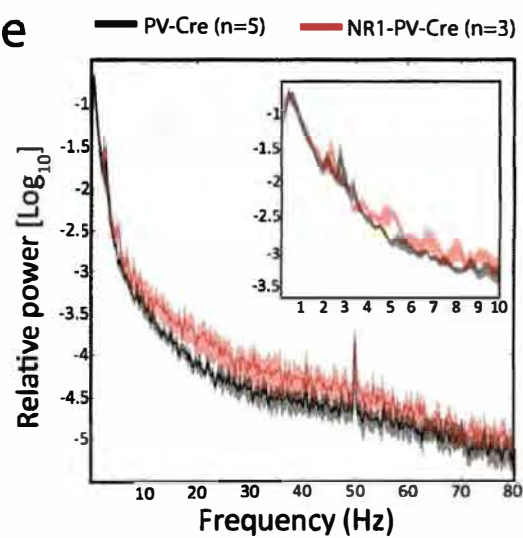
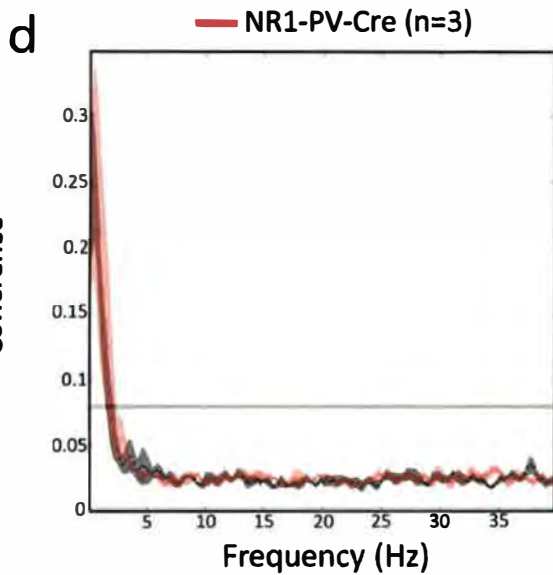
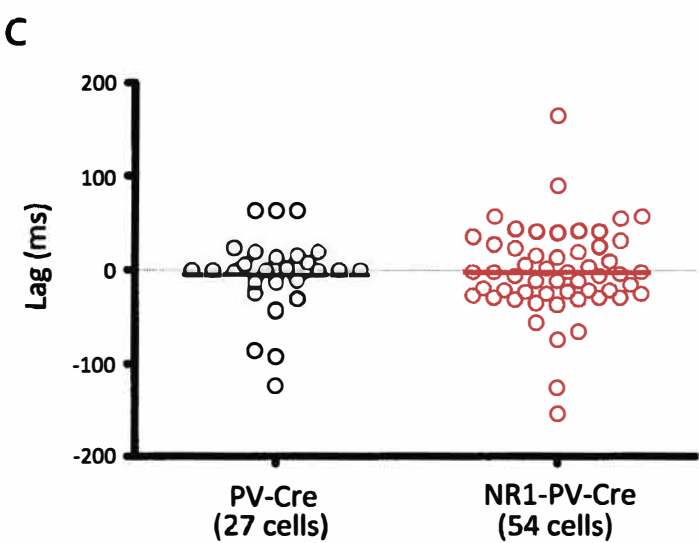


Figure 5. Relationship between LFPs and spikes during UP-and-DOWN states in PV-Cre and PV-Cre-NR1f/f. **(a)** Raw data displayed in Neuroexplorer illustrating an impressive proportion of cells aligned to the UP-states of a 10s-epoch LFP recorded in the mPFC of a PV-Cre-NR1-f/f mouse under urethane. One of these periods is highlighted by yellow rectangle. **(b)** Average of the temporal correlation between spike and LFPs in the PV-Cre (n=27 cells; grey) and PV-Cre-NR1f/f (n=54 cells; red) groups indicate that the lack of NR1 subunit in PV neurons did not disrupt synchrony spike-LFP during cortical UP-and-DOWN states. **(c)** Scatter plot with the time lag between spike and LFPs of all cells sorted for both groups. **(d)** Spectral coherence analysis between LFPs and spikes indicates a very specific frequency range of entrainment (0.5 – 1Hz) for both groups. **(e)** To assess possible alterations in basal oscillatory patterns in the mPFC of urethane-anesthetized PV-Cre-NR1f/f mice a 100s-epoch with the most stable UP-and-DOWN states was evaluated regarding its power spectrum. The average relative power spectral density suggests higher power at frequencies from theta to low gamma in PV-Cre-NR1f/f animals. Indeed, statistical analysis indicate that PV-Cre-NR1f/f group displayed LFPs with higher power in **(g)** theta and a trend towards higher power in **(h)** beta and **(i)** low-gamma. No differences were observed in **(f)** delta and **(j)** high-gamma ranges of frequency. * Statistical significant: $p=0.03$; Student t-test. Data are shown as mean \pm s.e.m.

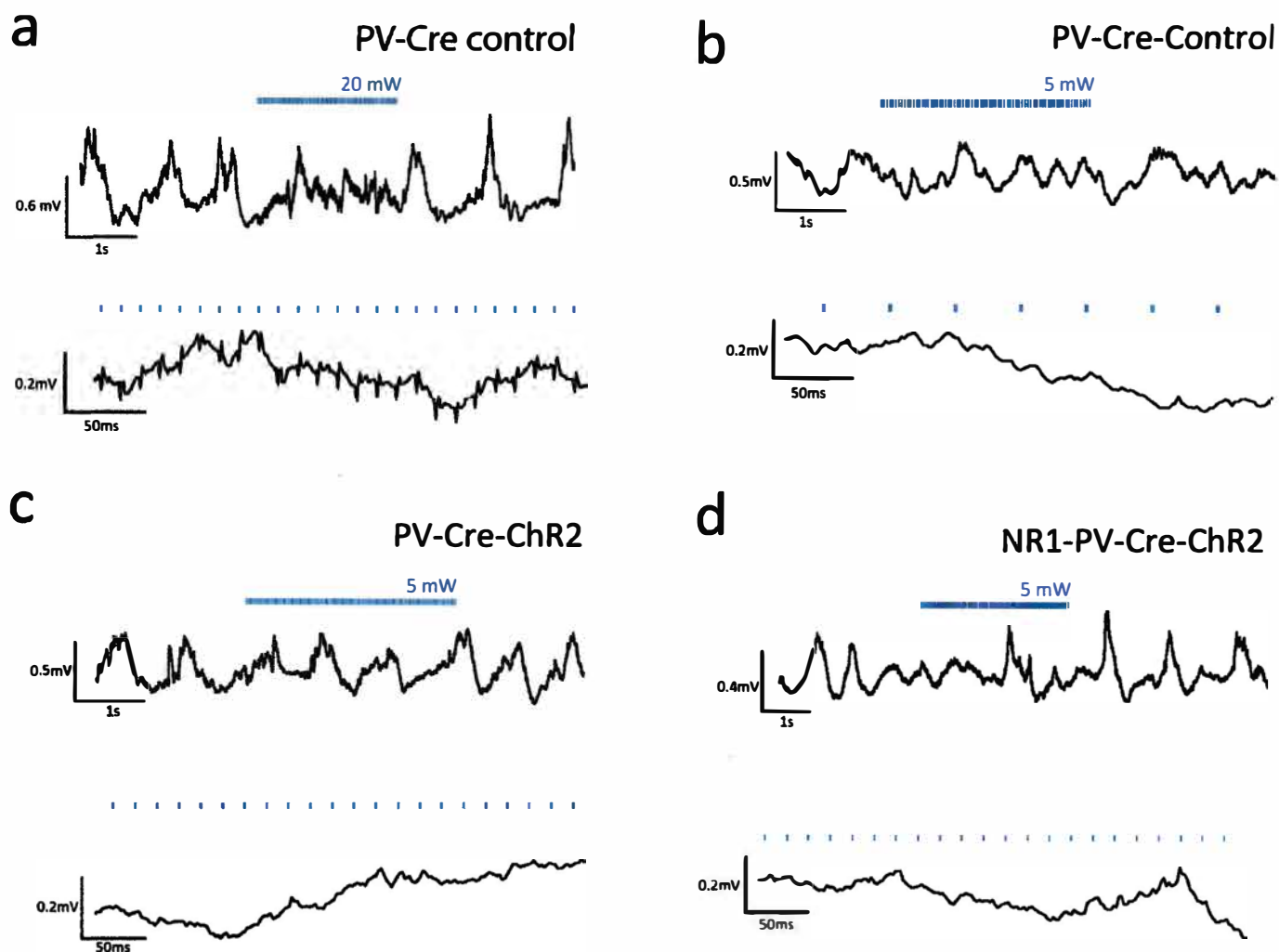


Figure 6. Elimination of light-induced artifacts in LFPs recordings. (a) Direct exposure of metal electrodes to the laser beam causes large electrical artifacts. This example was taken from recordings in the mPFC not transduced with AAV2-DIO-ChR2-mCherry. Although we were already using an oblique insertion of the optical fiber in relation to the silicon probe, it is possible to see that 1ms light-pulses applied at 20mW power caused a large and repeated artifact in the LFP recording (lower black trace). The artifact started at the onset of each light pulse and usually lasted more than the light pulse width. (b) Another sample of LFP during light stimulation. Now, a PV-Cre animal transfected with control virus AAV-DIO-EYFP displayed a cleaner LFP tracing when the laser power was reduced from 20 to 5mW. Artifacts in the metal sites of the silicon probe recordings were indeed eliminated by changing the angle of the fiber, associated to reduction in the power as can illustrated in (c) and (d).

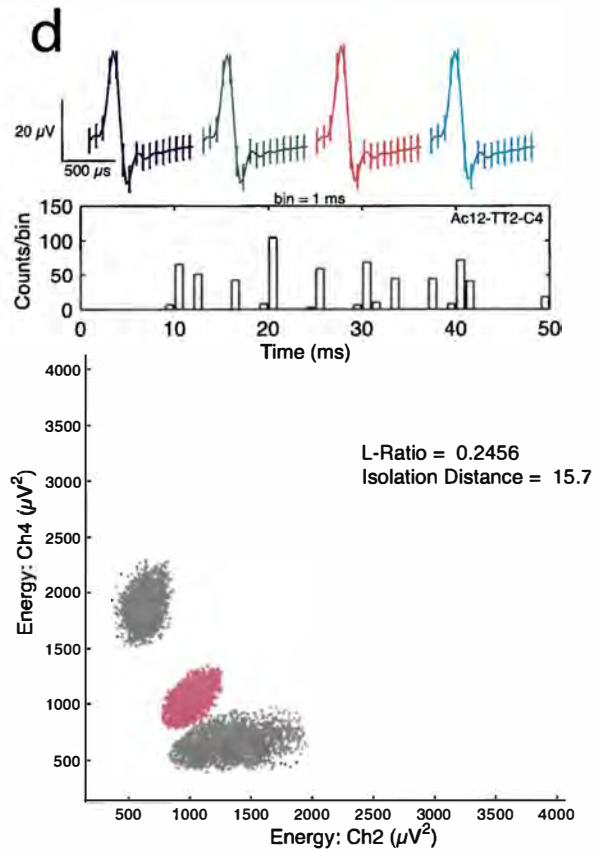
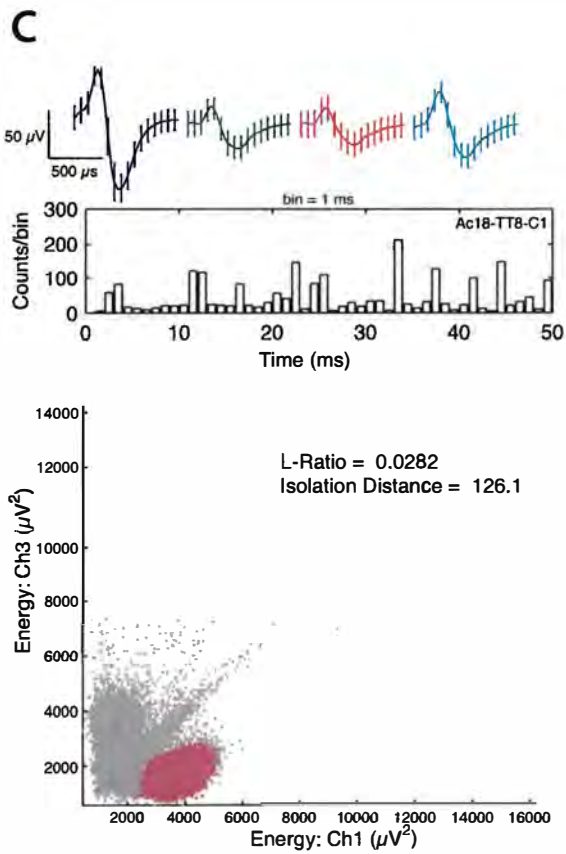
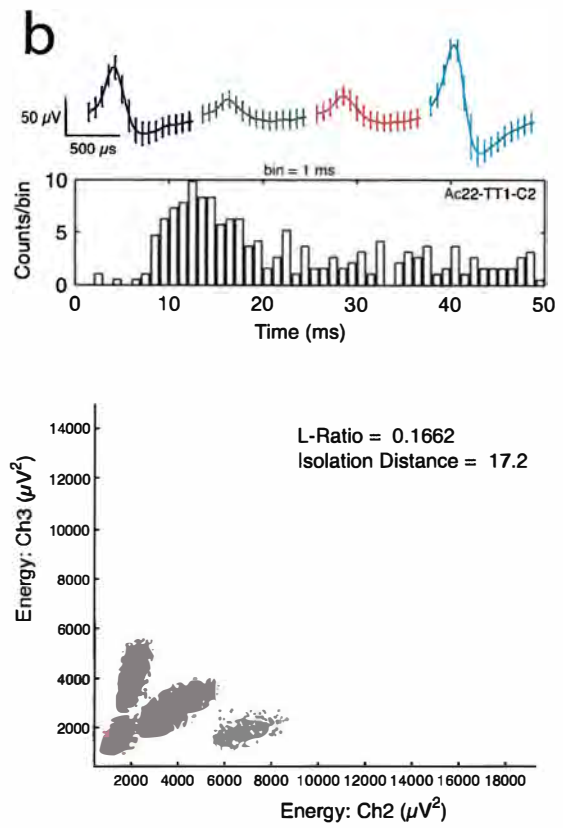
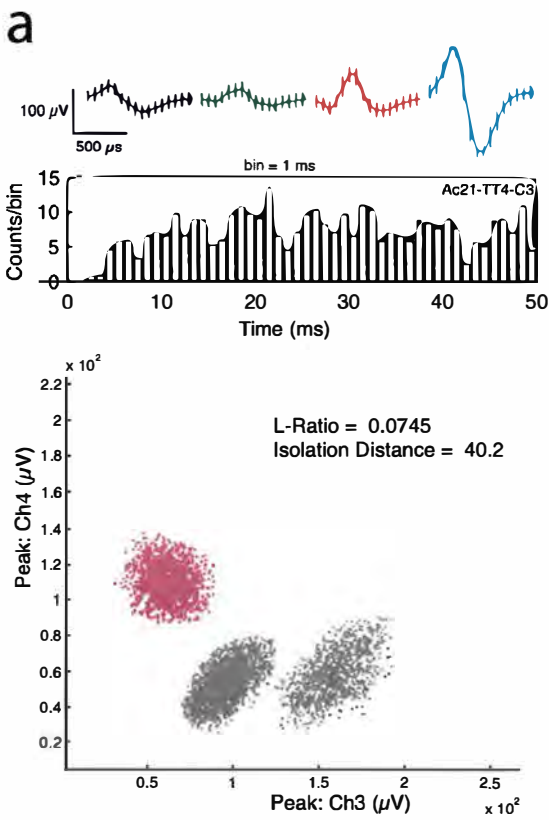


Figure 7. Checking clusters to detect light-artifacts. (a) Ac21-TT4-C3 is a sorted unit from a PV-Cre-NR1f/f mouse transfected with ChR2-mCherry. It shows good signal-to-noise ratio between the tetrode sites (top), excellent parameters of cluster quality (bottom; L-Ratio and Isolation Distance) and dispersed ISI (middle), indicating irregular firing. (b) Ac22-TT1-C2 is a sorted unit from a PV-Cre-NR1f/f mouse transfected with ChR2-mCherry as well. It shows a good signal-to-noise ratio between the tetrode sites, worse parameters of cluster quality (though still acceptable) and a more concentrated ISI, indicating a better spike timing. (c) Ac22-TT1-C2 is a sorted unit from a PV-Cre mouse transfected with ChR2-mCherry. It shows a good signal-to-noise ratio between the tetrode sites, remarkable parameters of cluster quality and an unusual ISI due to light-activation in specific frequencies. For instance, the peak of firing near to 30ms might be related to 32Hz stimulation ($F=1/0.03125s$) and the other ones, near to 20 and 25ms, might be caused by 40 and 48Hz stimulation. Importantly, it is possible to see firing activity in intermediate frequencies, suggesting spontaneous firing between light-pulses and/or trains. (d) Likewise the prior cluster, Ac12-TT2-C4 is a sorted unit from a PV-Cre mouse transfected with ChR2-mCherry. It displays a poor signal-to-noise ratio between the tetrode sites, worse parameters of cluster quality (though still acceptable) and a very unusual ISI, with peaks excessively locked to the frequencies of stimulation. Therefore, this waveform is a candidate to be considered as a light-artifact.

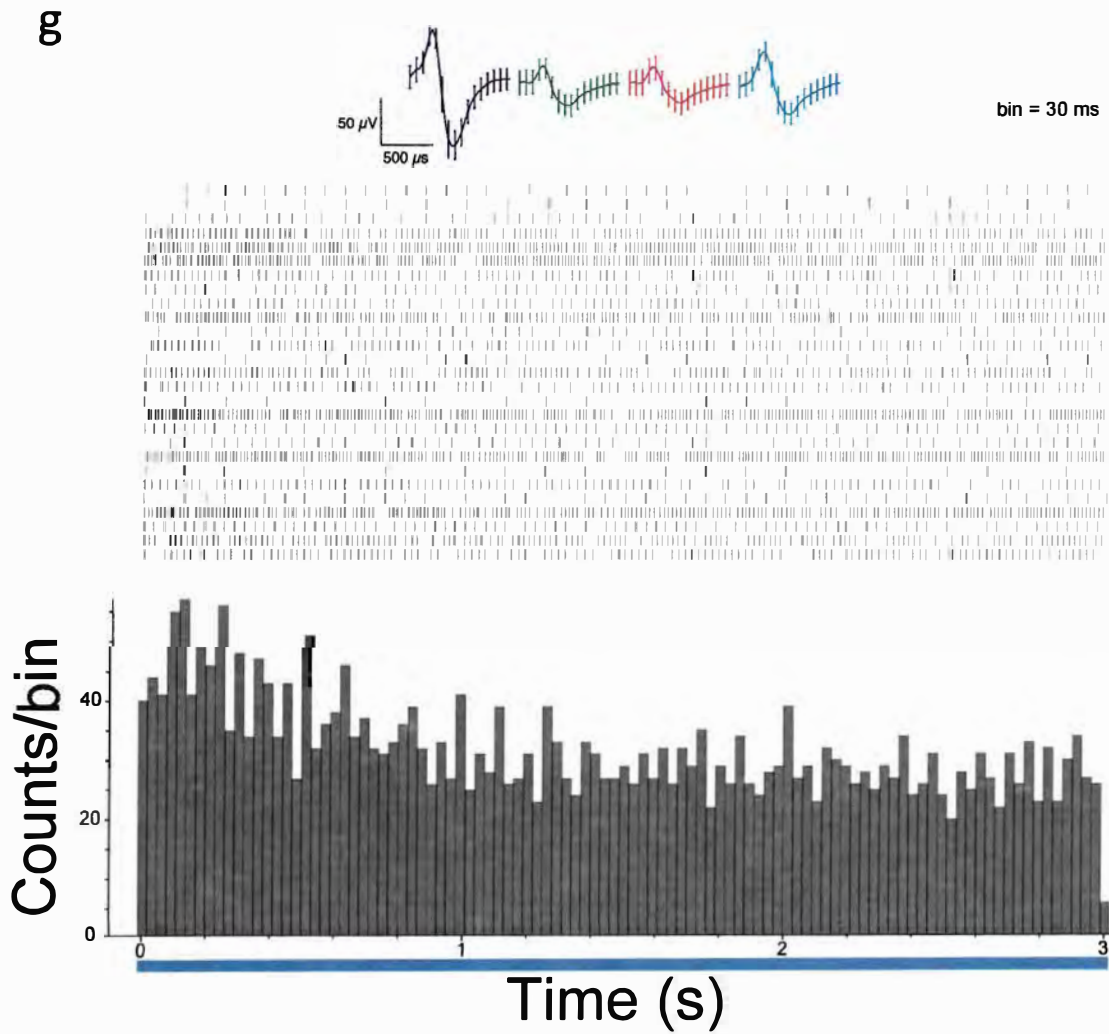
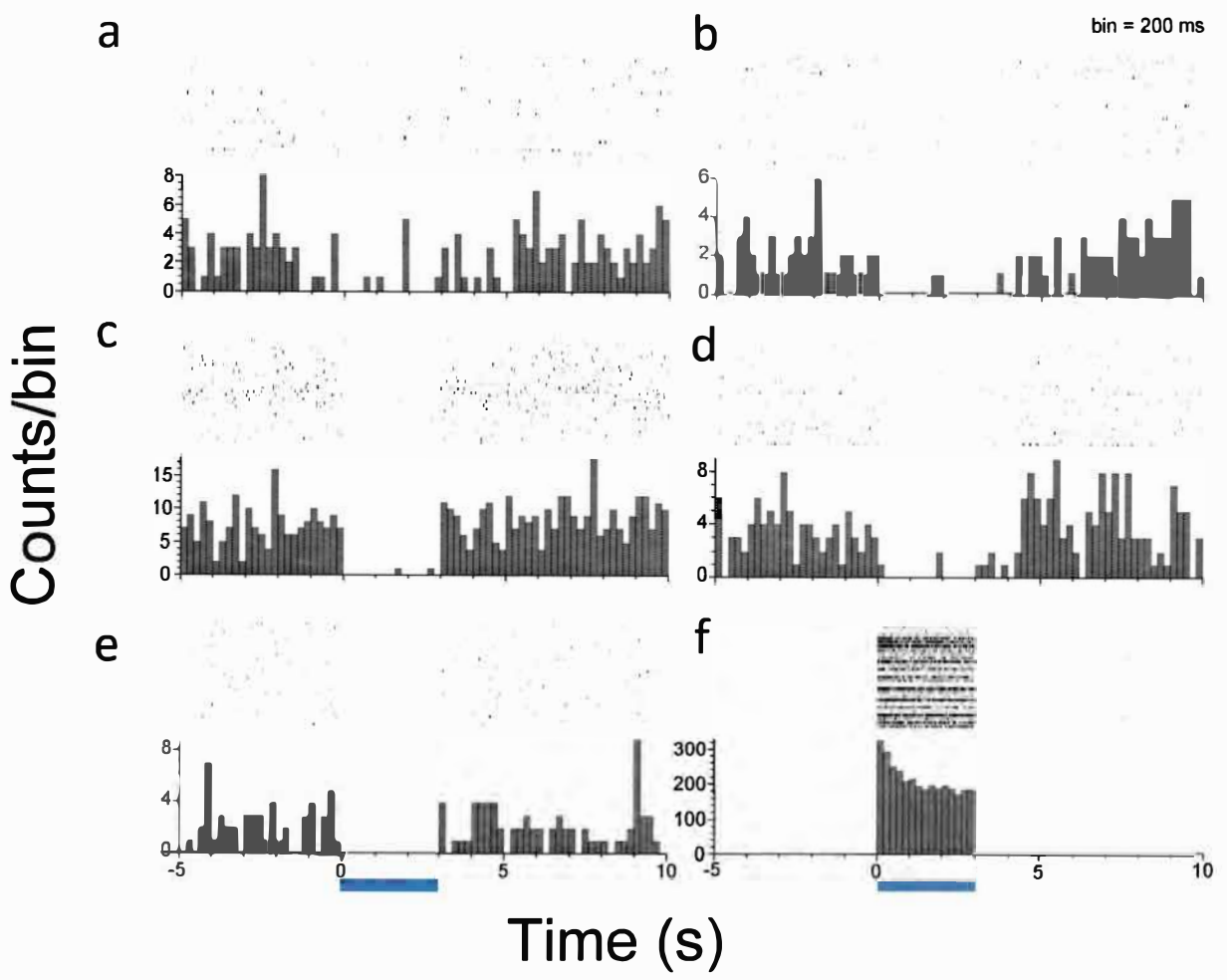


Figure 8. Optogenetics validation: Example of light-induced inhibition and activation in a PV-Cre mouse. A PV-Cre animal injected with ChR-mCherry was submitted to 27 trials of 3s-trains of stimulation (1ms pulses at 8, 16, 24, 32, 48, 60, 80 and 90 Hz; 5mW). **(a-e)** Peri-event raster and histogram of five different cells are shown to exemplify firing activity suppression during light stimulation. **(f)** Peri-event raster and time histogram of a putative FS cell showing a robust activation during light stimulation. **(g)** Shows the waveforms and a larger peri-event raster and time histogram of the same unit displayed in f.

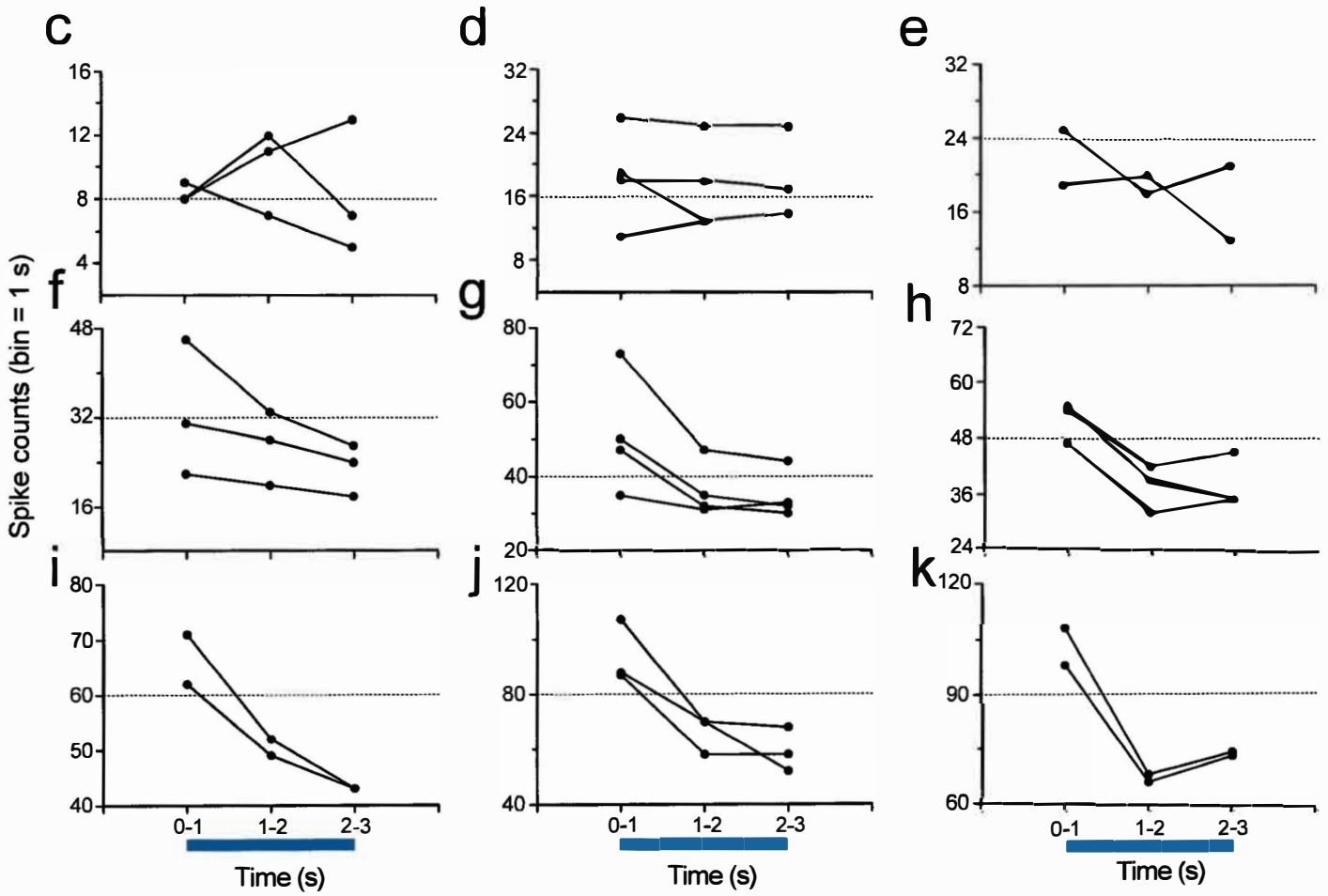
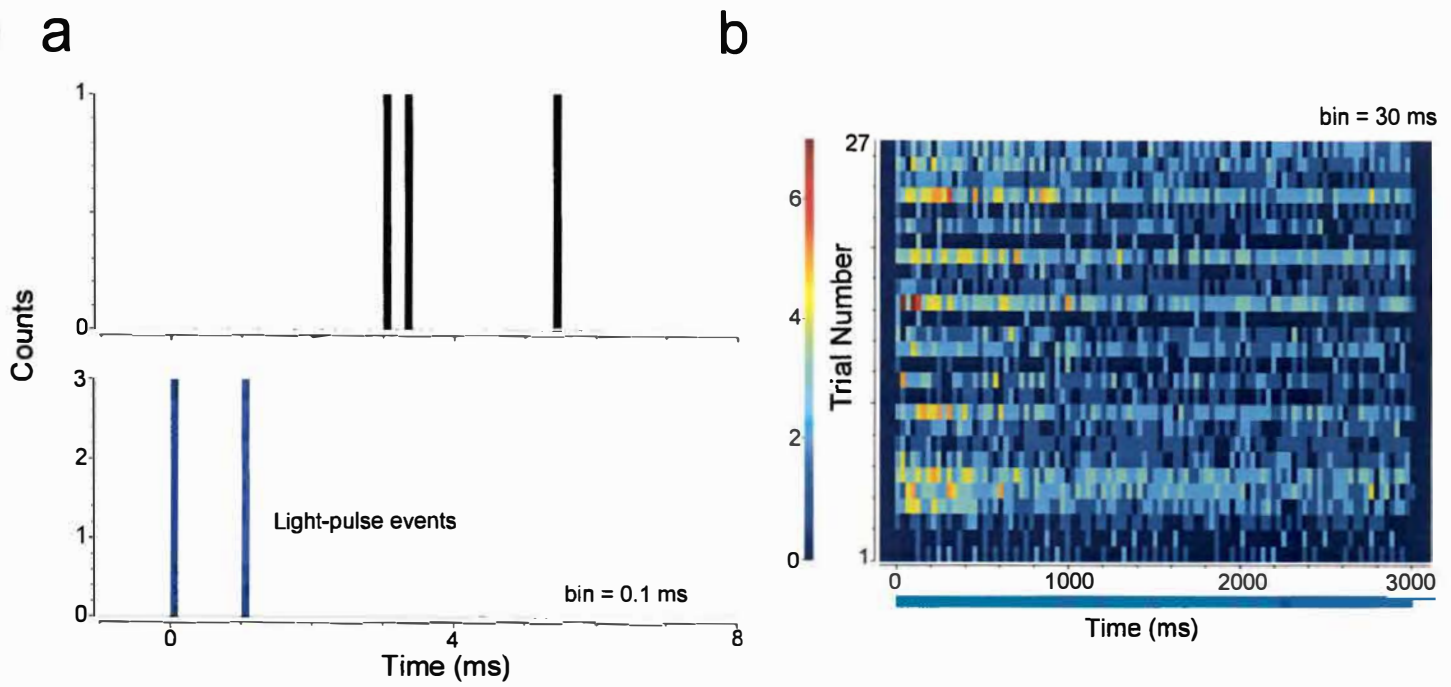


Figure 9. Putative FS cell displayed a rapid firing-rate increase followed by a decrease until a steady state under light-stimulation. (a) The event-related spike responses of the cell Ac18-TT8-C1 (above) display a biologically reasonable latency (3.05ms) to the stimulus (below); **(b)** Spike counting trial-by-trial during 3s of light stimulation highlights the rapid firing-rate increase followed by a decrease until a steady state under light-stimulation. Colormap is the number of spikes per bin. Then, the same data were grouped in bins of 1s and the trials were sorted according to the frequency of stimulation. Stimulation frequencies up to 16Hz were able to entrain the cell to firing around the same frequency. In this case, the entrainment lasted the whole period of optical stimulation **(c-d)**. However, in higher frequencies, the same cell failed to follow the stimulation frequency **(e-h)**. This was particularly more evident in frequencies above 60Hz **(i-k)**.

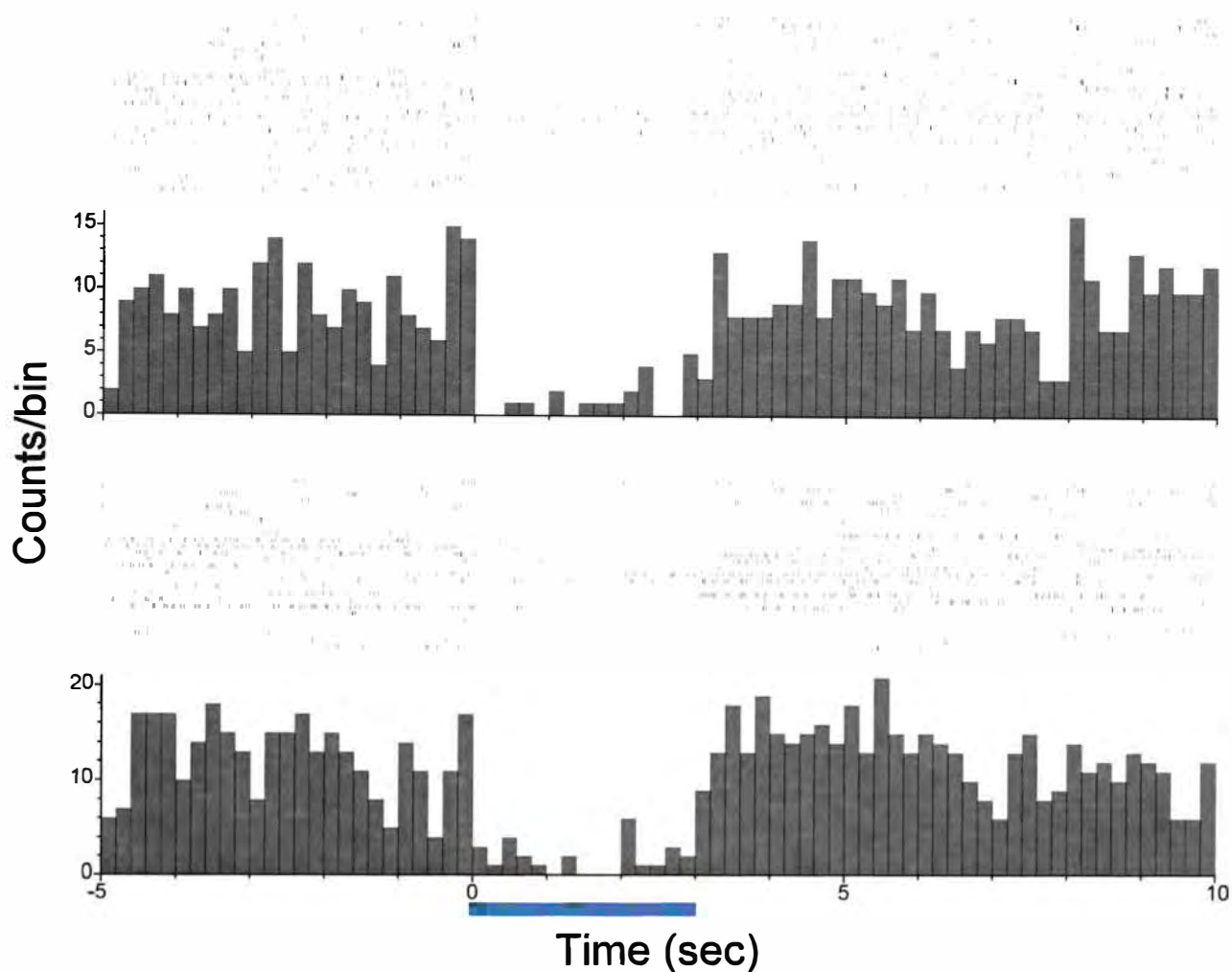


Figure 10. Optogenetics validation: Example of light-induced inhibition in a PV-Cre-NR1f/f mouse. A PV-Cre-NR1f/f animal injected with ChR-mCherry was submitted to 27 trials of 3s-trains of stimulation (1ms pulses at 8, 16, 24, 32, 48, 60, 80 and 90 Hz; 5mW). Perievent raster and histogram of two different cells from the same animal are shown to exemplify firing activity suppression during light stimulation.

bin = 500 ms

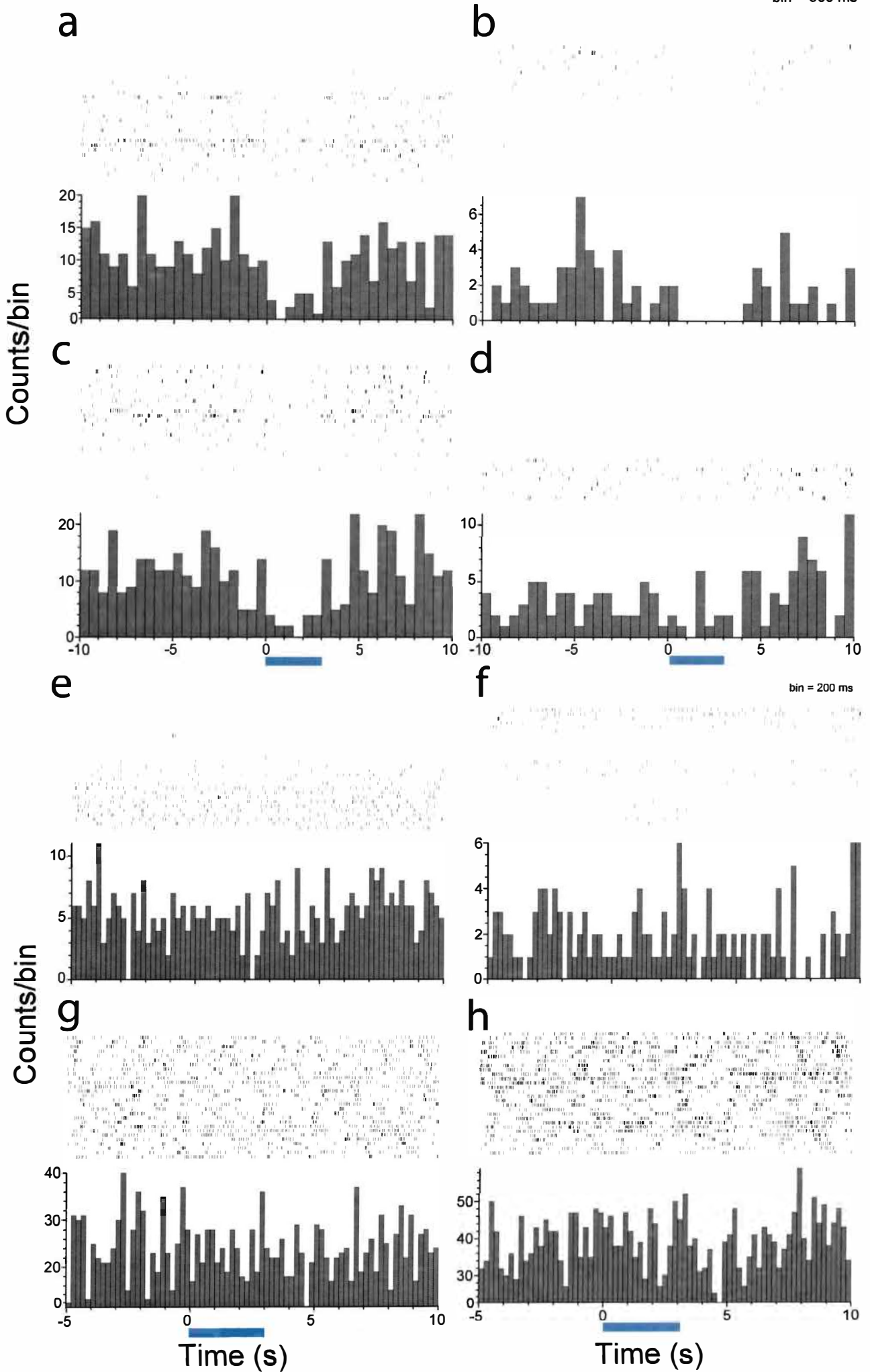


Figure 11. Optogenetics validation: Examples of partial light-induced inhibition and of absence of light-effect in control animals (a-c) Perievent raster and time histogram of three different cells from a PV-Cre ChR2 expressing mouse are shown to exemplify partial firing activity suppression during light stimulation; **(d)** Perievent raster and time histogram of one cell from the same mouse to exemplify no firing activity suppression during light stimulation; **(e-h)** Perievent raster and time histograms of four cells (two each control virus injected mouse) to exemplify no firing activity modulation during light stimulation.

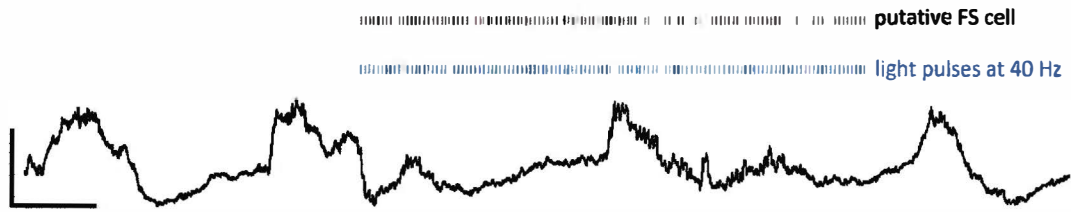
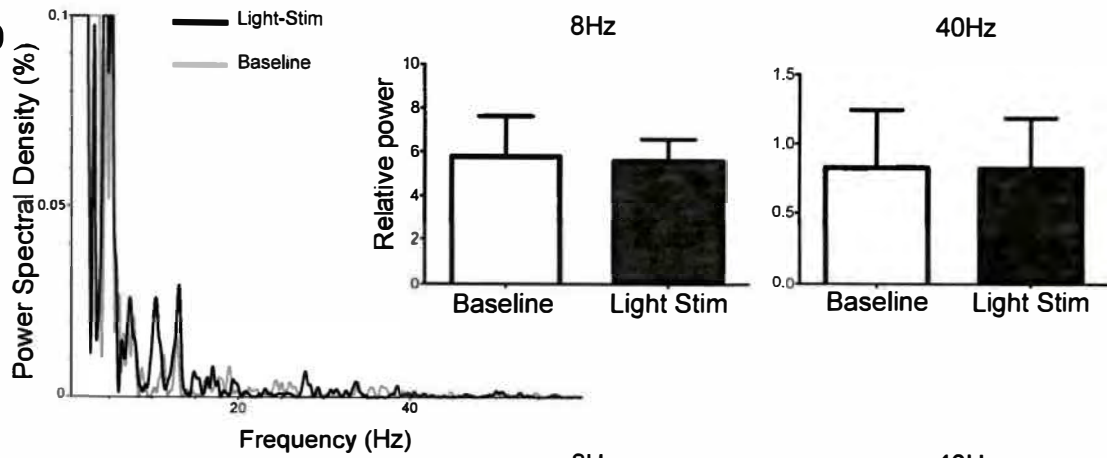
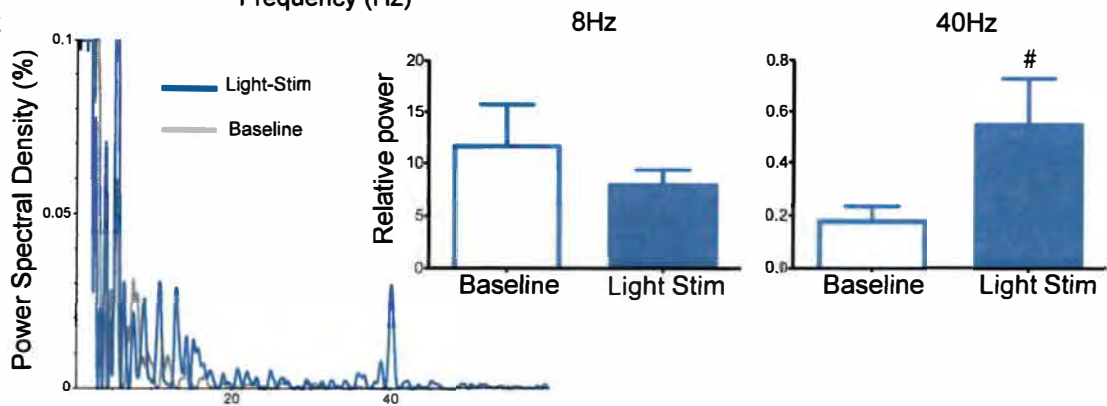
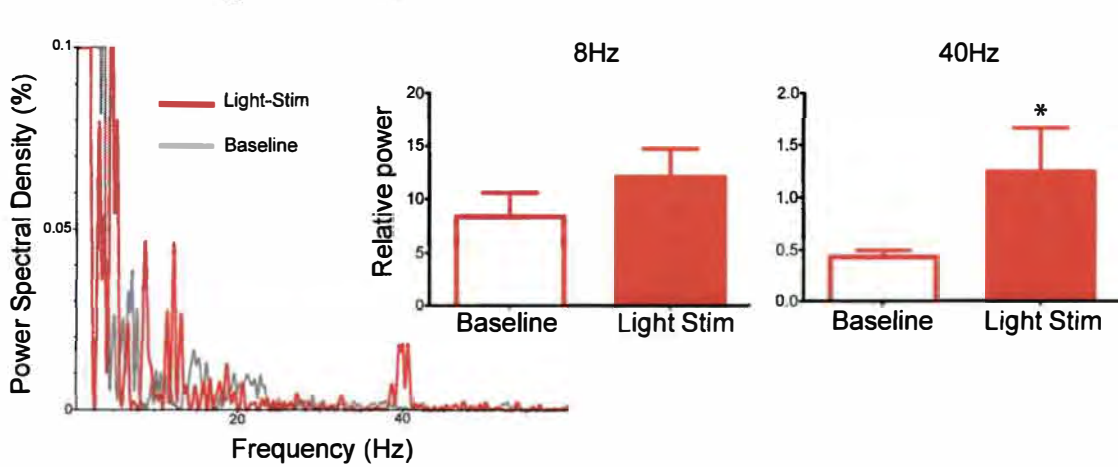
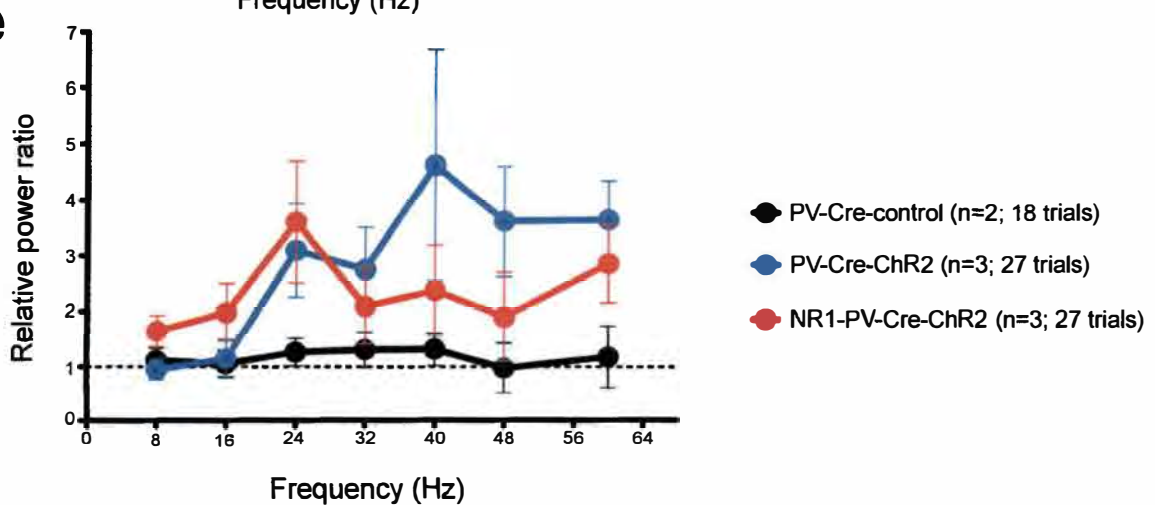
a**b****c****d****e**

Figure 12. Role of NMDARs in cortical PV+ cells during evoked gamma oscillations by optogenetics. (a) Single-unit recordings during optogenetic activation of a FS–PV+ interneuron. The protocol of stimuli consisted in 27 trials of 3s-trains of blue light stimulation (1ms pulses at 8, 16, 24, 32, 48, 60, 80 and 90 Hz; 5mW). The reliability of the FS cell in following the light stimulus is illustrated in figure 9. Left side: PSD% from a representative trial of (b) one PV-Cre mouse transfected with control virus, (c) one PV-Cre mouse transfected with ChR2-mCherry and (d) one PV-Cre-NR1f/f mouse transfected with ChR2-mCherry. (b-d: Right side): Average of PSDs (%) centered at 8Hz (4 to 12 Hz) and at 40 Hz (36 to 44 Hz) in three trials of 8 and 40Hz optical stimulation trains each. (b) No significant differences were observed when compared average of trials before and during light. (c) PV-Cre and (d) PV-Cre-NR1f/f mice both expressing ChR2, seem to produce LFP power enhancement preferentially in the gamma range when submitted to light pulses in the mPFC. In both groups, stimulation of FS cells at 8 Hz had no effect on LFP power at 4-12 Hz (centered at 8Hz). However, stimulation at 40 Hz did cause a significant increase LFP power at 36-44Hz. (e) The number of subjects is still not sufficient to perform statistics with the power ratio evaluation. However, it suggests a poorer optogenetic-induced gamma evocation in PV-Cre-NR1f/f mice (fig.12e), according to Carlén et al. (2012). * p = 0.039; # p = 0.054; baseline vs stimulation trial; paired Student t-test. Data are shown as mean ± s.e.m.

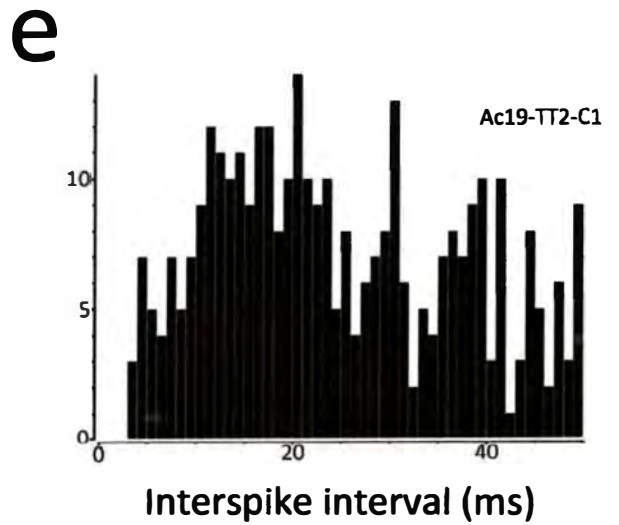
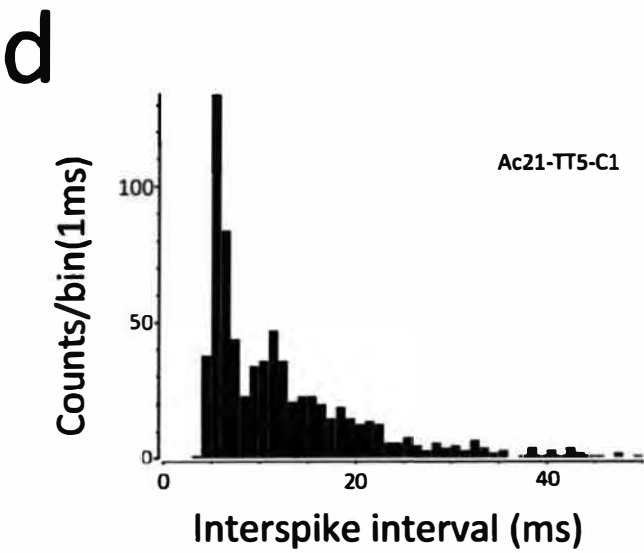
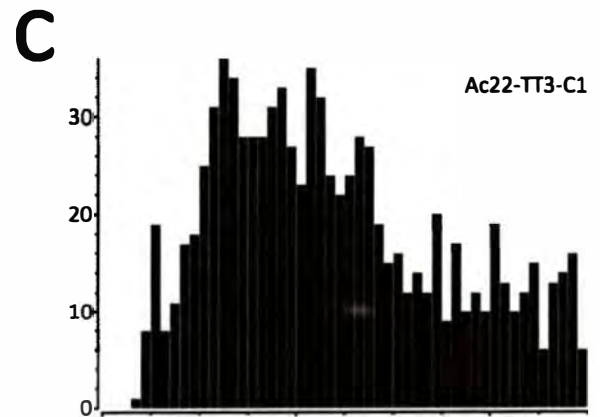
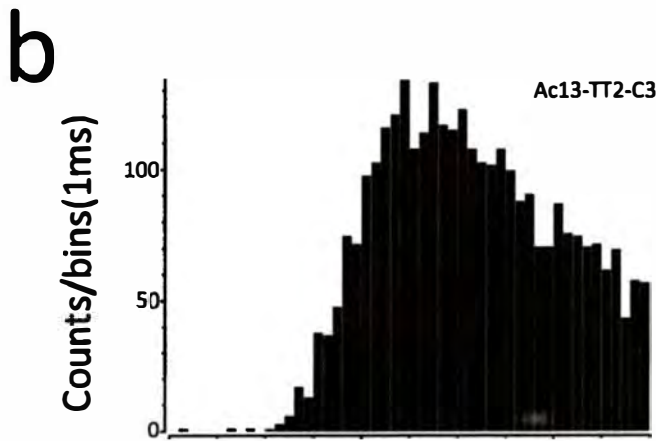
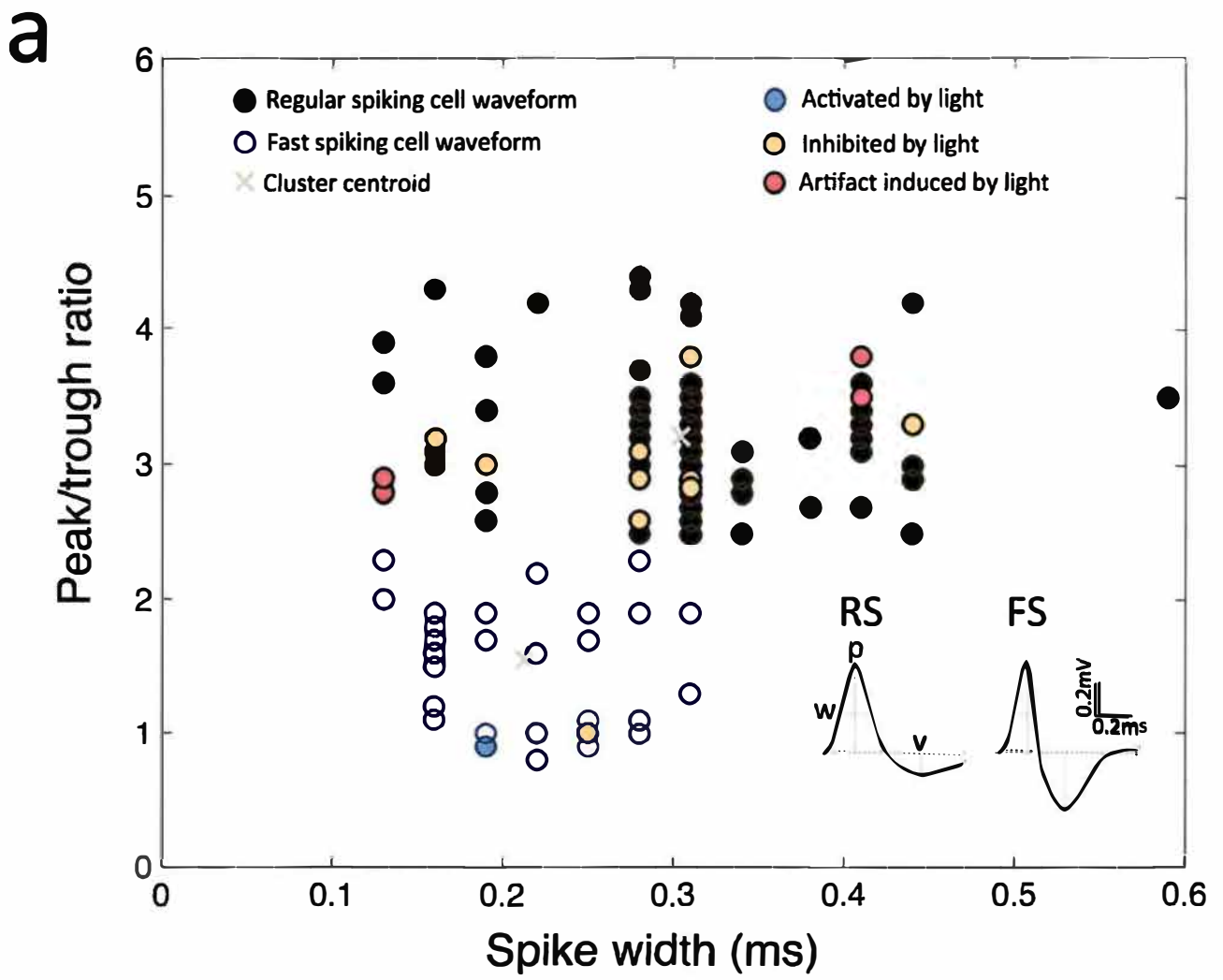


Figure 13. Classification of units in putative FS and RS cells. (a) Right-bottom corner: First, for each waveform, we calculated (1) the ratio between the amplitude of the initial peak (p) to the following trough (v) and (2) the duration of the spike at half height (w). Then, we plotted a scatter with the above-mentioned parameters for all sorted units (**main chart**; $n=8$ animals; 133 units) and performed k-means clustering to partition the population of waveforms between clusters of FS and RS putative cells. Consistently, 9/10 of the light-inhibited cells (orange dots) were included in the RS-like waveform cluster (black dots). Lastly, we also labeled the waveforms presumably generated by light-induced artifacts (red dots). As mentioned before, this strategy can be useful to help in the fine detection of light-artifacts. **(b-e)** Examples of ISI histogram distribution of cells classified as putative RS cells with random firing pattern revealed as dispersed ISIs **(b,c and e)** and one classified as putative FS cell, with ISI histogram revealing burst-firing pattern **(d)**.

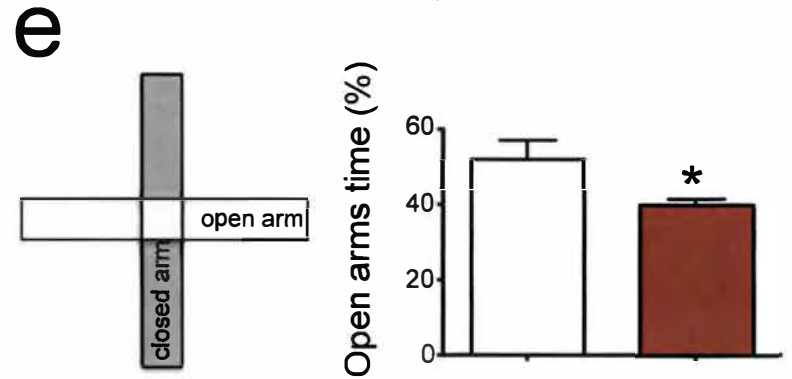
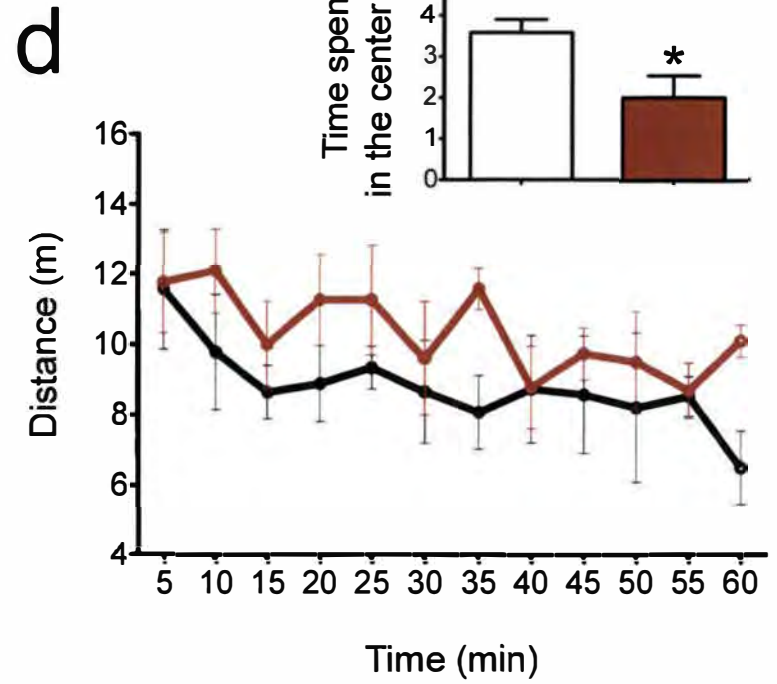
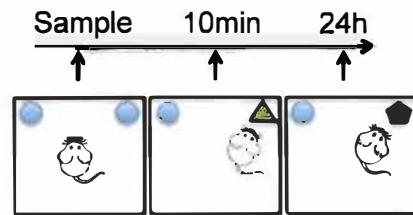
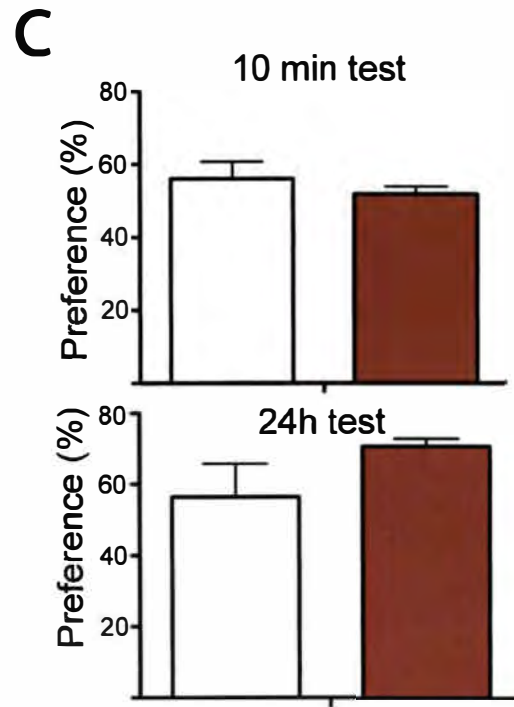
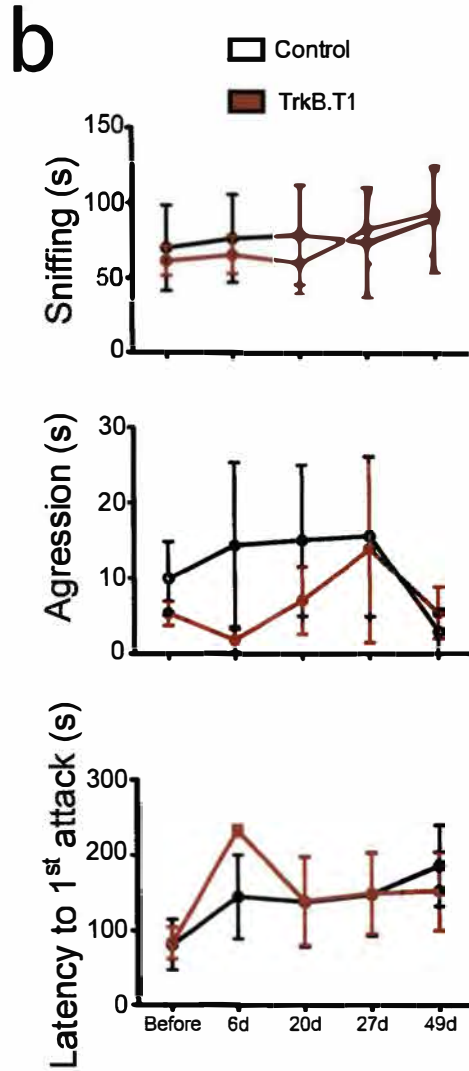
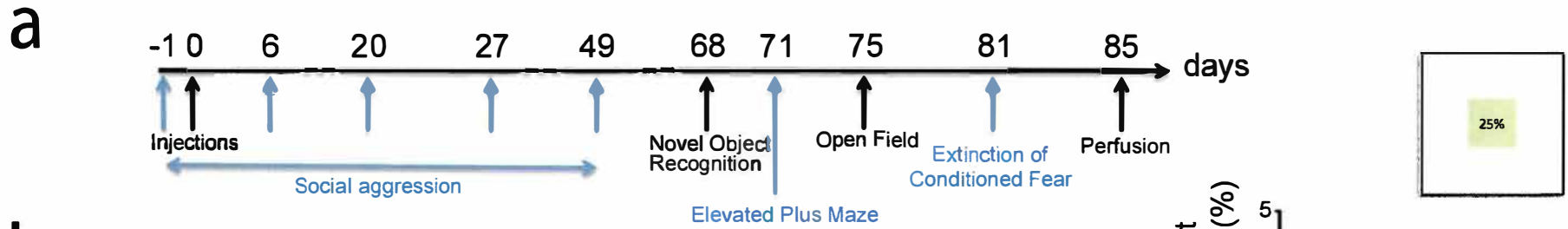


Figure 14. BDNF-TrkB signaling disruption specifically in PV+ interneurons of mPFC exacerbates anxiety-like behaviors without impacts social behavior, recognition memory, and locomotion. (a) Experimental design. Adult males PV-Cre mice were anesthetized and submitted to bilateral injection in the infralimbic mPFC of AAV5-DIO-TrkB.T1-mCherry. Control animals received AAV5-DIO-EYFP. Aggressive behavior was probed one day before and after microinjections to rule out possible effects induced by the surgical procedure. Then, a behavior battery was performed from the 6th to the 81th day after surgery, namely: resident-intruder test, novel object recognition, elevated plus maze, open field and extinction of non-contextual fear. Animals were perfused and the *trkB.t1* expression was confirmed by examination of 40 μ m mPFC coronal sections for the presence of mCherry-fluorescence. **(b)** Resident-intruder test. Top: Evaluation of the amount of time an adult male mouse (resident) spent sniffing a juvenile mouse (intruder) in 5 sessions over 7 weeks after virus injection. Middle: Assessment of the amount of time spent by the resident in offensive episodes (defined as an attack that included either biting or wrestling; Ogawa et al., 1999) towards the intruder. Bottom: Quantification of the latency to the first attack. No significant differences were observed between groups in all comparisons ($p > 0.05$; ANOVA Two way RM). **(c)** Novel object recognition test. Bottom: Following habituation, two identical objects were fixed in the arena and the animal was placed in the arena for 5-min (sample phase). After 10min from the sample phase, we replaced one of the objects by a novel one with similar size, but different shape and color/brightness; and the same animal was placed again in the arena for additional 5 min to explore the familiar and the novel objects (10min-test). After 24h, we kept the familiar object from the sample phase and replaced the novel from the 10min-test by a third one (totally different from the first two objects). Then, the animal was allowed to freely-explore the objects for 5 min (24h-test). Preference (%) was calculated as follows: $((\text{time spent exploring the novel object}) / (\text{the total time of object exploration})) * 100$. No significant differences were observed between groups in both 10min test (top) and 24h test (middle) ($p > 0.05$; non-paired Student t-test). **(d)** Open field. Briefly, each subject was placed near the wall-side of an arena, and the movement of the mouse was monitored for 60 min (TSE/ActiMot2). The total distance traveled and time in center (imaginary square with 25% of the open-field area) were measured. No significant differences were observed between groups ($p > 0.05$; ANOVA Two way RM). However, *trkB.T1* mice spent lesser time at center (central portion encompassing 25% of the arena) of the open field in the first 3min of test ($p < 0.05$; non-paired Student t-test). **(e)** Elevated plus maze. Consistent with the results obtained from the time spent in the center of the open field, *trkB.T1* animals displayed a reduced amount of time spent in the open arms as well ($p < 0.05$; non-paired Student t-test). * Statistical significant: $p < 0.05$; Student t-test. Data are shown as mean \pm s.e.m.

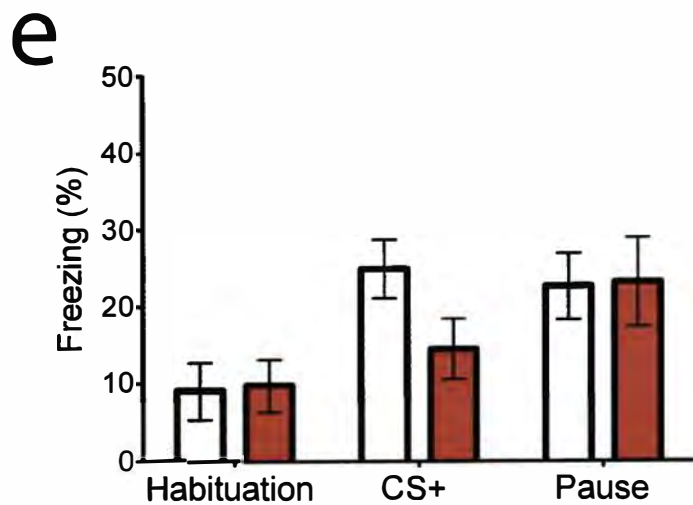
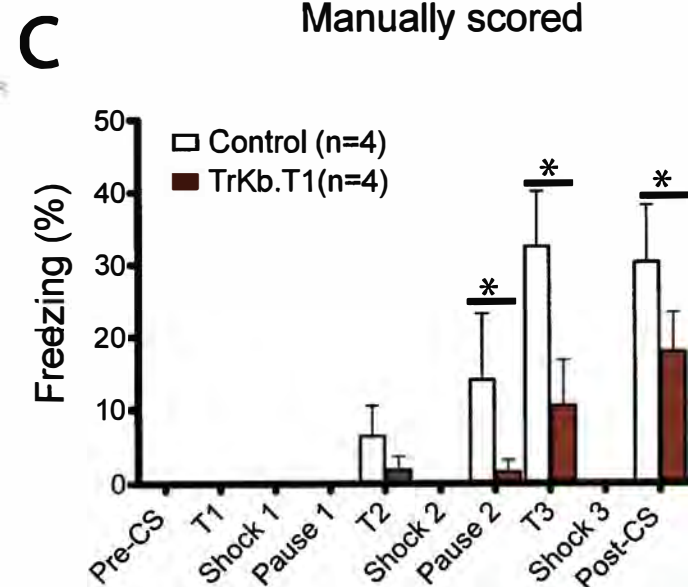
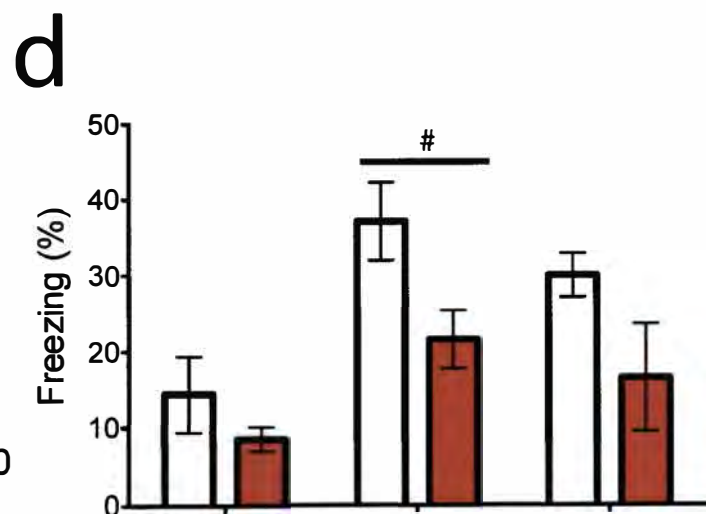
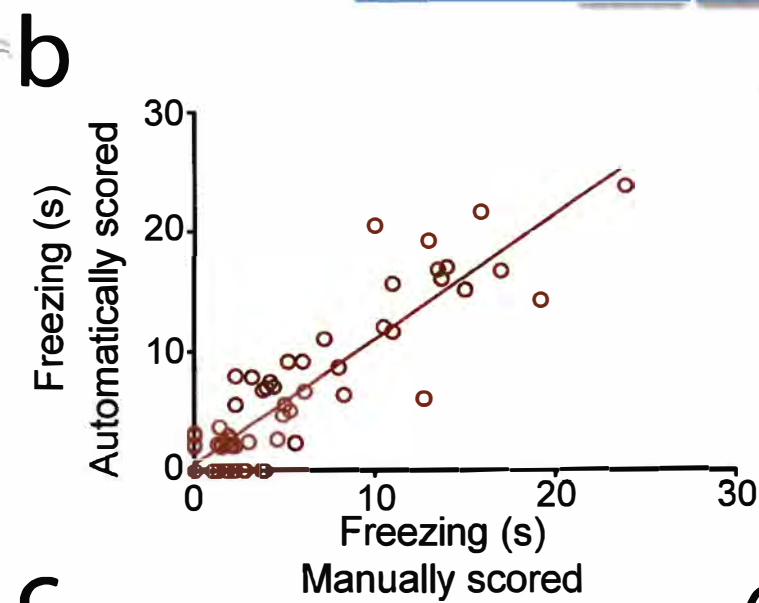


Figure 15. BDNF-TrkB signaling disruption specifically in PV+ interneurons of mPFC impairs acquisition of non-contextual fear memory. (a) Experimental design: On day 1, mice were habituated to the chamber for 150s (without tone and shock), followed by 3 CS+US trials (tone paired with shock; inter-trial interval (ITI) = 40 ± 4 s) and one resting trial (60s, without tone and/or shock). On day 2, all animals were submitted to habituation in a new chamber (circular shape, dark acrylic, diameter = 20cm x high = 40 cm) during 150s and received 15 extinction tones (without shock) with an ITI of 5s, besides a resting trial of 60s. On day 3, at the same chamber, all subjects received 15 additional extinction trials (only CS; ITI = 40 ± 4 s) to test for extinction of non-contextual fear. (b) To check the consistency of the automatic freezing behavior by the TSE-Multiconditioning software, we performed a correlation between manual versus automatic quantifications from the same animal. Linear correlation analysis revealed a significant and robust association between manual and automatic quantification, which gave us more conviction to keep using the software to assess freezing (Number of XY Pairs: 66; Pearson $r = 0.8994$; 95% confidence interval: 0.8403 to 0.9374; P value (two-tailed) < 0.0001; R squared = 0.8090). (c) During the conditioning phase (day 1), TrkB.T1 mice displayed significant reduction of freezing behavior during the pause that followed the second presentation of the CS, besides during the third presentation of CS and its subsequent pause. (d) On the day 2, the fear memory retrieval elicited by CS was poorer in the TrkB.T1 group compared to control animals. (e) On the day 3, no significant differences were observed between groups.). * Statistical significant: $p < 0.05$; Two way ANOVA RM. Data are shown as mean \pm s.e.m.

Only 1 of 14254 spikes shown.



TT3--Cluster2

Cut by cleitonlopesaguiar on 30-Jan-2014

14254 spikes

firing rate = 1.0734 spikes/sec

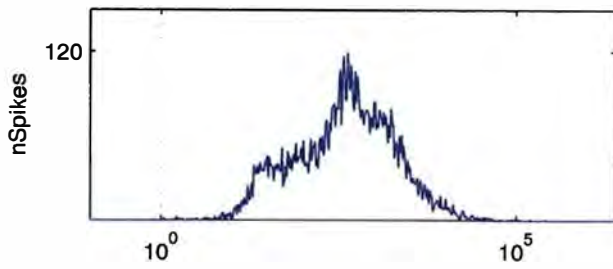
spikewidth (Ch1,2) = 11.34 +/- 9.52 8.60 +/- 11.34

spikewidth (Ch3,4) = 11.97 +/- 9.16 12.72 +/- 6.91

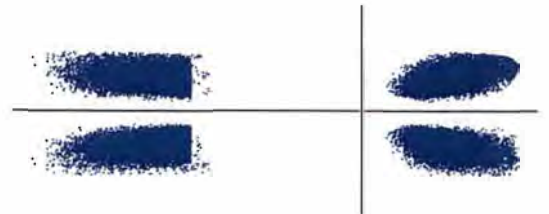
peak/valley (Ch1,2) = 1.42 +/- 0.58 1.27 +/- 0.51

peak/valley (Ch3,4) = 1.51 +/- 0.60 2.16 +/- 0.62

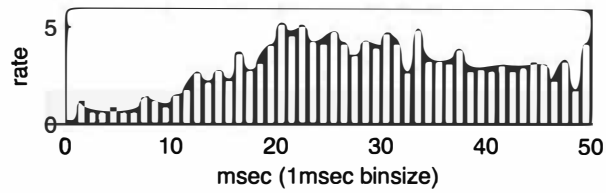
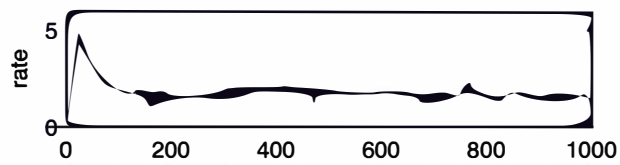
histogram of log(ISI)



Peak Plot



Autocorrelation



Separation: L-Ratio = 0.1783 ID = 17.0

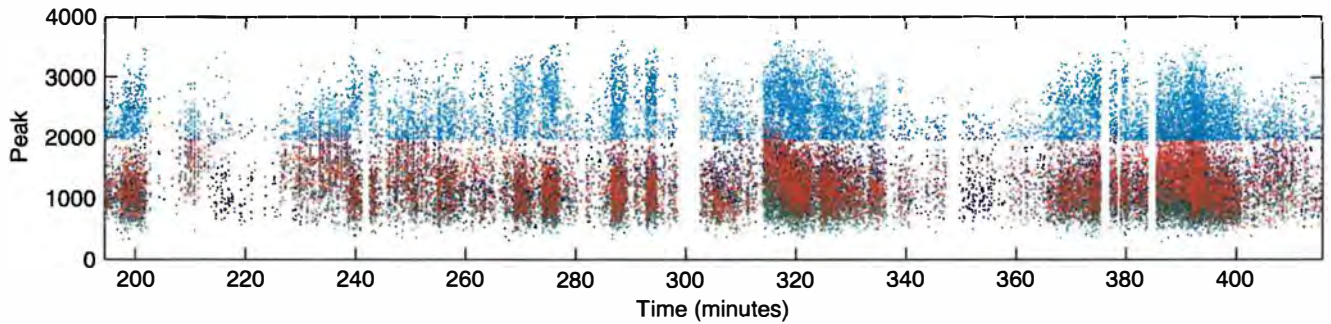
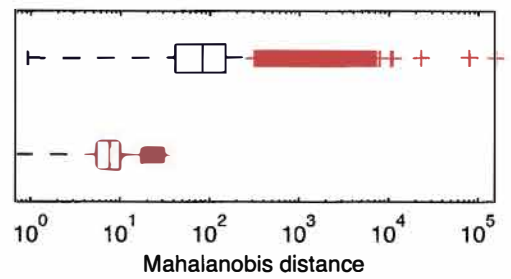
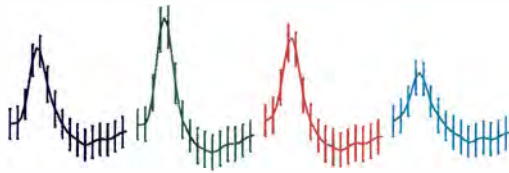


Figure S1. Cluster checking file of unit Ac13-TT3-C2 generated by MClust after sorting

Average Waveform



TT4--Cluster2

Cut by cleitonlopesaguiar on 30-Jan-2014

5085 spikes

firing rate = 0.3829 spikes/sec

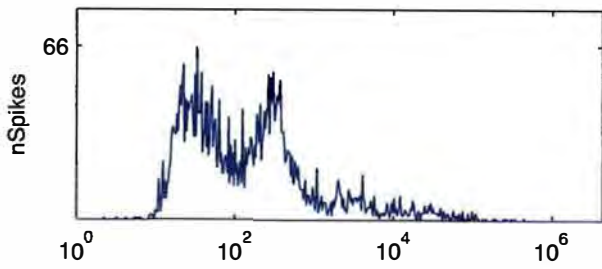
spikewidth (Ch1,2) = 14.02 +/- 5.70 13.78 +/- 5.05

spikewidth (Ch3,4) = 14.61 +/- 5.15 15.03 +/- 6.12

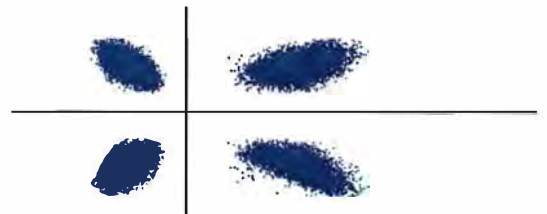
peak/valley (Ch1,2) = 1.99 +/- 0.67 2.35 +/- 0.61

peak/valley (Ch3,4) = 1.96 +/- 0.61 1.54 +/- 0.61

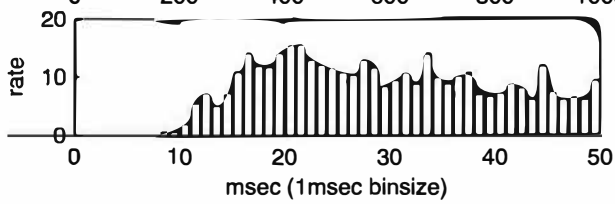
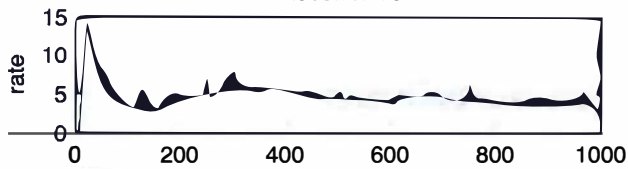
histogram of log(ISI)



Peak Plot



AutoCorrelation



Separation: L-Ratio = 0.1873 ID = 17.2

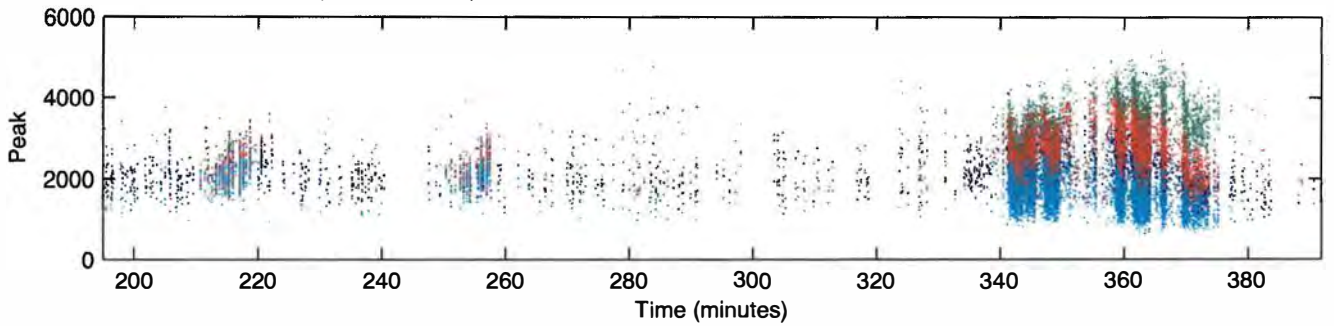
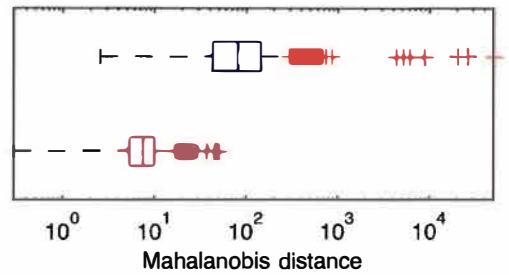


Figure S2. Cluster checking file of unit Ac13-TT4-C2 generated by MClust after sorting

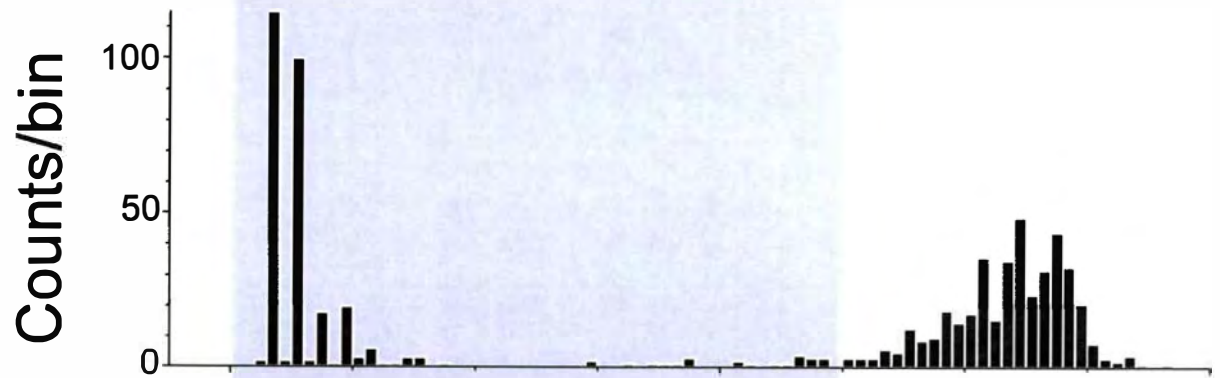
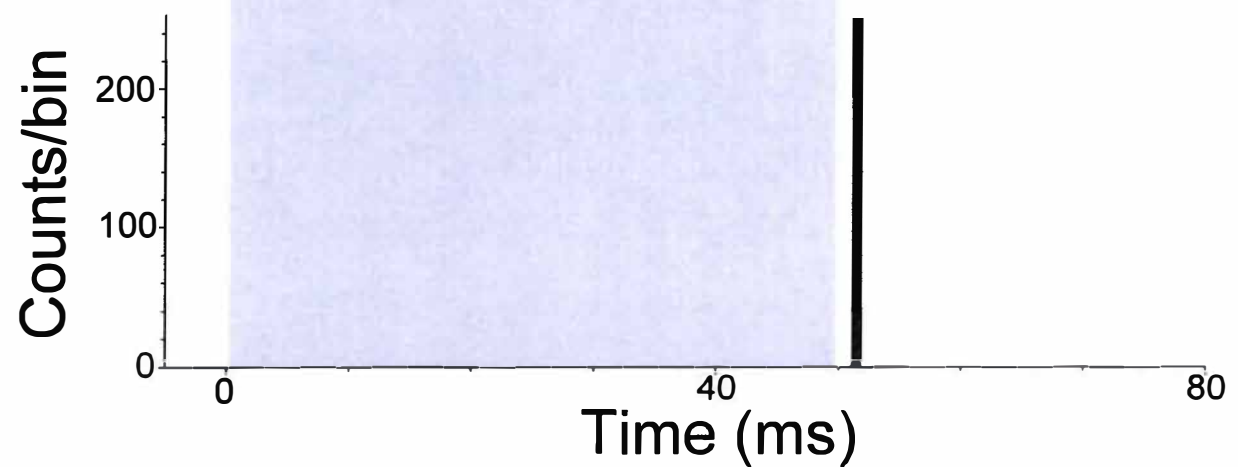
a**b**

Figure S3. Peri-stimulation raster and time histogram during 150 trials of 50ms light-pulse of a putative FS cell Ac18-TT8-C1 (a) and a waveform produced by light-artifact, Ac12-TT4-C3 (b). Interestingly, the Ac18-TT8-C1 displayed persistence of firing activity up to 20ms after light cessation, contrasting with Ac12-TT4-C3, which displayed an extremely time-locked response related to the event.

ANEXO 4



ELSEVIER

Revista Brasileira de Psiquiatria

RBP Psychiatry

Official Journal of the Brazilian Psychiatric Association
Volume 34 • Number 4 • December 2012



SPECIAL ARTICLE

Psychiatric comorbidities in temporal lobe epilepsy: Possible relationships between psychotic disorders and involvement of limbic circuits

Ludmyla Kandratavicius,^{1,3} Cleiton Lopes-Aguiar,¹ Lézio Soares Bueno-Júnior,¹
Rodrigo Neves Romcy-Pereira,² Jaime Eduardo Cecilio Hallak,^{1,3} João Pereira Leite¹

¹Faculdade de Medicina de Ribeirão Preto, Department of Neurosciences and Behavior, Universidade de São Paulo, Brazil

²Brain Institute, Universidade Federal do Rio Grande do Norte, Natal, Brazil

³National Institute of Science and Technology in Translational Medicine
(Instituto Nacional de Ciência e Tecnologia - INCT-TM; CNPq)

Submitted on March 9, 2012; accepted on April 23, 2012

DESCRIPTORS:

Temporal Lobe
Epilepsy;
Psychosis;
Psychiatric
Comorbidities;
Neuropathology;
Limbic Circuits.

Abstract

Objective: Mounting evidence suggests that the limbic system is pathologically involved in cases of psychiatric comorbidities in temporal lobe epilepsy (TLE) patients. Our objective was to develop a conceptual framework describing how neuropathological and connectivity changes might contribute to the development of psychosis and to the potential neurobiological mechanisms that cause schizophrenia-like psychosis in TLE patients. **Methods:** In this review, clinical and neuropathological findings, especially brain circuitry of the limbic system, were examined together to enhance our understanding of the association between TLE and psychosis. Finally, the importance of animal models in epilepsy and psychiatric disorders was discussed. **Conclusions:** TLE and psychiatric symptoms coexist more frequently than chance would predict. Damage and deregulation among critical anatomical regions, such as the hippocampus, amygdala, thalamus, and the temporal, frontal and cingulate cortices, might predispose TLE brains to psychosis. Studies of the effects of kindling and injection of neuroactive substances on behavior and electrophysiological patterns may offer a model of how limbic seizures in humans increase the vulnerability of TLE patients to psychiatric symptoms.

Corresponding author: Ludmyla Kandratavicius, PhD Faculdade de Medicina de Ribeirão Preto, Department of Neurosciences and Behavior, Universidade de São Paulo. Av Bandeirantes 3900, CEP 14049-900, Ribeirão Preto, SP, Brazil.

Phone: (+55 16) 3602 2796; Fax: (+55 16) 3633 0866. E-mail: ludykandra@gmail.com

1516-4446 - ©2012 Elsevier Editora Ltda. All rights reserved.

doi: 10.1016/j.rbp.2012.04.007

DESCRITORES:

Epilepsia do lobo temporal;
 Psicose;
 Esquizofrenia;
 Comorbidades psiquiátricas;
 Neuropatologia;
 Circuitos límbicos.

Comorbidades psiquiátricas na epilepsia do lobo temporal: Possíveis relações entre desordens psicóticas e comprometimento de circuitos límbicos
Resumo

Objetivo: Existem cada vez mais evidências de que o sistema límbico está envolvido na patologia das comorbidades psiquiátricas em pacientes com epilepsia do lobo temporal (ELT). Nosso objetivo foi elaborar um desenho conceitual descrevendo como aspectos neuropatológicos e de conectividade podem contribuir para o desenvolvimento de psicose em pacientes com ELT. *Métodos:* Nesta revisão, achados clínicos e neuropatológicos, e especialmente os aspectos da circuitaria límbica, foram examinados em conjunto para auxiliar nossa compreensão sobre a associação entre ELT e psicose. Achados em modelos animais de epilepsia e esquizofrenia também foram levados em consideração. *Conclusões:* ELT e comorbidades psiquiátricas coexistem com maior frequência que o predito pela associação ao acaso. Dano e desregulação entre estruturas anatómicas críticas, como hipocampo, amígdala, tálamo, e córtices temporal, frontal e cíngulo podem predispor o cérebro com ELT à psicose. Estudos sobre efeitos comportamentais e eletrofisiológicos do abrasamento elétrico e injeções de substâncias neuroativas em modelos animais podem oferecer pistas sobre como crises límbicas em humanos aumentam a vulnerabilidade de pacientes com ELT a sintomas psiquiátricos.

Background

Temporal lobe epilepsy (TLE) is a focal neurological condition, in which seizures are able to spread and compromise a whole set of limbic structures and neighboring cortices.¹ In contrast, various forms of psychosis are not clearly related to any consistent pathological localization. Instead, they have been attributed to neurochemical and ultrastructural dysfunctions in a much wider set of limbic circuits, including the ones directly affected by TLE.² However, it is noteworthy that the high prevalence of psychosis in TLE patients³⁻⁷ indicates a possible shared mechanism between the two etiologies, despite their distinct degree of substrate commitment and localization. While the specific mechanisms generating psychosis in TLE are still poorly understood, neuroanatomical knowledge of limbic network connectivity might help to define potential brain targets for investigation and lead to a better understanding of this pathophysiological issue. The present article conducts a survey of TLE and psychosis, analyzing historical, clinical and neuropathological observations within the framework of limbic connectivity. Additionally, we reviewed experimental studies with electrical kindling or pharmacological treatment of the hippocampal formation, the amygdaloid complex, and the prefrontal cortex circuits. We focused on the dopaminergic and glutamatergic mechanisms that are potentially involved in both TLE and psychosis.

Early observations and clinical aspects

In 1825, two of Esquirol's assistants reported that the Ammon's horn was strikingly abnormal in the brains of some epileptic and a few psychotic patients.⁸ Fifty-three years later, Paul Broca would describe the great limbic lobe as "the seat of those lower faculties which predominate in the beast."⁸ This ample region regained attention more than thirty years later, especially with the study of Papez stating that, "the hypothalamus, the anterior thalamic nuclei, the

gyrus cinguli, the hippocampus and their interconnections constitute a harmonious mechanism which may elaborate the functions of central emotion, as well as participate in emotional expression".⁹ The amygdala was not included in Papez's original theory of emotion, but after Klüver and Bucy's findings,¹⁰ MacLean made the amygdala one of the epicenters of a more extensive system, later called the limbic system.^{11,12} Beyond the limbic lobe structures cited above, the existence of anatomical connections among the frontal lobes, the hypothalamus and temporal lobes, as well as the effects of experimental lesions, suggested that the frontal lobes influence the basic instinctive and emotional drives.¹³ In addition to emotional disturbances, another important feature of several types of epilepsy is the presence of periods of short, intermittent lack of the awareness of the environment and of the self, indicating that the brainstem and most of the thalamus are also affected.¹⁴

A distinct syndrome of behavior abnormalities occurs in many patients with temporal lobe epilepsy. This constellation of interictal personality changes includes hyposexuality, hyperreligiosity/deeply held convictions, viscosity (a striking preoccupation with detail, especially concerned with moral and ethical issues), and, occasionally, hypergraphia or the urge to express in forms other than writing.¹⁵ Frequent symptoms of TLE patients also include psychic or experiential phenomena: intellectual auras or dreamy states, complex visual or auditory hallucinations or illusions, memory "flashbacks", *déjà vu*, *jamais vu*, and emotions, most commonly fear.¹⁶ It is important to stress that these patients, who characteristically exhibit a preserved or even deepened affect, do not fall into any established nosologic category and often do not appear schizophrenic.¹⁵ Indeed, as described by Gloor et al.,¹⁷ "the patients are never in doubt that these phenomena occur incongruously, that is, out of context, as if they were superimposed upon the ongoing stream of consciousness (...). This insight clearly distinguishes these phenomena from psychotic hallucinations and illusions".¹⁷

In 1957, Desmond Pond made the first explicit clinical recognition of schizophrenic-like psychoses of epilepsy, as reviewed by Beard and Slater.¹⁸ Typically, the psychotic state closely resembles schizophrenia, with paranoid ideas which might become systematized, ideas of influence, and auditory hallucinations often of a menacing quality. The points of difference with classic schizophrenia are the common religious coloring of the paranoid ideas, the tendency of the affect to remain warm and appropriate, and the lack of typical deterioration to the hebephrenic state¹⁸. Although auditory hallucinations are common, visual hallucinations are relatively rare. Other forms of delusions, including grandiose, referential, religious and Schneiderian symptoms, have also been reported, especially when a history of traumatic brain injury is present.¹⁹

The nature of the relationship between psychosis and epilepsy is controversial, and existent hypotheses are not mutually exclusive. One hypothesis suggests that there is a basic antagonism between epilepsy and psychosis. Psychosis in TLE is regularly associated with fewer or no psychomotor seizures,^{3,20} and normalization of the EEG and elimination of seizures through anticonvulsant medication - though they relieve epileptic symptomatology - often exacerbate an underlying psychiatric disorder and lead to the emergence of a psychotic state.²¹ Indeed, this supposed mutual antagonism was the basis for the development of electroconvulsive therapy, wherein seizure induction is used to treat psychosis, as reviewed by Pollock.²² Gamma-amino butyric acid (GABA) and dopamine also exert antagonistic effects in epilepsy and psychosis. For instance, dopamine antagonists are commonly used as antipsychotic drugs, and the drugs can trigger seizures.²³ On the other hand, dopamine agonists are able to exacerbate or trigger psychotic symptoms, while having anticonvulsant properties.^{24,25} In contrast to this antagonist relationship, epilepsy also predisposes a patient to the development of schizophrenia-like psychosis. This last view is in line with the extensive works of Slater, Beard and Glithero,²⁶ and of Kristensen and Sindrup,²⁰ which recognize epileptic psychoses as truly organic phenomena, caused by structural damage to the limbic parts of the temporal lobe responsible for both the epilepsy and the psychosis.

Psychiatric disorders in epilepsy can be classified into ictal (the psychiatric symptoms are a clinical manifestation of the seizure), periictal (symptoms precede and/or follow the seizure occurrence) and interictal (symptoms occur independently of the seizure occurrence) disorders. In the present review, our focus will be primarily interictal psychosis, which includes schizophrenia-like psychosis of epilepsy, as defined by the International League Against Epilepsy (ILAE, Commission on Neuropsychiatric Aspects).²⁷ Because interictal symptoms are not related to any "seizure collateral effect", psychiatric manifestations are much like the pure form of the psychopathology. For instance, chronic interictal psychosis of epilepsy is also referred to as schizophrenia-like psychosis of epilepsy, due to its resemblance to schizophrenia's phenomenological manifestations.²⁸ Interictal psychosis is usually prodigal in florid symptoms, whereas postictal psychosis exhibits few common schizophreniform psychotic traits such as perceptual delusions or voices.²⁹ Of note, recurrent postictal psychosis in human TLE is considered to be a risk factor for the development

of interictal psychosis,³⁰ which makes animal models of postictal psychosis suitable for the study of the possible gradual commitment of the limbic circuits. The increased risk of psychiatric symptoms in epilepsy may be related to several risk factors, such as genetic background and illness chronicity, which are liable to facilitate psychopathological manifestations. In the next two sections, the contributions of structural neurologic factors and their possible imbalance among connected neuroanatomical regions will be examined.

Neuropathological aspects

Schizophrenic patients often have abnormal electrical activity in the temporal lobes and sometimes in the frontal lobes.³¹ Early descriptions suggested that the sites of maximum abnormalities were in the hippocampus, amygdala, septum, uncus, anterior-temporal, and orbito-frontal areas, even in patients with no history of epilepsy.³² For more than 50 years, studies have suggested that any given brain tumor affecting the limbic system can present as classical schizophrenia.⁵ In Malamud's studies of eighteen patients with temporal lobe tumors, ten had been diagnosed and treated as schizophrenics, three as melancholics, one as a psychotic depressive, one as maniac, two as psychoneurotics, and one as anxious.³³ In Taylor's series of TLE post-mortem brains, 23% of the cases with "alien tissue" (tumors, hamartomas and focal dysplasias) were psychotic, contrasting with only 5% in the mesial temporal sclerosis group.⁷ Although some authors agree that psychiatric symptoms presage temporal lobe tumors and that presence of mesial temporal sclerosis is protective against schizophrenia-like psychosis in patients with epilepsy,³⁴ recent neuropathological evidence suggests that there is a structural basis for psychiatric symptoms in TLE patients with hippocampal sclerosis.³⁵ In our series of patients³⁵ with no dual pathology or alien tissue, we did not observe a predominance of female patients or of left handedness in the psychosis group (as did Taylor)⁷ nor a predominance of patients with left or bilateral temporal foci (as did Flor-Henry).³ Other studies also indicate that the presence of hippocampal sclerosis is not protective against psychosis. In Roberts's series of 249 TLE patients, the largest epilepsy series analyzed to date for their neuropathological features and schizophrenia-like psychosis, 6.4% had a preoperative diagnosis of TLE and psychosis; 40% of the cases with TLE and psychosis had hippocampal sclerosis with left sided foci and approximately 20% had gangliogliomas.⁴ It is noteworthy that gangliogliomas usually have origin in and predilection for the temporal lobe,⁴ meaning that, more important than the type of lesion, the location of a lesion within the hippocampal-amygdalar-temporal gyri may represent a true predisposition factor for psychosis.

With a focal brain lesion, hallucinations may arise after compensatory over-activation of nearby sensory pathways. Complex auditory hallucinations are most common in TLE and schizophrenia, and the affected areas mainly comprise the primary auditory pathway (the pons, inferior colliculus, medial geniculate body and temporal lobe).³⁶ In fact, fMRI studies in schizophrenic patients during auditory hallucinations have revealed activation of areas related not only to the auditory pathway but also to inner speech as follows: transverse temporal gyrus of the dominant hemisphere, posterior superior temporal gyrus, middle temporal gyrus,

frontoparietal operculum, orbitofrontal cortex, hippocampus, amygdala, sensorimotor cortex, right inferior colliculus, right and left insula, left parahippocampal gyrus, right temporal gyrus, right thalamus, middle frontal and anterior cingulate gyri.³¹ The structural lesions most often seen in auditory verbal hallucinations are a reduction in grey matter volume in the superior temporal and middle temporal gyri of the dominant hemisphere, and in the insula, temporal pole, thalamus and right prefrontal cortex.³⁶ Interestingly, auditory hallucinations have been associated with impaired effective connectivity between the left superior temporal, frontal and anterior cingulate cortex, suggesting that such patients tend to misattribute their own speech to an external source (external speech).³⁶ In addition to hallucinations, another classic feature exhibited by patients with psychosis is a reduction in the operational index of sensorimotor gating. This index is obtained by measuring the prepulse inhibition (PPI) of the startle response, which refers to the ability of a weak prestimulus to transiently inhibit the response to a closely following strong sensory stimulus. Both schizophrenia patients and their relatives show gating deficits that are significantly heritable, consistent with the endophenotype criteria.^{37,38} In fact, reduced PPI has been observed in subjects with schizotypal personality and in normal subjects with high scores of self-transcendence in Personality Questionnaire scales.³⁹ TLE patients with psychosis⁴⁰ and non-psychotic patients with psychogenic "non-epileptic" seizures⁴¹ also exhibit reductions in PPI. It is important to stress that, although patients with psychogenic seizures may not exhibit epileptiform brain activity, all of them present with hysterical features.⁴² Often - in more than 90% of the cases⁴³ - they also present with psychiatric comorbidities. Definite neuropathological substrates adjunct to PPI impairment in humans are not known, but experimental data suggest that kindling of the amygdala⁴⁴ and precommissural lesions of the fornix⁴⁵ are effective ways to disrupt PPI in rats.

Neuropathological abnormalities are frequently observed in the brains of schizophrenic⁴⁶ and TLE patients.⁴⁷ TLE patients with hippocampal sclerosis exhibit hippocampal neuronal loss, often accompanied by neuronal loss and gliosis in the amygdala and entorhinal cortex.⁴⁸ The same set of mesial structures may appear atrophic under magnetic resonance imaging, in addition to being consistently recruited at the onset of electrographical seizure activity.⁴⁹ The search for an organic basis in the post-mortem brains of schizophrenic patients has resulted in controversial findings, mostly because methodological approaches are rarely consistent in their selection of patients and controls.⁴⁶ Common findings include neuronal loss, shrinkage or disarray in the cortical layers and occasional gliosis; affected areas comprise prefrontal cortical areas, the pons, the nucleus accumbens, the hypothalamus, the substantia innominata (part of the basal forebrain), the cingulate, superior, middle and inferior temporal gyri, the amygdala and the hippocampus.^{46,50,51} The hippocampal formation has been the subject of intensive study. Left hemisphere neuronal loss in Ammon's horn without gliosis, entorhinal cortex layer II neuronal loss and reduced density of the interneurons have been described in the post-mortem brains of schizophrenic patients, the former being more noticeable in paranoid than in catatonic patients.^{50,52} As reviewed by Roberts and Bruton,⁵⁰ although, in the early 1900's,

Kraepelin believed schizophrenia had an organic cause and the characteristics of a degenerative process, the majority of contemporary neuropathological studies have not shown signs of progressive features, such as reactive gliosis or correlations between structural abnormalities and the length of illness. Current theories consider prenatal and perinatal effects, as well as environmental factors, to be risk factors for disease manifestation.⁵²

Excision of parts of the limbic system or the temporal lobe of schizophrenic patients usually decreases the florid symptoms (i.e., delusions, hallucinations, disorganized speech or thinking, and chaotic or confused behavior in their fully developed form), but it leaves the psychosis untouched.⁵ Therefore, it is not the complete destruction which gives rise to psychosis, but possibly the irritation process during the development of destruction.³² On some occasions, psychosis or deep personality changes may arise after temporal lobectomy in TLE patients who were previously psychiatrically normal.^{34,53} Not only the recruitment and/or partial damage of the limbic structures are necessary to generate psychiatric disturbances. As postulated by Racine,⁵⁴ the kindling process may gradually develop and spread throughout brain structures distal to the stimulated focus. In patients with epilepsy, there is evidence of a time-dependent spread of epileptic excitability that is independent of tissue pathology.⁵⁵ It is generally assumed that a human limbic seizure disorder results in enhancement of affective limbic functions, rather than their flattening.⁵⁶ Again, the relatively long interval between TLE onset and the onset of comorbid psychiatric symptoms suggests that damage to key structures is necessary and that it builds up over time.^{19,57} Such gradual commitment of connected systems might be determinant to the sum of neurobiological events that eventually will lower the psychopathological threshold of a normal or prodromal psychiatric state.

Limbic lobe and major connections

Through clinical and pathological observation, it is well accepted that TLE is attributable to focal mesial structures of the temporal lobe, especially the amygdaloid complex and the hippocampal formation. The hippocampal formation consists of the hippocampus proper - the dentate gyrus (DG) and Ammon's horn/*Cornus Ammonis* (CA) subfields - along with the subicular and rhinal cortices.⁵⁸ Despite the focal nature of TLE, it is possible that recurrent limbic seizures gradually compromise remote encephalic areas, which may be due to the axonal connectivity of the mesial temporal lobe. Indeed, according to tract-tracing studies in non-human primates and rodents, the hippocampus, amygdaloid complex, and neighboring cortices are embedded within a broad network of limbic connections, whose dysfunctions are involved in at least some of the psychiatric morbidities that are related to TLE. Therefore, it seems reasonable to consider that efferent axons arising from the mesial temporal lobe may convey paroxysmal activity to the entire limbic circuitry, ultimately promoting ictal and periictal psychiatric symptoms. In the same vein, it is possible that seizure recurrence is responsible for the chronic pathological commitment of subcortical and neocortical sites targeted by mesial temporal lobe axons, which would explain the increased susceptibility of TLE patients to interictal psychiatric symptoms.

Hippocampal formation connectivity

The hippocampal formation is the largest structure of the mesial temporal lobe. Intrinsic connections between the DG and CA subfields constitute a well-known tri-synaptic circuit, primarily represented by a unidirectional sequence from DG granule cells to CA3 pyramidal cells (mossy fibers) and then from CA3 to CA1 pyramidal cells (Schaffer axonal collaterals).⁵⁹ Despite evidence for some CA3-DG back-projections,⁶⁰ the DG acts as the major starting point for the circuit, receiving most of its extrahippocampal afferents from superficial cells of the entorhinal cortex via the perforant path of the angular bundle.^{61,62} At the other end of the sequence, CA1 pyramidal cells provide the main hippocampal output, which may or may not be relayed through subiculum cells.^{63,64} Interestingly, part of the CA1 and subiculum axons project back to the entorhinal cortex, specifically to its deep layers, making the entorhinal cortex a critical link in the excitatory loop of the hippocampal formation.⁶⁵ Intrinsically, in the entorhinal cortex an inhibitory system between deep layers receiving CA1/subiculum axons and DG-projecting superficial layers seems to gate the flow of information from, and to, the hippocampus, thereby controlling its excitatory loop.^{66,67} Finally, in addition to the strong entorhinal-DG unidirectional pathway, there are lighter projections from the entorhinal cortex to all CA subfields and to the subiculum, which means that entorhinal cortex reciprocates the CA1 and subiculum inputs.^{65,68} The hippocampal formation and its main connections are shown in Figures 1 and 2.

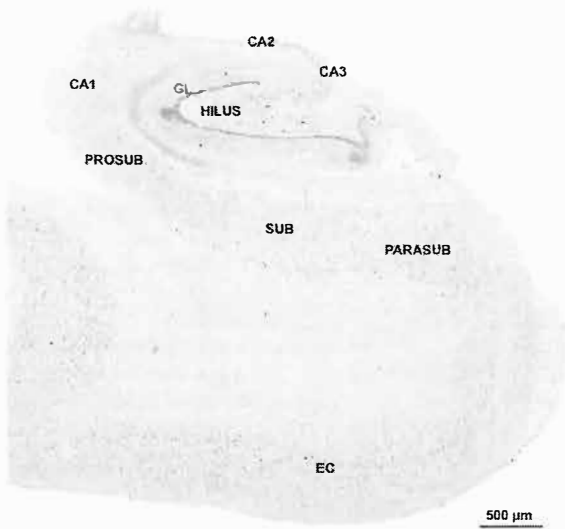


Figure 1 Human hippocampal formation immunostained with the neuronal marker NeuN.

Section from a necropsy subject without history of neurological disorders. The dentate gyrus comprehends the granular layer (GL) and the hilus. CA3-1 are part of Ammon's horn, and together with the dentate gyrus they constitute the hippocampus proper. PROSUB: prosubiculum; SUB: subiculum; PARASUB: parasubiculum; and EC: entorhinal cortex.

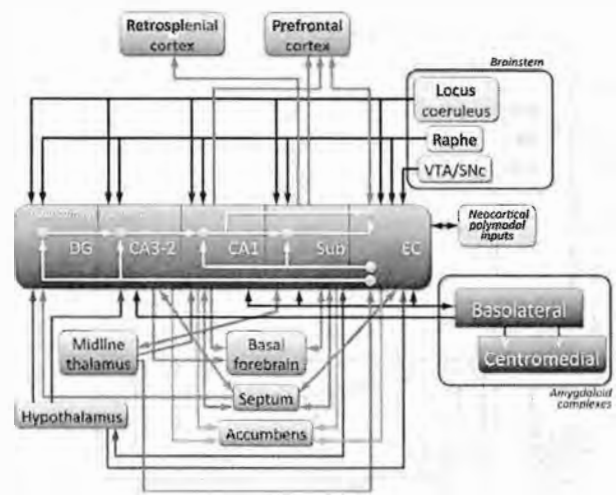


Figure 2 Overview of hippocampal formation connectivity with other limbic structures.

Bold arrows depict conspicuous and well-known afferents/efferents of hippocampus proper (DG, CA3-2, CA1), subiculum (Sub), and entorhinal cortex (EC). Light grey arrows and boxes represent part of the amygdaloid complex connectivity. The topography of axonal pathways according to subdivisions of structures was not detailed. NST: nucleus of the solitary tract; PAG: periaqueductal grey; PBN: parabrachial nucleus; SNC: substantia nigra pars compacta; VTA: ventral tegmental area.

In turn, subicular cells that do not project back to the hippocampal formation send axons through the fimbria-fornix bundles, forwarding hippocampal output to several limbic sites, including specific regions of the basal forebrain (e.g., vertical limb of diagonal band), septum, nucleus accumbens, amygdaloid complex (with particularly dense projections to the basolateral division), mammillary bodies of hypothalamus and adjacent nuclei, midline thalamus (especially nucleus reuniens), retrosplenial cortex, and prefrontal cortex.^{63,69,72} The CA1 subfield, itself, also sends direct projections to the vertical limb of diagonal band, septum, nucleus accumbens, basolateral amygdaloid complex, and prefrontal cortex,^{63,70,71,73,74} as well as weaker efferents to retrosplenial cortex and sensorial neocortical areas.^{74,75} Roughly, all these efferents are accompanied by returning afferents, except for from the nucleus accumbens, retrosplenial cortex, and prefrontal cortex, which do not send projections back to the hippocampus proper.^{68,76} In addition to the preferential hippocampal output by the CA1/subiculum system, CA3 also sends direct efferents to the vertical limb of the diagonal band, septum, and nucleus accumbens, with returning axons from the septum.^{70,77,78} Additionally, CA3-2 receives projections - presumably unidirectional - from basolateral amygdala,⁷¹ and substance P-containing afferents from the supramammillary hypothalamic nucleus.⁷⁹ In contrast with CA subfields, the DG is a mere receiver of extrahippocampal afferents, projecting axons solely to CA3.^{68,80} Beyond the substantial input from the entorhinal cortex, few subcortical sites target the DG (the septum and some parts of the hypothalamus, mainly its supramammillary area, are among these sites).^{81,82}

In spite of the mammillary nuclei and adjacencies that are reciprocally connected with the subiculum, none of the CA subfields project to the hypothalamus,⁸³ although CA2 and CA3 do receive hypothalamic projections.⁷⁹ Mostly, the non-entorhinal afferents directed to the DG and CA subfields use the fimbria-fornix system as their main route, along with the majority of hippocampal efferents described above.⁶⁸ Last but not least, the entire hippocampal formation (Figure 1) receives noradrenergic, serotonergic, and dopaminergic inputs, respectively from locus coeruleus, raphe nuclei and ventral tegmental area of the brainstem.^{84,86} Particularly in the DG and CA subfields, dopaminergic innervation is much more meager than the others, preferentially targeting the entorhinal cortex.⁶⁸

Because there are unknown efferents from the DG and CA2-3 to the neocortex, it seems that CA1 unidirectional projections to retrosplenial and prefrontal cortices are the strongest communication between the hippocampus proper and neocortical areas outside the hippocampal formation.^{63,75} Unlike the hippocampus proper, the entorhinal cortex is reciprocally connected with a wider neocortical domain, with a preference for higher-order association areas. Therefore, the entorhinal cortex acts as the principal link between the polymodal neocortical inputs and the hippocampus.^{68,87} Although this neuroanatomical and functional distinction exists, subcortical connections of the entorhinal cortex are similar to those of the hippocampus proper, including bidirectional pathways with the septum and basolateral amygdala, as well as unidirectional projections to nucleus accumbens, and unidirectional projections from distributed parts of the hypothalamus and midline thalamus, once again with major participation of nucleus reuniens.^{72,88-91} Among the neocortical sites reciprocally connected to the entorhinal cortex are the perirhinal, postrhinal, and prefrontal cortices, including a weak communication with the retrosplenial cortex.⁶⁸ As part of the hippocampal formation, the entorhinal cortex is also subjected to neuromodulatory influence by the monoaminergic ascending systems, including significant dopaminergic afferents from the ventral tegmental area.^{90,92} In Figure 2, the arrows outside the hippocampal formation represent the extrinsic connections depicted here.

Amygdaloid complex and its efferents and afferents

Another important part of the mesial temporal lobe is represented by the amygdaloid complex, a group of functionally and structurally diverse nuclei, with intricate interconnections and widely distributed communication with cortical and subcortical limbic sites.⁹³ In particular, the basolateral group projects strong efferents to CA3, CA1, the subiculum, entorhinal cortex and perirhinal cortex, receiving back-projections from all sites except CA3.^{72,94,95} as seen in Figure 3. The same basolateral group is responsible for most of the amygdaloid innervation of the prefrontal cortex (which is also a recipient of CA1/subiculum axons, as previously mentioned), nucleus accumbens (a target of the whole hippocampal formation), and the striatum.⁹⁶⁻⁹⁸ Specifically, the prefrontal cortex sends returning projections to the basolateral complex⁹⁹ (Figure 3). Considering the emotional roles of the amygdala, as well as the mnemonic/

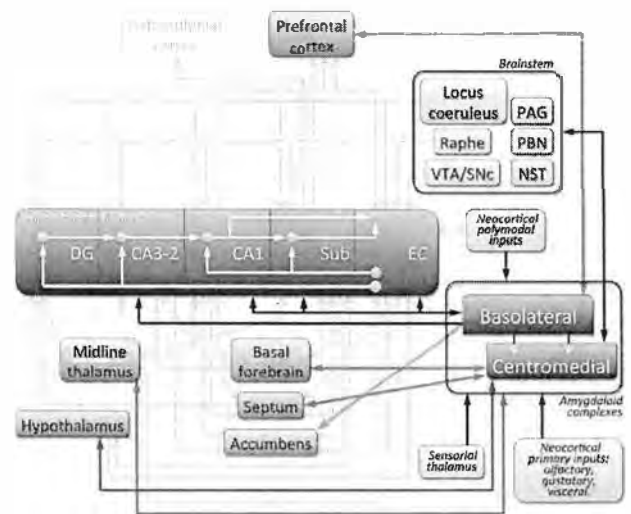


Figure 3 Overview of amygdaloid complex connectivity with other limbic structures.

Bold arrows depict conspicuous and well-known afferents/efferents of basolateral and centromedial groups of amygdaloid nuclei. Light grey arrows and boxes represent part of the hippocampal formation connectivity. The topography of axonal pathways according to subdivisions of structures was not detailed. NST: nucleus of the solitary tract; PAG: periaqueductal grey; PBN: parabrachial nucleus; SNc: substantia nigra pars compacta; VTA: ventral tegmental area.

attentive functions of the hippocampus and the prefrontal cortex, this basolateral-hippocampal reciprocity, along with its common limbic targets, comprises a wide network that is well positioned to control cognitive aspects of behavior.¹⁰⁰⁻¹⁰²

In contrast, the centromedial group of amygdaloid nuclei preferentially sends projections to neuromodulatory sites, including brainstem ascending monoaminergic centers (noradrenergic locus coeruleus, dopaminergic substantia nigra and ventral tegmental area, and serotonergic raphe nuclei), and cholinergic regions of the basal forebrain and septum.¹⁰³⁻¹⁰⁶ Moreover, this centromedial division of the amygdala sends efferents to several different autonomic, reproductive, and defensive-related sites, including some brainstem regions (periaqueductal grey, parabrachial nucleus, and nucleus of the solitary tract), and various portions of the hypothalamus.^{105,107-110} In particular, the medial nucleus of the amygdala sends projections to the nucleus reuniens of midline thalamus.¹⁰⁴ An important conduit of the amygdala fibers that are directed to the brainstem, the basal forebrain, and the diencephalon is the stria terminalis, whose bed nucleus contributes to additional innervation of these sites.¹¹¹ Finally, the corticomedial nuclei of the amygdala, which are also referred to as cortical-like nuclei due to their superficial location and layered structure, are the main source of efferents to the olfactory system.⁹³ In general, all of these efferent connections of the centromedial division are reciprocated⁹³ (Figure 3).

The amygdaloid complex, as a whole, receives afferents from regions that are not preferentially targeted by amygdala projections, such as higher-order areas of somatosensory,

auditory, and visual cortices, as well as primary areas of the olfactory system, and gustatory and visceral portions of the insular cortex.¹¹²⁻¹¹⁵ Thalamic nuclei directly related to specific sensorial functions also contribute with afferents to the amygdala,^{116,117} along with the paraventricular and reuniens nuclei of the midline thalamus¹¹⁸. Overall, the various afferents terminate onto virtually all the amygdaloid divisions, despite some intricate patterns of specificity not detailed here. Nevertheless, the basolateral group acts as the main input receiver, which processes the information locally, forwarding it to the centromedial nuclei as a preferential output station⁹³ (Figure 3).

Each one of the projection systems mentioned above have specific patterns of ipsilateral and/or contralateral connectivity not detailed in the present article. The majority of connections are mediated by glutamatergic neurotransmission, regardless of termination onto glutamatergic projection cells or GABAergic interneurons, with specific exceptions, for instance, monoaminergic and cholinergic projections arising from the brainstem and basal forebrain, GABAergic projections from the septum that coexist with septal cholinergic axons, and GABAergic projections from central amygdala. There are differential patterns of topographical connectivity throughout the long axis of the hippocampal formation, which are not explained here. Because comparative neuroanatomy is not the main purpose of the present review, information on differences between mammalian species was omitted for clarity.

According to Bear,⁵⁷ psychopathological states in TLE would derive from intrinsic mechanisms leading to anatomical sensory limbic hyper connectivity. This psychiatric manifestation would be the result of a long epileptogenic process throughout the limbic system, and progressive changes in limbic structures secondary to seizure activity would be the underlying physiopathology.⁵⁷ Such changes would explain the fact that some patients have incomplete seizure remission after surgical resection of the mesial temporal lobe.¹ The extra-temporal commitment would be due to the spread of seizures by critical subcortical synchronizers, possibly represented by thalamo-hippocampal circuits.¹ Specifically, the midline nuclei of the thalamus are well positioned to act as major synchronizers,¹¹⁸ because some of them are interconnected with both the hippocampal formation and the amygdaloid complex (Figures 2 and 3). Importantly, the same thalamic nuclei project to the nucleus accumbens and are interconnected with the prefrontal cortex, forming a behaviorally flexible circuit whose dysfunction contributes to the pathophysiology of psychosis and schizophrenia.¹¹⁹ Therefore, the hippocampal and amygdala connectivity summarized here may be the common context for TLE and psychotic-like symptoms. Although these network dysfunctions are not fully understood, there is increasing evidence from animal models showing how particular pathways of the limbic circuitry may underlie the relationship between psychosis and TLE.

Evidence from animal models

The relationship between psychosis and epilepsy has been investigated experimentally through electrical kindling in specific circuits and through single electrically evoked hippocampal afterdischarge protocols,¹²⁰⁻¹²³ dopaminergic

sensitization by pharmacological challenge,^{124,125} and acute or chronic treatments with non-competitive antagonists of N-methyl D-aspartate (NMDA) receptors.^{126,127}

Kindling by electrical stimulation in specific circuits provides evidence for dopaminergic involvement in the putative shared mechanisms between epilepsy and psychosis. For example, kindling in the ventral tegmental area generates progressive fearfulness, hiding and loss of social behavior in cats,¹²⁸ enhancing amphetamine- or methamphetamine-induced locomotor activity in rodents.^{129,130} Hippocampal kindling increases the density of dopaminergic receptors, as well as dopamine release in nucleus accumbens.^{131,132} These dopaminergic changes in mesolimbic circuits after ictal episodes seem to depend on the hippocampal activity. Hyperlocomotion, PPI deficits and aberrant increases of fast oscillations elicited by prefrontal or nucleus accumbens kindling are reverted if the hippocampus is previously inactivated.¹²² Unlike to hippocampal stimulation, prefrontal cortex stimulation is unable to significantly depolarize nucleus accumbens neurons.^{133,134} Other studies have shown that kindling in the basolateral amygdala down-regulates dopamine transporters in the striatum, while disrupting PPI.^{44,135} Altogether, kindling data reinforce the idea that, in experimental psychosis, the hippocampus becomes unable to regulate the source of convergent information flow to the nucleus accumbens, especially those from the prefrontal cortex, ventral tegmental area and amygdala¹³⁶ (Figure 4).

Abnormalities in the cortico-frontal-mesolimbic circuits observed in experimental models may be useful to understand how dopaminergic dysfunctions could be related to the high rates of psychosis in TLE patients.¹³⁷ Postictal psychosis models based on single electrically evoked hippocampal afterdischarge also induce psychotic-like behaviors, such as hyperlocomotion and stereotyped movements.¹²¹ This postictal locomotor activity is mediated by D2 dopaminergic receptors in the nucleus accumbens and requires ventral pallidum activity, suggesting that the nucleus accumbens-ventral pallidum pathway is critical for the expression of postictal abnormal behaviors.¹²⁰ Impairment of sensorimotor gating induced by afterdischarge is related to increased neural activity in the medial septum and increased hippocampal gamma waves induced by local afterdischarges through GABAergic, not cholinergic, septo-hippocampal neurons.¹²³ Experimental studies on seizure-induced pathological sensitization of the dopaminergic system have also been useful to elucidate the relationship between mesolimbic circuits, psychosis and epilepsy.¹²⁴ Seizure activity transiently elevates extracellular dopamine levels at various brain sites, including the hippocampus, striatum, nucleus accumbens and prefrontal cortex^{132,138,139} (Figure 4). In fact, rats subjected to the pilocarpine model of TLE display significantly higher spontaneous firing rates of ventral tegmental area neurons compared to control rats.¹²⁴ This population activity of dopaminergic neurons, defined as the proportion of spontaneously firing neurons, is regulated in intact rats by a ventral subicular-nucleus accumbens-ventral pallidal-ventral tegmental area pathway.¹¹⁹ However, the underlying mechanisms by which hippocampal hyperactivity influences the dopaminergic neurons in TLE are not well recognized. Neonatal seizures affect both dopaminergic and glutamatergic systems in the prefrontal-striatal circuitry, resulting in enhanced behavioral

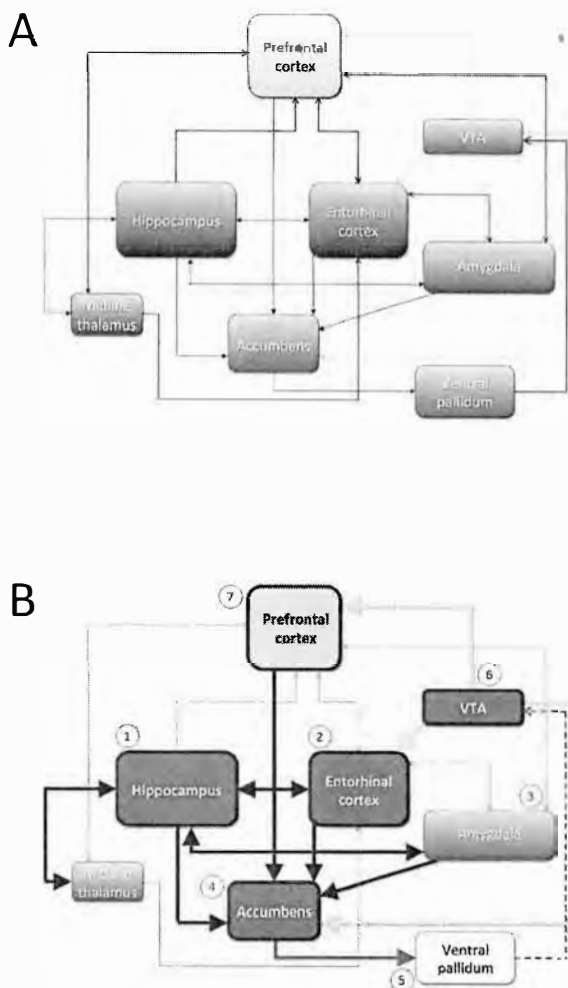


Figure 4. Direct and indirect output in psychosis pathways.

A. Non-pathological circuit. **B.** Hypothetic pathological circuit in temporal lobe epilepsy. Hippocampal hyperactivity may disrupt the fine dopaminergic control of limbic and extralimbic circuits via polysynaptic projections. **1.** Epileptogenic process and neuropathological changes may drive hippocampal hyperexcitability. **2.** Increased excitability seen in TLE patients and animal models might be associated with neurodegeneration in the entorhinal cortex. Robust projections between hippocampus and entorhinal cortex reverberate neuronal hyperactivity. **3.** Strong projections between hippocampal formation and amygdala may propagate the excitability to the emotional circuit. **4.** Consequently, nucleus accumbens is overactivated by convergent projections. **5.** Nucleus accumbens, in turn, strongly inhibits ventral pallidum. **6.** Given that the ventral pallidum provides an inhibitory tone to dopaminergic neurons of the ventral tegmental area (VTA), limbic hyperactivation will result in increased dopamine neuron activity by disinhibition. **7.** The pathological increase of dopamine levels in the prefrontal cortex disrupts working memory and behavioral flexibility leading to stereotyped behaviors. Arrows: Black (excitatory projections), gray (inhibitory projections), light gray (dopaminergic projections). The dashed line represents a decrease in the inhibitory tone from the ventral pallidum to VTA. The weight of remaining lines indicates hypothetical efficacy of information flow between areas. Figure based on Sesack and Grace¹⁵⁵ and Lodge and Grace.¹³⁹

sensitization to methamphetamine in adolescence.¹²⁵ The increased excitability observed in patients and in TLE models might be associated with a pronounced neurodegeneration in layer III of the medial entorhinal cortex.^{140,141} This pattern of neuronal loss eventually results in hippocampal and parahippocampal hyperexcitability, which have an important role in epileptogenesis and enhanced susceptibility to seizures and epileptiform discharges.^{142,143} Such hyperexcitability could be related to the cognitive deficits and psychiatric comorbidities observed in some cases of TLE because entorhinal-hippocampus projections are crucial to temporal association memory in mice.¹⁴⁴ Their dysfunction is involved in the potentiation of drug-induced locomotor hyperactivity in pilocarpine-treated rats.¹²⁴ In fact, recent data on human TLE suggest that decreased neuronal density is found in entorhinal cortex layer III of TLE patients with hippocampal sclerosis and psychosis.³⁵ Therefore, according to kindling and hippocampal afterdischarge studies, the increased sensitization to psychostimulants observed in TLE models is likely attributable to an increase in tonic dopaminergic transmission, secondary to an augmented activity within the hippocampal and parahippocampal circuits¹⁴⁵ (Figure 4B). Increased hippocampal and parahippocampal drive is also found in patients with schizophrenia.¹⁴⁶

Despite the available data, putative shared mechanisms between epilepsy and psychosis remain poorly understood. The non-competitive NMDA antagonists ketamine (KET), phencyclidine (PCP), and dizocilpine (MK-801) produce robust psychotic-like behaviors, PPI deficits, memory impairments and hippocampal synaptic plasticity disruptions probably associated with increased excitability in limbic thalamo-cortical circuits.^{147,148} Non-competitive NMDA antagonists generate disinhibition of specific circuits by blocking the action of NMDA receptors on GABAergic neurons, resulting in decreased firing of GABAergic neurons (mainly parvalbumin-positive chandelier cells) and increased excitability of limbic circuits and the prefrontal cortex.¹⁴⁹⁻¹⁵³ Treatment with non-competitive NMDA antagonists can also decrease parvalbumin expression¹⁵⁴ and produce epileptiform activity in limbic circuits.¹⁵⁵ NMDA antagonists can also damage and kill cortical neurons by increasing cytoplasmic vacuoles in pyramidal neurons of the posterior cingulate and retrosplenial cortex of adult rats.¹⁵⁶ In the same vein, KET significantly potentiates kainic acid-elicited gamma power in slices of the mouse prefrontal cortex.¹⁵⁷ Moreover, the dopaminergic system is also involved in the behavioral changes observed in NMDA-antagonist-based models.¹⁵⁸ Impairment of executive tasks in rodents treated with KET is mediated by D2 receptors.¹⁵⁹ In addition, a single dose of PCP promotes an increase of dopamine levels in the prefrontal cortex.¹⁶⁰ Jackson et al.¹⁵² demonstrated that a single MK-801 injection increases random firing and decreases burst firing activity in the prefrontal cortex. The reduction in burst activity is associated with a decrease in synaptic efficacy, which in turn could affect the control of behavioral outputs. Similarly, increases in the random firing rates of prefrontal neurons are associated with deficits in PPI and working memory.¹⁵² Suzuki et al.¹²⁷ showed that systemic injection with PCP significantly changes neuronal firing rates in the prefrontal cortex of rats. No changes were seen after local frontal cortex microinjection. However, when PCP was microinjected into the ventral

hippocampus, prefrontal neurons showed responses similar to those observed after systemic injection.¹⁶¹ Altogether, a set of evidence indicates the involvement of the dopaminergic system and points to a possible role of hippocampal to prefrontal cortex projections in the expression of aberrant behaviors induced by non-competitive NMDA antagonists in rats. Considering that the main source of direct hippocampal afferents to the cortex (CA1 subfield of the hippocampus) is especially affected in TLE, and that psychotic-like effects produced by the administration of NMDA antagonists require a preserved communication between the hippocampus (CA1) and the prefrontal cortex, we speculate that synaptic plasticity in this pathway may represent a point of vulnerability for the development of psychosis in TLE patients.

Conclusions

The investigation on TLE and psychosis has independently provided important pathophysiological hallmarks. The best-known observations include hippocampal sclerosis in TLE, related to a chronic state of recurrent seizures, and heterogeneous cortico-striato-pallido-thalamic disturbances in psychosis, possibly due to interactions between genetic and environmental influences on the maturation of these circuits. The relatively high prevalence of psychotic-like symptoms in TLE patients suggests shared mechanisms and/or substrates between these two conditions. However, few studies have addressed this issue, despite the interesting reports on electrical kindling, dopaminergic manipulation, and NMDA antagonism reviewed here. Considering mesial temporal lobe connectivity along with the midline thalamus, the prefrontal cortex and the nucleus accumbens, as well as the ascending neuromodulatory influence on these circuits, future studies involving a convergence of approaches would be useful. For instance, investigations into the relationship between behavioral symptoms (e.g., sensorimotor gating), synaptic plasticity (e.g., long-term potentiation/depression in limbic pathways), and pathology in animal models of TLE (e.g., lithium-pilocarpine or electrical kindling in the hippocampus or amygdala) are scant. Nevertheless, such animal studies would be necessary to gain a better understanding of clinical cases. In summary, present clinical, neurophysiological and neuropathological data demonstrate the existence of an intricate mesh of both antagonistic and also shared mechanisms between TLE and psychosis. As once mentioned by Slater et al. "like effects commonly have similar causes"²⁶, and the underlying pathogenesis of psychosis in TLE still needs clarification.

Acknowledgments

Supported by Fundação de Amparo à Pesquisa do Estado de São Paulo (FAPESP), Conselho Nacional de Desenvolvimento Científico e Tecnológico (National Counsel of Technological and Scientific Development - CNPq) and Fundação de Amparo à Pesquisa do Estado do Rio Grande do Norte (FAPERN), Brazil.

Disclosures

Ludmyla Kandratavicius, PhD

Employment: *Faculdade de Medicina de Ribeirão Preto, Department of Neurosciences and Behavior, Universidade de São Paulo, Brazil.*

Cleiton Lopes-Aguiar, MSc

Employment: *Faculdade de Medicina de Ribeirão Preto, Department of Neurosciences and Behavior, Universidade de São Paulo, Brazil.*

Lézio Soares Bueno-Júnior, PhD

Employment: *Faculdade de Medicina de Ribeirão Preto, Department of Neurosciences and Behavior, Universidade de São Paulo, Brazil.*

Rodrigo Neves Romcy-Pereira, MSc, PhD

Employment: *Brain Institute, Universidade Federal do Rio Grande do Norte, Natal, Brazil.*

Jaime Eduardo Cecilio Hallak, MD, PhD

Employment: *Faculdade de Medicina de Ribeirão Preto, Department of Neurosciences and Behavior, Universidade de São Paulo, Brazil.* Other: *National Institute of Science and Technology in Translational Medicine (Instituto Nacional de Ciência e Tecnologia - INCT-TM; CNPq).*

Joao Pereira Leite, MD, PhD

Employment: *Faculdade de Medicina de Ribeirão Preto, Department of Neurosciences and Behavior, Universidade de São Paulo, Brazil.*

* Modest

** Significant

*** Significant. Amounts given to the author's institution or to a colleague for research in which the author has participation, not directly to the author.

References

- Bertram EH. Temporal lobe epilepsy: where do the seizures really begin? *Epilepsy Behav.* 2009;14(Suppl 1):32-7.
- Swerdlow NR. Integrative circuit models and their implications for the pathophysiologies and treatments of the schizophrenias. *Curr Top Behav Neurosci.* 2010;4:555-83.
- Flor-Henry P. Psychosis and temporal lobe epilepsy. A controlled investigation. *Epilepsia.* 1969;10(3):363-95.
- Roberts GW, Done DJ, Bruton C, Crow TJ. A "mock up" of schizophrenia: temporal lobe epilepsy and schizophrenia-like psychosis. *Biol Psychiatry.* 1990;28(2):127-43.
- Serafetinides EA, Falconer MA. The effects of temporal lobectomy in epileptic patients with psychosis. *J Ment Sci.* 1962;108:584-93.
- Stevens JR. Epilepsy, psychosis and schizophrenia. *Schizophr Res.* 1988;1(1):79-89.
- Taylor DC. Factors influencing the occurrence of schizophrenia-like psychosis in patients with temporal lobe epilepsy. *Psychol Med.* 1975;5(3):249-54.
- Editorial: Epilepsy, schizophrenia, and limbic system. *Lancet.* 1974;2(7886):935-6.
- Papez JW. A proposed mechanism of emotion. *J Neuropsychiatry Clin Neurosci.* 1937;7(1):103-12.
- Klüver H, Bucy P. "Psychic blindness" and other symptoms following bilateral temporal lobectomy in rhesus monkeys. *American Journal of Physiology.* 1937;119:352-3.
- MacLean P. Psychosomatic disease and the visceral brain; recent developments bearing on the Papez theory of emotion. *Psychosom Med.* 1949;11(6):338-53.
- Heimer L, Van Hoesen GW, Trimble M, Zahn DS. The limbic system: a concept in perpetual search for a definition. In: Heimer L, Van Hoesen GW, Trimble M, Zahn DS, eds. *Anatomy of Neuropsychiatry.* U.S.A.: Academic Press Elsevier; 2008:1-13.
- Brain L. Psychosomatic Medicine and the Brain-Mind Relationship. *Lancet.* 1964;2(7355):325-8.
- Cairns H. Disturbances of consciousness with lesions of the brain-stem and diencephalon. *Brain.* 1952;75(2):109-46.
- Waxman SG, Geschwind N. The interictal behavior syndrome of temporal lobe epilepsy. *Arch Gen Psychiatry.* 1975;32(12):1580-6.
- Penfield W, Perot P. The Brain's Record of Auditory and Visual Experience. A Final Summary and Discussion. *Brain.* 1963;86:595-696.
- Gloor P, Olivier A, Quesney LF, Andermann F, Horowitz S. The role of the limbic system in experiential phenomena of temporal lobe epilepsy. *Ann Neurol.* 1982;12(2):129-44.
- Beard AW, Slater E. The schizophrenic-like psychoses of epilepsy. *Proc R Soc Med.* 1962;55:311-6.

19. Fujii D, Ahmed I. Psychotic disorder following traumatic brain injury: a conceptual framework. *Cogn Neuropsychiatry*. 2002;7(1):41-62.
20. Kristensen O, Sindrup EH. Psychomotor epilepsy and psychosis. I. Physical aspects. *Acta Neurol Scand*. 1978;57(5):361-9.
21. Landolt H. Some correlations between the electroencephalogram and normal and pathologic mental processes. *Epilepsy Behav*. 1963;14(3):448-51.
22. Pollock DC. Models for understanding the antagonism between seizures and psychosis. *Prog Neuropsychopharmacol Biol Psychiatry*. 1987;11(4):483-504.
23. Trimble M. The relationship between epilepsy and schizophrenia: a biochemical hypothesis. *Biol Psychiatry*. 1977;12(2):299-304.
24. Ogren SO, Pakh B. Effects of dopamine D1 and D2 receptor agonists and antagonists on seizures induced by chemoconvulsants in mice. *Pharmacol Toxicol*. 1993;72(4-5):213-20.
25. Turski L, Cavalheiro EA, Bortolotto ZA, Ikonomidou-Turski C, Kleinrok Z, Turski WA. Dopamine-sensitive anticonvulsant site in the rat striatum. *J Neurosci*. 1988;8(11):4027-37.
26. Slater E, Beard AW, Glithero E. The schizophrenia-like psychoses of epilepsy. *Br J Psychiatry*. 1963;109:95-150.
27. Krishnamoorthy ES, Trimble MR, Blumer D. The classification of neuropsychiatric disorders in epilepsy: a proposal by the ILAE Commission on Psychobiology of Epilepsy. *Epilepsy Behav*. 2007;10(3):349-53.
28. Toone BK. The psychoses of epilepsy. *J Neurol Neurosurg Psychiatry*. 2000;69(1):1-3.
29. Kanemoto K, Kawasaki J, Kawai I. Postictal psychosis: a comparison with acute interictal and chronic psychoses. *Epilepsia*. 1996;37(6):551-6.
30. Tarulli A, Devinsky O, Alper K. Progression of postictal to interictal psychosis. *Epilepsia*. 2001;42(11):1468-71.
31. Braun CM, Dumont M, Duval J, Hamel-Hebert I, Godbout L. Brain modules of hallucination: an analysis of multiple patients with brain lesions. *J Psychiatry Neurosci*. 2003;28(6):432-49.
32. Torrey EF, Peterson MR. Schizophrenia and the limbic system. *Lancet*. 1974;2(7886):942-6.
33. Malamud N. Psychiatric disorder with intracranial tumors of limbic system. *Arch Neurol*. 1967;17(2):113-23.
34. Taylor DC. Mental state and temporal lobe epilepsy. A correlative account of 100 patients treated surgically. *Epilepsia*. 1972;13(6):727-65.
35. Kandravicius L, Hallak JE, Young LT, Assirati JA, Carlotti CG, Jr., Leite JP. Differential aberrant sprouting in temporal lobe epilepsy with psychiatric co-morbidities. *Psychiatry Res*. 2012;195(3):144-50.
36. Allen P, Laroi F, McGuire PK, Aleman A. The hallucinating brain: a review of structural and functional neuroimaging studies of hallucinations. *Neurosci Biobehav Rev*. 2008;32(1):175-91.
37. Braff DL. Gating in schizophrenia: from genes to cognition (to real world function?). *Biol Psychiatry*. 2011;69(5):395-6.
38. Quednow BB, Ettinger U, Mossner R et al. The schizophrenia risk allele C of the TCF4 rs9960767 polymorphism disrupts sensorimotor gating in schizophrenia spectrum and healthy volunteers. *J Neurosci*. 2011;31(18):6684-91.
39. Takahashi H, Iwase M, Yasuda Y et al. Relationship of prepulse inhibition to temperament and character in healthy Japanese subjects. *Neurosci Res*. 2012;72(2):187-93.
40. Braff DL, Geyer MA, Swerdlow NR. Human studies of prepulse inhibition of startle: normal subjects, patient groups, and pharmacological studies. *Psychopharmacology (Berl)*. 2001;156(2-3):234-58.
41. Pouretmad HR, Thompson PJ, Fenwick PB. Impaired sensorimotor gating in patients with non-epileptic seizures. *Epilepsy Res*. 1998;31(1):1-12.
42. Syed TU, LaFrance WC, Jr., Kahrman ES et al. Can semiology predict psychogenic nonepileptic seizures? A prospective study. *Ann Neurol*. 2011;69(6):997-1004.
43. Mokleby K, Blomhoff S, Malt UF, Dahlstrom A, Tauboll E, Gjerstad L. Psychiatric comorbidity and hostility in patients with psychogenic nonepileptic seizures compared with somatoform disorders and healthy controls. *Epilepsia*. 2002;43(2):193-8.
44. Howland JG, Hannesson DK, Barnes SJ, Phillips AG. Kindling of basolateral amygdala but not ventral hippocampus or perirhinal cortex disrupts sensorimotor gating in rats. *Behav Brain Res*. 2007;177(1):30-6.
45. Miller EJ, Saint Marie LR, Breier MR, Swerdlow NR. Pathways from the ventral hippocampus and caudal amygdala to forebrain regions that regulate sensorimotor gating in the rat. *Neuroscience*. 2010;165(2):601-11.
46. Weinberger DR, Wagner RL, Wyatt RJ. Neuropathological studies of schizophrenia: a selective review. *Schizophr Bull*. 1983;9(2):193-212.
47. Thom M. Hippocampal sclerosis: progress since Sommer. *Brain Pathol*. 2009;19(4):565-72.
48. Cavanagh JB, Meyer A. Aetiological aspects of Ammon's horn sclerosis associated with temporal lobe epilepsy. *Br Med J*. 1956;2(5006):1403-7.
49. Bonilha L, Rorden C, Appenzeller S, Coan AC, Cendes F, Li LM. Gray matter atrophy associated with duration of temporal lobe epilepsy. *Neuroimage*. 2006;32(3):1070-9.
50. Roberts GW, Bruton CJ. Notes from the graveyard: neuropathology and schizophrenia. *Neuropathol Appl Neurobiol*. 1990;16(1):3-16.
51. Sokolov BP, Tcherepanov AA, Haroutunian V, Davis KL. Levels of mRNAs encoding synaptic vesicle and synaptic plasma membrane proteins in the temporal cortex of elderly schizophrenic patients. *Biol Psychiatry*. 2000;48(3):184-96.
52. Falkai P, Parlapani E, Gruber O, Schmitt A. The Neuropathology of Schizophrenia: Central Role for the Hippocampus? In: Gattaz WF, Busatto G, eds. *Advances in Schizophrenia Research 2009*. New York: Springer Science; 2010:149-65.
53. Shaw P, Mellers J, Henderson M, Polkey C, David AS, Toone BK. Schizophrenia-like psychosis arising de novo following a temporal lobectomy: timing and risk factors. *J Neurol Neurosurg Psychiatry*. 2004;75(7):1003-8.
54. Morimoto K, Fahnstock M, Racine RJ. Kindling and status epilepticus models of epilepsy: rewiring the brain. *Prog Neurobiol*. 2004;73(1):1-60.
55. Flor-Henry P. Lateralized temporal-limbic dysfunction and psychopathology. *Ann N Y Acad Sci*. 1976;280:777-97.
56. Adamec RE. Does kindling model anything clinically relevant? *Biol Psychiatry*. 1990;27(3):249-79.
57. Bear DM. Temporal lobe epilepsy--a syndrome of sensory-limbic hyperconnection. *Cortex*. 1979;15(3):357-84.
58. Duvernoy HM. *The Human Hippocampus*. Berlin: Springer-Verlag; 1988.
59. Andersen P, Soleng AF, Raastad M. The hippocampal lamella hypothesis revisited. *Brain Res*. 2000;886(1-2):165-71.
60. Scharfman HE. The CA3 "backprojection" to the dentate gyrus. *Prog Brain Res*. 2007;163:627-37.
61. Heinemann U, Schmitz D, Eder C, Gloveli T. Properties of entorhinal cortex projection cells to the hippocampal formation. *Ann N Y Acad Sci*. 2000;911:112-26.
62. Witter MP, Wouterlood FG, Naber PA, Van Haften T. Anatomical organization of the parahippocampal-hippocampal network. *Ann N Y Acad Sci*. 2000;911:1-24.
63. Aggleton JP. Multiple anatomical systems embedded within the primate medial temporal lobe: Implications for hippocampal function. *Neurosci Biobehav Rev*. 2012;36(7):1579-96.

64. Gigg J. Constraints on hippocampal processing imposed by the connectivity between CA1, subiculum and subicular targets. *Behav Brain Res.* 2006;174(2):265-71.
65. Naber PA, Lopes da Silva FH, Witter MP. Reciprocal connections between the entorhinal cortex and hippocampal fields CA1 and the subiculum are in register with the projections from CA1 to the subiculum. *Hippocampus.* 2001;11(2):99-104.
66. Canto CB, Wouterlood FG, Witter MP. What does the anatomical organization of the entorhinal cortex tell us? *Neural Plast.* 2008;2008:381243.
67. de Curtis M, Pare D. The rhinal cortices: a wall of inhibition between the neocortex and the hippocampus. *Prog Neurobiol.* 2004;74(2):101-10.
68. Amaral DG, Lavenex P. Hippocampal Neuroanatomy. In: Andersen P, Morris RG, Amaral DG, Bliss TV, O'Keefe J, eds. *The Hippocampus Book.* New York: Oxford University Press; 2007:37-114.
69. Finch DM, Nowlin NL, Babb TL. Demonstration of axonal projections of neurons in the rat hippocampus and subiculum by intracellular injection of HRP. *Brain Res.* 1983;271(2):201-16.
70. Friedman DP, Aggleton JP, Saunders RC. Comparison of hippocampal, amygdala, and perirhinal projections to the nucleus accumbens: combined anterograde and retrograde tracing study in the Macaque brain. *J Comp Neurol.* 2002;450(4):345-65.
71. Pitkanen A, Pikkarainen M, Nurminen N, Ylinen A. Reciprocal connections between the amygdala and the hippocampal formation, perirhinal cortex, and postrhinal cortex in rat. A review. *Ann N Y Acad Sci.* 2000;911:369-91.
72. Saunders RC, Rosene DL, Van Hoesen GW. Comparison of the efferents of the amygdala and the hippocampal formation in the rhesus monkey: II. Reciprocal and non-reciprocal connections. *J Comp Neurol.* 1988;271(2):185-207.
73. Jay TM, Witter MP. Distribution of hippocampal CA1 and subicular efferents in the prefrontal cortex of the rat studied by means of anterograde transport of Phaseolus vulgaris-leucoagglutinin. *J Comp Neurol.* 1991;313(4):574-86.
74. van Groen T, Wyss JM. Extrinsic projections from area CA1 of the rat hippocampus: olfactory, cortical, subcortical, and bilateral hippocampal formation projections. *J Comp Neurol.* 1990;302(3):515-28.
75. Cenquizca LA, Swanson LW. Spatial organization of direct hippocampal field CA1 axonal projections to the rest of the cerebral cortex. *Brain Res Rev.* 2007;56(1):1-26.
76. Vertes RP, Hoover WB, Szigeti-Buck K, Leranath C. Nucleus reuniens of the midline thalamus: link between the medial prefrontal cortex and the hippocampus. *Brain Res Bull.* 2007;71(6):601-9.
77. Gaykema RP, van der Kuil J, Hersh LB, Luiten PG. Patterns of direct projections from the hippocampus to the medial septum-diagonal band complex: anterograde tracing with Phaseolus vulgaris leucoagglutinin combined with immunohistochemistry of choline acetyltransferase. *Neuroscience.* 1991;43(2-3):349-60.
78. Swanson LW, Cowan WM. An autoradiographic study of the organization of the efferent connections of the hippocampal formation in the rat. *J Comp Neurol.* 1977;172(1):49-84.
79. Leranath C, Nitsch R. Morphological evidence that hypothalamic substance P-containing afferents are capable of filtering the signal flow in the monkey hippocampal formation. *J Neurosci.* 1994;14(7):4079-94.
80. Swanson LW, Wyss JM, Cowan WM. An autoradiographic study of the organization of intrahippocampal association pathways in the rat. *J Comp Neurol.* 1978;181(4):681-715.
81. Vertes RP. PHA-L analysis of projections from the supramammillary nucleus in the rat. *J Comp Neurol.* 1992;326(4):595-622.
82. Wyss JM, Swanson LW, Cowan WM. Evidence for an input to the molecular layer and the stratum granulosum of the dentate gyrus from the supramammillary region of the hypothalamus. *Anat Embryol (Berl).* 1979;156(2):165-76.
83. Swanson LW, Cowan WM. Hippocampo-hypothalamic connections: origin in subicular cortex, not ammon's horn. *Science.* 1975;189(4199):303-4.
84. Bobillier P, Seguin S, Degueurce A, Lewis BD, Pujol JF. The efferent connections of the nucleus raphe centralis superior in the rat as revealed by radioautography. *Brain Res.* 1979;166(1):1-8.
85. Loughlin SE, Foote SL, Grzanna R. Efferent projections of nucleus locus coeruleus: morphologic subpopulations have different efferent targets. *Neuroscience.* 1986;18(2):307-19.
86. Oades RD, Halliday GM. Ventral tegmental (A10) system: neurobiology. 1. Anatomy and connectivity. *Brain Res.* 1987;434(2):117-65.
87. Insausti R, Herrero MT, Witter MP. Entorhinal cortex of the rat: cytoarchitectonic subdivisions and the origin and distribution of cortical efferents. *Hippocampus.* 1997;7(2):146-83.
88. Insausti R, Amaral DG, Cowan WM. The entorhinal cortex of the monkey: III. Subcortical afferents. *J Comp Neurol.* 1987;264(3):396-408.
89. Ohtake T, Yamada H. Efferent connections of the nucleus reuniens and the rhomboid nucleus in the rat: an anterograde PHA-L tracing study. *Neurosci Res.* 1989;6(6):556-68.
90. Room P, Groenewegen HJ. Connections of the parahippocampal cortex in the cat. II. Subcortical afferents. *J Comp Neurol.* 1986;251(4):451-73.
91. Witter MP, Groenewegen HJ. Connections of the parahippocampal cortex in the cat. IV. Subcortical efferents. *J Comp Neurol.* 1986;252(1):51-77.
92. Beckstead RM, Domesick VB, Nauta WJ. Efferent connections of the substantia nigra and ventral tegmental area in the rat. *Brain Res.* 1979;175(2):191-17.
93. Sah P, Faber ES, Lopez De Armentia M, Power J. The amygdaloid complex: anatomy and physiology. *Physiol Rev.* 2003;83(3):803-34.
94. Canteras NS, Swanson LW. Projections of the ventral subiculum to the amygdala, septum, and hypothalamus: a PHAL anterograde tract-tracing study in the rat. *J Comp Neurol.* 1992;324(2):180-94.
95. McDonald AJ, Mascagni F. Projections of the lateral entorhinal cortex to the amygdala: a Phaseolus vulgaris leucoagglutinin study in the rat. *Neuroscience.* 1997;77(2):445-59.
96. Mitrano DA, Pare JF, Smith Y. Ultrastructural relationships between cortical, thalamic, and amygdala glutamatergic inputs and group I metabotropic glutamate receptors in the rat accumbens. *J Comp Neurol.* 2010;518(8):1315-29.
97. Porrino LJ, Crane AM, Goldman-Rakic PS. Direct and indirect pathways from the amygdala to the frontal lobe in rhesus monkeys. *J Comp Neurol.* 1981;198(1):121-36.
98. McDonald AJ. Organization of amygdaloid projections to the prefrontal cortex and associated striatum in the rat. *Neuroscience.* 1991;44(1):1-14.
99. Gabbott PL, Warner TA, Jays PR, Salway P, Busby SJ. Prefrontal cortex in the rat: projections to subcortical autonomic, motor, and limbic centers. *J Comp Neurol.* 2005;492(2):145-77.
100. Ghashghaei HT, Barbas H. Pathways for emotion: interactions of prefrontal and anterior temporal pathways in the amygdala of the rhesus monkey. *Neuroscience.* 2002;115(4):1261-79.
101. Ishikawa A, Nakamura S. Convergence and interaction of hippocampal and amygdalar projections within the prefrontal cortex in the rat. *J Neurosci.* 2003;23(31):9987-95.

102. Vertes RP. Interactions among the medial prefrontal cortex, hippocampus and midline thalamus in emotional and cognitive processing in the rat. *Neuroscience*. 2006;142(1):1-20.
103. Caffé AR, van Leeuwen FW, Luiten PG. Vasopressin cells in the medial amygdala of the rat project to the lateral septum and ventral hippocampus. *J Comp Neurol*. 1987;261(2):237-52.
104. Price JL, Amaral DG. An autoradiographic study of the projections of the central nucleus of the monkey amygdala. *J Neurosci*. 1981;1(11):1242-59.
105. Usunoff KG, Schmitt O, Itzev DE et al. Efferent projections of the anterior and posterodorsal regions of the medial nucleus of the amygdala in the mouse. *Cells Tissues Organs*. 2009;190(5):256-85.
106. Wallace DM, Magnuson DJ, Gray TS. Organization of amygdaloid projections to brainstem dopaminergic, noradrenergic, and adrenergic cell groups in the rat. *Brain Res Bull*. 1992;28(3):447-54.
107. Jia HG, Zhang GY, Wan Q. A GABAergic projection from the central nucleus of the amygdala to the parabrachial nucleus: an ultrastructural study of anterograde tracing in combination with post-embedding immunocytochemistry in the rat. *Neurosci Lett*. 2005;382(1-2):153-7.
108. Petrovich GD, Canteras NS, Swanson LW. Combinatorial amygdalar inputs to hippocampal domains and hypothalamic behavior systems. *Brain Res Brain Res Rev*. 2001;38(1-2):247-89.
109. Rizvi TA, Ennis M, Behbehani MM, Shipley MT. Connections between the central nucleus of the amygdala and the midbrain periaqueductal gray: topography and reciprocity. *J Comp Neurol*. 1991;303(1):121-31.
110. Saha S, Batten TF, Henderson Z. A GABAergic projection from the central nucleus of the amygdala to the nucleus of the solitary tract: a combined anterograde tracing and electron microscopic immunohistochemical study. *Neuroscience*. 2000;99(4):613-26.
111. Dong HW, Swanson LW. Projections from bed nuclei of the stria terminalis, dorsomedial nucleus: implications for cerebral hemisphere integration of neuroendocrine, autonomic, and drinking responses. *J Comp Neurol*. 2006;494(1):75-107.
112. LeDoux JE, Farb CR, Romanski LM. Overlapping projections to the amygdala and striatum from auditory processing areas of the thalamus and cortex. *Neurosci Lett*. 1991;134(1):139-44.
113. Scalia F, Winans SS. The differential projections of the olfactory bulb and accessory olfactory bulb in mammals. *J Comp Neurol*. 1975;161(1):31-55.
114. Yasui Y, Breder CD, Saper CB, Cechetto DF. Autonomic responses and efferent pathways from the insular cortex in the rat. *J Comp Neurol*. 1991;303(3):355-74.
115. McDonald AJ. Cortical pathways to the mammalian amygdala. *Prog Neurobiol*. 1998;55(3):257-332.
116. Doron NN, Ledoux JE. Organization of projections to the lateral amygdala from auditory and visual areas of the thalamus in the rat. *J Comp Neurol*. 1999;412(3):383-409.
117. Turner BH, Herkenham M. Thalamoamygdaloid projections in the rat: a test of the amygdala's role in sensory processing. *J Comp Neurol*. 1991;313(2):295-325.
118. Su HS, Bentivoglio M. Thalamic midline cell populations projecting to the nucleus accumbens, amygdala, and hippocampus in the rat. *J Comp Neurol*. 1990;297(4):582-93.
119. Floresco SB, Zhang Y, Enomoto T. Neural circuits subserving behavioral flexibility and their relevance to schizophrenia. *Behav Brain Res*. 2009;204(2):396-409.
120. Ma J, Brudzynski SM, Leung LW. Involvement of the nucleus accumbens-ventral pallidal pathway in postictal behavior induced by a hippocampal afterdischarge in rats. *Brain Res*. 1996;739(1-2):26-35.
121. Ma J, Leung LS. Schizophrenia-like behavioral changes after partial hippocampal kindling. *Brain Res*. 2004;997(1):111-8.
122. Ma J, Leung LS. Kindled seizure in the prefrontal cortex activated behavioral hyperactivity and increase in accumbens gamma oscillations through the hippocampus. *Behav Brain Res*. 2010;206(1):68-77.
123. Ma J, Leung LW. Medial septum mediates the increase in post-ictal behaviors and hippocampal gamma waves after an electrically induced seizure. *Brain Res*. 1999;833(1):51-7.
124. Cifelli P, Grace AA. Pilocarpine-induced temporal lobe epilepsy in the rat is associated with increased dopamine neuron activity. *Int J Neuropsychopharmacol*. 2011:1-8.
125. Lin TC, Huang LT, Huang YN, Chen GS, Wang JY. Neonatal status epilepticus alters prefrontal-striatal circuitry and enhances methamphetamine-induced behavioral sensitization in adolescence. *Epilepsy Behav*. 2009;14(2):316-23.
126. Olney JW, Newcomer JW, Farber NB. NMDA receptor hypofunction model of schizophrenia. *J Psychiatr Res*. 1999;33(6):523-33.
127. Suzuki Y, Jodo E, Takeuchi S, Niwa S, Kayama Y. Acute administration of phencyclidine induces tonic activation of medial prefrontal cortex neurons in freely moving rats. *Neuroscience*. 2002;114(3):769-79.
128. Stevens JR, Livermore A, Jr. Kindling of the mesolimbic dopamine system: animal model of psychosis. *Neurology*. 1978;28(1):36-46.
129. Ehlers CL, Koob GF. Locomotor behavior following kindling in three different brain sites. *Brain Res*. 1985;326(1):71-9.
130. Watanabe T, Morimoto K, Nakamura M et al. Kindling of the ventral tegmental area induces supersensitivity in the central dopamine system. *Brain Res*. 2004;1003(1-2):194-8.
131. Csernansky JG, Kerr S, Pruthi R, Prosser ES. Mesolimbic dopamine receptor increases two weeks following hippocampal kindling. *Brain Res*. 1988;449(1-2):357-60.
132. Strecker RE, Moneta ME. Electrical stimulation of the kindled hippocampus briefly increases extracellular dopamine in the nucleus accumbens. *Neurosci Lett*. 1994;176(2):173-7.
133. Goto Y, O'Donnell P. Network synchrony in the nucleus accumbens in vivo. *J Neurosci*. 2001;21(12):4498-504.
134. O'Donnell P, Grace AA. Synaptic interactions among excitatory afferents to nucleus accumbens neurons: hippocampal gating of prefrontal cortical input. *J Neurosci*. 1995;15(5 Pt 1):3622-39.
135. Gordon I, Mintz M, Rosenne E, Rehavi M. Long-term effects of amygdaloid kindling on striatal dopaminergic terminals. *Brain Res Bull*. 1995;36(3):235-9.
136. Grace AA. Gating of information flow within the limbic system and the pathophysiology of schizophrenia. *Brain Res Brain Res Rev*. 2000;31(2-3):330-41.
137. Leung LS, Ma J, McLachlan RS. Behaviors induced or disrupted by complex partial seizures. *Neurosci Biobehav Rev*. 2000;24(7):763-75.
138. Dazzi L, Serra M, Porceddu ML, Sanna A, Chessa MF, Biggio G. Enhancement of basal and pentylentetrazol (PTZ)-stimulated dopamine release in the brain of freely moving rats by PTZ-induced kindling. *Synapse*. 1997;26(4):351-8.
139. Meurs A, Clinckers R, Ebinger G, Michotte Y, Smolders I. Seizure activity and changes in hippocampal extracellular glutamate, GABA, dopamine and serotonin. *Epilepsy Res*. 2008;78(1):50-9.
140. Du F, Eid T, Lothman EW, Kohler C, Schwarcz R. Preferential neuronal loss in layer III of the medial entorhinal cortex in rat models of temporal lobe epilepsy. *J Neurosci*. 1995;15(10):6301-13.
141. Du F, Whetsell WO, Jr., Abou-Khalil B, Blumenkopf B, Lothman EW, Schwarcz R. Preferential neuronal loss in layer III of the entorhinal cortex in patients with temporal lobe epilepsy. *Epilepsy Res*. 1993;16(3):223-33.
142. Spencer SS, Spencer DD. Entorhinal-hippocampal interactions in medial temporal lobe epilepsy. *Epilepsia*. 1994;35(4):721-7.

143. Wozny C, Gabriel S, Jandova K, Schulze K, Heinemann U, Behr J. Entorhinal cortex entrains epileptiform activity in CA1 in pilocarpine-treated rats. *Neurobiol Dis.* 2005;19(3):451-60.
144. Suh J, Rivest AJ, Nakashiba T, Tominaga T, Tonegawa S. Entorhinal cortex layer III input to the hippocampus is crucial for temporal association memory. *Science.* 2011;334(6061):1415-20.
145. Mitchell SN, Yee BK, Feldon J, Gray JA, Rawlins JN. Activation of the retrohippocampal region in the rat causes dopamine release in the nucleus accumbens: disruption by fornix section. *Eur J Pharmacol.* 2000;407(1-2):131-38.
146. Lodge DJ, Grace AA. Hippocampal dysregulation of dopamine system function and the pathophysiology of schizophrenia. *Trends Pharmacol Sci.* 2011;32(9):507-13.
147. Manahan-Vaughan D, von Haebler D, Winter C, Juckel G, Heinemann U. A single application of MK801 causes symptoms of acute psychosis, deficits in spatial memory, and impairment of synaptic plasticity in rats. *Hippocampus.* 2008;18(2):125-34.
148. Sharp FR, Tomitaka M, Bernaudin M, Tomitaka S. Psychosis: pathological activation of limbic thalamocortical circuits by psychomimetics and schizophrenia? *Trends Neurosci.* 2001;24(6):330-4.
149. Carlen M, Meletis K, Siegle JH et al. A critical role for NMDA receptors in parvalbumin interneurons for gamma rhythm induction and behavior. *Mol Psychiatry.* 2012;17(5):537-48.
150. Gunduz-Bruce H. The acute effects of NMDA antagonism: from the rodent to the human brain. *Brain Res Rev.* 2009;60(2):279-86.
151. Homayoun H, Moghaddam B. NMDA receptor hypofunction produces opposite effects on prefrontal cortex interneurons and pyramidal neurons. *J Neurosci.* 2007;27(43):11496-500.
152. Jackson ME, Homayoun H, Moghaddam B. NMDA receptor hypofunction produces concomitant firing rate potentiation and burst activity reduction in the prefrontal cortex. *Proc Natl Acad Sci U S A.* 2004;101(22):8467-72.
153. Kiss T, Hoffmann WE, Hajos M. Delta oscillation and short-term plasticity in the rat medial prefrontal cortex: modelling NMDA hypofunction of schizophrenia. *Int J Neuropsychopharmacol.* 2011;14(1):29-42.
154. Abdul-Monim Z, Neill JC, Reynolds GP. Sub-chronic psychotomimetic phencyclidine induces deficits in reversal learning and alterations in parvalbumin-immunoreactive expression in the rat. *J Psychopharmacol.* 2007;21(2):198-205.
155. Feinberg I, Campbell IG, Marrs JC. Intraperitoneal dizocilpine induces cortical spike-wave seizure discharges in rats. *Neurosci Lett.* 1995;196(3):157-60.
156. Olney JW, Labruyere J, Price MT. Pathological changes induced in cerebrocortical neurons by phencyclidine and related drugs. *Science.* 1989;244(4910):1360-2.
157. McNally JM, McCarley RW, McKenna JT, Yanagawa Y, Brown RE. Complex receptor mediation of acute ketamine application on in vitro gamma oscillations in mouse prefrontal cortex: modeling gamma band oscillation abnormalities in schizophrenia. *Neuroscience.* 2011;199:51-63.
158. Javitt DC. Glutamate and schizophrenia: phencyclidine, N-methyl-D-aspartate receptors, and dopamine-glutamate interactions. *Int Rev Neurobiol.* 2007;78:69-108.
159. Verma A, Moghaddam B. NMDA receptor antagonists impair prefrontal cortex function as assessed via spatial delayed alternation performance in rats: modulation by dopamine. *J Neurosci.* 1996;16(1):373-9.
160. Hondo H, Yonezawa Y, Nakahara T, et al. Effect of phencyclidine on dopamine release in the rat prefrontal cortex; an in vivo microdialysis study. *Brain Res.* 1994;633(1-2):337-42.
161. Jodo E, Suzuki Y, Katayama T, et al. Activation of medial prefrontal cortex by phencyclidine is mediated via a hippocampoprefrontal pathway. *Cereb Cortex.* 2005;15(5):663-9.

ANEXO 5

Indução Prévia de LTP na Via CA1-Córtex Pré-Frontal Medial de Ratos Bloqueia os Prejuízos de Plasticidade Pré-Sináptica Induzidos por Modelo de Psicose Pós-Ictal *in vivo**

Lopes-Aguiar C^a, Rossignoli MT^a, Esteves IM^a, Ruggiero RN^a, Bueno Júnior LS^a, Romcy-Pereira RN^b, Leite JP^a

Faculdade de Medicina de Ribeirão Preto – USP

RESUMO

O objetivo do presente trabalho foi testar se a indução de potenciação de longa duração (LTP) no córtex frontal seria capaz de bloquear os efeitos depressores sobre a plasticidade pré-sináptica da via hipocampo (CA1)-córtex pré-frontal medial (mPFC) induzidos por pós-descarga no hipocampo (AD; atividade epiléptica) ou pela injeção sistêmica de cetamina (KET; modelo farmacológico de psicose). Ratos anestesiados com uretana receberam implantes de eletrodos de estimulação e registro, em CA1 e mPFC, respectivamente. Estímulos elétricos monofásicos pareados foram aplicados em CA1 a cada 20s para eliciar potenciais pós-sinápticos de campo (P1 e P2) no mPFC. Avaliamos a plasticidade de curta duração através da facilitação por pulso pareado (PPF), definida pela razão entre as amplitudes de P2 e P1. Após 90min de registros de linha de base, grupos independentes de animais receberam aplicação de AD, injeção de KET-S(+) (12,5 mg/kg i.p.) ou injeção de veículo (NaCl 0,15M), e foram registrados por mais 120min. Em outro experimento registramos 30min de linha de base e aplicamos estímulos de alta frequência (HFS) para indução de LTP aos 30 e 60min. Trinta minutos depois, os animais receberam KET, AD ou veículo e tiveram seus potenciais corticais registrados por mais 120 min. Nossos resultados mostram que AD gera significativa redução (-50%) da eficiência de transmissão basal na via CA1-mPFC, enquanto KET promove leve aumento (+10%). Ambos os tratamentos também promovem prejuízo significativo da PPF na mesma via (-15%). Além disso, observamos que a indução prévia de LTP atenua as alterações da eficiência basal e bloqueia os prejuízos da PPF na via CA1-mPFC induzidos por KET e AD. Nossos achados reforçam evidências recentes de que moduladores alostéricos positivos de NMDA e AMPA atenuam os prejuízos cognitivos em modelos animais de psicose. Acreditamos, portanto, que a aplicação prévia de HFS na região CA1 do hipocampo pode ser uma ferramenta útil para melhor entendermos como prevenir os prejuízos de plasticidade sináptica no mPFC em modelos de psicose e psicose pós-ictal.

Unitermos: psicose pós-ictal, plasticidade sináptica, via CA1-córtex pré-frontal medial, potenciação de longa duração, pós-descarga, cetamina.

ABSTRACT

Prevention of the CA1-mPFC pre-synaptic plasticity impairments in a post-ictal psychosis model 'in vivo'

The present work aimed to test whether the induction of cortical long-term potentiation (LTP) was able to prevent the presynaptic plasticity impairment in the hippocampus (CA1)-medial prefrontal cortex (mPFC) pathway induced by hippocampal after-discharge (AD; epileptic activity) or systemic injection of ketamine (KET; pharmacological model of psychosis). Electrodes were stereotaxically positioned into CA1 and mPFC in urethane-anesthetized rats. Monophasic paired-pulses of electrical stimuli were applied to CA1 in order to evoke field post-synaptic potentials (P1 and P2) in the mPFC every 20s. Short-term plasticity was evaluated by measuring paired-pulse facilitation (PPF), defined as the amplitude ratio P2/P1. After 90min of baseline

*Trabalho vencedor do Prêmio Aristides Leão – XXXIV Congresso Brasileiro de Epilepsia, 06-09 de junho de 2012, Ribeirão Preto, SP.

^a Departamento de Neurociências e Ciências do Comportamento – Faculdade de Medicina de Ribeirão Preto – USP, Ribeirão Preto, SP.

^b Instituto do Cérebro, Universidade Federal do Rio Grande do Norte – UFRN, Natal-RN.

Received Apr. 28, 2012; accepted Apr. 30, 2012.

recordings, three independent groups of animals received hippocampal-AD, KET-S(+) (12.5mg/kg, i.p.) or vehicle (NaCl 0.15M) followed by 120min of evoked response monitoring. In an additional experiment, two applications of high-frequency stimuli (HFS) were given at 30 and 60min after baseline. Thirty minutes after the second HFS, the rats received KET, AD or vehicle and their cortical evoked potentials were monitored for further 120min. Our results showed that AD significantly decreased (-50%) whereas KET enhanced (+10%) CA1-mPFC basal synaptic transmission. In addition, AD and KET similarly impaired short-term plasticity in the mPFC (-15%). Interestingly, pre-induction of LTP in the mPFC prevented the PPF disruption induced by KET and AD. Altogether, our findings support recent evidences that positive allosteric modulators of NMDA and AMPA receptors attenuate cognitive impairments in animal models of psychosis. We believe that controlled HFS in CA1 can be a useful tool to better understand how to prevent synaptic plasticity disruptions observed in experimental models of psychosis and pos-ictal psychosis.

Keywords: post-ictal psychosis, synaptic plasticity, CA1-medial prefrontal cortex pathway, long-term potentiation, afterdischarge, ketamine.

INTRODUÇÃO

Vários estudos têm mostrado que a incidência de psicose – perturbação que envolve o início súbito de delírios, alucinações, discurso desorganizado ou comportamento amplamente desorganizado ou catatônico – chega a ser três vezes maior em pacientes com epilepsia do lobo temporal (ELT) do que em casos de epilepsia generalizada^{1,2}. Entretanto, os mecanismos neurais responsáveis pela ocorrência e fenomenologia dos episódios psicóticos em pacientes com epilepsia ainda são pouco compreendidos.

A relação entre psicose e epilepsia tem sido investigada experimentalmente por meio, principalmente, de (1) protocolos de avaliação comportamental em modelos animais de epilepsia (genéticos ou induzidos)^{3,4,5} e de abramento límbico (*kindling* do hipocampo e amígdala)^{6,7,8}; (2) protocolos de evocação de pós-descargas (AD) no hipocampo⁹; e (3) tratamentos agudos ou crônicos com antagonistas não competitivos do receptor de glutamato do tipo N-metil-D-aspartato (NMDA)¹⁰.

O modelo de AD única no hipocampo é considerado uma importante ferramenta, pois induz hiperlocomoção e movimentos estereotipados, logo que a atividade epileptiforme cessa, reproduzindo alguns aspectos característicos de um episódio psicótico pós-ictal¹¹. Além disso, o prejuízo nas funções do filtro sensorio-motor gerado por indução de AD apresenta-se associado a aumento de oscilações gama (30-100Hz) no hipocampo e córtex pré-frontal medial (mPFC), como observado no modelo de psicose induzido por cetamina (KET)¹¹.

Os modelos de psicose gerados pela administração de antagonistas glutamatérgicos como a fenciclidina (PCP), KET ou a dizocilpina (MK-801) são baseados na hipótese de hipofunção glutamatérgica da esquizofrenia¹⁰. Recentemente foi demonstrado que a administração sistêmica de MK-801, além de potencializar oscilações

gama¹², também é capaz de alterar o perfil espectral dentro da faixa de oscilações lentas (0,5-2Hz) no córtex pré-frontal e reduzir a plasticidade sináptica de curta duração na via CA1-mPFC *in vivo*¹³. É interessante notar que ambos os efeitos foram imediatamente revertidos após administração de AMPA, um modulador alostérico positivo de receptores AMPA. Ainda em suporte à hipótese glutamatérgica, estudos pré-clínicos com roedores têm mostrado que a inibição de transportadores de glicina (um co-agonista do receptor NMDA) é capaz de (1) reverter a hiperlocomoção e o excesso de liberação dopaminérgica, induzidos por PCP¹⁴, (2) potencializar a atividade do mPFC *in vivo*¹⁵ e (3) reverter os prejuízos de memória de trabalho induzidos por KET¹⁶. Uma série de inibidores de alta afinidade para o transportador de glicina têm sido desenvolvidos e também testados, com sucesso, em modelos experimentais de psicose¹⁴, em pacientes com esquizofrenia¹⁷ e em sujeitos sadios submetidos a administração de KET¹⁸. Consistente com esses achados, alguns estudos sugerem que a clozapina, um antipsicótico atípico, funciona pelo menos em parte como um agonista do sítio de glicina presente nos receptores NMDA¹⁴. Portanto, considerando as evidências sobre o envolvimento da neurotransmissão glutamatérgica nas alterações eletrofisiológicas e comportamentais em modelos experimentais de psicose, nosso objetivo foi testar a hipótese de que a potencialização sináptica de longa duração (LTP) cortical é capaz de bloquear os efeitos depressores da injeção sistêmica de KET ou da aplicação de AD hipocampal, sobre a plasticidade pré-sináptica na via hipocampo (CA1)-mPFC *in vivo*.

MÉTODOS

Ratos Wistar adultos machos foram anestesiados com uretana (1,3g/kg, i.p.) para implantação estereotáxica de eletrodos em CA1 e mPFC segundo coordenadas anatômicas de referência¹⁹. No total, três eletrodos foram implantados:

(1) eletrodo monopolar de registro no mPFC; (2) eletrodo bipolar de estímulo na região CA1 do hipocampo posterior dorsal (com desnível entre as pontas de 0,5 mm) e (3) eletrodo monopolar de registro em CA1, localizado 1,5mm anterior ao eletrodo de estímulo. Estímulos monofásicos pareados (0,2ms de duração; intervalo inter-estímulos de 80ms) aplicados em CA1, a cada 20s, foram capazes de eliciar potenciais pós-sinápticos de campo denominados P1 e P2 no mPFC. A facilitação por pulso pareado (PPF) foi definida pela razão entre as amplitudes de P2 e P1, e foi estudada antes e depois da administração de AD-hipocampal, KET-S(+) (12,5 mg/kg i.p.) ou veículo (NaCl 0,15M i.p.).

Em resumo, após 90min de registro de linha de base, três grupos independentes de animais receberam AD-hipocampal, KET-S(+) ou veículo e tiveram seus potenciais monitorados por mais 120min. Para testar os efeitos da LTP sobre a PPF, três novos grupos de animais foram registrados por 30min de linha de base e, em seguida, receberam duas sessões de estímulos em alta frequência (HFS) aos 30 e 60min. Trinta minutos depois, cada grupo recebeu como tratamento AD, KET-S(+) ou veículo e tiveram seus potenciais corticais registrados por mais 120min. A indução de AD-hipocampal foi realizada por um único trem de estímulos em CA1 constituído por 200 pulsos a 20Hz (pulsos monofásicos; 1ms de duração) com duração total de 10 segundos¹¹. A indução de LTP foi realizada por meio da aplicação de HFS, aos 30 e 60min de registro. Cada HFS consistiu de duas séries de 10 trens (50 pulsos a 250Hz; 0,2ms de duração; a cada 10s), separados por 10min²⁰. A corrente de estimulação utilizada em todos os experimentos foi em intensidade capaz de gerar o maior PPF nessa via determinada a partir da curva de calibração¹⁴. Para analisar os potenciais evocados no mPFC consideramos amplitude de P1 e P2 medidas como a distância entre o ponto máximo do primeiro pico positivo e o ponto mínimo do primeiro pico negativo com latência de 16 a 20 ms. Esses valores foram normalizados com relação à linha de base, definida como 100%. Todas as variáveis analisadas apresentaram

distribuição normal e, por isso, utilizamos o teste estatístico ANOVA de duas vias com medidas repetidas, seguido do teste *post hoc* de Tukey.

RESULTADOS

A Tabela 1 sintetiza os principais efeitos de KET e AD sobre a transmissão e plasticidade pré-sináptica na via CA1-mPFC *in vivo*. Nossos resultados indicam que a injeção sistêmica de KET aumentou significativamente a amplitude do P1 em dois momentos específicos do experimento, de 120 a 130min e 170 a 190min [Interação tratamento-tempo: +10%, Sham-KET vs. Sham-SAL: $F(20, 260)=1,88, p<0,05$; ANOVA de duas vias medidas repetidas e teste *post hoc* de Tukey, $p<0,05$] sem afetar de maneira significativa o P2 da via CA1-mPFC *in vivo* ($p>0,05$). Em contrapartida, a indução de AD gera uma queda robusta de ambos, P1 [Tratamento: -50%; Sham-AD vs. Sham-Sham: $F(1, 12)=61,95, p<0,001$, ANOVA de duas vias medidas repetidas] e P2 [Tratamento: -60%; $F(1, 12)=95,88, p<0,001$] na mesma via. Além de robusto, esse efeito mostrou ser sustentado, mantendo a queda inicial dos potenciais de 50 a 60% por, no mínimo, 2 horas em relação ao grupo controle (teste *post hoc* de Tukey para P1 e P2; $p<0,05$). Embora KET e AD tenham efeitos bastante distintos sobre a eficiência basal da via CA1-mPFC, ambos geram prejuízo sobre sua plasticidade pré-sináptica, medida por PPF [Tratamento: -15%; Sham-KET vs. Sham-SAL: $F(1, 13)=39,34, p<0,001$ e -13%; Sham-AD vs. Sham-Sham: PPF, $F(1, 12)=6,31, p<0,05$, ANOVA de duas vias para medidas repetidas]. A Tabela 2 mostra as principais comparações referentes ao segundo estudo realizado para testar a hipótese de que a LTP seria capaz de bloquear os prejuízos de AD e KET. Observa-se que a indução prévia de LTP previne a queda dos PPF gerada por KET e AD. Ao contrário do experimento anterior, nenhuma diferença foi observada entre os grupos tratados com LTP+KET, AD ou SAL [Tratamento: $F(2, 20)=0,089; p=0,9$; ANOVA de duas vias para medidas repetidas].

Tabela 1. Efeitos de KET e AD sobre a eficiência basal e plasticidade pré-sináptica da via CA1-mPFC. P1: amplitude do primeiro potencial evocado no mPFC após estimulação de CA1. P2: amplitude do segundo potencial evocado. PPF: razão entre as amplitudes de P2 e P1.

Comparação	ANOVA		Parâmetros	Variação
	duas vias medidas repetidas			
Sham-KET vs. Sham-SAL	$F(20, 260)=1,88; p<0,05$		P1	10%
Sham-KET vs. Sham-SAL	n.s.		P2	n.s.
Sham-KET vs. Sham-SAL	$F(1, 13)=39,34; p<0,001$		PPF	-15%
Sham-AD vs. Sham-Sham	$F(1, 12)=61,95; p<0,001$		P1	-50%
Sham-AD vs. Sham-Sham	$F(1, 12)=95,88; p<0,001$		P2	-60%
Sham-AD vs. Sham-Sham	$F(1, 12)=6,31; p<0,05$		PPF	-13%

Tabela 2. Efeitos indução prévia de LTP sobre os efeitos depressores de plasticidade pré-sináptica induzidos por KET e AD.

Comparação	ANOVA duas vias medidas repetidas	Parâmetros	Varição
LTP-KET vs. LTP-SAL	n.s.	P1	n.s.
LTP-KET vs. LTP-SAL	n.s.	P2	n.s.
LTP-KET vs. LTP-SAL	n.s.	PPF	n.s.
LTP-AD vs. LTP-SAL	n.s.	P1	n.s.
LTP-AD vs. LTP-SAL	n.s.	P2	n.s.
LTP-AD vs. LTP-SAL	n.s.	PPF	n.s.

CONCLUSÕES

A depressão sináptica observada na via CA1-mPFC gerada por AD pode ser considerada uma nova forma de depressão de longa duração (LTD), neste caso induzida por um evento tipo-ictal, particularmente por ter se mostrado robusta (~50%) e sustentada (duração de 120min). Esta atenuação da resposta do córtex pré-frontal subsequente à atividade epileptiforme hipocampal pode ser responsável por falhas no processamento sináptico límbico-cortical pós-ictal e contribuir para alterações comportamentais observadas neste período. Além disso, os efeitos provenientes de uma única AD são importantes para o entendimento de como crises espontâneas isoladas, da ordem de segundos, podem afetar a comunicação entre áreas de controle executivo interligadas ao foco epiléptico. Por outro lado, o fato da KET e da AD promoverem reduções semelhantes na plasticidade pré-sináptica, mesmo com efeitos distintos nos potenciais evocados basais, sugere que esses tratamentos possam ter atuado diferencialmente nos terminais pré e pós-sinápticos, alterando tanto a eficiência sináptica quanto a excitabilidade local da rede. Por fim, os efeitos da LTP sobre a queda do PPF induzido por KET e AD, estão de acordo com evidências recentes mostrando que a ativação de NMDA e AMPA revertem prejuízos cognitivos em modelos animais de psicose. Consideramos, portanto, que a indução prévia de LTP possa ser uma ferramenta útil para melhor investigarmos como prevenir os prejuízos de plasticidade sináptica no mPFC em modelos de psicose e psicose pós-ictal.

Agradecimentos: Os autores agradecem a Sra. Renata Scandiuzzi e o Sr. Renato Meirelles, pelo excelente suporte técnico, aos colegas de laboratório, Ana Clara Broggin, Ludmyla Kandravicius, Raquel do Val da Silva e José Peixoto, pelas valiosas discussões, e às agências financiadoras FAPESP/CInAPCe; FAPESP; CAPES; CNPq e FAEPa pelo apoio financeiro.

REFERÊNCIAS

- Gaitatzis A, Carroll K, Majeed A, W Sander J. The epidemiology of the comorbidity of epilepsy in the general population. *Epilepsia*. 2004;45(12):1613-22.
- Tellez-Zenteno JF, Patten SB, Jetté N, Williams J, Wiebe S. Psychiatric comorbidity in epilepsy: a population-based analysis. *Epilepsia*. 2007;48(12):2336-44.
- Gorji A, Scheller D, Speckmann EJ. The lateral spread of epileptiform discharges in rat neocortical slices: effect of focal phencyclidine application. *Pharmacopsychiatry*. 2003; 36(3):113-20
- Jones NC, Martin S, Megatia I, Hakami T, Salzberg MR, Pinault D, Morris MJ, O'Brien TJ, van den Buuse M. A genetic epilepsy rat model displays endophenotypes of psychosis. *Neurobiol Dis*. 2010;39(1):116-25.
- Cifelli P, Grace AA. Pilocarpine-induced temporal lobe epilepsy in the rat is associated with increased dopamine neuron activity. *Int J Neuropsychopharmacol*. 2012;15(7):957-64.
- Smith PF, Darlington CL. The development of psychosis in epilepsy: a re-examination of the kindling hypothesis. *Behav Brain Res*. 1996;75(1-2):59-66.
- Howland JG, Hannesson DK, Barnes SJ, Phillips AG. Kindling of basolateral amygdala but not ventral hippocampus or perirhinal cortex disrupts sensorimotor gating in rats. *Behav Brain Res*. 2007;177(1):30-6.
- Koch M, Ebert U. Deficient sensorimotor gating following seizures in amygdala-kindled rats. *Biol Psychiatry*. 1998;44(4):290-7.
- McCracken CB, Roberts DCS. A single evoked afterdischarge produces rapid time-dependent changes in connexin36 protein expression in adult rat dorsal hippocampus. *Neurosci. Lett*. 2006; 405(1-2):84-8.
- Corlett PR, Honey GD, Krystal JH, Fletcher PC. Glutamatergic model psychoses: prediction error, learning, and inference. *Neuropsychopharmacology*. 2011;36(1):294-315.
- Ma J, Leung LS. Schizophrenia-like behavioral changes after partial hippocampal kindling. *Brain Res*. 2004;997(1):111-8.
- Carlén M, Meletis K, Siegle JH, Cardin JA, Futai K, Vierling-Claassen D, Rühlmann C, Jones SR, Deisseroth K, Sheng M, Moore CI, Tsai LH. A critical role for NMDA receptors in parvalbumin interneurons for gamma rhythm induction and behavior. *Mol Psychiatry*. 2012;17(5):537-48
- Kiss T, Hoffmann WE, Hajós M. Delta oscillation and short-term plasticity in the rat medial prefrontal cortex: modelling NMDA hypofunction of schizophrenia. *Int J Neuropsychopharmacol*. 2011;14(1):29-42.
- Moghaddam B, Javitt D. From revolution to evolution: the glutamate hypothesis of schizophrenia and its implication for treatment. *Neuropsychopharmacology*. 2012;37(1):4-15.

15. Chen L, Muhlhauser M, Yang CR. Glycine transporter-1 blockade potentiates NMDA-mediated responses in rat prefrontal cortical neurons *in vitro* and *in vivo*. *J Neurophysiol*. 2003;89(2):691-703.
16. Roberts BM, Shaffer CL, Seymour PA, Schmidt CJ, Williams GV, Castner SA. Glycine transporter inhibition reverses ketamine induced working memory deficits. *Neuroreport*. 2010;21(5):390-4.
17. Alberati D, Moreau J-L, Lengyel J, Hauser N, Mory R, Borroni E, et al. Glycine reuptake inhibitor RG1678: a pharmacologic characterization of an investigational agent for the treatment of schizophrenia. *Neuropharmacology*. 2012;62(2):1152-61.
18. D'Souza DC, Singh N, Elander J, Carbutto M, Pittman B, de Haes JU, et al. Glycine transporter inhibitor attenuates the psychotomimetic effects of ketamine in healthy males: preliminary evidence. *Neuropsychopharmacology*. 2012;37(4):1036-46.
19. Paxinos G, Watson C. *The Rat Brain in Stereotaxic Coordinates*, Sixth Edition: Hard Cover Edition. 6th ed. Academic Press; 2007.
20. Lopes Aguiar C, Romcy-Pereira RN, Escorsim Szawka R, Galvis-Alonso OY, Anselmo-Franci JA, Pereira Leite J. Muscarinic acetylcholine neurotransmission enhances the late-phase of long-term potentiation in the hippocampal-prefrontal cortex pathway of rats *in vivo*: a possible involvement of monoaminergic systems. *Neuroscience*. 2008;153(4):1309-19.

Endereço para correspondência:

Rodrigo Romcy-Pereira
Instituto do Cérebro, Universidade Federal do Rio Grande do Norte (UFRN)
CEP 59056-450, Natal, RN, Brasil
Tel.: (+55-84) 3852-1551
E-mail: <mrpereira@gmail.com>, <mrpereira@neuro.ufrn.br>.

ANEXO 6

Muscarinic and Nicotinic Modulation of Thalamo-Prefrontal Cortex Synaptic Plasticity *In Vivo*

Lezio Soares Bueno-Junior¹, Cleiton Lopes-Aguiar¹, Rafael Naime Ruggiero¹, Rodrigo Neves Romcy-Pereira^{1,2*}, João Pereira Leite¹

¹ Department of Neuroscience and Behavioral Sciences, Ribeirão Preto School of Medicine, University of São Paulo, Ribeirão Preto, São Paulo, Brazil, ² Brain Institute, Federal University of Rio Grande do Norte, Natal, Rio Grande do Norte, Brazil

Abstract

The mediodorsal nucleus of the thalamus (MD) is a rich source of afferents to the medial prefrontal cortex (mPFC). Dysfunctions in the thalamo-prefrontal connections can impair networks implicated in working memory, some of which are affected in Alzheimer disease and schizophrenia. Considering the importance of the cholinergic system to cortical functioning, our study aimed to investigate the effects of global cholinergic activation of the brain on MD-mPFC synaptic plasticity by measuring the dynamics of long-term potentiation (LTP) and depression (LTD) *in vivo*. Therefore, rats received intraventricular injections either of the muscarinic agonist pilocarpine (PILO; 40 nmol/ μ L), the nicotinic agonist nicotine (NIC; 320 nmol/ μ L), or vehicle. The injections were administered prior to either thalamic high-frequency (HFS) or low-frequency stimulation (LFS). Test pulses were applied to MD for 30 min during baseline and 240 min after HFS or LFS, while field postsynaptic potentials were recorded in the mPFC. The transient oscillatory effects of PILO and NIC were monitored through recording of thalamic and cortical local field potentials. Our results show that HFS did not affect mPFC responses in vehicle-injected rats, but induced a delayed-onset LTP with distinct effects when applied following PILO or NIC. Conversely, LFS induced a stable LTD in control subjects, but was unable to induce LTD when applied after PILO or NIC. Taken together, our findings show distinct modulatory effects of each cholinergic brain activation on MD-mPFC plasticity following HFS and LFS. The LTP-inducing action and long-lasting suppression of cortical LTD induced by PILO and NIC might implicate differential modulation of thalamo-prefrontal functions under low and high input drive.

Citation: Bueno-Junior LS, Lopes-Aguiar C, Ruggiero RN, Romcy-Pereira RN, Leite JP (2012) Muscarinic and Nicotinic Modulation of Thalamo-Prefrontal Cortex Synaptic Plasticity *In Vivo*. PLoS ONE 7(10): e47484. doi:10.1371/journal.pone.0047484

Editor: Michelle L. Block, Virginia Commonwealth University, United States of America

Received: May 9, 2012; **Accepted:** September 11, 2012; **Published:** October 30, 2012

Copyright: © 2012 Bueno-Junior et al. This is an open-access article distributed under the terms of the Creative Commons Attribution License, which permits unrestricted use, distribution, and reproduction in any medium, provided the original author and source are credited.

Funding: This work was supported by grants from FAPESP (#2008/57413-7), FAPESP-CinAPCe (#2005/56447-7) and CNPq (#502726/2009-1). Respectively, these are the funder's websites: <http://www.fapesp.br/en/>, <http://www.fcm.unicamp.br/cinapce/>, <http://www.cnpq.br/english/cnpq/index.htm>. The funders had no role in study design, data collection and analysis, decision to publish, or preparation of the manuscript.

Competing Interests: The authors have declared that no competing interests exist.

* E-mail: rnrpereira@neuro.ufrn.br

Introduction

In the prefrontal cortex (PFC), the rescaling of synaptic weights mediated by long-term potentiation (LTP) and long-term depression (LTD) is thought to play an important role in working memory, decision-making, behavioral inhibition and attention shifting [1–3]. Much of the LTP/LTD dynamics in the PFC takes place at afferent terminals from subcortical structures, including the basolateral amygdala, ventral tegmental area, CA1 of the hippocampus, and medial thalamic nuclei [4]. In particular, the mediodorsal thalamic nucleus (MD) is one of the most prominent sources of excitatory projections to the PFC, both in primates and rodents [5–10].

Several studies, ranging from functional imaging of the human brain to behavioral tests in animal models, have demonstrated the involvement of MD-PFC reciprocal projections in cognitive functions [11–16] and in pathological conditions, especially schizophrenia [17–20]. Electrophysiological studies in rodents have also shown that changes in PFC responses mediated by MD stimulation are involved in the modulation of hippocampus-evoked activity in the PFC [21], fear extinction [22,23], and propagation of limbic seizures [24–27].

The MD-PFC circuit can be influenced by ascending cholinergic projections from the brainstem and basal forebrain [28–30], which represent important modulators of cognitive processes [31–34] and oscillatory activity throughout the sleep-wake cycle [35–37]. Unbalanced cholinergic neurotransmission is associated with cognitive decline, schizophrenia, Alzheimer's disease, and temporal lobe epilepsy [38–43]. In addition, several studies have shown that cholinergic activation regulates synaptic plasticity in adult thalamocortical loops comprising sensorial areas of the cortex [44–48]. However, the cholinergic modulation of thalamus-induced plasticity in associative cortical areas is still poorly understood. In one of the few studies *in vivo* [49], it was shown that nicotinic agonists into the medial prefrontal cortex of rats (mPFC, pre-limbic area) facilitated MD-evoked spikes and increased glutamate levels in the mPFC. However, the authors did not evaluate long-term synaptic plasticity in the MD-mPFC pathway. Synaptic plasticity in this pathway was also shown to occur associated with fear learning in mice in the absence of any pharmacological treatment [22,23].

Recently, we have shown that muscarinic activation of the brain, by an M1 preferential agonist, enhances the hippocampal-mPFC plasticity in two different ways. It specifically potentiates the

late-phase LTP induced by high frequency stimulation [50], and promotes a long-lasting LTD in the mPFC induced by trains of low frequency stimulation [51]. Therefore, considering (1) that CA1 and MD project and influence a common set of neurons in the mPFC [52,53], suggesting a possible substrate for the local interaction between hippocampal inputs and thalamocortical activity; and (2) that these projections can be modulated during general states of cholinergic activation achieved by the administration of muscarinic and nicotinic agonists, we decided to further investigate the muscarinic and nicotinic effects on LTP and LTD in the MD-mPFC circuit *in vivo*.

Materials and Methods

2.1. Subjects

A total of 71 adult male Wistar rats (250–450 g) were housed in standard rodent cages in a colony room maintained at 24°C under a 12 h light/12 h dark cycle with free access to food and water. All procedures were performed according to the Brazilian Council for Animal Experimentation (CONCEA) guidelines and approved by the Ethics Committee of the Ribeirão Preto School of Medicine (protocol number 125/2008). These guidelines abide by the National Institutes of Health rules for the care and use of laboratory animals (NIH Publications No. 8023, revised 1978). Experiments were designed to minimize the number of animals used and their suffering.

2.2. Surgery and electrophysiology

Rats were anesthetized with urethane (1.2–1.5 mg/kg, *i.p.*, in NaCl 0.15 M; Sigma-Aldrich, USA) and placed in a stereotaxic frame (David Kopf Instruments, USA), and their body temperature was maintained at $37 \pm 0.5^\circ\text{C}$ by using a heating pad (Insight Ltda, Brazil). When necessary, the level of anesthesia was maintained with supplementary injections of the anesthetic (10% of the initial dose) after checking the tail pinch reflex. For electrode and cannula implantation, the skull was exposed and small holes were drilled to allow access to the left hemisphere prelimbic area (PrL₁) of the mPFC (antero-posterior, AP: +3.0 mm; lateral to midline, L: -0.4 mm; ventral to dura mater, V: -3.2 mm), left hemisphere MD (AP: -1.9 mm, L: -0.4 mm, V: -4.8 mm) and right hemisphere lateral ventricle (LV; AP: -0.5 mm, L: +1.3 mm, V: -2.5 mm) according to the rat brain atlas [54]. An additional hole was drilled over the parietal cortex in the right hemisphere to implant a micro-screw used as recording reference. Thereafter, a 23-gauge stainless-steel cannula was inserted into the brain and positioned 1 mm above the LV. The cannula was fixed to the skull with dental acrylic resin.

Teflon-insulated tungsten wires (60 μm diameter) were used to prepare stimulating and recording electrodes. A twisted bipolar electrode (vertical tip separation: 500 μm) was used for constant current stimulation of the MD and a monopolar electrode was used to record field post-synaptic potentials (fPSPs) in the mPFC. Both electrodes were lowered into the brain through the holes drilled on the skull, after removing the dura mater. Monophasic test pulses (200 μs duration, 150–200 μA ; S88 Stimulator, Grass Technologies, USA) were delivered through the bipolar electrode every 20 s, and the final position of the electrodes was adjusted to obtain the highest negative-going fPSP in the mPFC (amplitude $\geq 150 \mu\text{V}$). fPSPs were amplified and filtered ($\times 100$, 0.01–1 KHz; P55-AC Pre-amplifier, Grass Technologies, USA) before digitization at 10 KHz (PowerLab/16S; ADInstruments, Australia). For some animals, it was necessary to invert the polarity of the stimulation prior to the beginning of the experiments in order to increase the regularity of the fPSP. Although polarity influenced

direction of stimulus artifact, it did not affect the latencies of fPSP negative peaks. Once the electrodes were positioned and the stimulation polarity was defined, electrical pulses were delivered every 20 s at increasing intensities (60–500 μA) and the fPSP amplitudes were used to calculate input-output curves for each animal. Based on the input-output curves, we obtained the intensity necessary to produce maximum fPSP amplitudes and used 60–70% of such intensity to stimulate the MD during baseline, LTP or LTD induction and post-LTP or LTD recordings.

Baseline fPSPs were recorded for 30 min with single electrical pulses (200 μs duration; every 20 s). Then, the drugs were microinjected through a 30-gauge needle inserted into the cannula and connected to a 10 μL microsyringe (Hamilton Company, USA) via a polyethylene tube. After microinjection, LTP or LTD was induced by delivery of high-frequency (HFS) or low-frequency (LFS) trains of stimuli into the MD, respectively. Post-HFS/LFS recordings of fPSPs resumed for an additional 240 min to monitor the dynamics of mPFC responses. The HFS protocol consisted of two series (10 min apart) of 10 trains of 50 pulses (250 Hz). These trains were delivered every 10 s [23,50,55]. LFS consisted of a single train of 1200 pulses (2 Hz) [23].

2.3. Cholinergic drugs

We used the following drugs: (1) pilocarpine hydrochloride (PILO, Sigma-Aldrich, USA), a non-selective muscarinic agonist with high affinity for M1-like receptors [56,57]; and (2) (-)-nicotine hydrogen tartrate (NIC, Sigma-Aldrich, USA), an agonist with high affinity for neural nicotinic receptors, especially $\alpha 7$ and $\alpha 4\beta 2$ subtypes [58,59]. Artificial cerebrospinal fluid (aCSF; in mM: 2.7 KCl, 1.2 CaCl₂, 1.0 MgCl₂, and 135.0 NaCl, with pH 7.3 at room temperature) was used to dissolve both PILO (40 nmol/ μL) and NIC (320 nmol/ μL) salts. The concentrations of PILO and NIC were chosen based on a pilot experiment that measured the duration of the oscillatory changes induced in the mPFC and MD, and did not produce alteration of the physiological parameters of the animals, such as heart rate and salivation. aCSF without PILO or NIC was used as the control vehicle. The injections of PILO, NIC, or aCSF were delivered by intracerebroventricular route (*i.c.v.*) in a volume of 1 μL over a two-minute period.

2.4. Experimental design

To investigate the cholinergic modulation of MD-evoked synaptic plasticity in the mPFC, three experiments were carried out. Experiment I tested the effects of cholinergic modulation on the induction and maintenance of LTP. For that, animals received PILO, NIC, or aCSF immediately before HFS and were divided into three groups: PILO-HFS, NIC-HFS, and aCSF-HFS, respectively. Experiment II tested the effects of cholinergic modulation on the induction and maintenance of LTD. Animals received PILO, NIC, or aCSF just before LFS and were also divided into three groups: PILO-LFS, NIC-LFS, and aCSF-LFS, respectively. Experiment III assessed the effects of PILO, NIC, or aCSF on basal mPFC responses induced by MD stimulation. Animals received PILO, NIC, or aCSF, but did not receive train stimulation and were grouped as PILO-Ctrl, NIC-Ctrl, and aCSF-Ctrl. Synaptic plasticity was analyzed by quantifying the average fPSP amplitude normalized to the baseline at different time points after synaptic plasticity induction. For that, fPSP amplitudes were averaged every 10 min and normalized as percentage of the baseline mean amplitude.

2.5. Local field potential analysis

To monitor the state of brain activity associated to the muscarinic (PILO) and nicotinic (NIC) modulation, we recorded local field potentials (LFP) simultaneously in the MD and mPFC through the same electrodes used to induce and record LTP or LTD. Thalamic and neocortical LFPs were recorded during a 6 min period divided into 2 min blocks: before, during and after i.c.v. microinjection. After down sampling to 200 Hz and low-pass filtering (0.5–100 Hz), Welch's power spectral densities (Hanning window) were calculated every 10 s epochs. Spectral densities were estimated for each epoch after averaging periodograms calculated from eight sections with 50% overlap. Delta (0.5–4 Hz), theta (4–12 Hz), beta (12–30 Hz) and gamma (30–80 Hz, removing 58–62 Hz noise) normalized powers were calculated using custom-made MATLAB scripts (The MathWorks, Natick, MA). Normalized band powers were compared to evaluate the effects of PILO and NIC on the oscillatory activity recorded in the MD and mPFC.

2.6. Histology

After each recording session, a current pulse (1 mA, 1 s) was delivered through the stimulation and recording electrodes to produce a small electrolytic lesion for electrode localization. The animals received an additional injection of the anesthetic and had their brains removed after decapitation. The brains were post-fixed in 10% formaldehyde-saline solution for 14 h at 4°C and cryoprotected for 48 h in 20% sucrose solution (in 0.1 M sodium phosphate buffer, pH 7.4). After rapid freezing in dry ice-chilled isopentane, 30 μ m-thick slices were cut in a cryostat, mounted on gelatinized slides and stained with cresyl violet. Electrode tip positions and cannula tracts were determined after analysis of brain sections under the optic microscope (AxioPhot, Carl Zeiss Inc.).

2.7. Statistical analysis

Analysis of group differences following HFS or LFS was carried out by two-way ANOVA with repeated measures (group: fixed factor vs. time: repeated measures). The same ANOVA was used to test power spectrum differences in the mPFC and MD along the 6 min recording of LFPs. The Newman-Keuls *post hoc* test was applied following ANOVAs when necessary. All results are expressed as the mean \pm SEM and significance level was set to 0.05.

Results

3.1. Accuracy of implants

All animals included in our analysis had the stimulation electrode tips positioned within the MD, most often in its anterior and medial aspects, which contain the highest density of mPFC-projecting cells according to retrograde tracing [60]. Recording electrode tips were most frequently observed in the medial wall of the ipsilateral mPFC, at the level of PrL. Cannulae placement was observed approximately 1 mm above the LV, so that only the microinjection needle reached the LV (Figure 1).

3.2. Characteristics of mPFC responses evoked by MD stimulation

In all experiments, we first positioned the recording electrode at the PrL area of the mPFC based on stereotaxic coordinates [54] and then, lowered the stimulation electrode in 200 μ m steps while applying pulses each 20 s (electrical parameters described in the methods section). No fPSP was found until the stimulation

electrode reached 3.0 mm below the dura mater (presumably at the corpus callosum level), from where we consistently elicited fPSPs with a negative peak at latency of \sim 9 ms (Figure 1). As the stimulation electrode crossed the hippocampus on its way towards the MD, the same profile of fPSP was repeatedly elicited until approximately 4.2–4.4 mm below the dura mater, when we observed a shift of the negative peak from a latency of \sim 9 to \sim 13 ms. From that point on, we continued to lower the electrode until 4.8–5.2 mm below dura mater (at the MD level), when we obtained the strongest and most reliable negative-going fPSP and concluded the implantation. The prefrontal fPSPs obtained by stimulation throughout the hippocampus may occur due to the activation of passing fibers, since retrograde tracing data from the literature do not show hippocampal cells projecting to the mPFC at the anteroposterior level where our stimulation electrodes were implanted [59]. Nevertheless, fPSPs elicited during the trajectory of the stimulating electrode were useful as references for the refinement of the dorso-ventral implant position.

In approximately half of the subjects, the MD-evoked fPSPs showed two distinct negative peaks, which we termed N1 and N2 (Figure 1). When clearly detected, N1 was a low-amplitude ($108.20 \pm 9.32 \mu$ V) short-latency (6.85 ± 0.15 ms) negative peak, but in some cases it was too subtle to be defined. Differently, N2 was a negative peak characterized by high amplitude ($270.00 \pm 17.10 \mu$ V) and long latency (13.43 ± 0.17 ms), and was consistently detected in all subjects. fPSPs recorded in the present study had latency and amplitude profiles resembling those previously described in awake mice [22,23]. As reported by these authors, it was difficult to dissociate the short-latency component of the fPSP depending on the case. Thus, we adopted a similar definition and used measurements of the consistent N2 peak amplitude as an index of field synaptic response in the mPFC. Table 1 shows baseline N2 parameters for all groups in the present study. As expected, no significant differences were detected between groups when latency and amplitude were analyzed (one-way ANOVA; $p > 0.05$).

Pirot et al. [5,61] showed that MD stimulation evoked two categories of unitary responses in the mPFC, which were distinguished by their latencies: short (3.46 ± 0.05 ms) and long (13.67 ± 0.22 ms). Short-latency responses correspond to the actual recruitment of MD-mPFC thalamocortical fibers, whereas long-latency responses correspond to the activation of intracortical axon collaterals, originating from mPFC-MD corticothalamic fibers. Indeed, electrical pulses applied within the MD inevitably stimulate mPFC-derived axon terminals, eliciting antidromic action potentials towards the mPFC, and thereby recruiting the axon collaterals of corticothalamic fibers [6]. Differently from Pirot et al. [5,61], Herry et al. [22] were the first to examine MD-evoked fPSPs in the mPFC to study long-term synaptic plasticity in the thalamocortical circuit, interpreting the short-latency component of their fPSPs as a response to MD-mPFC activation. However, given that they were not always able to identify the short-latency component depending on the subject, the authors (as well as Herry and Garcia [23]) measured the amplitude of the long-latency component (N2) of the fPSPs. Similarly, we decided to use N2 as an index of mPFC plasticity. Despite the low selectivity of MD electrical stimulation, we consider that MD-evoked plasticity may control the excitatory reverberation in the MD-mPFC circuit as a whole. In addition, Herry et al. [22] and Herry and Garcia [23] showed that LTD of MD-evoked fPSPs correlate to learning behaviors (i.e., resistance to extinction of conditioned fear), reinforcing the functional implications of MD-mPFC long-term plasticity.

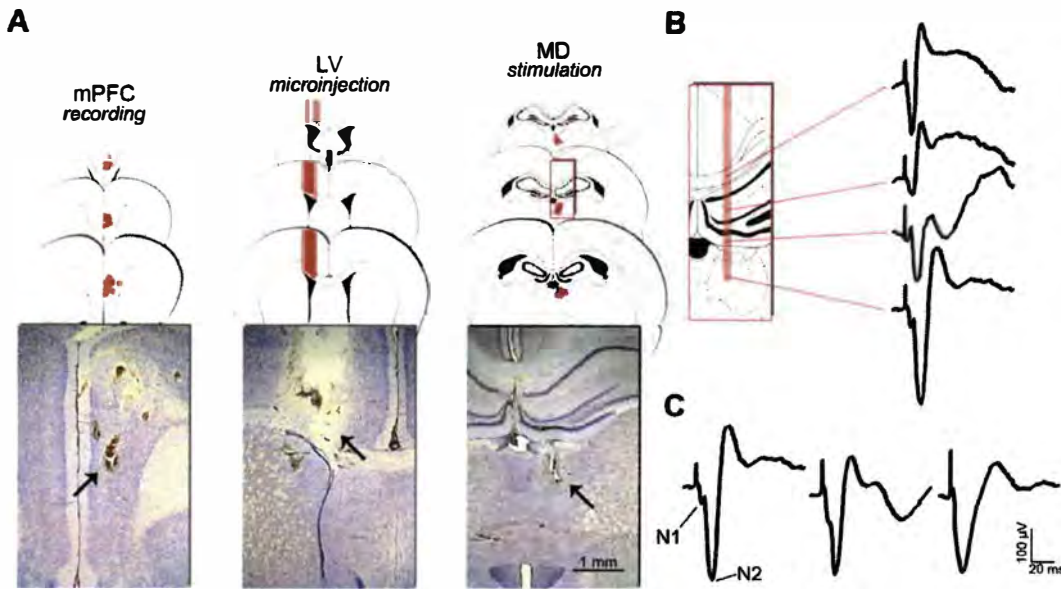


Figure 1. Histological validation of implants and typical prefrontal fPSPs. (A) Positioning of electrodes and cannulae from a coronal point of view. For mPFC and MD, coronal plates represent the anteroposterior variation of the electrode tip positioning (red dots), preferentially at the PrL of mPFC (layer-inespecific) and the anterior half of MD (subdivision-inespecific), both in the left hemisphere. For LV, the coronal plates show the variation of the cannula positioning (red bars) just above the right lateral ventricle, where the experimental drugs were injected. In the representative Nissl-stained coronal sections, the arrows point to typical electrolytic lesions (applied after the end of the experiments) and cannula tract. (B) Once the recording electrode was positioned at the mPFC, a typical dorsoventral profile of fPSPs was consistently evoked across subjects, while the stimulation electrode was lowered towards the MD (see details in the text). (C) Diversity of MD-evoked fPSPs recorded in the mPFC. The first fPSP shows a clear differentiation between two distinct negative peaks, which we termed N1 (amplitude $108.20 \pm 9.32 \mu\text{V}$; latency $6.85 \pm 0.15 \text{ ms}$) and N2 (amplitude $270.00 \pm 17.10 \mu\text{V}$; latency $13.43 \pm 0.17 \text{ ms}$). Such an aspect of fPSP was obtained in approximately half the subjects. In some cases, like the second fPSP, the N1 peak was subtle. Finally, in some other cases, like the third fPSP, the N1 peak was indistinguishable.
doi:10.1371/journal.pone.0047484.g001

3.3. Concentration-dependent effects of PILO and NIC on MD and mPFC oscillations

We have recently determined the latency and duration of the muscarinic effect of PILO on LFP oscillations in the hippocampus and mPFC following i.c.v. injections of different concentrations of the drug. PILO $40 \text{ nmol}/\mu\text{L}$ (injected volume of $1 \mu\text{L}$) shifts the pattern of urethane-driven slow waves to a transient state of increased high-frequency oscillations for $\sim 15 \text{ min}$ with a latency $\sim 1 \text{ min}$. In the present study, we show that LFPs recorded in the

MD and mPFC are also shifted towards faster oscillations in a concentration-dependent manner in response to NIC (Figure 2). In particular, the effect of NIC $320 \text{ nmol}/\mu\text{L}$ ($1 \mu\text{L}$, i.c.v.) on thalamic and cortical LFPs lasted for $\sim 12 \text{ min}$, matching the duration of HFS and LFS protocols used in this study. Therefore, PILO and NIC were used at these concentrations (respectively, $40 \text{ nmol}/\mu\text{L}$ and $320 \text{ nmol}/\mu\text{L}$) in all experiments.

3.4. Cholinergic modulation of the oscillatory activity in the hippocampus and mPFC

We quantified the spectral content of cortical and thalamic LFPs before, during, and after PILO and NIC microinjections. Figure 3 shows the integrated relative power spectra changes in MD and mPFC LFPs along the 6 min period of LFP continuous recording. We can see that PILO and NIC significantly decreased delta and proportionally potentiated theta, beta, and gamma oscillations. Particularly, the NIC effects on the four frequency bands had shorter latencies than the PILO effects, since the latter were already evident during the microinjection window. In addition, NIC induced a stronger potentiating effect on beta and gamma. Microinjection of aCSF by itself did not alter the urethane-induced slow-wave context. The ANOVA F values for interaction effects are as follows. mPFC delta: $F_{(58,1653)} = 5.181$; mPFC theta: $F_{(58,1653)} = 4.039$; mPFC beta: $F_{(58,1653)} = 8.930$; mPFC gamma: $F_{(58,1653)} = 13.880$; MD delta: $F_{(58,1653)} = 6.040$; MD theta: $F_{(58,1653)} = 5.538$; MD beta: $F_{(58,1653)} = 13.643$; MD gamma: $F_{(58,1653)} = 16.578$. The p values for all the ANOVAs were less than 0.001.

Table 1. Amplitude and latency of MD-evoked fPSPs recorded in the mPFC during baseline.

Groups	Amplitude (μV)	Latency (ms)
PILO-HFS	231.25 ± 31.19	13.22 ± 0.31
NIC-HFS	250.00 ± 56.78	14.57 ± 0.39
aCSF-HFS	335.00 ± 83.00	13.41 ± 0.42
PILO-LFS	277.50 ± 31.83	13.22 ± 0.51
NIC-LFS	262.50 ± 64.96	13.65 ± 0.68
aCSF-LFS	341.25 ± 63.82	13.16 ± 0.36
PILO-Ctrl	255.00 ± 31.40	11.99 ± 0.44
NIC-Ctrl	285.00 ± 50.92	14.01 ± 0.60
aCSF-Ctrl	190.00 ± 14.52	13.72 ± 0.57

Intergroup oneway ANOVA showed no significant differences. Data are shown as the mean \pm SEM.

doi:10.1371/journal.pone.0047484.t001

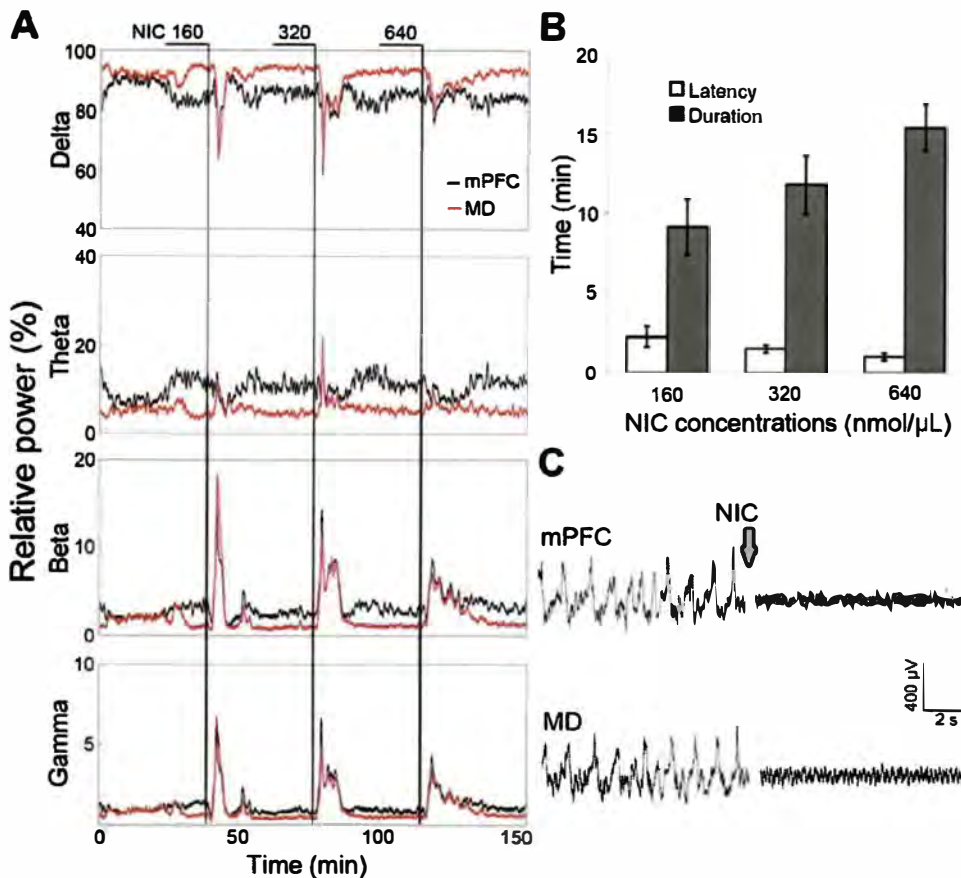


Figure 2. Concentration-dependent effect of NIC on forebrain oscillatory activity. Different concentrations of NIC (160, 320, and 640 nmol/μL; 1 μL icv) were injected while LFPs were continuously recorded during 120 min for analysis of the power spectrum at delta (0.5–4 Hz), theta (4–12 Hz), beta (12–30 Hz), and gamma (30–80 Hz) frequency bands. (A) Continuous thalamic and cortical LFP recording from a representative subject. (B) Analysis of latency and duration of LFP changes induced by the injection of the different NIC concentrations in a sample of eight rats. The sequence of injections at the different concentrations was randomized (data shown as the mean ± SEM). (C) Representative EEG tracings from mPFC and MD before and after NIC injection. Based on these experiments, we decided to use NIC 320 nmol/μL to induce a transient effect matching the duration of HFS and LFS protocols. doi:10.1371/journal.pone.0047484.g002

3.5. Cholinergic activation triggers a delayed form of LTP in the mPFC

Application of HFS in the MD did not induce LTP in the mPFC by itself. The amplitude of mPFC fPSPs recorded following aCSF injection (aCSF-HFS group) did not change for 4 h (Figure 4). In contrast, we observed that both PILO and NIC induced a delayed-onset form of LTP, with similar kinetics (PILO-HFS and NIC-HFS groups; interaction effect: $F_{(46,460)} = 1.714$; $p = 0.003$). As depicted in figure 4, LTP induced by PILO and by NIC began to emerge approximately 2 h after HFS, with values reaching approximately 120–130% of baseline level.

3.6. Cholinergic activation suppresses a long-lasting form of LTD in the mPFC

In the groups in which LFS was applied after aCSF microinjection, we observed stable LTD with duration of 4 h, at 80–90% of baseline level (Figure 5). In contrast, PILO-LFS and NIC-LFS subjects showed a complete suppression of LTD throughout the 4 h monitoring period. The effects had similar kinetics for both groups and apparently converted the LTD into a

subtle, but stable LTP (Figure 6; group effect: $F_{(2,21)} = 6.719$; $p = 0.006$).

3.7. Basal mPFC fPSPs are not affected by NIC or PILO in the long term

While PILO and NIC modulated HFS and LFS effects on MD-evoked prefrontal responses, these agonists alone did not affect mPFC responses in the long term. Although we observed a brief potentiation induced by NIC in the first 20 min (interaction effect: $F_{(46,480)} = 2.148$; $p < 0.001$), mPFC responses quickly recovered and did not show the sustained effect observed after HFS and LFS (Figure 6). These results support the fact that the cholinergic modulation observed after HFS and LFS is due to the interaction between the stimulation protocols and the cholinomimetic states promoted by PILO and NIC.

By separately comparing aCSF-LFS with aCSF-Ctrl or aCSF-HFS curves, we showed that LTD was significantly induced after LFS, but our HFS protocol was not sufficient to induce LTP (aCSF-LFS vs. aCSF-Ctrl: group effect, $F_{(1,14)} = 7.638$, $p = 0.015$, and time effect, $F_{(23,315)} = 1.587$, $p = 0.045$; aCSF-LFS vs. aCSF-HFS: group effect, $F_{(1,14)} = 19.074$, $p < 0.001$, and interaction

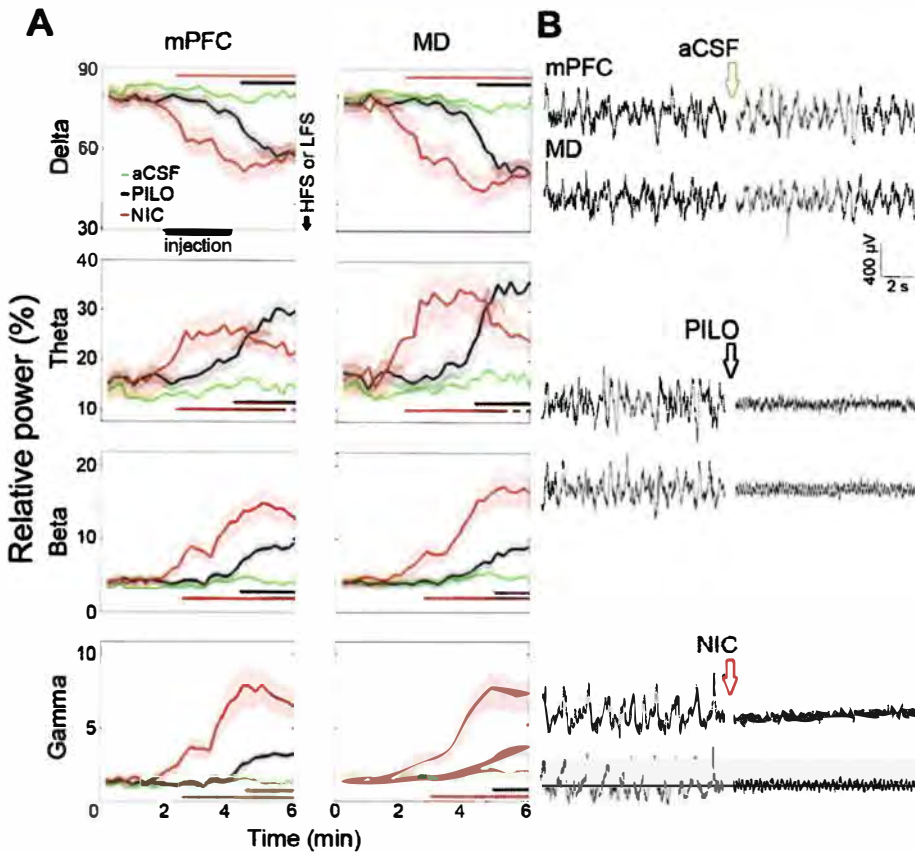


Figure 3. LFP power spectrum comparing mPFC and MD oscillatory activity before, during, and after microinjection. (A) Charts detailing PILO and NIC effects on LFPs, showing a decrease in delta (0.5–4 Hz), as well as an increase in theta (4–12 Hz), beta (12–30 Hz), and gamma (30–80 Hz) relative power. The LFP changes induced by NIC occurred earlier than those induced by PILO, with a shorter duration of theta potentiation, and a stronger potentiation of beta and gamma waves. The data were obtained from all aCSF, PILO and NIC rats of the synaptic plasticity experiments. Significant differences are indicated by two-way repeated measures ANOVA followed by the Newman-Keuls post-hoc test (black bar: aCSF vs. PILO; red bar: aCSF vs. NIC). (B) Representative EEG tracings from mPFC and MD before and after icv microinjections. Data are shown as the mean \pm SEM.

doi:10.1371/journal.pone.0047484.g003

effect, $F_{(23,315)}=1.734$, $p<0.021$; two-way repeated measures ANOVA; Figure S1). Given the subtle and stable LTP ($\sim 110\%$) observed in PILO-LFS and NIC-LFS groups, four additional comparisons were made: PILO-LFS vs. PILO-Ctrl, PILO-LFS vs. PILO-HFS, NIC-LFS vs. NIC-Ctrl, and NIC-LFS vs. NIC-HFS. All comparisons showed no intergroup differences. Thus, PILO and NIC were able to induce LTP (up to $\sim 130\%$, Figure 4) when applied before an ineffective HFS protocol, whereas they promoted a stable but of lower magnitude LTP following the LTD-inducing LFS protocol.

3.8. Thalamic and cortical oscillatory activity correlates with the peak of prefrontal LTP

To test whether the magnitude of prefrontal fPSPs correlated to the level of oscillatory changes induced by PILO and NIC in the MD and mPFC, we pooled data from all rats used in the synaptic plasticity experiments and divided them into three major groups (HFS, LFS, and Ctrl), regardless the injection they received. We then calculated the Pearson's linear correlation between the relative power at four frequency bands (delta, theta, beta, and gamma) and the mean fPSP amplitude every 10 min blocks following HFS, LFS, or Ctrl.

In HFS rats, the most evident results show a negative correlation between the amplitude of cortical fPSPs and the relative power of delta recorded in the mPFC and MD throughout the experiments. In addition, we observed a positive correlation of the amplitude of cortical fPSPs with the relative power of theta and beta recorded specifically in the mPFC. Therefore, the lower the relative delta power after microinjection, the higher the prefrontal responses to MD stimulation during the 4 h monitoring. Similarly, the higher the relative theta and beta powers after microinjection, the higher the prefrontal responses. The significant correlations were particularly concentrated 120 min after HFS, nearly matching the peak of prefrontal LTP in our HFS experiments (Figure 7).

Significant correlations were also found in LFS rats although they were less frequent and occurred only during the first 150 min of monitoring. Significant results were restricted to delta (negative correlations) and theta oscillations (positive correlations) recorded both in the mPFC and MD (e.g., at 20 min after LFS, MD delta: $r = -0.497$, $p = 0.026$; MD theta: $r = 0.489$, $p = 0.028$; at 30 min after LFS, mPFC delta: $r = -0.521$, $p = 0.038$; mPFC theta: $r = 0.537$, $p = 0.032$). Therefore, delta and theta powers after microinjection were negatively and positively correlated with the

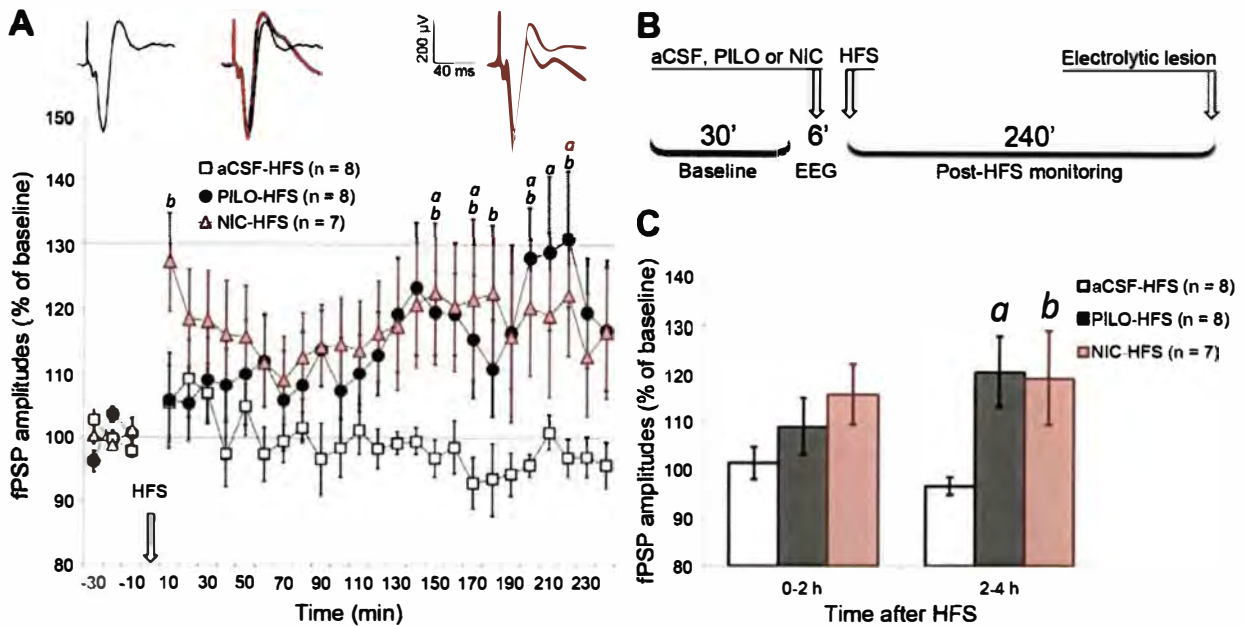


Figure 4. HFS induced a late LTP in mPFC only when applied under PILO and NIC effects. (A) fPSP amplitude throughout baseline (30 min) and post-HFS monitoring (240 min), depicting amplitudes averaged in 10-min blocks and normalized in relation to baseline mean amplitude. Significant differences are indicated by two-way ANOVA with repeated measures, followed by the Newman-Keuls post-hoc test (a = PILO vs. aCSF; b = NIC vs. aCSF; $p < 0.05$). The sequence of averaged fPSPs above the chart represents a typical PILO-HFS experiment, where post-HFS fPSPs (red) are superimposed on baseline fPSPs (black). Such fPSPs are roughly aligned with the time course of the chart. (B) Timeline summarizing the procedures for HFS experiments. (C) Data from chart A clustered in blocks of 2 h after HFS, highlighting PILO and NIC significant effects restricted to the second half of the monitoring. Data are shown as the mean \pm SEM. doi:10.1371/journal.pone.0047484.g004

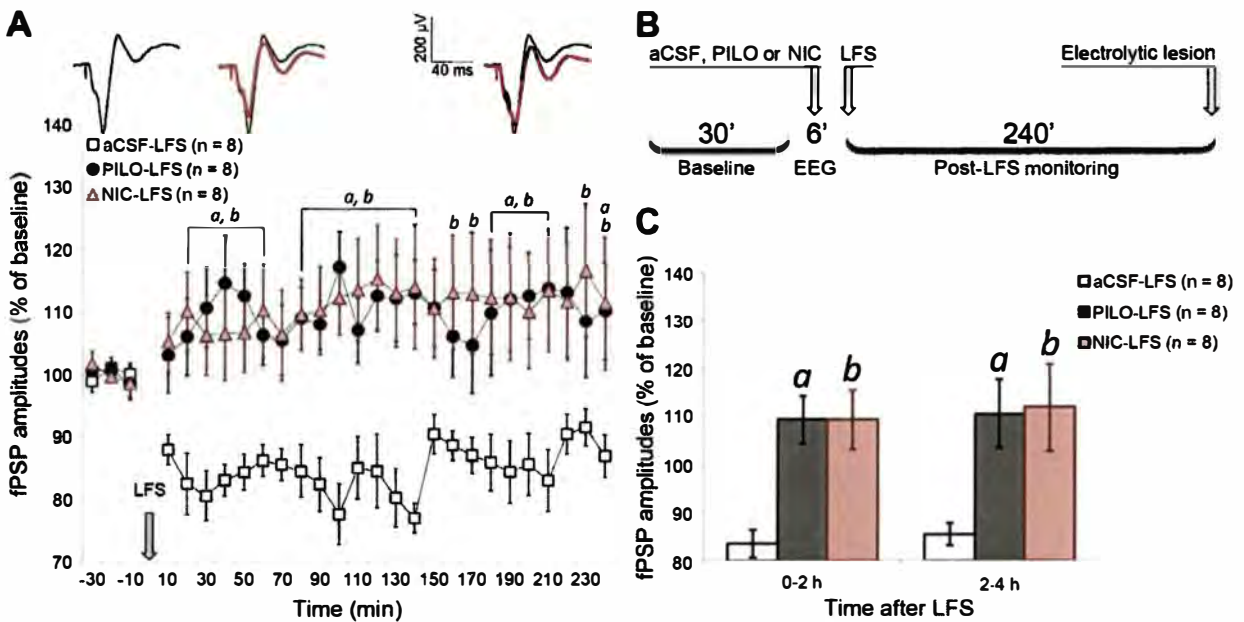


Figure 5. LFS induced a stable LTD in mPFC only when applied under urethane-driven slow-wave context. (A) fPSP amplitude throughout baseline (30 min) and post-LFS monitoring (240 min), depicting amplitudes averaged in 10 min blocks and normalized in relation to baseline mean amplitude. Significant differences are indicated by two-way ANOVA with repeated measures, followed by the Newman-Keuls post-hoc test (a = PILO vs. aCSF; b = NIC vs. aCSF; $p < 0.05$). The sequence of averaged fPSPs above the chart represents a typical aCSF-LFS experiment, where post-LFS fPSPs (red) are superimposed on baseline fPSPs (black). Such fPSPs are roughly aligned with the time course of the chart. (B) Timeline summarizing the procedures for LFS experiments. (C) Data from chart A clustered in blocks of 2 h after LFS, showing the stability of PILO and NIC effects throughout the monitoring. Data are shown as mean \pm SEM. doi:10.1371/journal.pone.0047484.g005

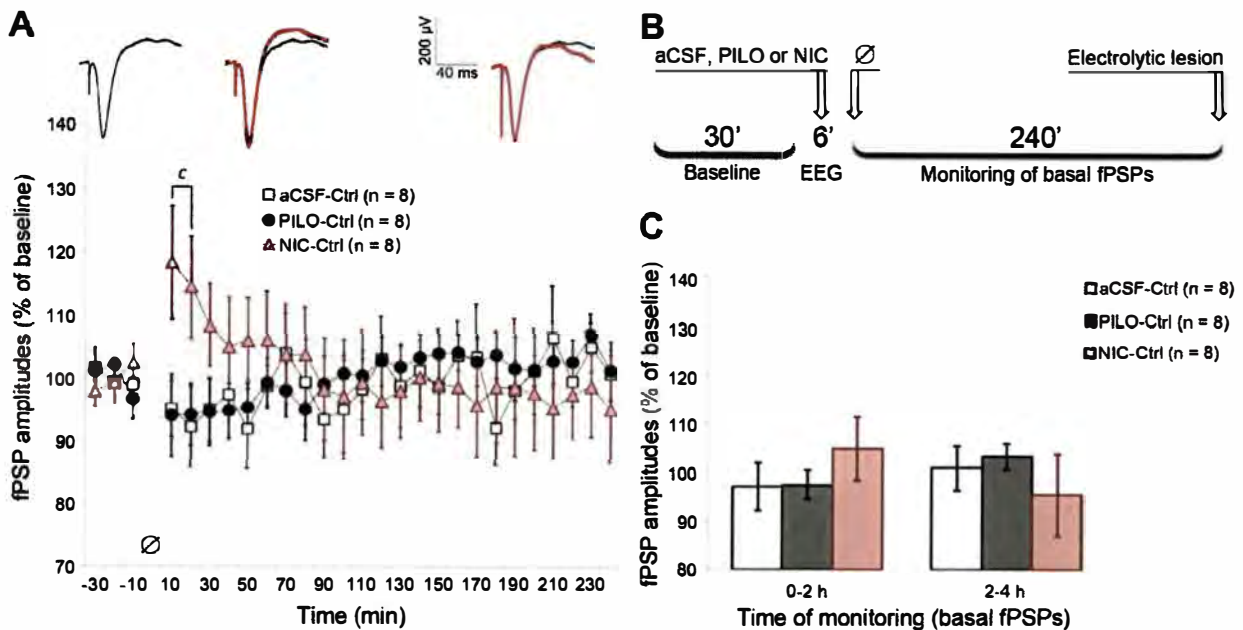


Figure 6. PILO and NIC microinjection alone did not induce long-term changes in MD-evoked prefrontal fPSPs. (A) fPSP amplitude throughout baseline (30 min) and monitoring (240 min), depicting amplitudes averaged in 10 min blocks and normalized in relation to baseline mean amplitude. Significant differences are indicated by two-way ANOVA with repeated measures, followed by the Newman-Keuls post-hoc test ($c = \text{NIC vs. both aCSF and PILO}$; $p < 0.05$). The sequence of averaged fPSPs above the chart represents a typical NIC-Ctrl experiment, where fPSPs recorded during the 4 h monitoring (red) are superimposed on baseline fPSPs (black). Such fPSPs are roughly aligned with the time course of the chart. (B) Timeline summarizing the procedures for Ctrl experiments, in which the empty-set symbol represents absence of train stimulation. (C) Data from chart A clustered in blocks of 2 h of monitoring. Data are shown as the mean \pm SEM. doi:10.1371/journal.pone.0047484.g006

prefrontal responses to MD stimulation during the first half of the monitoring respectively, which is consistent with the LTD-suppressing effects of PILO and NIC in our experiments.

Discussion

The present study describes the effects of the muscarinic and nicotinic brain activation on the long-term synaptic plasticity in the mPFC induced by electrical stimulation of the MD *in vivo*. We can divide our results into five main findings: (1) the muscarinic and nicotinic activation, induced by PILO and NIC, promoted a delayed-onset LTP in the mPFC when applied prior to HFS; (2) in contrast, both PILO and NIC suppressed LTD in the mPFC triggered by LFS; (3) PILO and NIC did not affect basal synaptic transmission in the long term, but NIC showed a transient potentiating effect both in the control and HFS condition with a mean duration of 20 min; (4) the network effects of PILO and NIC were detected by a transient decrease in the prevalence of delta waves (0.5–4 Hz) and a proportional increase of fast oscillations (4–80 Hz) in the cortex and thalamus; and (5) although PILO and NIC induced brief oscillatory changes in the MD and mPFC, such changes showed significant correlation to the increase in fPSP amplitudes recorded more than two hours after HFS or LFS.

In two recent reports, we used a similar design in anesthetized rats to assess the muscarinic modulation of LTP and LTD in the hippocampus-mPFC pathway [50,51]. We showed that muscarinic activation, produced by systemic administration of PILO prior to HFS in CA1, prevented the decay of LTP 2 h after its induction [50]. In contrast, the intracerebroventricular administration of PILO converted a subthreshold transient synaptic depression into a robust and stable LTD, lasting up to 4 h [51].

These results indicate that the brain muscarinic activation enhances both forms of synaptic plasticity in the mPFC suggesting an important cholinergic role in the bidirectional control of hippocampo-prefrontal plasticity. Our present findings, on the other hand, support a distinct function for the cholinergic modulation of MD-evoked mPFC plasticity, in which both muscarinic and nicotinic agonists either enhance LTP or suppress LTD. In fact, PILO and NIC converted a subthreshold HFS into a late-onset LTP and completely blocked LTD induced by LFS, with a net potentiating effect after HFS and a net suppressive effect after LFS. Besides, in the absence of stimulation, the application of NIC induced a transient enhancement of MD-mPFC responses that decayed to basal levels in 20 min. However, it is still unknown if NIC produces similar effects on the CA1-mPFC responses *in vivo*.

Neurochemically, the reciprocal communication between MD and mPFC is mediated by AMPA and NMDA receptors, and regulated by several neuromodulators [5,49,61–65]. It is well described that NMDA-dependent LTP and LTD relies on the intracellular signaling mediated by cytosolic Ca^{2+} , which controls AMPA receptor trafficking to and from the postsynaptic density [67]. These mechanisms can be triggered by HFS or LFS, and enhanced by simultaneous activation of M1-like muscarinic receptors that are widely distributed in the frontal cortex, resulting in sustained or reduced membrane depolarization [31,68–71]. Moreover, some reports have shown that presynaptic nicotinic receptors, mainly the low-affinity $\alpha 7$ and high-affinity $\alpha 4\beta 2$ subtypes, can exert a calcium-dependent potentiation of the thalamocortical transmission [34,47,59,72,73], which could explain the net potentiating effects of PILO and NIC. Consistently, Giovanni et al. [49] have shown that nicotinic agonists facilitate MD-evoked firing and promote glutamate release in the mPFC.

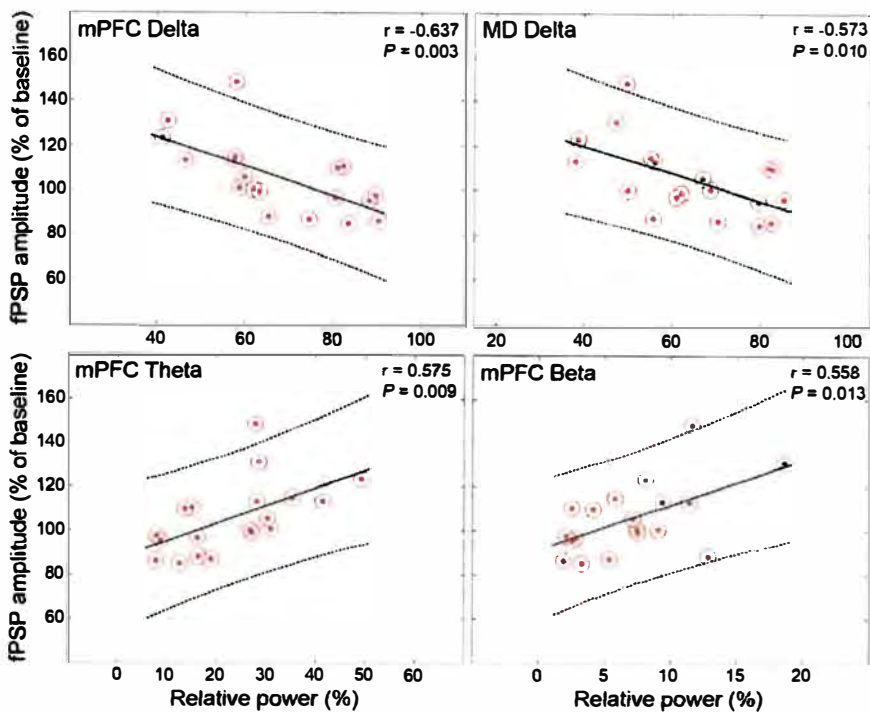


Figure 7. There were correlations between the level of LFP changes and fPSP amplitudes throughout the monitoring. The four plots represent the highest concentration of significant correlations, specifically between the delta, theta, and beta bands recorded prior to HFS and the 120–150 min time point after HFS. The lower the delta in mPFC and MD, the higher the fPSP amplitudes (top). The higher the theta-beta in mPFC, the higher the fPSP amplitudes (bottom).
doi:10.1371/journal.pone.0047484.g007

The authors also observed that unilateral MD lesions reduced in ~40% the binding of 3H-nicotine in the mPFC, indicating that thalamic presynaptic terminals in the mPFC are rich in nicotinic receptors. However, our data do not allow us to make a clear dissection of the individual effects of PILO and NIC on specific receptor subtypes, as we did not use cholinergic antagonists to block their actions.

Although previous studies have shown that excitability and neurotransmission in thalamocortical loops are susceptible to cholinergic modulation [46,48,66], there is still a lack of understanding on how synaptic plasticity in the MD-mPFC is affected by cholinergic-driven brain states. Here, our strategy of injecting PILO or NIC into the ventricle of anesthetized rats allowed us to achieve a global cholinergic activation that tried to mimic a physiological state of arousal or rapid-eye-movement (REM) sleep, which are endogenously regulated by ascending projections from the brainstem, basal forebrain, and septum [29,30]. Despite the limitation of recording during anesthesia, it was recently shown that urethane anesthesia mimics the state alternations of sleep, suggesting its possible use as a model to study sleep oscillations [95]. Interestingly, the cholinergic control of oscillatory states of sleep is relatively preserved by urethane [90–95]. Indeed, the transient effects of PILO and NIC on LFPs under urethane resembled the oscillatory pattern observed in REM sleep episodes [84], which are primarily induced by cholinergic projections depolarizing thalamocortical cells and inducing their tonic firing [36,85,88–89].

A plausible implication of our findings is that acetylcholine through muscarinic and nicotinic receptors might favor MD inputs

to the mPFC during cholinergic-driven states such as in sleep or during cognitive demands during waking, leading to a long lasting strengthening of thalamo-prefrontal communication. More specifically, high-frequency inputs to mPFC during REM sleep might induce LTP in thalamocortical synapses, as shown from the effects of PILO and NIC following HFS. In agreement to that, cortical synaptic plasticity seems to occur in sleep and is thought to be a mechanism of consolidation of memories traces [37,86,87]. In contrast, low-frequency trains of MD spikes would more efficiently cause synaptic depression in the mPFC in a low cholinergic activity condition. Such LTD-favoring effect would be congruent with the hypothesis of sleep-dependent synaptic homeostasis, according to which slow-wave activity down-scales prefrontal synapses, preparing them for ensuing wakefulness [96]. It is known that cholinergic cells of the basal forebrain and septum are also particularly active during wakefulness and are involved in the phasic and tonic cholinergic discharges during cue-detection tasks [81]. Such neuromodulation is thought to raise the sensitivity of cortical networks to afferent inputs, supporting arousal [33,46–48,74–76] and enhancing the thalamocortical signal-to-noise ratio during cognitive and attention-demanding tasks [77–81]. It is possible that cognitive processes requiring mPFC activity, such as working memory and action planning, could undergo a state-dependent bimodal cholinergic modulation [2,82–83].

In conclusion, the present study shows that the brain cholinergic activation by PILO and NIC differentially modulate LTP and LTD in the mPFC driven by the thalamus. Considering that a cholinergic unbalance in limbic circuits connected to the prefrontal cortex may contribute to major disorders, such as

Alzheimer's disease and schizophrenia, new studies on network plasticity in freely behaving animals under low and high-cholinergic tone may help to elucidate some of the prefrontal roles in such dysfunctions.

Supporting Information

Figure S1 Pairwise comparisons between drug-treated groups (aCSF, PILO and NIC) in all experimental conditions (Control, LFS and HFS). Normalized amplitude of IPSPs recorded during baseline (30 min) and post-tetanzation (240 min) are plotted in 10-min blocks. (A) aCSF; (B) PILO; (C) NIC. Significant differences were evaluated by two-way ANOVA with repeated measures, followed by Newman-Keuls post-hoc test.

References

- Otani S (2003) Prefrontal cortex function, quasi-physiological stimuli, and synaptic plasticity. *J Physiol Paris* 97: 423–430.
- Dalley JW, Cardinal RN, Robbins TW (2004) Prefrontal executive and cognitive functions in rodents: neural and neurochemical substrates. *Neurosci Biobehav Rev* 28: 771–784.
- Goto Y, Yang CR, Otani S (2010) Functional and dysfunctional synaptic plasticity in prefrontal cortex: roles in psychiatric disorders. *Biol Psychiatry* 67: 199–207.
- Vertes RP (2006) Interactions among the medial prefrontal cortex, hippocampus and midline thalamus in emotional and cognitive processing in the rat. *Neuroscience* 142: 1–20.
- Pirot S, Jay TM, Glowinski J, Thierry AM (1994) Anatomical and electrophysiological evidence for an excitatory amino acid pathway from the thalamic mediodorsal nucleus to the prefrontal cortex in the rat. *Eur J Neurosci* 6: 1225–1234.
- Kuroda M, Yokofujita J, Murakami K (1998) An ultrastructural study of the neural circuit between the prefrontal cortex and the mediodorsal nucleus of the thalamus. *Prog Neurobiol* 54: 417–458.
- Uyilings HB, Groenewegen HJ, Kolb B (2003) Do rats have a prefrontal cortex? *Behav Brain Res* 146: 3–17.
- Negyessy L, Goldman-Rakic PS (2005) Morphometric characterization of synapses in the primate prefrontal cortex formed by afferents from the mediodorsal thalamic nucleus. *Exp Brain Res* 164: 148–154.
- Klein JC, Rushworth MFS, Behrens TFJ, Mackay CE, Crespigny AJ, et al. (2010) Topography of connections between human prefrontal cortex and mediodorsal thalamus studied with diffusion tractography. *Neuroimage* 51: 553–564.
- Eckert U, Metzger CD, Buchmann JE, Kaufmann J, Osoba A, et al. (2011) Prefrontal networks of the mediodorsal nucleus and centromedian-parafascicular complex of the thalamus - A DTT tractography study. *Hum Brain Mapp* doi:10.1002/hbm.21389.
- Bailey KR, Mair RG (2005) Lesions of specific and nonspecific thalamic nuclei affect prefrontal cortex-dependent aspects of spatial working memory. *Behav Neurosci* 119: 410–419.
- Antoniadis EA, McDonald RJ (2006) Fornix, medial prefrontal cortex, nucleus accumbens, and mediodorsal thalamic nucleus: roles in a fear-based context discrimination task. *Neurobiol Learn Mem* 85: 71–85.
- Izquierdo A, Murray EA (2010) Functional interaction of medial mediodorsal thalamic nucleus but not nucleus accumbens with amygdala and orbital prefrontal cortex is essential for adaptive response selection after reinforcer devaluation. *J Neurosci* 30: 661–669.
- Metzger CD, Eckert U, Steiner J, Sartorius A, Buchmann JE, et al. (2010) High field fMRI reveals thalamocortical integration of segregated cognitive and emotional processing in mediodorsal and intralaminar thalamic nuclei. *Front Neuroanat* 4: 138.
- Padilla-Garzon N, Do-Monte FH, Quirk GJ (2012) A time-dependent role of midline thalamic nuclei in the retrieval of fear memory. *Neuropharmacology* 62: 457–463.
- Watanabe Y, Funahashi S (2012) Thalamic mediodorsal nucleus and working memory. *Neurosci Biobehav Rev* 36: 134–142.
- Mitelman SA, Byrne W, Kemether EM, Hazlett EA, Buchsbaum MS (2006) Correlations between volumes of the pulvinar, centromedian, and mediodorsal nuclei and cortical Brodmann's areas in schizophrenia. *Neurosci Lett* 392: 16–21.
- Kito S, Jung J, Kobayashi T, Koga Y (2009) Fiber tracking of white matter integrity connecting the mediodorsal nucleus of the thalamus and the prefrontal cortex in schizophrenia: a diffusion tensor imaging study. *Eur Psychiatry* 24: 269–274.
- Pakkenberg B, Scheel-Kruger J, Kristiansen LV (2009) Schizophrenia: from structure to function with special focus on the mediodorsal thalamic prefrontal loop. *Acta Psychiatr Scand* 120: 345–354.
- Volk DW, Lewis DA (2010) Prefrontal cortical circuits in schizophrenia. *Curr Top Behav Neurosci* 4: 485–508.
- Floresco SB, Grace AA (2003) Gating of hippocampal-evoked activity in prefrontal cortical neurons by inputs from the mediodorsal thalamus and ventral tegmental area. *J Neurosci* 23: 3930–3944.
- Herry C, Vouimba RM, Garcia R (1999) Plasticity in the mediodorsal thalamo-prefrontal cortical transmission in behaving mice. *J Neurophysiol* 82: 2827–2832.
- Herry C, Garcia R (2002) Prefrontal cortex long-term potentiation, but not long-term depression, is associated with the maintenance of extinction of learned fear in mice. *J Neurosci* 22: 577–583.
- Bertram EH, Zhang D, Williamson JM (2008) Multiple roles of midline dorsal thalamic nuclei in induction and spread of limbic seizures. *Epilepsia* 49: 256–263.
- Sloan DM, Bertram EH (2009) Changes in midline thalamic recruiting responses in the prefrontal cortex of the rat during the development of chronic limbic seizures. *Epilepsia* 50: 556–565.
- Sloan DM, Zhang D, Bertram EH (2011) Excitatory amplification through divergent-convergent circuits: the role of the midline thalamus in limbic seizures. *Neurobiol Dis* 43: 435–443.
- Sloan DM, Zhang D, Bertram EH (2011) Increased GABAergic inhibition in the midline thalamus affects signaling and seizure spread in the hippocampus-prefrontal cortex pathway. *Epilepsia* 52: 523–530.
- Buzsáki G, Gage BH (1989) The cholinergic nucleus basalis: a key structure in neocortical arousal. *EXS* 57: 159–171.
- Lucas-Munier E, Fossier P, Baux G, Amar M (2003) Cholinergic modulation of the cortical neuronal network. *Pflügers Arch* 446: 17–29.
- Parent M, Descarries L (2004) Acetylcholine innervation of the adult rat thalamus: distribution and ultrastructural features in dorsolateral geniculate, parafascicular, and reticular thalamic nuclei. *J Comp Neurol* 511: 678–691.
- Gu Q (2002) Neuromodulatory transmitter systems in the cortex and their role in cortical plasticity. *Neuroscience* 111: 815–835.
- Giocomo LM, Hasselmo ME (2007) Neuromodulation by glutamate and acetylcholine can change circuit dynamics by regulating the relative influence of afferent input and excitatory feedback. *Mol Neurobiol* 36: 184–200.
- Hasselmo ME, Giocomo LM (2006) Cholinergic modulation of cortical function. *J Mol Neurosci* 30: 133–135.
- Hasselmo ME, Sarter M (2011) Modes and models of forebrain cholinergic neuromodulation of cognition. *Neuropsychopharmacology Rev* 36: 52–73.
- McCormick DA (1989) Cholinergic and noradrenergic modulation of thalamo-cortical processing. *Trends Neurosci* 12: 215–221.
- Steriade M (2004) Acetylcholine systems and rhythmic activities during the waking-sleep cycle. *Prog Brain Res* 145: 179–196.
- Dickelmann S, Born J (2010) The memory function of sleep. *Nat Rev Neurosci* 11: 114–126.
- Raggenbass M, Bertrand D (2002) Nicotinic receptors in circuit excitability and epilepsy. *J Neurobiol* 53: 580–589.
- Friedman A, Behrens CJ, Heinemann U (2007) Cholinergic dysfunction in temporal lobe epilepsy. *Epilepsia* 48 Suppl 5: 126–130.
- Raedler TJ, Bymaster FP, Tandon R, Copolov D, Dean B (2007) Towards a muscarinic hypothesis of schizophrenia. *Mol Psychiatry* 12: 232–246.
- Herholz K, Weisenbach S, Kalbe E (2008) Deficits of the cholinergic system in early AD. *Neuropsychologia* 46: 1642–1647.
- Scarr E, Dean B (2009) Role of the cholinergic system in the pathology and treatment of schizophrenia. *Expert Rev Neurother* 9: 73–86.
- Craig LA, Hong NS, McDonald RJ (2011) Revisiting the cholinergic hypothesis in the development of Alzheimer's disease. *Neurosci Biobehav Rev* 35: 1397–1409.
- Metherate R, Ashe JH (1993) Nucleus basalis stimulation facilitates thalamo-cortical synaptic transmission in the rat auditory cortex. *Synapse* 14: 132–143.

*, $p < 0.05$. All curves correspond to data shown in figures 4–6. Data are shown as mean \pm SEM. (TIF)

Acknowledgments

We would like to thank Renata Caldo Scanduzzi and Antônio Renato Meirelles Silva for their excellent technical support, and Matheus Teixeira Rossignoli for valuable discussions.

Author Contributions

Conceived and designed the experiments: LSBJ RRP. Performed the experiments: LSBJ CLA RNR. Analyzed the data: LSBJ RRP. Contributed reagents/materials/analysis tools: JPL RRP. Wrote the paper: LSBJ RRP.

45. Dringenberg HC, Kuo MC, Tomaszek S (2004) Stabilization of thalamo-cortical long-term potentiation by the amygdala: cholinergic and transcription-dependent mechanisms. *Eur J Neurosci* 20: 357–365.
46. Dringenberg HC, Hamze B, Wilson A, Speechley W, Kuo MC (2007) Heterosynaptic facilitation of in vivo thalamocortical long-term potentiation in the adult rat visual cortex by acetylcholine. *Cereb Cortex* 17: 839–848.
47. Kawai H, Lazar R, Metherate R (2007) Nicotinic control of axon excitability regulates thalamocortical transmission. *Nat Neurosci* 10: 1168–1175.
48. Kuo MC, Rasmusson DD, Dringenberg HC (2009) Input-selective potentiation and rebalancing of primary sensory cortex afferents by endogenous acetylcholine. *Neuroscience* 163: 430–441.
49. Giovanni Y, Rougeot C, Clarke PB, Lepoué C, Thierry AM, et al. (1999) Nicotinic receptors in the rat prefrontal cortex: increase in glutamate release and facilitation of mediolateral thalamo-cortical transmission. *Eur J Neurosci* 11: 18–30.
50. Lopes-Aguiar C, Romcy-Pereira RN, Escorsim-Szawka R, Galvis-Alonso OY, Anselmo-Franci JA, et al. (2008) Muscarinic acetylcholine neurotransmission enhances the late-phase of long-term potentiation in the hippocampal-prefrontal cortex pathway of rats in vivo: a possible involvement of monoaminergic systems. *Neuroscience* 153: 1309–1319.
51. Lopes-Aguiar C, Bueno-Júnior LS, Ruggiero RN, Romcy-Pereira RN, Leite JP (2012) NMDA receptor blockade impairs the muscarinic conversion of sub-threshold transient depression into long-lasting LTD in the hippocampus-prefrontal cortex pathway in vivo: correlation with gamma oscillations. *Neuropharmacology*. 10.1016/j.neuropharm.2012.09.013. *In press*.
52. Gigg J, Tan AM, Finch DM (1994) Glutamatergic hippocampal formation projections to prefrontal cortex in the rat are regulated by GABAergic inhibition and show convergence with glutamatergic projections from the limbic thalamus. *Hippocampus* 4: 189–198.
53. Groenewegen HJ, Wright CJ, Uylings HB (1997) The anatomical relationships of the prefrontal cortex with limbic structures and the basal ganglia. *J Psychopharmacol* 11: 99–106.
54. Paxinos G, Watson C (2007) *The Rat Brain in Stereotaxic Coordinates*. London: Academic Press. 462 p.
55. Romcy-Pereira RN, Pavlides C (2004) Distinct modulatory effects of sleep on the maintenance of hippocampal and medial prefrontal cortex LTP. *Eur J Neurosci* 20: 3453–3462.
56. Hoss W, Woodruff JM, Ellerbrock BR, Periyasamy S, Ghodsi-Hovsepian S, et al. (1990) Biochemical and behavioral responses of pilocarpine at muscarinic receptor subtypes in the CNS. Comparisons with receptor binding and low-energy conformations. *Brain Res* 533: 232–238.
57. Cavalheiro EA (1995) The pilocarpine model of epilepsy. *Ital J Neurol Sci* 16: 33–37.
58. Dani JA, Bertrand D (2007) Nicotinic acetylcholine receptors and nicotinic cholinergic mechanisms of the central nervous system. *Annu Rev Pharmacol Toxicol* 47: 699–729.
59. McKay BE, Placzek AN, Dani JA (2007) Regulation of synaptic transmission and plasticity by neuronal nicotinic acetylcholine receptors. *Biochem Pharmacol* 74: 1120–1133.
60. Hogarty WB, Vertes RP (2007) Anatomical analysis of afferent projections to the medial prefrontal cortex in the rat. *Brain Struct Funct* 212: 149–179.
61. Pirot S, Glowinski J, Thierry AM (1995) Excitatory responses evoked in prefrontal cortex by mediolateral thalamic nucleus stimulation: influence of anesthesia. *Eur J Pharmacol* 285: 45–54.
62. Ferron A, Thierry AM, Le Douarin C, Glowinski J (1984) Inhibitory influence of the mesocortical dopaminergic system on spontaneous activity or excitatory response induced from the thalamic mediolateral nucleus in the rat medial prefrontal cortex. *Brain Res* 302: 257–265.
63. Mantz J, Godbout R, Tassin JP, Glowinski J, Thierry AM (1990) Inhibition of spontaneous and evoked unit activity in the rat medial prefrontal cortex by mesencephalic raphe nuclei. *Brain Res* 524: 22–30.
64. Mantz J, Milla C, Glowinski J, Thierry AM (1988) Differential effects of ascending neurons containing dopamine and noradrenaline in the control of spontaneous activity and of evoked responses in the prefrontal cortex. *Neuroscience* 27: 517–526.
65. Puig MV, Celada P, Diaz-Mataix L, Artigas F (2003) In vivo modulation of the activity of pyramidal neurons in the rat medial prefrontal cortex by 5-HT_{2A} receptors: relationship to thalamocortical afferents. *Cereb Cortex* 13: 870–882.
66. Hogsden JL, Dringenberg HC (2009) Decline of long-term potentiation (LTP) in the rat auditory cortex in vivo during postnatal life: involvement of NR2B subunits. *Brain Res* 1283: 25–33.
67. Citri A, Malenka RC (2008) Synaptic plasticity: multiple forms, functions, and mechanisms. *Neuropharmacology* 33: 18–41.
68. Rasmusson DD (2000) The role of acetylcholine in cortical synaptic plasticity. *Behav Brain Res* 115: 205–218.
69. Carr DB, Surmeier DJ (2007) M1 muscarinic receptor modulation of Kir2 channels enhances temporal summation of excitatory synaptic potentials in prefrontal cortex pyramidal neurons. *J Neurophysiol* 97: 3432–3438.
70. Broicher T, Wetschreck N, Munsch T, Coulon P, Meuth SG, et al. (2008) Muscarinic ACh receptor-mediated control of thalamic activity via G(q)/G(1)-family G-proteins. *Pflügers Arch* 456: 1049–1060.
71. Buchanan KA, Petrovic MM, Chamberlain SEL, Marrión NV, Mellor JR (2010) Facilitation of long-term potentiation by muscarinic M1 receptors is mediated by inhibition of SK channels. *Neuron* 68: 948–963.
72. Lambe EK, Picciotto MR, Aghajanian GK (2003) Nicotine induces glutamate release from thalamocortical terminals in prefrontal cortex. *Neuropsychopharmacology* 28: 216–225.
73. Clarke PB (2004) Nicotinic modulation of thalamocortical neurotransmission. *Prog Brain Res* 145: 253–260.
74. Hsieh CY, Cruikshank SJ, Metherate R (2000) Differential modulation of auditory thalamocortical and intracortical synaptic transmission by cholinergic agonist. *Brain Res* 880: 51–64.
75. Robbins TW, Roberts AC (2007) Differential regulation of fronto-executive function by the monoamines and acetylcholine. *Cereb Cortex* 17 Suppl 1: i131–160.
76. Metherate R (2011) Functional connectivity and cholinergic modulation in auditory cortex. *Neurosci Biobehav Rev* 35: 905A–906A.
77. Fanselow EE, Sameshima K, Baccala LA, Nicoletis MA (2001) Thalamic bursting in rats during different awake behavioral states. *Proc Natl Acad Sci USA* 98: 15330–15335.
78. Castro-Alamancos MA (2002) Role of thalamocortical sensory suppression during arousal: focusing sensory inputs in neocortex. *J Neurosci* 22: 9651–9655.
79. Usrey VM (2002) The role of spike timing for thalamocortical processing. *Curr Opin Neurobiol* 12: 411–417.
80. Hirata A, Castro-Alamancos MA (2010) Neocortex network activation and deactivation states controlled by the thalamus. *J Neurophysiol* 103: 1147–1157.
81. Parikh V, Sarter M (2008) Cholinergic mediation of attention: contributions of phasic and tonic increases in prefrontal cholinergic activity. *Ann NY Acad Sci* 1129: 225–235.
82. Del Arco A, Mora F (2009) Neurotransmitters and prefrontal cortex-limbic system interactions: implications for plasticity and psychiatric disorders. *J Neural Transm* 116: 941–952.
83. Mansvelder HD, Mertz M, Role LW (2009) Nicotinic modulation of synaptic transmission and plasticity in cortico-limbic circuits. *Semin Cell Dev Biol* 20: 432–440.
84. Stenborg D (2007) Neuroanatomy and neurochemistry of sleep. *Cell Mol Life Sci* 64: 1187–1204.
85. McCormick DA, Prince DA (1986) Mechanisms of action of acetylcholine in the guinea-pig cerebral cortex in vitro. *J Physiol* 375: 169–194.
86. Ribeiro S, Nicoletis MA (2004) Reverberation, storage, and postsynaptic propagation of memories during sleep. *Learn Mem* 11: 686–696.
87. Romcy-Pereira RN, Erraji-Benchekroun L, Smyrniotopoulos P, Ogawa S, Mello CV, et al. (2009) Sleep-dependent gene expression in the hippocampus and prefrontal cortex following long-term potentiation. *Physiol Behav* 98: 44–52.
88. McCormick DA, Pape HC (1990) Properties of a hyperpolarization-activated cation current and its role in rhythmic oscillation in thalamic relay neurons. *J Physiol* 431: 291–318.
89. Llinás RR, Steriade M (2006) Bursting of thalamic neurons and states of vigilance. *J Neurophysiol* 93: 3297–3308.
90. Détéari I, Semba K, Rasmusson DD (1997) Responses of cortical EEG-related basal forebrain neurons to brainstem and sensory stimulation in urethane-anesthetized rats. *Eur J Neurosci* 9: 1153–1161.
91. Horner RL, Kubin L (1999) Pontine carbachol elicits multiple rapid eye movement sleep-like neural events in urethane-anesthetized rats. *Neuroscience* 93: 215–226.
92. Balatoni B, Détéari I (2003) EEG related neuronal activity in the pedunculopontine tegmental nucleus of urethane anaesthetized rats. *Brain Res* 959: 304–311.
93. Dringenberg HC, Olmstead MC (2003) Integrated contributions of basal forebrain and thalamus to neocortical activation elicited by pedunculopontine tegmental stimulation in urethane-anesthetized rats. *Neuroscience* 119: 839–853.
94. Toth A, Hajnik T, Détéari I (2012) Cholinergic modulation of slow cortical rhythm in urethane-anesthetized rats. *Brain Res Bull* 87: 117–129.
95. Clement EA, Richard A, Thwaites M, Ailon J, Peters S, et al. (2008) Cyclic and sleep-like spontaneous alternations of brain state under urethane anesthesia. *PLoS One* 3: e2004.
96. Tononi G, Cirelli C (2003) Sleep and synaptic homeostasis: a hypothesis. *Brain Res Bull* 62: 143–150.